DISSERTATION

SORCS2 activity in pancreatic α cells safeguards insulin secretion from pancreatic β cells under glucose stress

Die Aktivität von SORCS2 in den pankreatischen α-Zellen schützt die Insulinsekretion der pankreatischen β-Zellen bei Glukosebelastung

zur Erlangung des akademischen Grades
Doctor of Philosophy (PhD)

vorgelegt der Medizinischen Fakultät

Charité – Universitätsmedizin Berlin

von

Oleksandra Kalnytska

Erstbetreuung: Prof. Dr. Thomas Willnow

Datum der Promotion: 29.11.2024

Preface

Partial results of this work were published in:

Kalnytska O, Qvist P, Kunz S, Conrad T, Willnow TE, Schmidt V. SORCS2 activity in pancreatic α-cells safeguards insulin granule formation and release from glucose-stressed β-cells. iScience. 2024;27(1)

on 19th of January 2024

Table of contents

List of tables

List of figures

List of abbreviations

AChR	-	Acetylcholine receptor
ACTH	-	Adrenocorticotropic hormone
ADHD	-	Attention deficit/hyperactivity disorder
AKT	-	Protein kinase B
AMPAR	-	α-amino-3-hydroxy-5-methyl-4-isoxazolepropionic acid receptor
AMPK	-	AMP-activated protein kinase
AP-1	-	Activator protein-1
APCs	-	Antigen-presenting cells
ASK1	-	Apoptosis signal-regulating kinase 1
ATF6	-	Transcription factor 6
BDNF	-	Brain-derived neurotrophic factor
BiP	-	Binding immunoglobulin protein
BDNF	-	Brain-derived neurotrophic factor
BMI	-	Body mass index
CA2	-	Cornu Ammonis 2
CAPN10	-	Calpain 10
CART	-	Cocaine-amphetamine-regulated transcript
CBP	-	p300/CREB-binding protein
CDKN2A/B	-	Cyclin-dependent kinase inhibitor 2A/B
CDC42	-	Cell division control protein 42
CDX2	-	Caudal-type homeobox 2
CGI-58	-	Comparative gene identification-58
CHOP	-	C/EBP homologous protein
CIITA	-	The class II major histocompatibility complex trans-activator
CNS	-	Central nervous system
COX-2	-	Cyclooxygenase-2
CRE	-	Cyclic AMP response element
CREB	-	CAMP response element-binding protein
CRTC2	-	CREB Regulated Transcription Coactivator 2
CXCL10	-	C-X-C motif chemokine ligand 10
DDX1	-	ATP-dependent RNA helicase DEAD-box helicase 1

DEG	-	Differentially expressed genes
df	-	Degrees of freedom
dH2O	-	Distilled water
EGF	-	Epidermal growth factor
EIF3a	-	Eukaryotic initiation factor 3a
ELKS	-	ETS-domain-containing proteins
EPAC2	-	Exchange protein directly activated by cAMP 2
ER	-	Endoplasmic reticulum
ERα	-	Estrogen receptor α
ERβ	-	Estrogen receptor β
ERγ	-	Estrogen receptor γ
ERAD	-	ER-associated protein degradation
eIF2α	-	α Subunit of eukaryotic initiation factor 2
G6P	-	Glucose-6-phosphate
GADD34	-	Growth arrest and DNA damage-inducible protein
GDP	-	Binding guanosine diphosphate
GIRK	-	G protein-coupled inwardly rectifying potassium channels
GIP	-	Glucose-dependent insulinotropic peptide
GIPR	-	Glucose-dependent insulinotropic polypeptide receptor
GLP-1	-	Glucagon-like peptide 1
GLP1R	-	Glucagon-like peptide 1 receptors
GLUTs	-	Glucose transporters
GHS-R1a	-	Growth hormone secretagogue receptor
GO	-	Gene ontology
GP	-	Glycogen phosphorylase
GPK	-	Glycogen phosphorylase kinase
GSK-3	-	Glycogen synthase 3
GSIS	-	Glucose-stimulated insulin secretion test
GWAS	-	Genome-wide association studies
HAB	-	Head-activating binding protein
HAP-1	-	Huntingtin-associated protein 1
HHEX	-	Haematopoietically expressed homeobox
HSL	-	Hormone-sensitive lipase

IAPP	-	Islet amyloid polypeptide
IGRP	-	Islet-specific glucose-6-phosphatase catalytic subunit-related protein
IFN-γ	-	Interferon-γ
IGF-1	-	Insulin-like growth factor-1
IGF1R	-	Insulin growth factor 1 receptor
IL-1β	-	Interleukin-1β
IL-15	-	Interleukin-15
IL-21	-	Interleukin-21
IRS	-	Insulin receptor substrate
JNK	-	c-Jun N-terminal kinase
KCNJ11	-	IRS-2, potassium inwardly-rectifying channel, subfamily J, member 11
LDL	-	Low-density lipoprotein
LEPR	-	Leptin receptor
limma	-	Linear models for microarray data
MAFA	-	MAF BZIP transcription factor A
MAST	-	Model-based analysis of single-cell transcriptomics
MHCII	-	Major histocompatibility complex class II
mTORC1	-	Mammalian target of rapamycin complex 1
NADPH	-	Nicotinamide adenine dinucleotide phosphate
NGF	-	Nerve growth factor
NLRP3	-	NLR family pyrin domain-containing 3
NOX	-	NADPH oxidase
NOX1	-	JAK2/STAT3/NADPH oxidase 1
n.s.	-	Not significant
NOD mice	-	Non-obese diabetic mice
NP	-	Nucleus pulposus
NR2A	-	N-methyl-D-aspartate receptor 2A
p	-	p-value
PACAP	-	Pituitary adenylate-cyclase-activating polypeptide
PAX6	-	Paired box 6
PDE3B	-	Phosphodiesterase 3B
PDPK1	-	3′phosphoinoside-dependent kinase 1
PDIA1	-	Disulfide isomerase

PERK	-	Protein kinase RNA-like ER kinase
PFA	-	Paraformaldehyde
PIP3	-	Phosphatidylinositol (3,4,5)-trisphosphate
PK	-	Pyruvate kinase
PKA	-	Protein kinase A
PKD	-	Polycystic kidney domain
PKG	-	Protein kinase G
PKM	-	Pyruvate kinase M1/2
PP	-	Pancreatic polypeptide
POMC	-	Proopiomelanocortin
proIAPP	-	Pro-form of islet amyloid polypeptide
qRT-PCR	-	Quantitative real-time PCR
Rab11FIP5	-	Rab11 GTPase effector Rab11 family-interacting protein 5
Rip11	-	Rab11-interacting protein
ROS	-	Reactive oxygen species
RYRs	-	Ryanodine receptors
scRNA-seq	-	Single-cell RNA sequencing
S1/2P	-	Site 1/2 proteases
SD	-	Standard deviation
SG	-	Secretory granules
SGLTs	-	Sodium-glucose transporters
SLC30A8	-	Solute carrier family 30 member 8
SORCS2	-	Sortilin-related VPS10 domain containing receptor 2
SORLA	-	Sorting protein-related receptor containing LDLR class A repeats
SRE	-	Sterol-regulatory element
SREB1	-	Sterol regulatory element-binding protein 1
SSTR5	-	Somatostatin receptor 5
t	-	t-test
T1D	-	Type 1 Diabetes
T2D	-	Type 2 Diabetes
TCF7L2	-	Transcription factor 7-like 2
TGN	-	*trans*-Golgi network
TNF-α	-	Tumor necrosis factor α

TNF-β	-	Tumor necrosis factor β
TMM	-	Trimmed mean of M values
TRAF2	-	TNF-receptor-associated factor 2
TRIB3	-	Tribbles homolog 3
TRK	-	Transports tropomyosin receptor
TXNIP	-	Thioredoxin interaction protein
TXNIP	-	Thioredoxin-interacting protein
U	-	U-test
UMAP	-	Uniform manifold approximation and projection
UPR	-	Unfolded protein response
VIP	-	Vasoactive intestinal peptide
VPS10P	-	Vacuolar protein sorting 10 protein domain receptors
WFS1	-	Wolfram syndrome 1
ZnT8	-	Zinc transporter 8

Abstract

Systemic glucose levels, an essential metabolic fuel in the mammalian organism, undergo intricate regulation to prevent hypo- or hyperglycemia. Insulin secretion deficiencies in Type 1 Diabetes (T1D) or altered tissue insulin sensitivity in Type 2 Diabetes (T2D) significantly impact glucose homeostasis. Genome-wide association studies linked the gene encoding the sortilin-related VPS10 domain-containing receptor 2 (*SORCS2*) to T2D and body mass index (BMI), another indicator of glucose imbalance. Yet, SORCS2's underlying mechanism remained unclear. Intriguingly, SORCS2 shares structural homology with T2D-associated SORCS1, implicated in regulating insulin vesicle production in pancreatic β cells.

Hypothesizing SORCS2's role in pancreatic glucose metabolism, I conducted comparative studies in wild-type mice (*Sorcs2*$^{+/+}$) and genetically deficient mice (*Sorcs2*$^{-/-}$). Investigations substantiated SORCS2's involvement in glucose metabolism by showing its' expression in pancreatic α, δ, and pancreatic polypeptide (PP) cells, crucial for insulin secretion regulation. Studies on insulin secretion dynamics, *in vivo* and *in vitro*, revealed reduced insulin secretion upon glucose stimulation in *Sorcs2*$^{-/-}$ mice islets. By contrast, hormone secretion from α, δ, and PP cells was unchanged, and morphological analyses found no SORCS2-related changes in β cell mass or areas of α, δ, and PP cell types. However, the β cell insulin vesicles maturation was altered upon SORCS2 deficiency.

Single-cell RNA sequencing (scRNA-seq) of *Sorcs2*$^{-/-}$ and *Sorcs2*$^{+/+}$ pancreatic islets revealed a loss of metabolically active and a gain of proliferative β cell clusters in *Sorcs2*$^{-/-}$ islets, with unaffected α, δ, and PP cells. Transcriptomics confirmed *Sorcs2's* predominant expression in α, δ, and PP cell types, and in progenitor β cells. Gene ontology (GO) analysis indicated dampened endoplasmic reticulum (ER) stress in α and β cells, while δ or PP cell types showed minimal impact from *Sorcs2* deficiency.

Differentially expressed genes (DEG) analysis in α cells revealed decreased *Spp1* expression, encoding osteopontin (OPN), a stress response factor capable of inducing glucose-stimulated insulin secretion through Ca^{2+}-dependent mechanisms. Reduced OPN expression and secretion in *Sorcs2*$^{-/-}$ islets suggested SORCS2's role in *Spp1*

expression control. Additionally, AKT pathway activation, regulating OPN expression in α cells, was diminished in *Sorcs2*$^{-/-}$ islets.

In conclusion, my findings underscore SORCS2's pivotal role in pancreatic α-cells, controlling OPN expression and secretion via modulation of the AKT pathway. This regulatory mechanism improves insulin secretion, possibly by fostering an adaptive ER stress response in β cells under glucose stress. Future studies should unveil SORCS2's molecular role in promoting AKT signaling during ER stress and identify SORCS2-dependent factors secreted from α cells, potentially enhancing ER stress responses and fine-tuning insulin secretion in β cells.

Zusammenfassung

Die systemischen Glukosespiegel im Säugerorganismus werden aufwendig reguliert, um Zustände einer Hypo- oder Hyperglykämie zu verhindern. Insbesondere Insulinsekretionsdefizite bei Typ 1 Diabetes oder reduzierte Insulinempfindlichkeit bei Typ 2 Diabetes (T2D) beeinträchtigen die Glukosehomöostase beträchtlich. Genetische Studien zeigten eine Assoziation des Gens für SORCS2 mit T2D und dem Body-Mass-Index. SORCS2 ist dem SORCS1 strukturell verwandt, einem an der Insulinvesikelproduktion in β-Zellen beteiligten Rezeptor. Die Rolle von SORCS2 im Glukosestoffwechsel war jedoch ungeklärt.

Um die Funktion von SORCS2 im Glukosestoffwechsel aufzuklären, führte ich Studien an Wildtypen (*Sorcs2*$^{+/+}$) und genetisch defizienten Mäusen (*Sorcs2*$^{-/-}$) durch. Meine Untersuchungen zeigten die Expression von SORCS2 in α-, δ- und PP-Zellen der Langerhans-Inseln bei Wildtypen sowie eine verminderte Insulinsekretion bei *Sorcs2*$^{-/-}$ Mäusen. Morphologische Untersuchungen deuteten auf einen Defekt in der Reifung von Insulinvesikeln der β-Zellen als Ursache dieser Sekretionsstörung hin.

In der Einzelzell-RNA-Sequenzierung von murinen Inselzellen zeigten sich transkriptionelle Veränderungen in einzelnen *Sorcs2*$^{-/-}$ β-Zellclustern, welche auf eine gestörte Insulinvesikelproduktion sowie einen Verlust metabolisch aktiver β-Zelltypen schließen ließen. Obwohl transkriptionelle Veränderungen in *Sorcs2*$^{-/-}$ α-Zellen weniger ausgeprägt waren, deuteten weiterführende bioinformatische Analysen auf eine verminderte Stressantwort in diesen Zellen hin. Diese verminderte Stressantwort zeigte sich insbesondere in einer reduzierten Expression von Osteopontin (OPN), einem von α-Zellen sezernierten Stressfaktor zur Stabilisierung der Glukose-stimulierten Insulinsekretion in β-Zellen. Eine Rolle von SORCS2 in der Expressionskontrolle von OPN wurde durch Befunde untermauert, welche zeigten, dass Signalwege zur Induktion der OPN Expression in *Sorcs2*$^{-/-}$ Inseln weniger aktiv waren als in Wildtypen.

Zusammenfassend deuten meine Ergebnisse auf eine wichtige Rolle von SORCS2 in der protektiven Stressantwort pankreatischer α-Zellen hin. Diese SORCS2-abhängige Stressantwort induziert die Expression und Ausschüttung von OPN und möglicher weiterer Stressfaktoren, welche eine adaptive Stressantwort in β-Zellen auslösen. Diese

adaptive Stressantwort fördert die pankreatische Insulinausschüttung unter Glukosestress. Zukünftige Studien sollten die zugrunde liegende molekulare Wirkungsweise von SORCS2 in der pankreatischen Stressantwort und der Entstehung von T2D aufklären.

1 Introduction

1.1 Structure and function of vacuolar protein sorting 10 protein domain receptors

The family of vacuolar protein sorting 10 protein (VPS10P) domain receptors comprises seven evolutionarily conserved receptors: mammalian sorting protein-related receptor containing LDLR class A repeats (SORLA), sortilin, and sortilin-related VPS10 domain-containing receptors 1-3 (SORCS1, SORCS2, SORCS3), as well as yeast VPS10P and hydra (head-activating binding) HAB protein [1] (Figure 1). All seven receptors share a 700 amino acid residue VPS10P domain at the extracellular N-terminus, forming a ten-bladed β-propeller and serving as the primary ligand binding site. Additional unifying motifs include a 10CC domain and a 164-residue cytoplasmic tail, crucial for receptor internalization and recycling [1,2]. Furthermore, the structure of receptors varies based on additional structural domains [1,2]. While all seven receptors function in sorting proteins between the cell surface and endocytic or secretory compartments, their intracellular localization and sorting paths differ [3].

The first VPS10P domain receptor was discovered in Saccharomyces cerevisiae, differing from other family members by having two extracellular VPS10P domains instead of one [1] (Figure 1). The yeast VPS10P domain receptor binds the soluble vacuolar hydrolase carboxypeptidase Y (CPY) in a late Golgi compartment to segregate it from the constitutive secretory pathway [4]. Subsequently, receptor-CPY complexes are packaged into clathrin-coated vesicles and transported to a pre-vacuolar endosomal compartment [4]. There, CPY is released, and VPS10P domain receptors are recycled back to the Golgi [4,5].

Similar to the yeast VPS10P receptor, the sortilin receptor carries only an extracellular VPS10P domain, a 10CC domain, and an intracellular cytoplasmic tail, lacking additional structural elements [1] (Figure 1).

On the contrary, the HAB hydra protein possesses additional structural domains, including low-density lipoprotein (LDL)-receptor class A and B repeats, epidermal growth factor (EGF)-type repeats, and a fibronectin type III domain [6].

SORLA is composed of complement-type and EGF-type repeats, along with six fibronectin type III domains crucial for protein-protein interactions [7]. Additionally, it features a six-bladed β-propeller facilitating pH-dependent ligand release in endosomes [1,8] (Figure 1).

The subgroup of sortilin-related receptors, central nervous system (CNS) expressed (SORCS1, SORCS2, SORCS3), existing in homo- and dimeric configurations, are characterized by one VPS10P domain, two 10CC domains (10CC-a and 10CC-b), and a leucine-rich domain [1,9]. This leucine-rich domain comprises two polycystic kidney disease domains (PKD1 and PKD2), in addition to a cytoplasmic tail [1,9] (Figure 1).

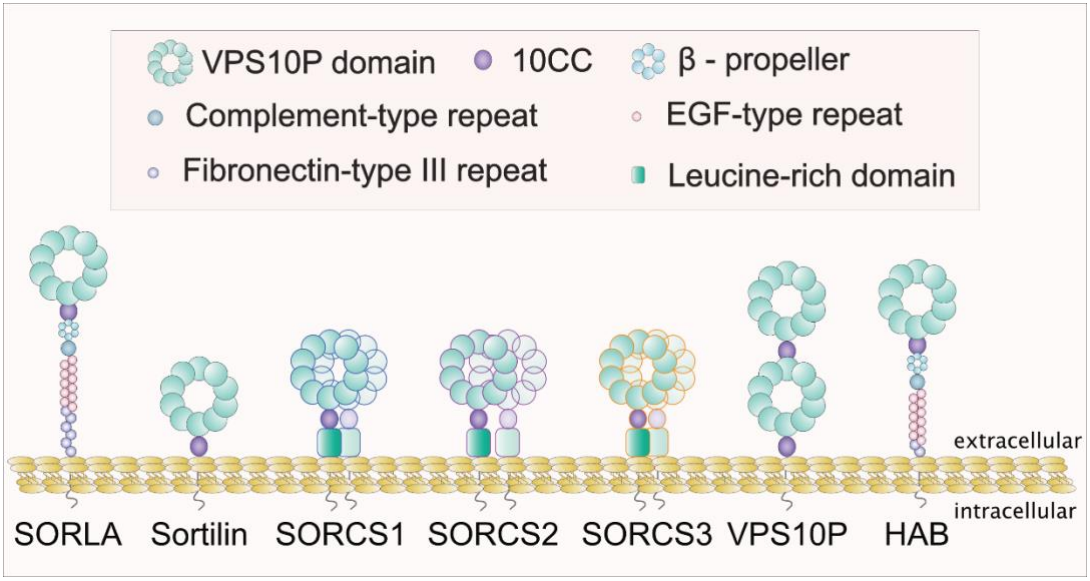

Figure 1: Structure of VP10P domain receptors

The figure depicts the structure of currently known VPS10P domain receptors. The structure and function of each varies depending on the additional domains (complement type repeats, fibronectin-type III repeats, leucin-rich domains, EGF-type repeats).
VPS10P, vacuolar protein sorting 10 protein; EGF, epidermal growth factor; SORLA, sorting protein-related receptor containing LDLR class A repeats; SORCS, sortilin-related receptor CNS expressed; HAB, head-activator binding protein.

Newly synthesized VPS10P receptors are activated in the *trans*-Golgi network (TGN) through the proteolytic removal of an amino-acid terminal propeptide by the pro-protein convertase furin [2,10,11] (Figure 2, step 0). Subsequently, VPS10P domain receptors can operate in ligand binding in various cell compartments, including secretory vesicles,

early and recycling endosomes, multivesicular bodies, lysosomes, exosomes, and the cell surface [3,12,13] (Figure 2).

Genome-wide association studies (GWAS) have linked VPS10P domain receptors to several brain diseases. *SORL1*, *SORCS1*, and *SORT1* were associated with Alzheimer's disease and other age-related dementias [14–19]. *SORT1* was also linked to brain aging [20], schizophrenia, bipolar disorder, and major depressive disorder [21]. Finally, *SORCS3* was associated with multiple psychiatric diseases, including insomnia, bipolar disorder, attention deficit/hyperactivity disorder (ADHD), schizophrenia, and major depressive disorder [22–24].

The importance of VPS10P domain receptors for functional integrity of neurons was confirmed by a multitude of studies.

Sortilin plays a crucial role in controlling neuron viability and function by sorting neurotrophins, a family of proteins that regulate neuronal survival, development, and function [25]. Specifically, sortilin associates with huntingtin-associated protein 1 (HAP-1) to sort pro- or mature BDNF, a key regulator of multiple neuronal processes, including synaptic transmission, cell survival, and growth of dendrites, from the TGN to the secretory vesicles for activity-dependent release [3,25–29] (Figure 2, steps 1, 1.1). In the absence of HAP-1, sortilin/BDNF or sortilin/pro-BDNF complexes are directed to late endosomes/lysosomes for degradation [28,29] (Figure 2, step 1, 1.1). Additionally, sortilin transports tropomyosin receptor kinase (TRK) receptors, responsible for cellular signal reception from neurotrophins such as BDNF or nerve growth factor (NGF), from the TGN to constitutive vesicles and the cell surface [27,30,31] (Figure 2, step 2, 2.1).

SORLA performs multiple sorting functions at the TGN, particularly relevant in controlling proteolytic processing of the amyloid precursor protein (APP) into amyloid beta peptides, the cause of Alzheimer's disease. SORLA traps APP in the TGN, reducing APP processing in post-Golgi compartments and at the cell surface (Figure 2, steps 6-6.1). Additionally, SORLA facilitates the anterograde recycling of endocytosed APP from early endosomes back to the TGN (Figure 2, steps 6.3-6.4) [1,32,33]. These sorting paths involve interactions between the receptor tail and sorting adaptors such as phosphofurin acidic cluster sorting protein 1 (PACS1), activator protein-1 (AP-1), or retromer (Figure 2,

steps 6.3-6.4) [1,32,33]. The anterograde shuttling of SORLA from the TGN to endosomes requires the binding of sorting adaptors Golgi-localizing, γ-adaptin ear homology domain ARF-interacting proteins (GGA) and AP-1 (Figure 2, step 6.2) [1,32,33]. In pancreatic beta cells, SORLA acts as an endocytic receptor for the pro-form of islet amyloid polypeptide (proIAPP), preventing amyloid fibril formation in islets [34] (Figure 2, steps 7.1-7.2). Once internalized, proIAPP is transported to lysosomes from early endosomes for catabolism, while SORLA returns to the cell surface via recycling endosomes [34] (Figure 2, steps 8.2-8.4).

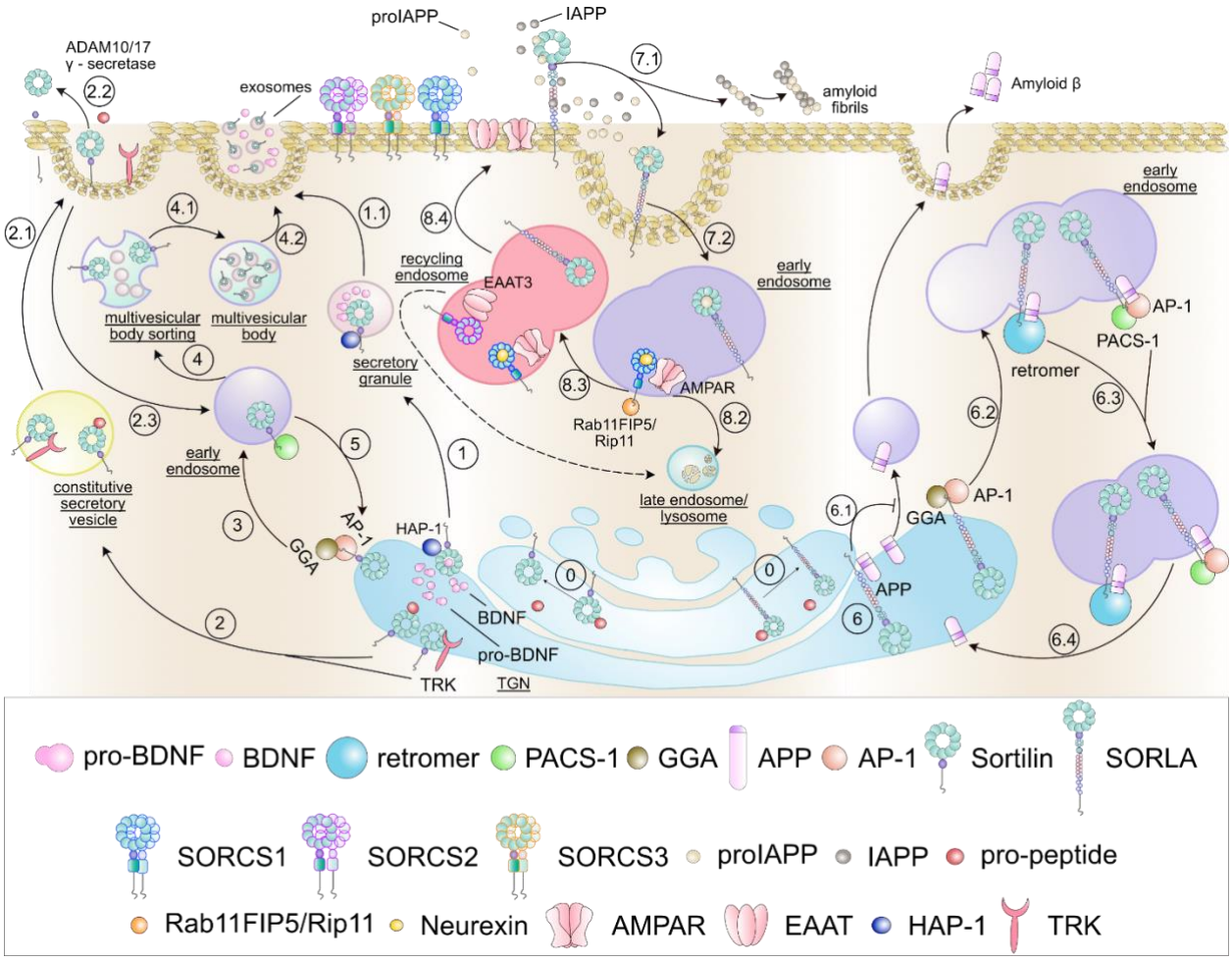

Figure 2: Sorting paths for VPS10P domain receptors

Step 0: Activation of VPS10P domain receptors starts at TGN, where the pro-peptide is cleaved from the receptor [8,9]. **Step 1-5:** Sortilin is present in the TGN wherefrom it can translocate to secretory granules (1) [11], to constitutive secretory vesicles [9,12,13] (2) and to early endosomes (via the interaction with GGA) (3) [9,14,15]. From secretory granules sortilin transports BDNF and pro-BDNF to the cell surface for secretion (1.1) [11]. From TGN and constitutive secretory vesicles sortilin transports TRK or pro-peptide to the cell surface (2-2.1) [12] . From the cell surface sortilin may either be endocytosed into early endosomes and transported back to the TGN (via PACS1) (2.3, 5) [12] or its' luminal domain may be cleaved from the

transmembrane and cytosolic domains with ADAM10/17 and γ-secretase (2.2) [9,12,13]. From early endosomes sortilin may also be transported to multivesicular bodies, wherefrom it is exported out of the cell in exosomes (4-4.2) [12]. **Step 6-7.2:** SORLA present in the TGN traps APP (6-6.1). SORLA can be transported to early endosomes (via the interaction with GGA and AP-1), wherefrom it anterogradely recycles endocytosed APP back to the TGN (via interaction with PACS1 and AP-1) (6.2-6.4) [1,19,20]. SORLA also functions on the cell surface (7.1), where it captures and transports proIAPP to an early endosome for further lysosomal degradation [1,16,17]. SORLA from early endosomes is transported back to the cell surface with recycling endosomes (8.3-8.4) [1,16,17]. **Steps 8.2-8.4:** SORCS1-3 are present at the cell surface. SORCS1 can transport AMPAR from early endosomes to recycling endosomes with the help of Rab11FIP5/Rab11 interacting protein and further to the cell surface to prevent AMPAR lysosomal destruction (8.2-8.4) [35,36]. SORCS2 can transport EAAT to the cell surface from recycling endosomes (8.4) [22–24].
The significance of the various sorting paths for directing receptor cargo is also detailed in the main text.
AMPAR, α-amino-3-hydroxy-5-methyl-4-isoxazolepropionic acid receptor; AP-1, Activator-protein 1; APP, amyloid precursor protein; BDNF, brain-derived neurotrophic factor; EAAT, Excitatory amino acid transporter; GGA, Golgi-localizing, γ-adaptin ear homology domain ARF-interacting proteins; HAP-1, huntingtin-associated protein 1; PACS1, phosphofurin acidic cluster sorting protein 1; proIAPP, Pro islet amyloid polypeptide; Rab11FIP5, Rab11 GTPase effector Rab11 family-interacting protein 5; Rip11, Rab11-interacting protein; TRK, receptor tyrosine kinase; TGN, trans-Golgi network.

As with sortilin, ligand sorting by SORCS1 also plays a crucial role in controlling neuronal plasticity, the ability of neurons to structurally and functionally reorganize their connectivity in response to stimuli [37]. For SORCS1, this function lies in its ability to sort α-amino-3-hydroxy-5-methyl-4-isoxazolepropionic receptor (AMPAR), glutamatergic receptors involved in synaptic plasticity during learning and memory acquisition [35,36] (Figure 2, steps 8.3-8.4).

Through interaction with the Rab11 GTPase effector Rab11 family-interacting protein 5 (Rab11FIP5)/Rab11 interacting protein, SORCS1 also sorts neuroligin and neurexin, adhesion molecules necessary for synapse assembly [38,39] (Figure 2, steps 8.3-8.4). Consistent with the association of SORCS1 with Alzheimer's disease [40], the receptor has also been documented to be involved in the trafficking of γ-secretase, the protease responsible for the final cleavage step in amyloid-β formation from APP [40,41].

1.2 Role of SORCS2 in protein function

1.2.1 Neuronal SORCS2 functions

Similar to other VPS10P domain receptors, SORCS2 is associated with bipolar disorder, schizophrenia, and ADHD [42,43]. Here, I will describe some of the underlying cellular mechanisms in which SORCS2 is implicated.

In the brain, SORCS2 is present in ~123 kDa and ~105 kDa forms, where the ~123 kDa form is a full-form protein, while the ~105 kDa form arises from the cleavage of the 18 kDa ectodomain [44,45]. Among brain regions, SORCS2 localizes to neurons in the hippocampal Cornu Ammonis 2 (CA2) region, specifically to the postsynaptic density and dendritic vesicles [44].

Similarly, to SORCS1, SORCS2 is also involved in the regulation of neuronal plasticity. Although the sorting mechanism is not yet clear, SORCS2 regulates the trafficking of glutamate-gated cation channels with high calcium permeability N-methyl-D-aspartate (NMDA) receptors to the dendritic and synaptic surface of neurons [44]. NMDA receptors are crucial for synaptic plasticity [48]. Consequently, their aberrant sorting in SORCS2-deficient mice leads to a decrease in dendritic spine density in the CA2 region and results in altered social memory [44].

Similarly, in striatum medium spiny neurons, SORCS2 traffics N-methyl-D-aspartate receptor 2A (NR2A), a subunit of NMDA receptors, to the dendritic membrane [46]. Sorting requires the interaction of SORCS2 with VPS35, a core component of the adaptor complex retromer [46]. SORCS2 deficiency in striatum medium spiny neurons leads to motor coordination deficit [46]. Additionally, SORCS2 selectively binds to mutant huntingtin (HTT), the etiological agent in Huntington's disease [46]. Binding leads to mislocalization of SORCS2, causing a decrease in the abundance of NR2A and, consequently, motor deficits in patients with Huntington's disease [46].

Brain specimens from individuals with temporal lobe epilepsy show an increased expression of SORCS2 in the hippocampal CA2 region [47,48]. This phenotype was confirmed in an epilepsy model in mice [47]. The reason for induced SORCS2 expression in epilepsy was shown in subsequent studies that identified a role for the receptor in

protection against epilepsy-induced oxidative stress in neurons through the sorting of excitatory amino acid transporter 3 (EAAT3) [47]. EAAT3 is responsible for neuronal uptake of cysteine, required for the production of the reactive oxygen species scavenger glutathione [47]. SORCS2 sorts EAAT3 to the neuronal cell surface, increasing cysteine uptake, glutathione production, and neuronal oxidative stress protection (Figure 2, step 8.4) [47].

1.2.2 Astrocytic SORCS2 functions

Mice subjected to middle cerebral artery occlusion, a murine model of stroke, exhibit increased expression of SORCS2 in astrocytes around the ischemic core [49]. Similar upregulation of SORCS2 expression is observed in stroke patients [49]. The induced expression of the receptor is associated with its ability to enhance the secretion of endostatin from astrocytes, a mechanism that promotes the revascularization of ischemic brain regions [49].

1.3 Role of VPS10P domain receptors in metabolic disorders

In addition to their involvement in brain diseases, VPS10P domain receptors are genetically associated with various metabolic conditions. For instance, SORCS1 [50–52], SORLA [53], and SORCS2 [54] are linked to T2D, SORLA [55] and SORCS2 [56] to BMI, SORCS2 to hypertension [57] and non-alcoholic fatty liver disease [58], while SORLA to obesity [59–61]. In the following sections, I will delve into our current understanding of the roles of VPS10P domain receptors in metabolism.

1.3.1 Role of SORCS1 in insulin secretion and sensitivity

The absence of SORCS1 in obese mice, attributed to a *leptin*^{ob} mutation, leads to impaired glucose-stimulated insulin secretion from pancreatic islets. This defect may be linked to the delayed replenishment of the insulin vesicle pool in pancreatic beta cells lacking the receptor [62]. The precise mechanisms through which SORCS1 deficiency hinders effective insulin vesicle replenishment, transport, and/or release remain unknown [62].

1.3.2 Role of SORLA in insulin receptor signaling

In adipocytes, SORLA regulates the sorting of insulin receptors (IR) to the cell surface [63]. Increased SORLA expression results in a higher abundance of IRs on the cell surface, enhancing insulin signaling and reducing lipolysis. This, in turn, contributes to obesity in mice overexpressing SORLA [63]. Specifically, after insulin binding, IRs undergo internalization and translocate to early endosomes (Figure 3, step 1). In the absence of SORLA, IRs are subsequently transported to lysosomes for degradation (Figure 3, step 2) [63]. However, in the presence of SORLA in early endosomes, IRs are sorted and directed to recycling endosomes before being transported back to the cell surface (Figure 3, steps 3-4) [63]. The continuous recycling of IRs by SORLA increases their abundance on the cell surface, allowing for prolonged inhibition of lipolysis (Figure 3, step 5) [63].

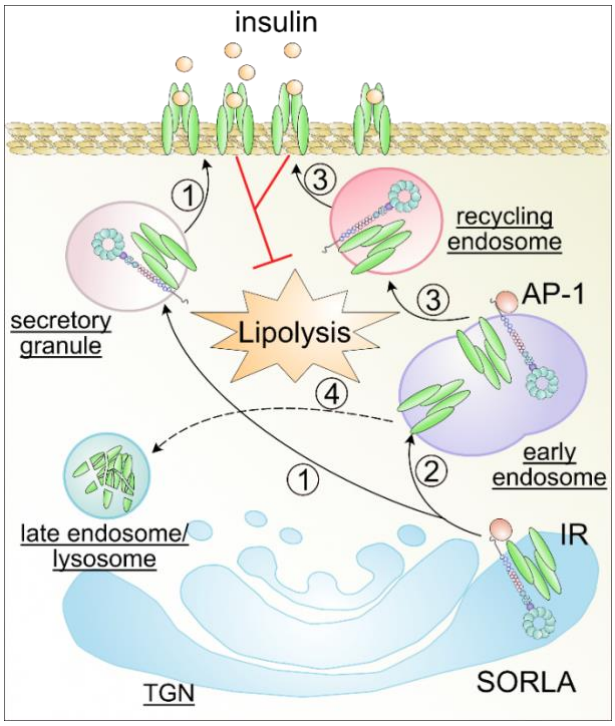

Figure 3: Sorting pathways of insulin receptor by SORLA in adipocytes

Step 1: Insulin binding leads to internalization and translocation of IR into early endosomes.

Step 2: Unsorted IR is transported to lysosomes/late endosomes for destruction.

Step 3: Sorting of IR by SORLA.

Step 4: Sorted IR together with SORLA is transported to recycling endosomes.

Step 5: From recycling endosomes IR is transported back to the cell surface.

Step 6: Increased number of IR on the cell surface due to SORLA sorting further inhibits lipolysis.

AP-1, activator-protein 1; IR, insulin receptor.

1.3.3 Role of sortilin in glucose metabolism

Studies on 3T3-L1 adipocytes have demonstrated the involvement of sortilin in the sorting of vesicles containing glucose transporter 4 (GLUT4), a glucose transporter facilitating insulin-stimulated glucose uptake in myocytes and adipocytes [64]. In non-stimulated cells, GLUT4 resides in specialized GLUT4 storage vesicles (GSVs). Insulin stimulation promotes GLUT4 translocation to the cell membrane, increasing glucose uptake [65,66].

Sortilin-deficient 3T3-L1 cells exhibit reduced levels of GLUT4, a decrease in the number of GSVs, and impaired glucose uptake [64]. It is hypothesized that sortilin, in complex with GGA-budding machinery, may interact with GLUT4 via its N-terminal domain to facilitate GLUT4 sorting into storage vesicles and prevent GLUT4 lysosomal degradation (Figure 4, step 1) [64]. Other studies suggest that sortilin is capable of retrograde sorting of GLUT4 to the trans-Golgi network through interaction with a retromer [67]. In this model, sortilin's luminal domain binds the first luminal loop of GLUT4, while its cytoplasmic tail binds to the retromer, stabilizing sortilin-GLUT4 complexes for sorting to the TGN (Figure 4, steps 4-5) [67].

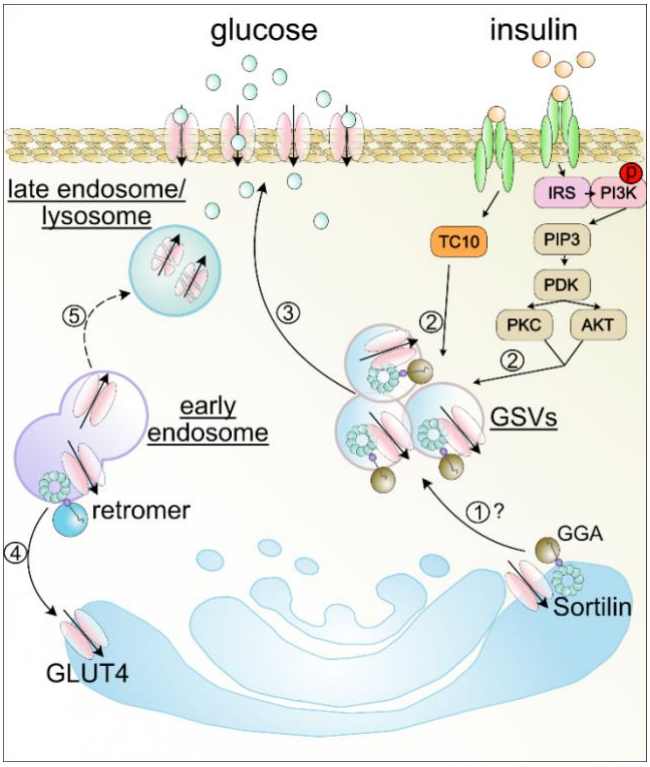

Figure 4: Sorting of GLUT4 by sortilin

Step 1: Formation of specialized GLUT4 vesicles via complex formation of the transporter with sortilin and GGA.

Step 2-3: Insulin signals through PI3K-PDK pathway or through indirect activation of TC10. Both PDK and TC10 stimulate translocation of GLUT4 vesicles to the plasma membrane.
Step 4: Sortilin complexed with retromer retrogradely transports GLUT4 to the TGN.
Step 5: GLUT4 not bound by sortilin is moved from early endosomes to lysosomes for degradation.
APS, Adaptor protein containing PH and SH2 domains; AKT, Protein kinase B; GGA, Golgi-localizing, γ-adaptin ear homology domain ARF-interacting proteins; GSVs, GLUT4 storage vesicles; IRS, Insulin receptor substrate; PDK, 3′phosphoinoside-dependent kinase 1; PI3K, Phosphoinositide 3-kinase; PIP3, Phosphatidylinositol (3,4,5)-trisphosphate.

Despite clear experimental evidence of sortilin's involvement in GLUT4 sorting and glucose uptake in adipocytes, mouse models of sortilin deficiency (*Sort1*$^{-/-}$) do not exhibit obvious insulin resistance or glucose intolerance phenotypes [12,68]. In fact, one study showed increased insulin sensitivity in mice lacking sortilin [12,69]. Additionally, GLUT4 protein levels in white adipose tissue or muscles were not affected in *Sort1*$^{-/-}$ mice [12,68].

1.4 Systemic regulation of the glucose metabolism

In consideration of the previously demonstrated involvement of SORLA, SORCS1, and sortilin in glucose metabolism, and the genetic association of SORCS2 with diabetes and changes in BMI [50–55,58–63,65,67], I will further discuss the mechanisms involved in the regulation of glucose metabolism.

Glucose stands as a primary metabolic fuel in mammalian organisms. Hence, precise regulation of glucose metabolism is crucial for survival, as both the lack and abundance of glucose can lead to severe complications or death

Hypoglycemia, defined as plasma glucose levels < 2.8-3.1 mmol/L, triggers adrenergic symptoms (sweating, hunger, tingling, trembling, palpitations, and anxiety) or neuroglycopenic symptoms (visual disturbance, poor concentration, drowsiness, lethargy, personality change, seizures, coma, confusion) [70]. Prolonged and severe hypoglycemia may also lead to permanent neurological damage and mortality [71–73].

Hyperglycemia, defined as plasma glucose levels > 125 mg/dL during fasting and > 200 mg/dL two hours after a meal [74], primarily damages neuronal cells, capillary endothelium, and renal mesangial cells due to their inability to control intracellular glucose concentrations [75]. Complications associated with hyperglycemia include retinopathy,

nephropathy, neuropathy, coronary artery diseases, cerebrovascular diseases, and peripheral vascular diseases [75].

Several tissues control glucose metabolism. The liver is a central hub for glucose production and storage [76,77]. The pancreas serves as a principal control center for glucose metabolism in the liver and other tissues through insulin and glucagon secretion [76,78]. The small intestine, brain, adipose tissue, adrenal glands, parasympathetic and sympathetic systems regulate pancreatic hormones secretion or directly influence glucose metabolism in tissues [76,78].

Glucose in the bloodstream originates from absorption in the small intestine from the diet or from breakdown processes such as glycogenolysis or new synthesis through gluconeogenesis in the liver [76]. Glucose metabolism is regulated by hormones released from the pancreas, small intestine, adrenal glands, and brain, as well as by the sympathetic and parasympathetic systems [76].

The anabolism and catabolism of glucose are tightly regulated by hormones, including insulin, glucagon, and amylin secreted from the pancreas [76]. Insulin stimulates glucose uptake and glycogen synthesis while inhibiting lipolysis, gluconeogenesis, and glycogenolysis [76]. Conversely, glucagon stimulates liver glucose production [76]. Amylin, by acting on calcitonin-like receptors and thereby stimulating vagal nerve efferent signals, suppresses glucagon synthesis [76]. Additionally, amylin slows down gastric emptying and reduces food intake, thereby limiting glucose availability [76].

Intestinal hormones, such as glucagon-like peptide 1 (GLP-1) and glucose-dependent insulinotropic peptide (GIP), regulate glucose metabolism by potentiating glucose-stimulated insulin release [76].

The adrenal glands play a role in regulating glucose metabolism via the secretion of glucocorticoids and epinephrine [76]. Glucocorticoids increase liver gluconeogenesis and glycogen synthesis [79]. However, they inhibit glucose uptake synthesis in skeletal muscles and white adipose tissue, as well as glycogen synthesis in muscles [79]. Epinephrine stimulates liver gluconeogenesis and glycogenolysis while inhibiting glucose utilization by insulin-dependent tissues [80].

Growth hormone, secreted from the pituitary gland, stimulates gluconeogenesis and lipolysis, thereby increasing circulating glucose and free fatty acids levels [81].

The sympathetic nervous system stimulates liver gluconeogenesis and glycogenolysis, thereby increasing bloodstream glucose concentration, while the parasympathetic system inhibits liver gluconeogenic pathways to lower circulating glucose levels [82].

1.4.1 Tissue glucose uptake

Two families of glucose transporters are involved in glucose handling in mammalian tissues, namely glucose transporters (GLUTs) and sodium-glucose transporters (SGLTs) [83]. GLUTs are present in all cell types of the organism. They transport glucose via facilitative diffusion along a concentration gradient in and out of the cell [83]. SGLTs are present on intestinal and kidney cortex cells and transport glucose inside cells together with two Na^+ molecules [83].

1.4.1.1 GLUTs

GLUTs involved in glucose transport include GLUT1, -2, -3, -4 as well as GLUT7 and GLUT11. GLUT7 and 11 transport both glucose and mannose [83].

Although GLUT1 is present in all tissues, it's function is most important in erythrocytes, neurons, and cell types at the blood-brain barrier, eye, placenta, and lactating mammary glands [84]. Low expression of GLUT1 is also seen in hepatocytes, endothelial, and Kupffer cells in the liver [85]. Protein kinase C (PKC) modulates GLUT1 transport activity via direct phosphorylation [86], while thioredoxin interaction protein (TXNIP) suppresses cellular glucose uptake by binding to GLUT1 and internalizing the transporter via clathrin-coated pits and by decreasing *GLUT1* mRNA [87].

GLUT2 is present on pancreatic β-cells, hepatocytes, enterocytes, and cells in the kidney and the CNS [88,89]. GLUT2 plays a crucial role in glucose sensing in enterocytes and pancreatic β-cells due to its low affinity for glucose [88]. In hepatocytes, GLUT2 is important for rapid glucose uptake and release upon hyper- or hypoglycemia, respectively [84,88]. In the CNS, GLUT2 is present in the brain stem nuclei where glucose sensing is crucial for the regulation of sympathetic and parasympathetic signaling, feeding behavior,

thermoregulation and energy expenditure [88,89]. In kidneys, GLUT2 regulates glucose reabsorption on the basolateral membrane of the epithelial cells [84].

GLUT3 has a predominantly neuronal expression [84]. It has the highest turnover among all GLUTs to ensure rapid control of glucose uptake in neurons. GLUT3 is also present in white blood cells [84]. However under normal condition, it stays in resting storage GLUT vesicles and translocates to the cell surface only upon proliferative stimuli [84].

GLUT4 is mainly expressed in skeletal muscles and adipocytes and translocates from storage vesicles to the cell surface in response to insulin stimulation. In detail, insulin is sensed by IRs on the cell surface which, on the one hand, activates IR substrate (IRS), phosphoinositide 3-kinase, and 3′phosphoinoside-dependent kinase 1 (PDK1), On the other hand, it indirectly activates TC10 and PDK1 [90]. Both stimulate GLUT4 translocation to the plasma membrane to facilitate glucose uptake [90].

1.4.1.2 SGLTs

Among the six SGLTs identified in the human organism, only the functions of SGLT1 and SGLT2 are described [83]. As mentioned above, SGLT1 is present in enterocytes where it facilitates glucose and galactose absorption from the intestine [83]. SGLT2 is present in the renal cortex and primarily facilitates glucose reabsorption in the kidney [83].

1.4.2 Intestinal control of glucose metabolism

Small intestine consists of different types of cells, such as enterocytes, goblet cells, Paneth cells, M-cells, enterochromaffin and enteroendocrine cells (L-, K-, I-, N-, and S-cells) [91]. Enterocytes are the major part of intestinal epithelium and they play role in nutrient absorption [91]. Goblet cells secrete mucus, which protects the small epithelium from digestive enzymes [91]. Paneth cells secrete antimicrobial peptides [91]. M-cells initiate mucosal immune response [92]. Enterochromaffin cells are mechanosensory cells, that secrete serotonin in response to epithelial mechanical forces [93]. I-cells secrete cholecystokinin, which promotes gull bladder contraction [94]. N-cells secrete neurotensin, which has numerous peripheral and central level functions, including the promotion of intestinal blood flow, nutrient absorption, and stimulation of pancreas exocrine function [95]. S-cells secrete secretin, which stimulates bile, bicarbonate, and

gastric pepsin secretion [96]. L-cells secrete GLP-1 and GLP-2, and Peptide YY (PYY) [97]. GLP-1 regulates glucose homeostasis by increasing glucose-stimulated insulin secretion; additionally, it reduces gastrointestinal motility and secretion of gastric enzymes and decreases food intake [97]. GLP-2 promotes gastric motility, gastric acid secretion and nutrient absorption [98]. PYY reduces food intake and weight [99]. K-cells secrete GIP, which regulates glucose metabolism by increasing glucose-stimulated insulin secretion and modulates fat absorption by reducing intestinal motility [97].

After food ingestion, glucose is absorbed in the small intestine into enterocytes and intestinal L-cells through SGLT-1 transporters located on the apical cell membrane (Figure 5) [100,101]. Enterocytes release glucose into the portal vein via facilitated diffusion and via GLUT2 transporters on their basolateral membranes (Figure 5) [100,101]. In response to glucose uptake, L-cells secrete GLP-1, GLP-2, and PYY, while K-cells secrete GIP [100–102] (Figure 5).

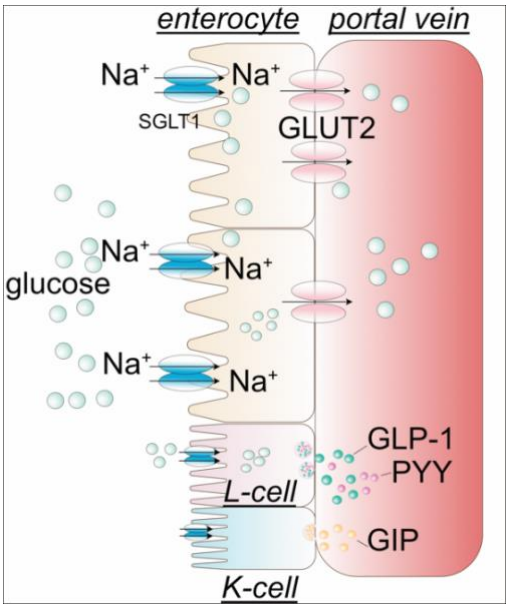

Figure 5: Regulation of glucose uptake by cells of the small intestine

Enterocytes as well as K- and L-cells absorb glucose through SGLT1 transporters on their apical cell membrane. Glucose is released into the portal vein via facilitated passive diffusion through GLUT2 transporters on the basolateral cell membrane. In response to glucose uptake, L-cell secrete GLP-1 and PYY, which function in regulation of glucose metabolism by potentiating insulin secretion. K-cell secrete GIP, which also stimulates insulin secretion.

GLP-1, glucagon-like peptide 1; GIP, glucose-dependent insulinotropic peptide; GLUT2, glucose transporter 2; PYY, peptide YY; SGLT1, sodium-dependent glucose transporter 1.

1.4.3 Pancreatic control of glucose metabolism

Increased glucose levels in the circulation are sensed by pancreatic β cells. Glucose is taken up by islet β cells through high-capacity and low affinity GLUT2 transporters [103,104]. In β cells glucose is phosphorylated to glucose-6-phosphate (G6P) by glucokinase, and subjected to glycolysis producing pyruvate, NADH, and ATP [103,104]. Glucokinase serves as a glucose sensor in β cells, as it has a lower glucose affinity compared to other hexokinases and it function is not inhibited by glucose metabolites [103,104]. Secreted insulin binds to IR on all mammalian cells and functions to decrease circulating glucose levels [76,105]. Insulin stimulates glucose uptake, which removes glucose from the circulation [76,105]. It also promotes glucose storage in a form of glycogen in liver and muscles by stimulating glycogenesis [76,105]. Similarly, insulin promotes triglycerides storage in adipose tissue, which prevents triglycerides catabolism with further glucose formation [76,105]. Moreover, insulin inhibits liver lipolysis and gluconeogenesis, to prevent new glucose formation [76,105]. And finally, insulin is able to inhibit glucagon secretion from α cells, to prevent activation of gluconeogenesis and lipolysis in the liver [76,105].

Prolonged low levels of circulating glucose lead to activation of glucagon secretion from pancreatic α cells [106,107]. The exact mechanism of activation of glucagon secretion is not entirely clear. However, the current model suggests that a lack of inhibitory action of GABA, Zn^{2+}, GLP-1, somatostatin, and insulin on α cells leads to glucagon secretion [106,107]. Additionally, glucagon secretion from α cells may be stimulated by adrenaline [108].

Furthermore, some studies report the importance of K^{+}_{ATP} channels for glucagon secretion [107]. In this model, α cells take up glucose through GLUT1 transporters, and similarly, to β cells, subject it to glycolysis to produce ATP. However, contrary to β cells, in α cells a decrease in ATP concentrations upon hypoglycemia closes K^{+}_{ATP} channels, leading to reduced K^{+} efflux, depolarization of α cells' plasma membrane, opening of voltage-gated Ca^{2+} channels, increase in Ca^{2+} influx, and glucagon secretion [107].
Ca^{2+} channels playing role in glucagon release in mice include L- and P/Q-type Ca^{2+} channels [109,110]. Similarly to mice, human α-cells also express L- and P/Q-type Ca^{2+}

channels but also a low-threshold T-type Ca^{2+} channels [109,110]. Additionally, voltage-gated Na^{+} channels have an important role in glucagon vesicles exocytosis [109,110].

Upon release, glucagon stimulates liver gluconeogenesis and glycogenolysis, and adipocytes lipolysis to increase circulating free fatty acids levels, which negatively regulate glucose production by influencing glucose-controlling hormone secretion in pancreas and gastrointestinal tract [76,111,112].

1.4.4 Liver control of glucose metabolism

The liver is the primary organ responsible for regulating glucose availability in the organism [113]. After intestinal absorption, dietary glucose travels via the portal vein to the liver, where hepatocytes take it up through GLUT2 transporters [113]. Internally, glucose undergoes conversion to G6P by glucokinase, which cannot be secreted back into the bloodstream [113]. Therefore, it is either metabolized to pyruvate via glycolysis, or NADPH via the pentose phosphate pathway, and can also serve as a precursor for glycogen synthesis [113].

1.4.4.1 Liver glycogen synthesis and glycogenolysis

In the fed state of the organism, insulin stimulates glycogen synthesis from G6P to promote the storage of glucose. The action of IRs in hepatocytes leads to a conformational change and activation of the tyrosine kinase activity of IRs [114]. Activated IRs recruit and phosphorylate IRS proteins on multiple tyrosine residues, allowing the binding of intracellular molecules with Src-homology 2 domains, such as phosphoinositide 3-kinase (PI3K) [114]. The binding of IRS and PI3K activates the PI3K catalytic subunit, which phosphorylates phosphatidylinositol 4,5-bisphosphate, producing phosphatidylinositol (3,4,5)-triphosphate and recruiting AKT [113–116] (Figure 6, step 1). AKT, in turn, phosphorylates glycogen synthase 3 (GSK-3), thereby inhibiting its inhibitory action on glycogen synthase (GS) and stimulating glycogen production and storage (Figure 6, step 1) [114].

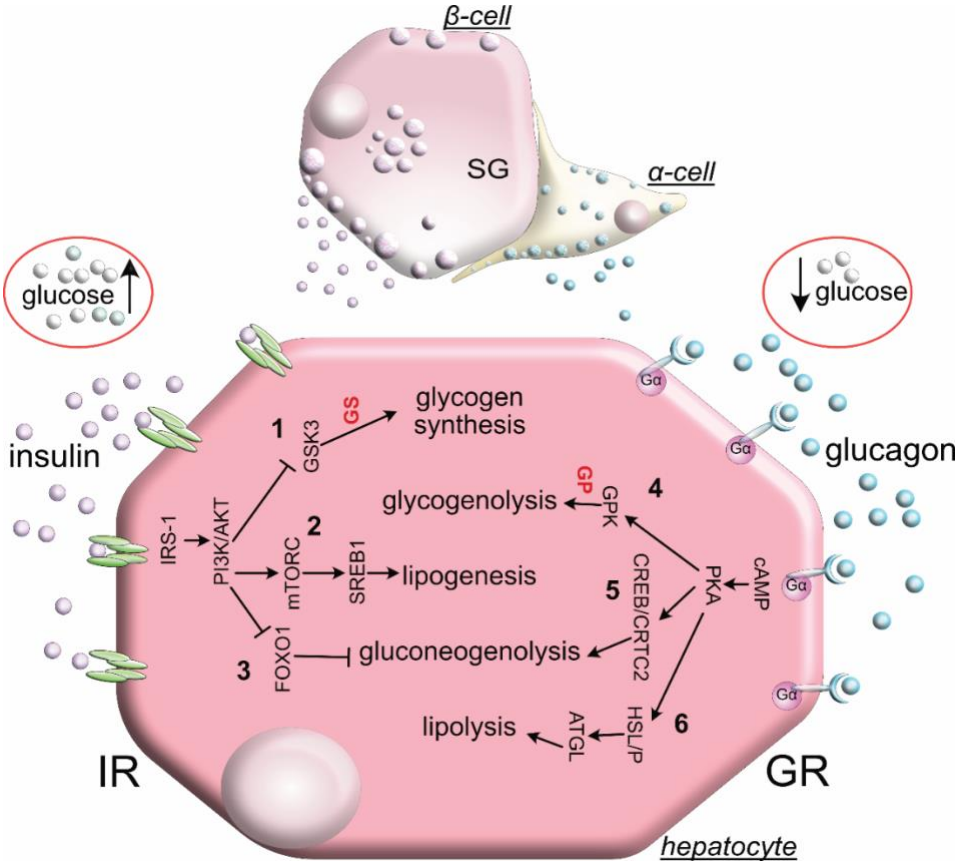

Figure 6: Liver metabolism is regulated by glucagon and insulin

Insulin and glucagon have opposite functions in regard of glucose metabolism in hepatocytes, where insulin stimulates storage of glucose, while glucagon triggers intrinsic glucose synthesis and glycogen breakdown to increase circulating glucose levels. This figure displays mechanisms by which insulin and glucagon affect glucose metabolism in hepatocytes.

Steps 1-3: Insulin secreted from pancreatic islet β cells activates the PI3K/AKT pathway by interacting with IR and phosphorylating insulin receptor substrate. Activation of the PI3K/AKT pathway leads to the inhibition of gluconeogenesis through the suppression of FOXO1 (3), stimulation of glycogen synthesis by suppressing GSK3 and releasing GS (1), and activation of lipogenesis through subsequent activation of mTORC and SREB1 (2).

Steps 4-6: Glucagon, secreted from pancreatic islet α cells, stimulates Gα-protein-coupled receptors, triggering cAMP and PKA. Activation of PKA stimulates gluconeogenesis by activating CREB/CRTC2 (5), activates lipolysis through the activation of ATGL (6), and induces glycogenolysis through the activation of GP (1).

ATGL, Adipocyte-Triglyceride-Lipase; AKT, Protein kinase B; CREB, CAMP response element-binding protein; cAMP, Cyclic adenosine 3',5'-monophosphate; CRTC2, CREB Regulated Transcription Coactivator 2; FOXO1, Forkhead box protein O1; GP, Glycogen phosphorylase; GPK, Glycogen phosphorylase kinase; GS, Glycogen synthase; GSK-3, Glycogen synthase kinase 3; HSL, Hormone-sensitive lipase; IRS-1, Insulin receptor substrate 1; mTORC1, Mammalian target of rapamycin complex 1; PI3K, Phosphoinositide 3-kinase; PKA, Protein kinase A; SREB1, Sterol regulatory element-binding protein 1.

During fasting, glycogen degradation is induced to release glucose into the circulation through GLUT2 or GLUT1 transporters [113,115,116]. This process is triggered by glucagon secreted from pancreatic α cells and by epinephrine and norepinephrine secreted from the adrenal medulla [117]. Glucagon binding to glucagon receptors induces a conformational change in the glucagon receptor, allowing interaction with the G_s protein [118]. The α subunit of the G_s protein, upon releasing guanosine triphosphate (GTP) and binding guanosine diphosphate (GDP), dissociates from the Gβ-γ protein subunits and interacts with adenylate cyclase [118]. This interaction leads to production of cyclic adenosine monophosphate (cAMP) from ATP [118]. cAMP changes the conformation of protein kinase A (PKA), leading to PKA activation [118]. PKA phosphorylates and activates glycogen phosphorylase kinase, which, in turn, phosphorylates glycogen phosphorylase [119]. Activated glycogen phosphorylase then phosphorylates glycogen, initiating glycogen breakdown (Figure 6, step 4). [117,119].

1.4.4.2 Liver lipogenesis and lipolysis

In a fed state of the organism, hepatocytes also produce fatty acids and store them in intracellular lipid droplets or export them to fat and other tissues [113,115,116]. During fasting, these fatty acids are oxidized by mitochondria as a metabolic fuel for energy production [113,115,116].

Insulin is able to stimulate lipogenesis in hepatocytes through PI3K/AKT and downstream target mTORC1, which activates sterol regulatory element-binding proteins (SREBP) (Figure 6, step 2) [120]. In absence of insulin stimulation, SREBP precursors are located in ER membranes bound with SREBP cleavage activating protein (SCAP) [121]. SCAP additionally interacts with insulin induced gene 2a (INSIG2A) [121]. Interaction of SREBP with both SCAP and INSIG2A keeps SREBP in the ER [121]. Upon insulin stimulation, AKT suppresses expression of *Insig2a*, allowing transport of SREBP/SCAP complex in coat protein II vesicles to the Golgi apparatus [120]. In the Golgi apparatus, SREBP is processed with Site-1 protease and Site-2 proteases [122]. Processing of SREBP with proteases allows the release of transcriptionally active SREBP fragment into the cytosol [123]. From the cytosol the transcriptionally active SREBP migrates to the nucleus, where it binds to sterol-regulatory element (SRE) sequences of genes that encode proteins involved in lipid uptake and synthesis [123]. Two types of SREBP are known: SREBP-1

(SREBP-1a and SREBP-1c) and SREBP-2 [123]. SREBP-1 proteins activate transcription of genes involved in synthesis and uptake of fatty acids and triglycerides, while SREBP-2 protein activates transcription of genes that control cholesterol synthesis and uptake [123]. AKT downstream target mTORC1 ensures SREB-1 nuclear accumulation via phosphorylation of Lipin-1, a phosphatidic acid phosphatase [121]. mTORC1 phosphorylation of Lipin-1 leads to Lipin-1 nuclear exclusion and cytoplasmic accumulation [121]. The absence of Lipin-1 in the nucleus allows SREBPs nuclear accumulation, by the mechanism yet to be determined [121].

Glucagon initiates lipolysis by increasing intracellular cAMP concentrations, activating PKA, hormone sensitive lipase (HSL), and perilins (P), which dissociates comparative gene identification-58 (CGI-58) from P and activates adipose triglyceride lipase (ATGL), thereby activating lipolysis (Figure 6, step 6) [124].

1.4.4.3 Liver gluconeogenesis

During prolonged fasting, liver glycogen stores are depleted, and gluconeogenesis is induced to generate glucose from lactate, pyruvate, glycerol, and amino acids [113,115,116]. Precursors for gluconeogenesis are either produced in hepatocytes or imported from the circulation [113,115,116]. Lactate is converted into pyruvate by lactate dehydrogenase [113,115,116]. Pyruvate is then translocated to the mitochondria, where pyruvate carboxylase turns it into oxaloacetate, which is then converted by malate dehydrogenase to malate [113,115,116]. Malate is then exported to the cytoplasm and converted back to oxaloacetate by malate dehydrogenase [113,115,116]. A critical step in gluconeogenesis is oxaloacetate's conversion to phosphoenolpyruvate by phosphoenolpyruvate carboxylase [113,115,116].

Gluconeogenesis is primarily stimulated by glucagon [117]. Secreted glucagon activates the cAMP-PKA pathway, which phosphorylates and activates cAMP response element-binding protein (CREB) and dephosphorylates its coactivator CREB Regulated Transcription Coactivator 2 (CRTC2) to prevent its degradation [117] (Figure 6, step 5). Additionally, PKA activates inositol-1,4,5-trisphosphate receptors (IP3Rs), thereby increasing ER-secreted Ca^{2+}, which activates calcineurin, thereby additionally stabilizing CRTC2 [117]. Glucagon may further stabilize CRTC2 by stimulating its acetylation by

p300/CREB-binding protein (CBP) [117]. Activation of CREB and its coactivator CRTC2 promotes gluconeogenesis [117].

In a fed state, insulin suppresses gluconeogenesis by activating IRS-1 and IRS-2, thereby activating the PI3-kinase/AKT pathway and mammalian target of rapamycin (mTORC2), which additionally activates AKT (Figure 6, step 3) [120]. Consequently, AKT phosphorylates and inactivates forkhead box protein O (FOXO) 1, -3, -4, and -6 to suppress gluconeogenesis (Figure 6, step 3) [120].

1.5 Regulation of insulin synthesis and secretion

1.5.1 Insulin synthesis regulation

Transcription of the insulin gene is regulated by the binding of several transcription factors to sequence elements known as A, C, E, Z, and CRE (cyclic AMP response element) in the promoter region [103,125,126]. Duodenal homeobox-1 (PDX-1), caudal-type homeobox 2 (CDX2), ISL LIM homeobox 1 (ISL-1) bind to sequence element A [103,125,126]. PDX-1 also binds to sequence element Z [103,125,126]. MAF BZIP transcription factor A (MAFA) binds to sequence element C1 and Z, while paired box 6 (PAX6) binds to sequence element C2 [103,125,126]. BETA2/NeuroD1, E2/5, E12, and E47 bind to sequence element E [103,125,126]. CREB/ATF family bind to sequence element CRE [103,125,126].

Insulin synthesis begins with the translation of a 110-amino acid preproinsulin mRNA, comprising an N-terminal signal peptide, B chain, connecting peptide (C-peptide), and C-terminal A chain (Figure 7) [103,125,126].

Preproinsulin translation is regulated by the mTOR pathway and the ATP-dependent RNA helicase DEAD-box helicase 1 (DDX1) complex with eukaryotic initiation factor 3a (EIF3a) and EIF4b [103,125,126]. The N-terminal signal peptide of preproinsulin is cleaved in the ER, resulting in a proinsulin molecule with intramolecular disulfide bridges connecting chains A and B, and one interchain disulfide bridge in the A chain (Figure 7) [103,125,126]. Proinsulin is then translocated to the TGN and sorted into secretory granules, where the C-terminal is cleaved by proprotein convertase 1/3 (PC1/3) (in humans) or PC2 (in rodents), and the dibasic residues are removed from the C-terminal

end of the B chain by exopeptidase carboxypeptidase E/H (CPE), forming mature insulin. Mature insulin exists in secretory vesicles as a hexamer formed from three insulin dimers joined by Zn^{2+} (Figure 7) [103,125,126].

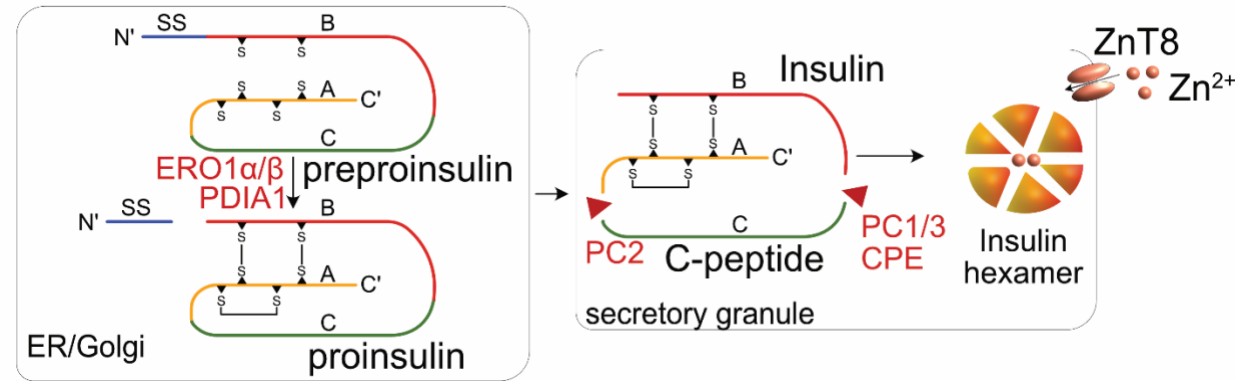

Figure 7: Insulin synthesis

Preproinsulin in the Golgi is converted to proinsulin though removal of the signaling sequence (SS) and formation of intramolecular disulfide bridges by PDIA1 and ERO1α/β. In the secretory granules, proinsulin is cleaved into insulin and the C-peptide by PC2, PC1/3 and CPE. Zn^{2+} imported through ZnT8 transporter shapes insulin molecules into hexamers.

CPE, exopeptidase carboxypeptidase E/H; ERO1α/β, oxidoreductases ER oxidoreductin 1α/β; PC1/3, proconvertase 1/3; PC2, proconvertase 2; PDIA1, disulfide isomerase; SS, signaling sequence; ZnT8, Zn transporter 8.

1.5.2 Glucose-stimulated insulin secretion

Although insulin secretion can be stimulated by amino acids, fatty acids, and monosaccharides, glucose is the main stimulator of insulin secretion, and the amplitude of secretion upon glucose stimulation is much higher than for any other nutrient [103]. Upon uptake into pancreatic β-cells, glucose is metabolized through glycolysis, initiating a two-phase insulin signaling process [110].

In the first phase of insulin secretion, increased intracellular ATP concentrations, produced in glycolysis, closes Potassium-ATP (K^{+}_{ATP}) channels, leading to an increase in potassium levels in the cells, an increase in membrane potential and subsequent membrane depolarization and influx of Ca^{2+} through voltage gated Ca^{2+} channels (Figure 8, step 1-6) [110]. Murine β-cells rely on Cav1.2 L-type Ca^{2+} channels as a primary Ca^{2+} channel, and on R-type Ca^{2+} channel to supply new vesicles to the plasma membrane [110]. By contrast, human β-cells depend on P/Q type and T-type Ca^{2+} channels [110].

Increased Ca^{2+} levels in β-cells induce insulin release from primed and docked vesicles (Figure 8, step 7) [103,104].

In the second phase of insulin secretion, Ca^{2+} influx is amplified by metabolic coupling factors produced from glucose (NADPH, pyruvate, malate, citrate, isocitrate, acyl-CoA and glutamate), as well as by GIP secreted from intestinal K-cells, GLP-1 from intestinal L-cells and pancreatic α-cells, acetylcholine from α-cells, vasoactive intestinal polypeptide, and gastrin-releasing polypeptide (Figure 8, step 8) [127–130].

1.5.3 Hormonal control of insulin secretion

GLP-1, GIP, and acetylcholine, vasoactive intestinal polypeptide and gastrin-releasing polypeptide all enhance insulin secretion through PKA, PKB, and exchange protein directly activated by cAMP 2 (EPAC2) (Figure 8, step 8) [130,131]. EPAC2 modulates insulin secretion by supporting the inhibitory action of ATP on K^+_{ATP} channels [132], while PKA and PKB modulate insulin secretion by increasing the number of Ca^{2+}-sensitive insulin vesicles (Figure 8, step 8) [133].

Another hormone involved in insulin secretion stimulation is estrogen. Estrogen acts through nuclear estrogen receptor α or β (ER α or β) or membrane ERγ, thereby activating protein kinase G (PKG), which directly phosphorylates CREB. CREB binds to CRE sequence element, activating transcription of genes with cAMP/Ca^{2+} response elements, ultimately amplifying intracellular Ca^{2+} oscillations and consequently insulin secretion [103].

Hormones exerting inhibitory action on insulin secretion include leptin, insulin growth factor-1 (IGF-1), somatostatin, neuropeptide Y (NPY), PYY and ghrelin. Adipocyte-secreted leptin and liver-produced IGF-1 exert their inhibitory function by activating phosphodiesterase 3B (PDE3B), which breaks down cAMP, inhibiting cAMP-dependent induction of insulin secretion (Figure 8, step 11) [103].

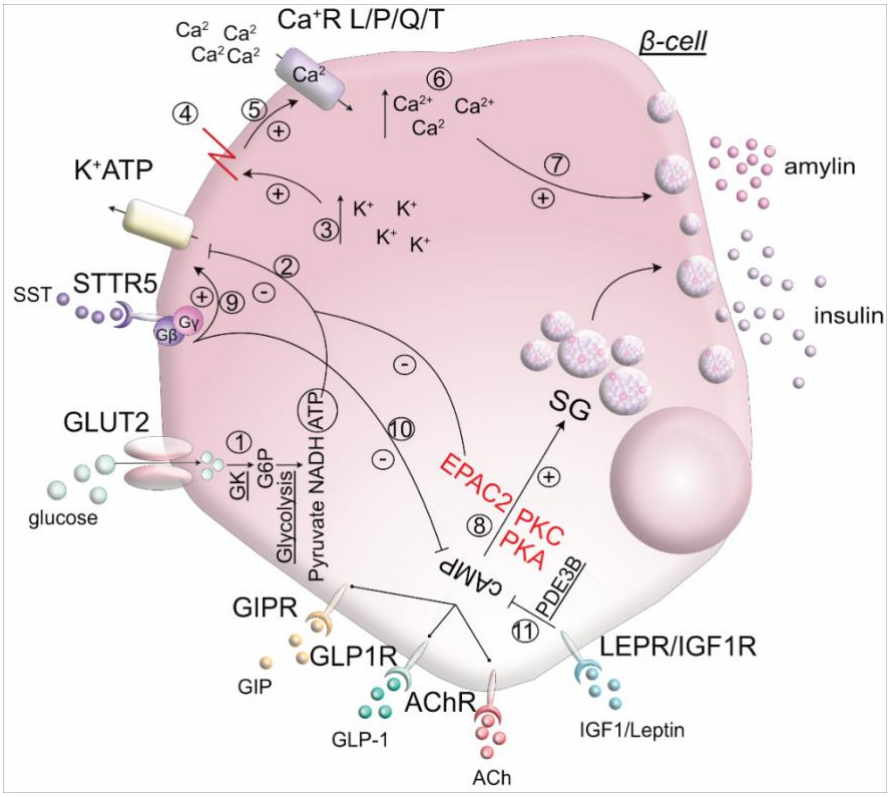

Figure 8: Glucose stimulated insulin secretion and its hormonal regulation

Step 1: Glucose conversion to G6P by hexokinase initiates glycolysis and ATP production.

Steps 2-3: Inhibition of ATP-mediated K^+ATP channels cause increase in intracellular K^+ levels.

Steps 4-7: Membrane depolarization leads to opening of Ca^{2+} channels, to increased intracellular Ca^{2+} concentration, and to insulin secretion from primed and docked cellular vesicles.

Step 8: Amplifying effects of GIP, GLP-1, and ACh signaling on insulin secretion through increase in cAMP concentration and further activation of EPAC2, which inhibits K^+ATP channels, PKC and PKA, which in turn stimulates new vesicles formation and priming.

Step 9: SST stimulates opening of K^+ATP channels, thereby hyperpolarizing the plasma membrane and inhibiting insulin secretion.

Step 10: SST may also decrease cAMP levels thereby inhibiting the cAMP insulin secretion amplifying pathway.

Step 11: Leptin and IGF-1 activate PDE3B, which breaks down cAMP and inhibits amplification of the insulin secretion pathway.

AChR, Acetylcholine receptor; cAMP, cyclic adenosine monophosphate; EPAC2, exchange protein directly activated by cAMP 2; G6P, glucose 6 phosphate; GIPR, glucose-dependent insulinotropic polypeptide receptor; GLP1R, glucagon-like peptide 1 receptors; GK, glucokinase; GLUT2, glucose transporter 2; IGF1R, insulin growth factor 1 receptor; LEPR, leptin receptor; PDE3B, phosphodiesterase 3B; PKA, phosphokinase A; PKC, phosphokinase C; SG, secretory granules; SSTR5, somatostatin receptor 5.

Somatostatin-28, predominantly expressed in intestinal D-cells, and Somatostatin-14 produced in the hypothalamus, peripheral nerves, and pancreatic δ cells both act on the somatostatin receptor 5 (SST5) on pancreatic β-cells [134,135]. This signal stimulates

Gβγ to induce the opening of K^+_{ATP} and G protein-coupled inwardly rectifying potassium channels (GIRK), which hyperpolarize β-cells plasma membranes and inhibits insulin secretion (Figure 8, step 9) [134,135]. Additionally, somatostatin may decrease cAMP levels, which also inhibits insulin secretion (Figure 8, step 10) [135].

NPY, secreted from the hypothalamus or pancreatic islets PP cells, elicits its insulin inhibitory functions via the NPY receptor Y1, which activates Gα subunit, thereby acting on pathways downstream of cAMP, excluding Ca^{2+} signaling [136]. PYY acts through similar mechanism as NPY as it binds to NPY receptors Y1, Y2 and Y4 [137].

Ghrelin, secreted from X/A-like cells in the stomach or pancreatic ε-cells, can directly and indirectly inhibit insulin secretion by mechanisms still not entirely clear [138,139]. Ghrelin directly binds to the growth hormone secretagogue receptor (GHS-R1a) on β-cells and elicits its inhibitory functions [138,139]. Additionally, ghrelin activates the afferent vagus nerve in the liver, which leads to the inhibition of efferent nerve fiber in the brain and reduces insulin secretion [138]. Furthermore, ghrelin can indirectly inhibit the sympathetic nervous system, decreasing stimulation of α-adrenergic receptors on β-cells [138,139].

1.5.4 Central regulation of insulin secretion

1.5.4.1 Sympathetic and parasympathetic control of insulin secretion

The sympathetic and parasympathetic nervous systems are both involved in the regulation of insulin secretion. Activation of sympathetic innervation inhibits insulin secretion through the action of noradrenaline on α2-adrenergic receptors on β cells [140,141]. In contrast, the parasympathetic nervous system stimulates insulin secretion by acting on muscarinic M3 receptors [142]. Vasoactive intestinal peptide (VIP), pituitary adenylate-cyclase-activating polypeptide (PACAP), gastrin-releasing peptide (GRP), and acetylcholine all stimulate insulin secretion [142–145]. The parasympathetic nervous system also stimulates insulin release in response to sensory stimuli (olfactory, visual information), ensuring insulin release before the elevation of blood glucose levels [142]. Furthermore, parasympathetic inputs from the intrapancreatic ganglia synchronize insulin secretion throughout islets in the pancreas [146].

1.5.4.2 Hypothalamic insulin secretion regulation

Oxytocin neurons in the paraventricular hypothalamic neurons exert inhibitory actions on insulin secretion via sympathetic preganglionic neurons located in the thoracic segments 9-13 of the spinal cord [147]. Postganglionic sympathetic neurons inhibit insulin secretion by releasing norepinephrine [148]. The hypothalamic ventromedial nucleus is also implicated in the inhibition of insulin secretion, as documented by the inhibition of hypothalamic prolyl endopeptidase expression leading to decreased fasting insulin secretion [149]. As mentioned above, hormones secreted by the hypothalamus, including NPY, somatostatin, leptin, and growth hormones, also regulate insulin secretion.

1.6 Beta cell dysfunction

Diseases linked to the loss of insulin function encompass T1D and T2D. Diabetes primarily arises from β cell dysfunction. Etiologically, it is classified into various subtypes, including gestational diabetes, monogenic diabetes (such as neonatal diabetes and maturity-onset diabetes of the young), and other forms like pancreatitis- or drug-induced diabetes [150,151]. Nevertheless, T1D and T2D are the most prevalent among them.

According to the 10th edition of the International Diabetes Federation Diabetes Atlas, approximately 10.5% of adults aged 20 to 79 worldwide are presently affected by diabetes. However, this number is projected to rise to 12.2% by the year 2045 [152]. T1D affects over 1.2 million individuals globally, while T2D accounts for 90% of all diabetes cases [152]. Tragically, diabetes claims the lives of around 6.7 million people worldwide [152]. Besides straining healthcare systems globally, with costs exceeding 966 billion US dollars and expected to surpass 1,054 billion US dollars by 2045 [153], diabetes diminishes the productivity of individuals by roughly 11% [154].

T1D is an autoimmune condition distinguished by immune-mediated β cell destruction, resulting in insulin insufficiency and hyperglycemia [155,156]. T1DM exhibits symptoms like polyuria, weight loss, constant hunger, blurred vision, polydipsia, and ketoacidosis [155,156]. The exact causes of T1D are still a subject of debate, but potential triggers for its etiology include genetic predisposition (specifically the DR3-DQ2 and DR4-DG8 haplotypes of HLA class II genes), viral infections (such as enterovirus and

coxsackievirus B), human endogenized retroviruses, epigenetic factors, and certain non-coding RNAs [155].

The central mechanism underlying T2D is tissue resistance to insulin, leading to decreased glucose uptake and the constantly activated lipolysis and gluconeogenesis, ultimately resulting in hyperglycemia [157,158]. While β cell function and viability remain intact during the early stages of T2D, the prolonged need for increased insulin production to combat tissue resistance eventually leads to β cell failure and death. Risk factors for T2D encompass obesity, hypertension, elevated triglyceride levels, polygenic changes, and genetic predisposition [157,158]. GWAS have identified risk genes for Type II diabetes, including calpain 10 (*CAPN10*), transcription factor 7-like 2 (*TCF7L2*), proliferator-activated receptor gamma (*PPARG*), insulin receptor substrate 1 (*IRS1*) and *IRS-2*, potassium inwardly-rectifying channel, subfamily J, member 11 (*KCNJ11*), Wolfram syndrome 1 (*WFS1*), HNF1 homeobox A (*HNF1A*), HNF1 homeobox B (*HNF1B*), hematopoietically expressed homeobox (*HHEX*), solute carrier family 30 member 8 (*SLC30A8*), cyclin-dependent kinase inhibitor 2A/B (*CDKN2A*/B), insulin-like growth factor 2 mRNA binding protein 2 (*IGF2BP2*), *SORCS2*, and *SORCS1*, among others [54,159,160].

Both diseases share a common feature of β cell population loss in the pancreas due to autoimmune-induced cell death in the case of T1D or the exhaustion of β cells in T2D. In the subsequent section, I will delve into various pathological mechanisms, such as inflammation and cellular stress, that trigger β cell death.

1.6.1 Effect of inflammation on beta cell function

The infiltration of immune cells into the pancreas plays a central role in the pathology of T1D [161,162]. This phenomenon arises from the production of auto-antibodies by compromised β cells, including insulin, proinsulin, islet antigen 2 (IA-2), glutamic acid decarboxylase 65 (GAD65), islet amyloid polypeptide (IAPP), glucose-regulated protein 78 (GRP78), islet-specific glucose-6-phosphatase catalytic subunit-related protein (IGRP), the cation efflux transporter zinc transporter 8 (ZNT8), and chromogranin [161,162]. Additionally, it can be attributed to the heightened immune presentation by β cells [161,162]. Nevertheless, the role of β cell auto-antibodies in the pathogenesis of

T1D remains a subject of debate. Therefore, the focus here will be on the mechanisms of β cell antigen presentation and immune cell-triggered cell death [163].

1.6.1.1 β cell as antigen-presenting cells

In some individuals with T1D and non-obese diabetic (NOD) mouse models, β cells take on the role of antigen-presenting cells (APCs), marked by the expression of major histocompatibility complex class II (MHCII) and the class II major histocompatibility complex trans-activator (CIITA) [161,162]. These elements are essential for the recognition and activation of $CD4^+$ T cells [161,162]. Furthermore, human β cells may also exhibit human leukocyte antigens of class I, which are necessary for engaging $CD8^+$ cytotoxic T cells [161,164].

Moreover, β cells possess the capability to release cytokines such as interleukin-1β (IL-1β), IL-6, IL-8, granulocyte colony-stimulating factor (G-CSF), and macrophage inflammatory protein-1 [165]. These cytokines can further enhance the infiltration of immune cells into the pancreas [165]. In response to metabolic challenges or exposure to cytokines, β cells can also produce intracellular proinflammatory factors, including nuclear transcription factor κB (NFκB), inducible nitric oxide synthase (iNOS), NADPH oxidase (NOX), and toll-like receptors (TLRs) [165].

1.6.1.2 Mechanism of immune cell-initiated β cell death

Multiple mechanisms underlie the immune cell-mediated death of β cells. These mechanisms encompass phagocytosis triggered by macrophages and dendritic cells, the production of cytokines by $CD4^+$ and $CD8^+$ T cells, and the activation of death receptors, leading to apoptosis [165–168].

1.6.1.2.1 Function of $CD8^+$ T cells in mediating β cell death

$CD8^+$ T cells employ three distinct mechanisms to induce β cell apoptosis. Firstly, upon recognizing auto-antigens or cytokines produced by β cells, $CD8^+$ T cells release specialized lysosomes known as lytic granules, containing perforin and granzymes [169]. Perforin creates pores in the lipid bilayer of target cells, enabling the influx of water and salts, leading to cell destruction [169]. Granzymes, which enter through these perforin-

formed pores, cleave caspase 3, initiating genomic DNA degradation through caspase-activated deoxyribonuclease [169]. Secondly, $CD8^+$ T cells carry ligands for Fas ligand (FasL) receptors in β cells. The formation of receptor-ligand complexes triggers caspase-dependent apoptosis in β cells [169]. Thirdly, $CD8^+$ T cells release interferon-γ (IFN-γ) along with tumor necrosis factors α and β (TNF-α and TNF-β) [169] . IFN-γ induces the expression of MHC class I on β cells, facilitating their swift recognition by immune cells for destruction [169]. Moreover, all three cytokines possess the capability to activate and engage macrophages [169].

1.6.1.2.2 Function of $CD4^+$ T cells in mediating β cell death

Three subsets of $CD4^+$ T cells play a crucial role in the progression of T1D, specifically Th1, Th17, and T follicular helper cells (Tfh) [170]. The Th1 subset of $CD4^+$ T cells is known for its production of IFN-γ [170]. The Th17 subset exerts a pro-diabetic effect by differentiating into the Th1 subtype [170]. Additionally, both Tfh and Th17 subsets secrete interleukin-21 (IL-21), which is essential for the proliferation of $CD4^+$ T cells and the activation of $CD8^+$ T cells [170]. $CD4^+$ T cells and macrophages collaborate to deactivate immunosuppressive Treg cells, promote the maturation and migration of dendritic cells, and reduce the production of immunosuppressive IL-10 by β-cells [170].

1.6.1.2.3 Macrophages directed β cell death

Macrophages are commonly found in the pancreatic islets. Under normal conditions, they play a vital role in sensing ATP released by β cells, along with insulin, through purinergic receptors [171,172]. This allows them to monitor β cell activity and secrete the anti-inflammatory cytokine IL-10, as well as metalloproteinase MMP9 [171,172]. Resident β cell macrophages also promote connective tissue growth factor (CTGF)-mediated β cell proliferation [173]. Moreover, macrophages serve as the primary source of IGF-1, transforming growth factor β (TGF-β), and epidermal growth factor (EGF) within the pancreatic islets [173]. These molecules stimulate β cell proliferation in response to β cell death [173].

However, under pathological conditions, cytokines and chemokines released by $CD4^+$ and $CD8^+$ T cells, such as IFN-γ, IL-1β, C-X-C motif chemokine ligand 10 (CXCL10), C-

C ligand 2 (CCL2), C-C ligand 20 (CCL20), and interleukin-15 (IL15), trigger the activation of a β cell destruction program by macrophages [171,174]. In particular, infiltrating macrophages secrete cytokines that activate the pro-apoptotic nuclear factor kappa-light-chain-enhancer of activated B cells (NFκB) pathway, and act as antigen-presenting cells to recruit cytotoxic T-cells, and directly phagocytose β cells [173].

1.6.2 ER stress initiated β cell apoptosis

Pancreatic β cells exhibit significant biosynthetic capacity to meet the continuous demand for insulin production, particularly in response to fluctuations in nutrient levels in the bloodstream [175–178]. However, the high rate of insulin synthesis and folding in the ER makes them susceptible to errors, resulting in the accumulation of improperly folded proteins and triggering ER stress [175–178]. During ER stress, binding immunoglobulin protein (BiP) binds to exposed hydrophobic regions of unfolded proteins, such as proinsulin, initiating factors in the unfolded protein response (UPR) [175–178]. These factors include protein kinase RNA-like ER kinase (PERK), transcription factor 6 (ATF6), and inositol-requiring enzyme type 1 (IRE1) [175–178].

PERK, functioning as an endoribonuclease, phosphorylates the α subunit of eukaryotic initiation factor 2 (eIF2α) upon activation, thereby inhibiting ER protein translation [175–178]. PERK also activates activating transcription factor 4 to regulate ER homeostasis [175–178]. ATF6 moves to the Golgi apparatus where it is cleaved by site 1/2 proteases (S1P, S2P), creating an active transcription factor that, upon translocation to the nucleus, activates the transcription of genes encoding chaperones and components of the ER-associated protein degradation (ERAD) machinery, as well as X-box binding protein 1 (XBP1) [175–178]. IRE1 is another endoribonuclease that splices XBP1 transcripts, generating an active transcription factor that in turn promotes the transcription of ERAD genes and the restoration of ER homeostasis [175–178].

While ER stress and the UPR are essential for restoring ER homeostasis and β-cell survival, prolonged or unresolved ER stress can lead to β cell apoptosis. Notably, IRE1 can recruit TNF-receptor-associated factor 2 (TRAF2) to phosphorylate c-Jun N-terminal kinase (JNK), which, in turn, induces apoptosis through the phosphorylation and

transactivation of c-Jun, resulting in increased expression of pro-apoptotic genes [178,179].
PERK triggers apoptosis through prolonged eIF2α-mediated activation of ATF4, leading to the activation of the C/EBP homologous protein (CHOP) [178,180]. CHOP promotes apoptosis by increasing the expression of pro-apoptotic Bcl-2 family proteins, enhancing Ca^{2+} release through IP_3Rs, boosting the expression of Tribbles homolog 3 (TRIB3) an AKT inhibitor, activating the growth arrest and DNA damage-inducible protein (GADD34), which inhibits eIF2α and boosts protein synthesis in the ER [178,180].

While the precise mechanism of how prolonged ATF6 activation can lead to β cell death remains unclear, studies have shown that prolonged inhibition of insulin gene expression leads to β cell dysfunction and death [178].

1.6.3 Oxidative stress initiated β cell apoptosis

Similar to ER stress, oxidative stress is essential for the normal functioning of β cells. Reactive oxygen species (ROS) generated during oxidative stress enhance insulin secretion by activating ryanodine receptors (RYRs) [181–184]. However, β cells have a weaker defense system against ROS compared to other cell types, making them more susceptible to cell death induced by oxidative stress [181–184].

ROS production in β cells is triggered by conditions like hyperglycemia or hyperlipidemia. In detail, an excess of metabolic fuel elevates the levels of nicotinamide adenine dinucleotide and flavin, overwhelming the electron transport chain [181–184]. As a result, electrons leak through complexes I and III of the mitochondrial electron transport chain and, upon reacting with molecular oxygen, are converted into H_2O_2 and further transformed into OH^- [181–184]. Other pathways involved in ROS production include the activation of PKC, the hexosamine and polyol pathways, oxidative phosphorylation, and advanced glycation [181–184].

Oxidative stress-induced β cell death is mediated by the prolonged activation of AMP-activated protein kinase (AMPK) and JNK, along with sustained inhibition of mTOR [181–184]. Overactivation of AMPK leads to an increase in extracellular-signal-regulated kinase (ERK) activity, which subsequently inhibits mTOR [181–184]. mTOR is crucial for

regulating β cell growth, proliferation, autophagy, and apoptosis [181–184]. Inactivation of mTOR induces cell death due to the lack of expression inhibition of thioredoxin-interacting protein (TXNIP) [181–184]. TXNIP translocates to the mitochondria and binds to TXN2, releasing apoptosis signal-regulating kinase 1 (ASK1) and initiating mitochondria-mediated apoptosis [181–184]. Furthermore, mTOR inhibition-induced cell death occurs because TXNIP promotes the formation of the NLR family pyrin domain-containing 3 (NLRP3) inflammasome, leading to pro-caspase 1 activation, microperforation of the plasma membrane, and activation of IL-1β [181–184].

1.7 Aim of the thesis project

Given the clinical significance of β cell malfunctions as the underlying cause of disturbances in glucose metabolism and the development of diabetes, investigating novel risk genes associated with β cell function and pathology is a timely and important pursuit. In this context, VPS10P domain receptors have emerged as intriguing candidate genes, connecting targeted protein sorting with metabolic cell functions. This concept is illustrated by SORCS1, a major risk gene for T2D with genome-wide significance [51,160]. Notably, SORCS1 bears a close structural resemblance to SORCS2, which is also genetically linked to diabetes [54]. However, the precise role of these receptors in the disease, if any, remains unknown.

Moreover, work conducted by Dr. V. Schmidt-Krüger in the Willnow lab has provided initial observations that support the functional relevance of SORCS2 in islet cell function and systemic glucose homeostasis. Dr. Schmidt used indirect gas calorimetry to investigate the primary metabolic fuel used by *Sorcs2*$^{-/-}$ mice [185]. The results of these studies showed a decreased respiratory exchange ratio in mutant mice, suggesting a preference for lipids over glucose as a fuel source [185].

Additionally, glucose tolerance tests, involving the injection of a glucose bolus and the measurement of blood glucose levels before and after the injection every 15 minutes for 120 minutes, revealed reduced glucose tolerance in mutant animals [185]. This suggests a potential defect in insulin secretion in response to glucose. In contrast, *Sorcs2*$^{-/-}$ mice performed normally in insulin tolerance tests, which involve the injection of an insulin bolus and the measurement of blood glucose levels before and after injection, showing

no significant changes [185]. These findings indicate that metabolic tissues were not resistant to insulin, and the glucose uptake machinery remained intact.

Based on this data and considering the structural similarity between SORCS2 and SORCS1, which is involved in insulin granule biogenesis, we hypothesized that SORCS2 might play a role in the regulation of insulin secretion through as yet unknown mechanisms.

Accordingly, the aim of my study was to investigate the role of SORCS2 in glucose metabolism and assess its influence on the control of insulin secretion. Utilizing a *Sorcs2*$^{-/-}$ mouse model and isolated pancreatic islets from *Sorcs2*$^{-/-}$ mice, we aimed to provide a comprehensive understanding of SORCS2's impact on insulin and glucose regulation, including the secretion of related hormones and the underlying molecular mechanisms. The outcomes of this research are anticipated to enhance our comprehension of the physiological significance of SORCS2 in metabolic regulation. Furthermore, the findings may carry implications for the development of potential therapeutic strategies targeting glucose-related disorders.

2 Methods

2.1 Materials

2.1.1 Oligonucleotides and TaqMan probes

Table 1: List of DNA primers used for genotyping PCR

Gene	Primer orientation	Primer sequence
Sorcs2	Forward	GTTCTGGGGACAAGGTCGTC
	Reverse	CTGAGCCAGTTGACTGATATGTC

Table 2: TaqMan Probes used for qRT-PCR

All TaqMan probes for RT-qPCR were ordered from Thermo Fisher Scientific.

Gene	TaqMan gene expression assay
Gapdh	Mm99999915_g1
18SRNA	Mm-03928990_g1
Sorcs2 (exon 14-15)	Mm00473063_m1
Sorcs2 (exon 15-16)	Mm01217942_m1
Spp1	Mm00436767_m1
Iba1	Mm00479862_g1
CD40	Mm00441891_m1
CD32	Mm00438875_m1
IL6	Mm00446190_m1
TNF-alpha	Mm00443260-g1
Nos2	Mm00440502_m1
CD3	Mm00446171_m1
CD40	Mm00441891_m1
Arg1	Mm00475988_m1

2.1.2 Antibodies

All peroxidase-labeled antibodies used for Western Blot were purchased from Sigma-Aldrich and used at a dilution of 1:10000. Fluorophore-conjugated antibodies Alexa Fluor® 488, 555, 647 used for immunohistochemistry were purchased from Thermo Fisher Scientific and utilized diluted to 1:1000.

Table 3: Primary antibodies used for immunohistochemistry and Western Blotting

Target protein	Source	Catalog number	Dilution	Application
SORCS2	R&D systems	AF4237	1:30	IF
Somatostatin	Abcam	ab111912	1:250	IF
Glucagon	Abcam	ab10988	1:150	IF
PPY	Abcam	ab9391	1:250	IF
Insulin	Cell Signaling Technology	8138	1:50	IF
Insulin	Dako	IR002	1:4	IF
SSP1	R&D systems	MAB808	1:30	IF
DAPI	Roche	10236276001	1:2000	IF
SORCS2	in-house		1:1000	WB
AKT	Cell Signaling Technologies	4691	1:1000	WB
pAKT-T	Cell Signaling Technologies	2965	1:1000	WB
pAKT-S	Cell Signaling Technologies	9271	1:1000	WB
ERK	Cell Signaling Technologies	9102	1:1000	WB
pERK	Cell Signaling Technologies	4370	1:2000	WB
cAMP	Abcam	ab136960	1:500	WB
PKCalpha	Sigma-Aldrich	SAB4502354	1:500	WB
Stat3	Cell Signaling Technologies	9139	1:1000	WB
pStat3	Cell Signaling Technologies	9145	1:2000	WB
pPI3K	Cell Signaling Technologies	4228	1:1000	WB
pJNK	Cell Signaling Technologies	9251	1:1000	WB
Vinculin	Invitrogen	700062	1:1000	WB
Alpha-tubulin	Sigma	DM1A	1:1000	WB

* WB, Western blotting; IF, immunofluorescence

2.1.3 Buffer solutions and cell culture media

Table 4: Buffer solutions used in the study

Buffer solution	Composition
Immunohistochemistry	
10xTBS (pH 7.6)	200 mM Tris-Base
	1500 mM NaCl
Wash buffer	1x TBS + 0.05 % Tween 20
Citrate buffer	10 mM Trisodium citrate dihydrate + 0.05% Tween 20
Blocking solution	10% Normal Donkey Serum (Linaris) + 1% Bovine Serum Albumin (Sigma) + 0.3% Triton X-100 (Sigma)
Primary antibody dilution solution	1x TBS + 1% Normal Donkey Serum + 1% Bovine Serum Albumin + 0.3% Triton X-100
Secondary antibody dilution solution	1xTBS + 0.05% Tween-20
Tissue lysate buffers	
Lysis buffer (pH 7.4)	20 mM Tris, pH 8+ 10 mM EDTA + 1 % Triton X-100 + 1% NP40 + phosphatase inhibitor (Thermo Fischer Scientific, Cat# 78427) + protease inhibitor (Roche, Cat# 11836145001)
Western Blotting buffers	
4x Laemmli sample buffer	250 mM Tris, pH 6.8 + 8% SDS + 1% Bromophenol blue + 40 % Glycerol + 5% 2-Mercaptoethanol
Running buffer	50 mM Tris + 384 mM Glycine + 0.1% SDS
Transfer buffer	18 mM Tris + 155 mM Glycine
Washing solution	20 mM Tris + pH 7.5, 150 mM NaCl + 0.1% Tween-20
Blocking solution	20 mM Tris, pH 7.5 + 150 mM NaCl + 0.1% Tween-20 + 5% Skimmed milk
Antibody diluent	5% BSA + 20 mM Tris, pH 7.5 + 150 mM NaCl + 0.1% Tween-20

Pancreatic islet lysate buffer	
NP40 lysis buffer	150 mM NaCl + 20 mM Tris + 1 mM EDTA + 0.5 mM EGTA + 5% Glycerol + 0.5% IGEPAL (NP40) + 1mM Phenylmethylsulfonyl fluoride (PMSF) (Serva, #32395.03) + 25 µg/ml Aprotinin (Serva, #13718.01) + 25 µg/ml Leupeptin (Serva, #51867.02) + 3.3 µg/ml Pepstatin (Serva, #52682.02)
Buffers for pancreatic islet secretion assay	
Kreb's Ringer's buffer Hepes (KRBH) (pH 7.4)	129 mM NaCl + 4.8 mM KCl + 1.2 mM $MgSO_4$-7H2O + 1.2 mM KH_2PO_4 + 5mM $NaHCO_3$ + 2.5 mM $CaCl_2$ + 10 mM HEPES
KRBH with glucose/KCl	KRBH + 1.6- or 16-mM Glucose, or 30 mM KCl + 0.25% Bovine serum albumin + 600 KIU/ml Aprotinin

Table 5: Colorimetric and fluorometric kits for lipid analyses

Name	Manufacturer	Catalog number
Free Fatty Acid Quantification Colorimetric/Fluorometric Kit	BioVision	K612-100
Triglyceride Colorimetric Assay Kit	Cayman Chemicals	10010303
Amplex Red Cholesterol Assay Kit	Invitrogen	A12216
Glycogen Colorimetric/Fluorometric Assay Kit	BioVision	K646-100

Table 6: ELISA kits used in the study

Name	Manufacturer	Catalog number
Insulin	Crystal Chemicals, USA	90080
C-peptide	Crystal Chemicals, USA	90050
Glucagon	Crystal Chemicals, USA	81518
GLP-1	Crystal Chemicals, USA	81508
Somatostatin	Phoenix Pharmaceuticals Inc, USA	EKE-060-03
Somatostatin-28	Phoenix Pharmaceuticals Inc, USA	FEK-060-14

Neuropeptide Y	Phoenix Pharmaceuticals Inc, USA	EK-049-03
Peptide YY	Phoenix Pharmaceuticals. Inc, USA	EK-059-04
Osteopontin	Abcam, USA	ab100734

2.2 *In vivo* experimental methods

2.2.1 *Sorcs2* deficient mice

The *Sorcs2* deficient mouse model was established following previously published protocols [186]. These mice were maintained through inbreeding on a C57BL6/N background and were housed in a controlled environment featuring a 12-hour light/dark cycle. The mice were provided with a standard chow diet containing 4.5% crude fat and 39% carbohydrates. For the study, male mice aged between 20 and 30 weeks were selected as experimental subjects. Ethical approval for all experimental procedures was obtained from the Berlin State Office for Health and Social Affairs (LAGESO, Berlin, Germany), ensuring compliance with ethical guidelines and standards.

2.2.2 Animal body weight and length measurement

Prior to and following a 16-hour fasting period, animals underwent weighing to assess changes in body weight. Additionally, the length of animals was measured from the nose to the base of the tail.

2.2.3 Lipid levels measurements in metabolic tissues and plasma

Mice underwent a 16-hour overnight fast before the collection of blood from the retro-orbital plexus into EDTA-coated tubes (Sarstedt, #20.1341). Plasma was obtained through centrifugation (2000 g at 4°C for 20 minutes). Subsequently, mice were sacrificed via cervical dislocation. Liver and gastrocnemius muscles were promptly dissected, placed in plastic tubes and flash-frozen in liquid nitrogen, and stored at -80°C until further analysis.

For lipid extraction, tissues from the liver and gastrocnemius muscles were processed following the protocols outlined in the Free Fatty Acid Quantification Kit (Table 5). Specifically, 200 µl of chloroform was added to 10 g of tissue, followed by homogenization using an Ultra-Turrax (IKA T25B) and subsequent centrifugation for 10 minutes at

161,000 g. The lower phase was collected, and to ensure complete chloroform evaporation, samples were air-dried overnight. Dried lipids were then dissolved in 200 µl of Free Fatty Acid Assay Buffer from the kit, vortexed vigorously for 5 minutes, and prepared for subsequent analyses.

Levels of cholesterol, triglycerides, and free fatty acids were quantified following the manufacturer's recommendations, utilizing commercially available colorimetric and fluorometric kits (Table 5).

2.2.4 Glycogen level measurement in metabolic tissues.

After an overnight fast lasting 16 hours, mice were subjected to the extraction of liver and skeletal muscles on the subsequent day. The extracted tissues were placed in plastic tubes, promptly frozen in liquid nitrogen and preserved at -80°C until further analysis. Glycogen extraction was carried out in accordance with the manufacturer's protocol (Table 5).

Briefly, 10 g of tissue was homogenized with ice-cold distilled water (dH2O), using an Ultra-Turrax (IKA T25B), followed by boiling for 10 minutes. The homogenate was then subjected to centrifugation for 10 minutes at 16,000 g. The resulting supernatant was analyzed using a commercially available colorimetric kit (Table 5).

2.2.5 Immunohistochemistry

2.2.5.1 Co-staining of SORCS2 with pancreatic islet cell markers

After initial weighing, mice were injected with a pentobarbital dose of 2.5 mg/kg body weight. Subsequently, transcardial perfusion was carried out consecutively using PBS and 4% paraformaldehyde (PFA). Pancreata were harvested, fixed overnight in 4% PFA at 4°C, and then subjected to a 24-hour dehydration process in sucrose solutions of increasing concentrations (10%, 20%, and 30%). Following dehydration, the tissues were frozen at -80°C in OCT-filled cryomolds (SAKURA, #4583). Tissue sections of 4 µm were prepared using a sliding microtome SM2000R (Leica Biosystems).

The tissue sections were rehydrated in 1x PBS for 15 minutes, underwent antigen retrieval in sodium citrate buffer pH 8.5 (Table 4) at 80°C for 30 minutes [187], and were

treated with a blocking solution for 1 hour at room temperature (Table 4). Primary antibodies were applied overnight at 4°C, followed by the application of secondary antibodies for 1 hour at room temperature. Nuclei were counterstained with DAPI. Imaging was conducted using a Leica SP8 DLS confocal microscope with a 63x objective.

To delineate the SORCS2 expression pattern in pancreatic islets, co-staining was performed with pancreatic cell markers, including glucagon (α cells), insulin (β cells), somatostatin (δ cells), and PPY (PP cells) (Table 3).

2.2.5.2 Pancreatic islet morphological analysis

Animals were initially weighed, followed by the administration of a pentobarbital dose of 2.5 mg/kg body weight. Subsequently, transcardial perfusion was conducted consecutively using PBS and 4% PFA. The harvested pancreata underwent fixation overnight in 4% PFA. Tissues were then dehydrated and embedded in paraffin utilizing an automatic tissue processor (Leica TP1020) with the following steps:

Step	Reagent	Time	Times
1	70 % Ethanol in distilled water	1 h	1x
2	90 % Ethanol in distilled water	1 h	1x
3	96 % Ethanol in distilled water	1 h	1x
4	100 % Ethanol in distilled water	1 h	3x
5	Roti-Histol	1 h	3x
6	Paroplast Plus	1 h	2x

The processed tissues were then sectioned into 4 µm slices using an automatic microtome (Thermo ScientificTM HM 355S). Subsequently, rehydration was performed with the following steps:

Step	Reagent	Time	Times
1	Roti-Histol	5 min	2x
2	100 % Ethanol in distilled water	5 min	2x
3	95 % Ethanol in distilled water	5 min	1x
4	80 % Ethanol in distilled water	5 min	1x
5	70 % Ethanol in distilled water	5 min	1x
6	50 % Ethanol in distilled water	5 min	1x
7	Distilled water	10 min	1x

The rehydrated tissues underwent antigen retrieval (citrate buffer, pH 6) at 95°C for 20 minutes (Table 4). Blocking and primary antibody solutions were prepared as previously described (Table 4). Tissues were stained for pancreatic cell markers including glucagon, insulin, somatostatin, and PPY (Table 3). Nuclei were counterstained with DAPI (Table 3). Images were captured using a Leica SP8 DLS confocal microscope with a 63x objective. The CellProfiler software was employed to measure the surface area occupied by different cell-type populations in islets of Langerhans [188]. Briefly, pancreata were stained for DAPI and cell markers mentioned above. The percentage of cell-type areas was quantified by dividing the marker area (defined by the software) by the total islet area (defined manually).

2.2.5.3 Pancreatic beta cell mass analysis

The mice were sacrificed by cervical dislocation. Pancreata were subsequently dissected, weighed, and fixed overnight in 4% PFA. The fixed tissues underwent process of dehydration and embedding in paraffin as described in 2.2.5.2. The processed tissues were sectioned into eight slices, each 6 µm thick and spaced 200 µm apart. The tissue sections were rehydrated using the previously described protocol (2.2.5.2). Following rehydration, immunostaining for insulin (Table 3) was performed, and the stained tissues were imaged on a Leica DMI6000 wide-field microscope with a 10x objective. Beta cell mass was quantified as described previously [189], using provided formulas:

$$\%\ insulin\ area\ = \frac{insulin\ area}{total\ tissue\ area} \times\ 100\%$$

$$beta\ cell\ mass = pancreas\ weight\ \times\ \%\ insulin\ area$$

2.2.6 Glucose-stimulated insulin secretion (GSIS) *in vivo*

The experimental procedure involved a 16-hour fasting period for the mice. On the subsequent day, the animals were weighed, and intraperitoneally (i.p.) injected with 2 g/kg of body weight of D-glucose in sterile filtered PBS [190,191]. Venous blood was collected at 0, 2, and 30 minutes from the retro-orbital plexus into EDTA-coated tubes containing 600 KIU/ml aprotinin. Plasma samples were obtained by centrifugation of blood samples at 2000g at 4°C for 20 minutes (Eppendorf 5415R centrifuge). Following

centrifugation, plasma samples were promptly frozen in liquid nitrogen and stored at -80°C until further use.

2.3 *In vitro* experimental methods

2.3.1 Islet of Langerhans isolation

The collagenase dissociation method was applied to obtain isolated islets of Langerhans from murine pancreata. Mice were sacrificed by cervical dislocation. The body cavity was opened, and the duodenal was clamped from both sides of the ampulla of Vater. The pancreas was inflated by injection of 3 ml of ice-cold dissociation solution (1000 U/ml collagenase (Sigma, #C9407-16), 1xHBSS (Gibco, #14175053), and 0.04 % FBS (Gibco, #0270106)) into the bile duct with a 27G needle. Pancreata were carefully removed and placed into 2 ml of dissociation solution at 37°C for 12 min, followed by 20 seconds of manual shaking. The activity of the collagenase was stopped with an ice-cold wash solution (1xHBSS, 0.04% FBS, 1 mM $CaCl_2$). The tissue lysate was centrifuged twice at 2000 g. After each centrifugation step, the supernatant was removed, and a fresh washing solution was added. The tissue pellet was dissociated in wash buffer and filtered through a 70 μm cell strainer (Falcon, #352350). Islets were handpicked into media (RPMI 1640 (PAN Biotech, #P04-16516)), 1% L-glutamine (Gibco, #25030-024), 1% Penicillin/Streptomycin (Gibco, #15140-122), 10% FBS) and cultured overnight at 37°C and with 5% CO_2.

2.3.2 Pancreatic islet collection for Western blot and RT-qPCR

Pancreatic islets were isolated following the procedure outlined in section 2.3.1. For Western Blotting, pancreatic islets from two to three mice were pooled to achieve 300 - 350 islets per sample. To investigate inflammatory cell infiltration into pancreatic islets, 150 - 200 islets per sample were allowed to rest for 2 hours in a culture medium, handpicked, washed in PBS, frozen in dry ice, and stored at -80°C for subsequent analysis. For the analysis of target genes in single-cell RNAseq, 150 - 200 pancreatic islets were isolated using the aforementioned method, left overnight in a culture medium, and, on the following day, washed in PBS, frozen in liquid nitrogen, and stored at -80°C for further use.

2.3.3 Glucose-stimulated insulin secretion (GSIS) *in vitro*

Thirty islets per sample were handpicked into low protein-binding tubes (ThermoFisher, #90410) and washed with KRBH containing 11 mM glucose. Following pre-incubation with KRBH buffer containing 1.6 mM glucose for 1 hour at 37°C, the islets underwent sequential incubation in 1.6 mM glucose KRBH and 16 mM glucose KRBH, for 1 hour at 37°C and in 30 mM KCl KRBH for 30 min at 37°C. Alternatively, islets were subjected to a sequence of 1.6 mM glucose in KRBH and 16 mM glucose in KRBH for 1 hour at 37°C each. The supernatant was collected after each round into new tubes coated with 600 KIU/ml aprotinin. After the final round, islets were washed once with 1x PBS (Gibco, #14200-067). Both the supernatant and islets were promptly frozen in liquid nitrogen and stored at -80°C until further use.

2.3.4 Isolated pancreatic islets perifusion studies

Islet perifusion studies were performed using the PERI4.2 set-up. Isolated and overnight recovered pancreatic islets were initially consecutively preincubated with fresh medium (30 min) and 1.6 mM glucose KRBH (30 min). Groups of 19-30 handpicked islets were equilibrated in 1.6 mM glucose KRBH (flow-through discarded) for 1 h (rest), followed by sequential perifusion with 1.6 mM glucose (18 min) and 16 mM glucose (1 h) in KRBH with a flow rate of 100 µl/min. At the end of the experiment, islets were lysed in TE buffer (10 mM Tris-HCl, 1 mM EDTA, 1% Triton X-100) and sonicated 10x for 30 sec with a 30 sec interval between sonication to measure DNA content. DNA content was measured with Quand-iT Picogreen DNA kit. Insulin levels were normalized to DNA content.

2.3.5 Pancreatic islet protein content analysis

To assess the protein content of the islets, a rigorous process was followed. Islets were vortexed for 1 minute and then incubated for 25 minutes at 4°C with NP40 lysis buffer (Table 4). Following this, the samples were centrifuged at 14,000g for 20 minutes at 4°C. The resulting supernatant was carefully transferred to a new tube. Subsequently, the protein concentration in the supernatant was determined using the Pierce BCA protein assay kit (ThermoFisher, #23225).

2.3.6 Total islet hormone content analysis

For the analysis of total islet hormone content, 30 handpicked islets were carefully collected into low-protein binding tubes and subsequently lysed as described in 2.3.5.

2.3.7 Osteopontin secretion analysis

Pancreatic islets were isolated following the procedure outlined in section 2.3.1 and allowed to rest in a cultural medium for 2 hours. Subsequently, 200 - 300 islets per sample were placed in 6-well plates with 1.5 ml of cultural medium and left for 16 hours at 37°C. The following day, both islets and the medium were collected for further analyses.

2.3.8 ELISA to determine secreted and total islet hormone levels

Hormone levels in plasma from *in vivo* GSIR experiments, supernatant from *in vitro* GSIR experiments, medium from osteopontin studies, or total islet lysates were quantified using commercially available ELISA kits, following the manufacturer's recommendations (Table 6). To ensure accuracy and relevance, hormone levels were normalized to the total islet protein content, providing a standardized measure for comparative analyses.

2.3.9 Electron Microscopy analysis

2.3.9.1 Samples preparation

Pancreatic islets were isolated following the procedure detailed in section 2.3.1. Subsequently, the isolated islets were cultured overnight in a culture medium. For further experimentation, one hundred fifty islets per sample were handpicked into low protein-binding tubes and washed with KRBH containing 11 mM D-glucose. The islets were then incubated for 1 hour in 1.6 mM glucose, followed by another hour in either 1.6 mM or 16 mM D-glucose in KRBH. After this incubation, the islets were washed with PBS and fixed by immersion in a solution comprising 4% (w/v) paraformaldehyde and 2.5% (v/v) glutaraldehyde in 0.1 M phosphate buffer for 2 hours at room temperature.

2.3.9.2 Postfixation, sectioning, and imaging

The postfixation, sectioning and imaging of samples was performed by electron microscopy facility in Max Delbueck Centre for Molecular Medicine. The samples were

postfixed in 1% (v/v) osmium tetroxide in 0.1 M phosphate buffer for 2 hours at room temperature, followed by an overnight incubation in 0.5% uranyl acetate at 4°C. The samples were then further dehydrated through a graded ethanol series and embedded according to the following protocol:

Step	Reagent	Time	Temperature	Times
1	30% Ethanol in distilled water	30 min	4 °C	1x
2	50% Ethanol in distilled water	30 min	4 °C	2x
3	70% Ethanol in distilled water	30 min	4 °C	1x
4	70% Ethanol in distilled water	Overnight	4 °C	1x
5	90% Ethanol in distilled water	30 min	4 °C	2x
6	100% Ethanol in distilled water	30 min	4 °C	2x
7	Propylene oxide	15 min	RT	2x
8	Propylene oxide:PolyBed ® 812 (1:1)	30 min	RT	2x
9	Propylene oxide: PolyBed ® 812 (1:2)	30 min	RT	2x
10	100% EPON	2 h	RT	1x
11	100% EPON	Overnight	RT	1x
12	100% EPON	3 h	RT	2x

After embedding, the samples were polymerized at 60°C for 2-3 days, cut into 60-80 nm sections, and stained consecutively with 0.5% uranyl acetate in H_2O for 30 minutes and with 3% lead citrate in H_2O for 7 minutes using a contrasting automat Leica AC20. They were then examined at 80 kV with an electron microscope Zeiss EM 910 equipped with a Quemesa CCD camera and iTEM software.

2.3.9.3 Image analysis

Fifteen to thirty β cell images per sample (n = 4) were analyzed through manual quantification of mature, immature, crystal-containing, and empty vesicles in the entire cell (total) or within 0.2 µm from the plasma membrane (docked). The numbers are reported as the total number of vesicles per cell area [192–194].

2.3.10 Preparation of single-cell islet cell suspension for scRNA-seq

Islets were isolated in accordance with the procedure outlined in section 2.3.1. Following an overnight recovery period, islets from three animals per genotype, totaling 400 - 600 islets per sample, were collected in tubes. The islets were washed once in PBS and

subjected to digestion in 200 µl Accutase (Innovative Cell Technologies, #AT-104) with the addition of 50 units/ml DNAse-1 (Roche, #EN0521) for 10 minutes at 37°C [195]. Throughout the digestion, islets were pipetted 10 times up and down every 5 minutes. The digestion reaction was halted by adding 1 ml of 0.5 mM EDTA, 2% FBS in HBSS. The resulting cell suspension was centrifuged for 3 minutes at 200 g and washed with the same solution. The cell pellet was resuspended in 1% BSA in PBS by pipetting four times up and down and subsequently filtered through a 40 µm Flowmi strainer (CarlRoth, #KKE3.1).

To eliminate apoptotic and duplet cells, the cell suspension underwent staining with propidium iodide (Invitrogen, #R37610), followed by flow cytometry using a BD FACSAria III (BD Biosciences, USA). Specifically, flow cytometry voltage and gain settings for the forward scatter and side scatter were optimized to identify a cluster of single-cell population based on the forward scatter area, as doublet and aggregated cells exhibit higher forward scatter areas. To exclude dead cells, the cell suspension was incubated with propidium iodide for 5 minutes before proceeding with flow cytometry analysis. Cells with excitation/emission at 535/617 nm were counted as apoptotic.

2.3.11 Single-cell RNA sequencing (scRNA-seq)

2.3.11.1 scRNA-seq library preparation

scRNA-seq library preparation and sequencing were conducted by Genomics Technology Platform, Max Delbrück Center for Molecular Medicine.

For scRNA-seq library generation, the Chromium Next GEM Single Cell 3' Reagent Kit v3.1 dual index (10X Genomics Inc., USA, Cat# PN-1000268) was employed. The experiment involved six samples and was performed on two separate days.

sRNA-seq library preparation workflow:

3.3.10.1.1. Cell barcoding and separation
3.3.10.1.2. cDNA barcoding with reverse transcription
3.3.10.1.3. cDNA purification
3.3.10.1.4. cDNA amplification
3.3.10.1.5. 3’ Gene expression library construction

3.3.10.1.5.1. cDNA fragmentation, end repair, and A-tailing
3.3.10.1. 5.2. cDNA post-fragmentation, A-tailing double-sided size selection
3.3.10.1.5.3. cDNA adaptor ligation
3.3.10.1.5.4. cDNA post-ligation purification
3.3.10.1.5.5. Sample index PCR
3.3.10.1.5.6. Post Sample Index PCR double-sided size selection
3.3.10.1.5.7. Quality control analysis

2.3.11.1.1 Cell barcoding and separation

To create a droplet emulsion targeting 10,000 cells, a 75 µl solution was prepared by combining 2 µl of nuclease-free water, 41.3 µl of single-cell suspension, and the Master Mix. This solution was carefully added to the first row of the microfluidic Next Gem Chip G (10X Genomics Inc., USA, Cat# PN-1000120).

Master Mix	**Catalog number**	**1x (µl)**
RT Reagent B	2000165	18.8
Template Switch Oligo	3000228	2.4
Reducing Agent B	2000087	2
RT enzyme C	2000085	8.7

To optimize the droplet generation process, the unused wells in the first row of the Next Gem Chip G were filled with 70 µl of 50% Glycerol. Moving to the second row, 50 µl of either Single-cell 3’ v3.1 Gel Beads (2000164) or 50% Glycerol (for unused wells) was added. The third row of the Next Gem Chip G was filled with 45 µl of Partitioning oil (2000190) or 45 µl of 50% Glycerol for unused wells.

Subsequently, the prepared Gem Chip G was promptly loaded into the Chromium Controller X (10X Genomics Inc., USA) and processed for 18 minutes. During this step, the partitioning oil droplet facilitated the combination of a single cell with a unique barcode, ensuring the separation of individual cells and the generation of droplets for downstream single-cell analysis.

2.3.11.1.2 cDNA barcoding with reverse transcription

After the completion of single-cell barcoding and separation, the next step involves reverse transcription to generate barcoded cDNA from polyadenylated mRNA. This

process is carried out by incubating samples in a thermal cycler using the following protocol:

Step	Temperature (°C)	Time (min)
1	53	45
2	85	5
3	4	Hold

Following the reverse transcription reaction, the recovery agent and partitioning oil were discarded. Simultaneously, the aqueous phase, which contains the generated cDNA, was retained for subsequent purification and amplification steps in the single-cell RNA sequencing workflow. This separation allows for the isolation and processing of the cDNA, ensuring the fidelity and quality of the sequencing data obtained from individual cells.

2.3.11.1.3 cDNA purification

For the purification of first-strand cDNA from the reverse transcription reaction, a 200 µl volume of Dynabeads Cleanup Mix was introduced to the aqueous phase. The entire solution was then subjected to pipetting ten times and incubated for 10 minutes at room temperature. An additional pipetting step was performed 5 minutes into the incubation period. This purification step is crucial for removing unwanted components and contaminants, ensuring the isolation of high-quality cDNA for subsequent analyses in the scRNA-seq workflow.

Dynabeads Cleanup Mix	Catalog number	1x (µl)
Cleanup buffer	2000088	182
Dynabeads MyOne SILANE	2000048	8
Reducing agent B	2000087	5
Nuclease-free water		5

Following the incubation period, magnetic separation was employed using a 10x Magnetic Separator to effectively separate the Dynabeads. Subsequently, the supernatant (containing the aqueous phase and recovery agent) was carefully removed, leaving the Dynabeads behind. The remaining Dynabeads underwent two washes with 200-300 µl of freshly prepared 80% ethanol, each lasting for 30 seconds. After each

wash, a brief centrifugation and magnetic separation were performed to remove the remaining ethanol. The washed Dynabeads were then subjected to incubation with Elution Solution I for 2 minutes, followed by one more round of magnetic separation to isolate the purified cDNA. This multi-step process ensures the efficient removal of contaminants and the recovery of high-quality cDNA for subsequent analyses.

Elution Solution I	**Catalog number**	**1x (µl)**
Buffer EB	Qiagen, 19086	98
10% Tween 20		1
Reducing Agent B	2000087	1

2.3.11.1.4 cDNA amplification

The cDNA amplification process involves mixing the samples with a cDNA amplification mix and incubating them in a thermal cycler. The amplification protocol followed these steps:

cDNA Amplification Reaction Mix	**Catalog number**	**1x (µl)**
Amp Mix	2000047	50
cDNA primers	2000089	15

Step	**Temperature (°C)**	**Time (min)**	**Cycles number**
1	98	3	1
2	98	15 s	11
3	63	20 s	11
4	72	1	11
5	98	15 s	11
6	72	1	1
7	4	Hold	

After cDNA amplification, the next steps involved purification and elution. The amplified cDNA was subjected to a 5-minute incubation with 0.6x SPRIselect reagent (Beckman Coulter, B23318). Following this, a magnetic separation process was applied to separate the cDNA from the reagent. Subsequently, the purified cDNA underwent two washes with ethanol, each followed by a brief centrifugation. After removing the remaining ethanol, the cDNA was eluted by pipetting it 15 times with 40.5 µl buffer EB. Finally, a final magnetic

separation step was performed to obtain the purified and eluted cDNA, ready for further downstream applications. This purification process ensures the removal of contaminants and the recovery of high-quality amplified cDNA.

2.3.11.1.5 3' Gene expression library construction

2.3.11.1.5.1 cDNA fragmentation, end repair, and A-tailing

For the library preparation of purified and amplified cDNA, a 10 µl of cDNA was employed. The library preparation process began by mixing the cDNA with 25 µl of buffer EB and 15 µl of Fragmentation mix. This mixture was then pipetted 15 times to ensure thorough mixing. The following protocol was applied to initiate fragmentation, end repair, and A-tailing:

Fragmentation Mix	**Catalog number**	**1x (µl)**
Fragmentation Buffer	200091	5
Fragmentation Enzyme	200090	10

Step	**Temperature (°C)**	**Time (min)**
Fragmentation	32	5
End repair and A-tailing	65	30
Hold	4	Hold

2.3.11.1.5.2 cDNA post-fragmentation, A-tailing double-sided size selection

After the fragmentation, end repair, and A-tailing steps in library preparation, the double-sided size selection process proceeded as follows. Samples were pipetted 15 times and incubated for 5 minutes at room temperature with 30 µl of 0.6x SPRIselect reagent, followed by magnetic separation. The supernatant was then mixed with 10 µl of 0.8x SPRIselect reagent, underwent a 5-minute incubation at room temperature, and was subjected to magnetic separation. Two washes with 80% ethanol were performed, followed by a final magnetic separation. The samples were mixed with 50.5 µl of buffer EB, incubated for 2 minutes at room temperature, and then subjected to a final magnetic separation. These steps ensure size selection, purification, and removal of unwanted fragments, preparing the library for downstream sequencing applications.

2.3.11.1.5.3 cDNA adaptor ligation

For adaptor ligation, the samples were combined with the Adaptor ligation mix and incubated in a thermal cycler following the specified protocol:

Adaptor Mix	Catalogue number	1x (µl)
Ligation Buffer	200092	20
DNA Ligase	220110	10
Adaptor Oligos	2000094	20

Step	Temperature (°C)	Time (min)
1	20	15
Hold	4	Hold

The process allows for the attachment of sequencing adaptors to the cDNA fragments, enabling the identification and sequencing of individual molecules in the subsequent steps.

2.3.11.1.5.4 cDNA post-ligation purification

Following adaptor ligation, post-ligation purification involved pipetting and a 5-minute incubation at room temperature with 80 µl of 0.8x SPRIselect reagent. This was followed by magnetic separation, two washes with 80% ethanol, brief centrifugation, addition, and 15x pipetting with buffer EB, and a final magnetic separation.

2.3.11.1.5.5 Sample index PCR

Samples (30 µl), were combined with 50 µl of Amp Mix (Cat# 20000470) and 20 µl of Dual Index TT Set A (Cat# 1000215). The sample index PCR was then carried out, following the specified protocol:

Step	Temperature (°C)	Time (min)	Cycles number
1	98	45	1
2	98	20 s	16
3	54	30 s	16
4	72	20 s	16
5	98	20 s	16
6	72	1	1
7	4	Hold	

2.3.11.1.5.6 Post Sample index double-sided size selection

Samples (30 µl) were combined with 60 µl of 0.6x SPRIselect reagent. They underwent 15x pipetting, followed by a 5-minute incubation at room temperature and magnetic separation. The supernatant was then mixed with 20 µl of 0.8x SPRIselect reagent, pipetted 15 times, incubated for 5 minutes at room temperature, and subjected to magnetic separation. Beads were washed twice with 80% ethanol, centrifuged, magnetically separated, combined with 35.5 µl of buffer EB, incubated for 3 minutes, and magnetically separated. This multi-step process ensured the purification and concentration of the PCR-amplified samples, preparing them for downstream sequencing applications.

2.3.11.1.5.7 Quality control analysis

Quality control was performed with High Sensitivity D1000 Screen Tape (Agilent, USA).

2.3.11.2 Sequencing

The library pools underwent denaturation by treating them with 0.2 M NaOH, followed by centrifugation at 280g for 1 minute and an 8-minute incubation. The reaction was neutralized by incubating the samples with 400 mM Tris-HCl pH 8.0 and then centrifuging at 280g for 1 minute. Subsequently, the samples were sequenced on a NovaSeq 6000 instrument (Illumina, USA) to achieve a depth of 40,000 mean read pairs per cell. This sequencing step is crucial for obtaining the genomic information from the prepared libraries.

2.3.11.3 Data analysis

Data analysis, encompassing sequence alignment, gene-level count analysis, data normalization, and dimensional reduction, was conducted by Per Qvist, an associate professor at the Department of Biomedicine of Aarhus University.

2.3.11.3.1 Data alignment to mouse genome

The sequence data underwent alignment to the mouse genome GRCm39 using STAR version 2.7.8a [196] on Galaxy [197]. The workflow for sequence alignment involved two main steps. First, genome index files were generated from the mouse reference genome sequences and annotations. Subsequently, scRNA-seq reads generated during sequencing were mapped to these genome index files. During the mapping process, CellRanger > 3 was utilized to filter out unique molecular identifiers with lower counts that matched to more than one gene.

2.3.11.3.2 Single count matrix creation

Gene-level counts for cells in each sample were aggregated into a single count matrix using the DropletUtils tool [198] on Galaxy [197]. The process involved generating a single count matrix from gene-level counts using the **createDropletObject** function. Quality control was performed to filter out low-quality cells with the **dropletFilter** function. Finally, the single counts matrix was obtained using the **DropletUtils::counts** function from DropletUtils.

2.3.11.3.3 Pretreatment analysis, normalization and dimensional reduction

Pretreatment analysis, normalization and dimensional reduction were performed using Automated Single Cell Analysis Platform VI (ASAP) [199]. The filtering criteria for cell exclusion were based on the following thresholds: quantity of genes per cell (1000), protein-coding gene count (80), mitochondrial content (20), ribosomal content (40), and sequence reading depth (1000). After the pretreatment process, 8,846 cells and 22,106 genes were retained for further analysis.

Normalization of the data was performed using Seurat [200]. During this step, feature counts for each cell were divided by the total counts for that cell, multiplied by the scale factor (10000), and then natural log-transformed.

Dimensional reduction was achieved through uniform manifold approximation and projection (UMAP) [201]. This method calculates pairwise distances between cells based on their gene expression profiles and identifies nearest neighbors for each cell [201]. Clusters of cells were annotated using Seurat based on highly upregulated differentially expressed genes (DEGs) for each cluster [202]. The gene count in cells from one cluster was compared to all the other cells, and upregulated genes for each cluster were utilized for cluster annotation.

2.3.11.3.4 Differential gene expression

Differentially expressed gene analysis was performed with linear models for microarray data (limma) [203] or model-based analysis of single-cell transcriptomics (MAST) [204] in RStudio.

Differentially expressed gene analysis workflow with limma:

1. Cluster data extraction
2. Gene filtering
3. Data normalization with trimmed mean of M values (TMM) method
4. Design and contrast matrix creation
5. Linear model fit creation with design and contrast matrix
6. Empirical Bayes moderation of the standard errors
7. Differential gene expression with linear models for microarray data (limma)

From the normalized single-count matrix, cell gene counts for each cluster were extracted based on a metadata file containing information on cell cluster accession, cell type, and genotype. The extracted data underwent filtering to exclude genes present in fewer than 3 cells. Subsequently, the extracted and filtered data were normalized using the TMM method, implemented through the **calcNormFactors** command [205,206]. The TMM method normalizes the read count for each gene based on the total sum of counts across all genes for each cell. It calculates the log2 fold change (M value) between *Sorcs2*$^{+/+}$ and *Sorcs2*$^{-/-}$ samples using the following formula:

$$M = log_2 \frac{Sorcs2^{-/-} samples\ count}{Sorcs2^{+/+} samples\ count}$$

M values are then used to calculate an absolute expression count (A) with the following formula:

$$A = \frac{log_2(Sorcs2^{-/-}\ sample) + log_2(Sorcs2^{+/+}\ sample)}{2}$$

For each cell, upper and lower percentages of the data were trimmed by 30% for M values and 5% for A values to eliminate DEGs [205,206]. Subsequently, a trimmed M value was determined for each cell, and the single-count matrix was scaled by the trimmed M value and the total count [205,206]. This process helps in normalizing and adjusting the data, ensuring that it is appropriately scaled for further analysis.

Following the normalization process, design and contrast matrices were created based on genotype and batch accession of cells in the metadata. These matrices were then utilized to fit the linear model on the gene expression data using the **lmFit()** function, facilitating the modeling of the relationship between gene expression levels and genotypes [203]. Subsequently, the linear model's standard errors were subjected to empirical Bayes moderation with the **eBayes()** function to enhance the stability of differential expression estimates [207]. The final step before conducting DEG analysis involved the application of the **topTable()** function. This function was used to identify highly differentially expressed genes based on significance criteria such as a p-value threshold (<0.05) and a false discovery rate (<0.05) [203].

In the pursuit of understanding the differential expression of genes associated with glucose and insulin handling, maturation, and transcription factors, data specific to *Sorcs2*$^{+/+}$ β cell clusters was extracted. This extracted matrix was then transformed into a Seurat object utilizing the **CreateSeuratObject()** function. The identification of differentially expressed marker genes was carried out through the MAST test, employing the **FindMarkers()** function. To enhance interpretability, the results were visualized with violin plot using the **ggplot()** function.

2.3.11.3.5 Data availability

The raw scRNA-seq data has been deposited in the GEO database under the accession number GSE231551. The detailed scRNA-seq data analysis is accessible at https://asap.epfl.ch/ with the public key: ASAP93.

2.3.11.3.6 Gene Ontology (GO) analysis

GO analysis was conducted using the clusterProfiler R package [208,209] within RStudio. The list of differentially expressed genes and log2(Fold change), obtained through limma analysis, served as input. The analysis utilized mouse genome-wide annotation packages from Bioconductor [210].

For cell-type-specific GO analysis between genotypes, differentially expressed genes were initially sorted by log2 (Fold change). Gene Set Enrichment Analysis (GSEA) [211] was then applied using the **gseGO()** function. GSEA was chosen for its capacity to consider the overall expression pattern of genes, providing insights into the impact of *Sorcs2*$^{-/-}$ on pathways [212]. Key parameters for GSEA included 10,000 permutations (nPerm), a minimum gene set size of 3 (minGSSize), a maximum gene set size of 800 (maxGSSize), a p-value cutoff of 0.05, and the Benjamini-Hochberg procedure for p-value adjustment.

Visualization of GO terms was achieved using the **dotplot()** and **cnetplot()** functions from the clusterProfiler R package [208,209]. The dot plot presents a list of activated or suppressed pathways, sorted by normalized enrichment score and linked to differentially expressed genes. The net plot illustrates all genes and their expression patterns found among the differentially expressed genes associated with a specific GO term, as presented in the dot plot.

To characterize beta clusters with aberrant cell numbers in *Sorcs2*$^{-/-}$ samples, gene counts in these clusters were compared with those in *Sorcs2*$^{+/+}$ samples using limma analysis. Overrepresentation analysis (ORA) was selected for this purpose due to its less stringent nature [212]. ORA analysis was conducted with the **enrichGO()** function, employing parameters such as 10,000 permutations (nPerm), a minimum gene set size of 3 (minGSSize), a maximum gene set size of 800 (maxGSSize), a p-value cutoff of 0.05,

and the Benjamini-Hochberg procedure for p-value adjustment. Visualization of GO terms was accomplished using a lolliplot plot created with the **ggplot()** function in RStudio.

2.4 General methods

2.4.1 PCR for mouse genotyping

Genomic DNA for genotyping PCR was extracted from mouse ear punch biopsies. The tissue was incubated for 30 minutes at 95°C in a base solution containing 25 mM NaOH and 0.2 mM EDTA. The reaction was halted by adding an equal volume of neutralizing solution (Tris-HCl). The extracted DNA was then utilized for PCR using the following cycling conditions:

Step #	Step	Temperature	Time	Cycles number
1	Initial denaturation	94°C	2 min	
2	Denaturation	94°C	15 sec	40
3	Annealing	53°C	15 sec	
4	Elongation	72°C	30 sec	

The PCR primers employed are detailed in Table 1. The reaction mixture comprised 0.025 U/µl Taq DNA polymerase, 1x Buffer, 0.2 mM of each deoxynucleotide triphosphate, 1x Cresol Red, and 0.2 µM primers. PCR products were separated on a 2% agarose gel. The anticipated sizes of PCR products used for determining mouse genotypes were 370 bp (*Sorcs2*$^{+/+}$) and 246 bp (*Sorcs2*$^{-/-}$).

2.4.2 Western Blotting

Protein concentration in islet lysates was determined through Western Blotting. After overnight recovery, pancreatic islets were collected in low-protein binding tubes and lysed using 80 µl of lysis buffer. The lysis was facilitated by sonicating the samples for 10 seconds, repeated twice, at 50% power, followed by a 2-hour incubation on ice. The total protein content was quantified using the Pierce BCA protein assay kit (Thermo Fischer Scientific, Cat# 23225). Following this, the sample's protein concentration was adjusted with sterile water. Then, 5 µl of 4x Laemmli sample buffer (Table 4) was added to 15 µl of the diluted samples. Subsequently, the samples were boiled at 97°C for 5 minutes. The prepared samples were then loaded into a 4-12% Tris-Glycine Mini Protein Gel and run

for 1.5 hours at 120 V using a running buffer in a Thermo Fisher Scientific vertical electrophoresis chamber. Gels were then transferred onto a 0.45 µm nitrocellulose membrane, running for 1.5 hours at 80V and 200 mA per blot with a transfer buffer in a Bio-Rad trans-blot cell.

Nitrocellulose membranes were incubated with a blocking solution (Table 4) for 1 hour, followed by three 5-minute washing steps using a washing solution (Table 4). Membranes were then incubated overnight at 4°C with primary antibodies (Table 3), which were diluted in an antibody diluent (Table 4). The following morning, membranes were washed three more times for 5 minutes each with the washing solution and subsequently incubated with secondary antibodies (Table 3) for 1 hour at room temperature in the antibody diluent. After three additional washing steps, the membranes were developed using chemiluminescent detection with SuperSignal West Femto maximum sensitivity substrate (Thermo Fischer Scientific, Cat#34096). Band intensities were analyzed by densitometry using ImageJ software.

2.4.3 RNA isolation and RT-qPCR

Total RNA extraction was performed using the RNeasy Micro kit (Qiagen, #74004), and RNA concentrations were measured using a NanoDrop ND-1000 spectrophotometer. Equal amounts of RNA (50 ng) were then reverse transcribed into cDNA using the high-capacity RNA to cDNA kit (Applied Biosystems, #4387406). The resulting cDNA samples underwent quantitative real-time PCR (qRT-PCR) using TaqMan Gene Expression Assays as detailed in Table 2. The 7900HT Fast Real-time PCR system (Thermo Fisher Scientific) was employed for qRT-PCR, and relative gene expression was quantified using the cycle threshold (CT) comparative method (2-ddCT) with normalization to *Gapdh* and *18sRNA* CT values.

2.4.4 Statistical data analysis

The data were analyzed using GraphPad Prism 7.0 (GraphPad Software, USA). Normal distribution was assessed using either the D'Agostino-Pearson omnibus normality test or the Shapiro-Wilk normality test, depending on the sample size. Student's t-test or Mann-Whitney test was employed for the analysis of two groups, depending on data distribution. The ROUT 1% outlier test was applied to insulin and C-peptide GSIR data, extreme

values were removed from the further analysis. Repeated measures two-way ANOVA with Sidak's multiple comparison's test was used for analysis of dependable variable over different time points. Non-repeated measured two-way ANOVA with Tukey's multiple comparison test was used for independent variables. The results are presented as the mean ± SD, and significance was considered at $p \leq 0.05$.

3 Results

3.1 SORCS2 deficiency affects the body weight of mice

Given the established genetic association between *SORCS2* and human BMI, I conducted an examination to assess the impact of receptor deficiency on the body weight of mice under different conditions, specifically before and after an overnight period of starvation. Notably, SORCS2-deficient mice exhibited a substantial weight reduction both prior to and following starvation in comparison to their wild-type counterparts (Figure 9 A). It is crucial to highlight that the observed decrease in weight among receptor mutants was not accompanied by a corresponding change in the length of the animals (Figure 9 B). This similarity in length across genotypes suggests that the weight reduction in SORCS2-deficient mice is likely attributable to factors beyond developmental considerations.

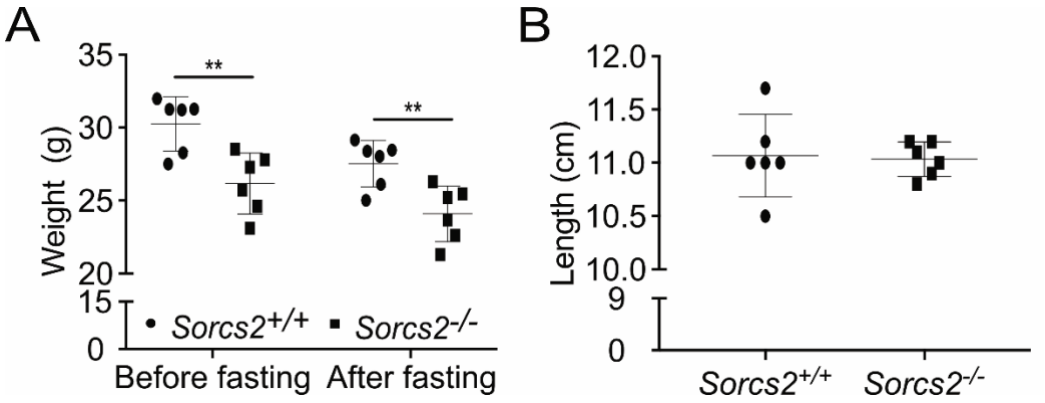

Figure 9: SORCS2 deficiency affects body weight in mice

(A) Body weights of *Sorcs2*$^{+/+}$ and *Sorcs2*$^{-/-}$ mice measured before and after 16 h of fasting (n=6 animals per genotype).

(B) The length of *Sorcs2*$^{+/+}$ and *Sorcs2*$^{-/-}$ animals was measured from the nose to the beginning of the tail (n=6 animals per genotype).

The significance of data was determined using two-way ANOVA followed by Sidak's multiple comparisons tests (A) or using an unpaired t-test (B). **, $p \leq 0.01$.

3.2 SORCS2 deficiency affects lipid and glycogen levels in metabolic tissues

The precise regulation of fat and glucose metabolism in peripheral tissues is under tight control by insulin and glucagon levels in the circulation [213,214]. With regards to lipid metabolism, insulin exerts inhibitory effects on lipolysis and fatty acid oxidation while concurrently promoting the biosynthesis of fatty acids, cholesterol, and triglycerides [215–217]. Conversely, glucagon operates in direct opposition, exerting effects that counterbalance insulin by promoting gluconeogenesis and inhibiting the synthesis of lipids [119,218].

Given the previously identified associations of *Sorcs2*$^{-/-}$ mice with decreased respiratory exchange ratios and impaired glucose tolerance [185], a comprehensive investigation was conducted to explore whether the loss of receptor activity also influences lipid and glycogen levels in plasma and metabolic tissues.

To investigate these dynamics, *Sorcs2*$^{+/+}$ and *Sorcs2*$^{-/-}$ I subjected mice to overnight starvation, following which I collected blood, liver, and gastrocnemius muscles the subsequent morning. Lipids were extracted from the liver and muscles following the protocol outlined in the Free Fatty Acid Quantification Kit (refer to the methods section 2.2.3). Subsequent analyses of free fatty acids, free and total cholesterol, and triglycerides were conducted utilizing fluorometric kits (Table 5). Glycogen extraction and analysis were performed in accordance with the Glycogen Colorimetric/Fluorimetric assay kit protocol (refer to the methods section 2.2.4).

While plasma and skeletal muscle lipid levels exhibited no significant alterations in SORCS2-deficient mice (Table 7 and Table 9), notable reduction in total and free cholesterol, along with a decrease in fatty acids, was observed in the liver (Table 8) compared to control groups. Additionally, both liver and muscle glycogen levels displayed a significant decrease (Table 8 and Table 9).

The observed reduction in storage lipids and glycogen aligns with the possibility of impaired insulin action in mutant mice. Notably, despite the previously established normal insulin tolerance in SORCS2-deficient mice, the substantial decrease in liver lipids and glycogen levels prompts the hypothesis of SORCS2 involvement in insulin secretion.

Table 7: Plasma lipids levels in Sorcs2$^{+/+}$ and Sorcs2$^{-/-}$ animals

Blood was collected from overnight starved *Sorcs2*$^{+/+}$ and *Sorcs2*$^{-/-}$ mice and centrifugated to obtain plasma. Lipid levels were analyzed by colorimetric or fluorometric kits (Table 5). The significance of data was determined using an unpaired t-test (Total cholesterol, Free cholesterol, Free fatty acids) or Mann-Whitney U test (Triglycerides). Data are given as mean ± standard deviation (SD) (Total cholesterol, Free cholesterol, Free fatty acids) or median with 25 and 75 quartiles (Triglycerides). Data were considered significant if $p \leq 0.05$. df, degrees of freedom; t, t-test; p, p-value; U, U-test.

	Sorcs2$^{+/+}$		*Sorcs2*$^{-/-}$					
	mean ± SD median [25; 75 quartiles]	n	mean ± SD median [25; 75 quartiles]	n	df	t	U	p
Total cholesterol (μg/ml)	1717 ± 994.6	12	1371 ± 648	12	22	1.01		0.3235
Free cholesterol (μg/ml)	558.5 ± 188.1	12	516.8 ± 147.9	12	22	0.6		0.5528
Free fatty acids (nmol/ml)	1716 ± 547.8	12	2023 ± 669.3	12	22	1.23		0.2309
Triglycerides (mg/dl)	78.57 [73.2; 97.55]	12	84.89 [71.22; 98.07]	12	22		64	0.6707

Table 8: Liver lipids and glycogen levels in *Sorcs2*$^{+/+}$ and *Sorcs2*$^{-/-}$ animals

Liver from *Sorcs2*$^{+/+}$ and *Sorcs2*$^{-/-}$ animals was extracted from overnight starved mice. Lipids and glycogen were isolated and analyzed by commercially available colorimetric or fluorometric kits (Table 5). The significance of data was determined using an unpaired t-test (Total cholesterol, Triglycerides, Glycogen) or Mann-Whitney U test (Free cholesterol, Free fatty acids). Data are given as mean ± standard deviation (SD) or median with 25 and 75 quartiles. Data were considered significant if $p \leq 0.05$. df – degrees of freedom, t, t-test, U, U-test, p, p-value.

	Sorcs2$^{+/+}$		*Sorcs2*$^{-/-}$					
	mean ± SD/ median [25; 75 quartiles]	n	mean ± SD/ median [25; 75 quartiles]	n	df	t	U	p
Total cholesterol (μg/ml)	127.5 ± 15.7	10	98.66 ± 15.27	11	19	4.3		0.0004
Free cholesterol (μg/ml)	99.95 [88.97; 104.5]	10	77.96 [65.74; 85.29]	11			10	0.0008
Free fatty acids (nmol/ml)	67.97 [47.29; 92.31]	10	16.31 [10.42; 39.8]	11			3	<0.0001
Triglycerides (mg/dl)	155.5 ± 47.12	10	125 ± 52.41	11	19	1.4		0.1757
Glycogen (μg/ml)	215.1 ± 139.1	17	86.96 ± 46.91	16	31	3.5		0.0014

Table 9: Skeletal muscles lipids and glycogen levels in *Sorcs2*$^{+/+}$ and *Sorcs2*$^{-/-}$ animals

Gastrocnemius muscles were extracted from overnight starved *Sorcs2*$^{+/+}$ and *Sorcs2*$^{-/-}$ mice. Lipids and glycogen were isolated and analyzed by colorimetric or fluorometric kits (Table 5). The significance of data was determined using an unpaired t-test (Glycogen) or Mann-Whitney U test (Total cholesterol, Free cholesterol, Free fatty acids; Triglycerides). Data are given as mean ± standard deviation (SD) or median with 25 and 75 quartiles. Data were considered significant if $p \leq 0.05$. df, degrees of freedom; t, t-test; p, p-value; U, U-test.

	Sorcs2$^{+/+}$		*Sorcs2*$^{-/-}$					
	mean ± SD median [25; 75 quartiles]	n	mean ± SD median [25; 75 quartiles]	n	df	t	U	p
Total cholesterol (μg/ml)	15.85 [14.25;20.31]	10	18.83 [16.88; 20.58]	11			39	0.2816
Free cholesterol (μg/ml)	16.92 [13.91; 24.58]	10	16.44 [14.88; 19.76]	11			52	0.8633
Free fatty acids (nmol/ml)	6.839 [6.054; 8.75]	10	6.589 [5.33; 7.143]	11			39	0.2734
Triglycerices (mg/dl)	51.4 [30.89; 78.53]	10	68.32 [36.07; 119.6]	11			46	0.5573
Glycogen (μg/ml)	27.78 ± 18.32	17	15.91 ± 10.98	17	32	2.3		0.0286

3.3 SORCS2 expression in pancreatic islets is specific to non-β cell types

To determine a possible role for SORCS2 in insulin secretion, I first analyzed SORCS2 expression in pancreatic islet cell types. Previous transcriptomic studies on human [219,220] pancreases showed modest levels of *SORCS2* transcripts in non-β islet cell types. Studies on human stem-derived pancreatic islets showed moderate *SORCS2* expression in all cell types except PP cells [221]. Moreover, *SORCS2* had a prominent expression in differentiating α and β stem cells [221]. Transcriptomic studies on mouse pancreases, except for expression in all non-β cells, showed a slight level of *Sorcs2* transcripts in a low population of β cells [222,223].

To substantiate expression at the protein level, I analyzed SORCS2 protein expression in isolated pancreatic islets with western blotting. I confirmed SORCS2 expression in overnight cultured isolated pancreatic islets from *Sorcs2*$^{+/+}$ animals and lack of expression in *Sorcs2*$^{-/-}$ tissue (Figure 10 A).

To substantiate protein expression of SORCS2 in individual cell types, I co-stained SORCS2 with pancreatic islets markers (glucagon for α-cells, insulin for β-cells, polypeptide Y for PP-cells and somatostatin for δ-cells).

Co-staining showed predominant expression of SORCS2 in α, δ, and PP cells, with no apparent protein expression in β-cells (Figure 10 B and C).

As mouse pancreatic islet *Sorcs2* transcript levels in β-cells were low and only in a minuscule β-cell population, I believe the sensitivity of SORCS2 antibody was not high enough to capture SORCS2 in β-cells. Another explanation may lie in the nature of transcriptomic data, which only by 40% predicts protein expression due to post-transcriptional regulation of protein expression and measurement noise, which may have occurred during the preparation of transcriptomic data [224].

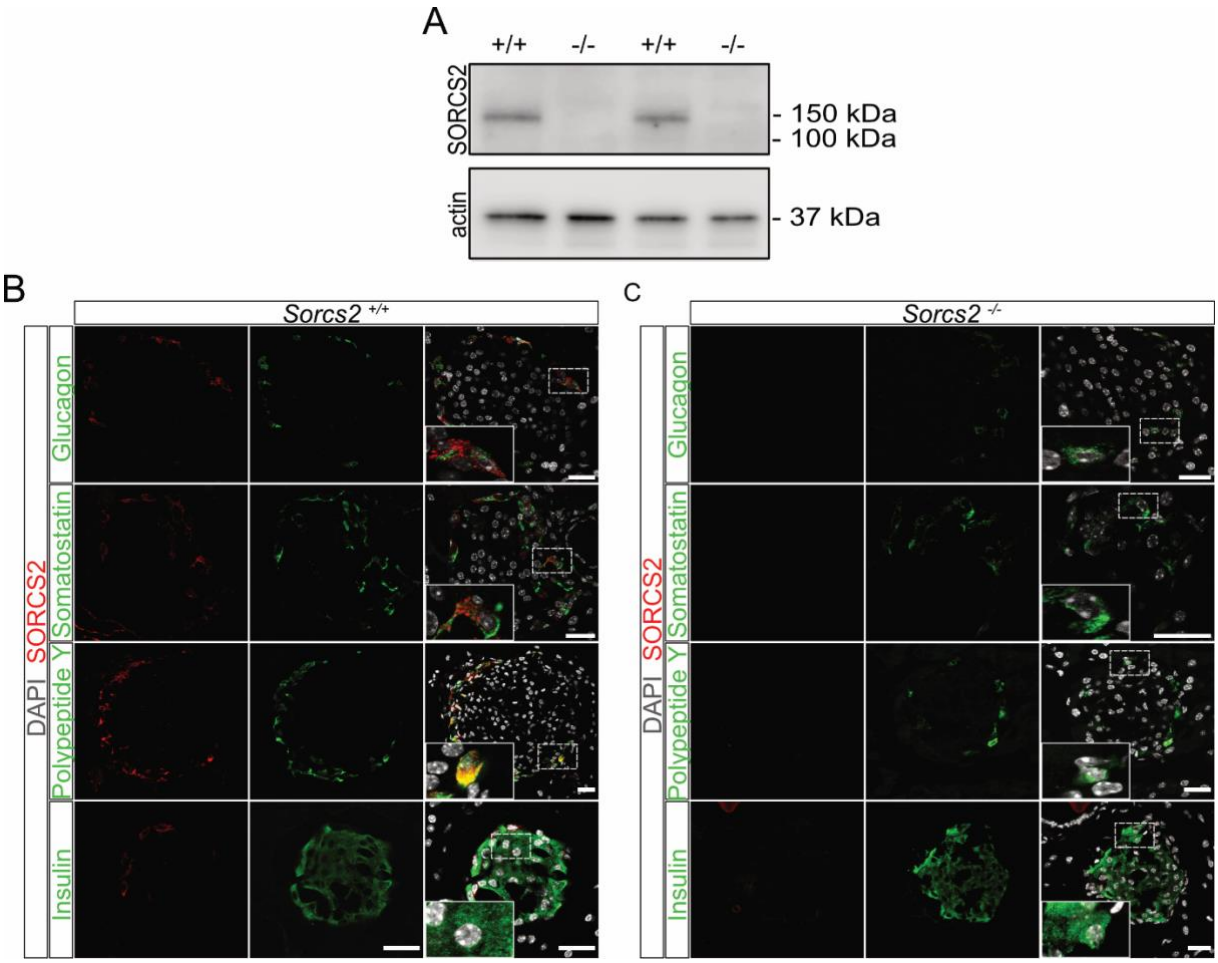

Figure 10: SORCS2 expression in mouse pancreatic islets

(A) Analysis of SORCS2 expression in total lysate from murine islets using western blotting analysis. The receptor is detected in samples from two *Sorcs2*$^{+/+}$ but not two *Sorcs2*$^{-/-}$ mice. Detection of actin served as loading control. The migration of marker proteins of the indicated molecular weights in the gel is given.

(B, C) Immunofluorescent staining of pancreatic sections from *Sorcs2*$^{+/+}$ (B) and *Sorcs2*$^{-/-}$ (C) animals for SORCS2 (red), as well as glucagon, somatostatin, polypeptide Y or insulin (green). Nuclei were counterstained with DAPI (grey). Individual and merged channel configurations are given. Stippled boxes indicate the area of sections shown in the higher magnification insets in the respective panels. SORCS2 is most prominently expressed in α (glucagon+), δ (somatostatin+), and PP (polypeptide Y+) cells of wild-type pancreatic islets. The receptor is not expressed in SORCS2-deficient pancreatic islets. Scale bars, 25 µm

3.4 SORCS2 deficiency blunts insulin secretion *in vivo*

To investigate the impact of *Sorcs2*$^{-/-}$ on insulin secretion, I conducted a glucose-stimulated insulin secretion test (GSIS) to affirm the deficiency in insulin secretion *in vivo*.

Various factors, such as free fatty acids, amino acids, and incretins, can stimulate insulin secretion from β-cells; however, glucose serves as the primary stimulator [103,225,226]. The biphasic nature of insulin secretion upon glucose stimulation is well-documented [103,225,226]. Following glucose uptake through GLUT2 transporters by β-cells, glucose undergoes metabolism to ATP [226]. This process blocks K_{ATP} channels, preventing K^+ outflow and membrane depolarization [226]. Consequently, L-type Ca^{2+} channels are activated, increasing intracellular Ca^{2+} concentration and facilitating the secretion of vesicles from the readily releasable pool of insulin vesicles [226]. This initial process occurs within the first 2-5 minutes, constituting the first phase of insulin secretion [227]. The second phase of insulin secretion gradually develops after the first and lasts for several hours [226,228]. During this phase, reserve insulin vesicles are modified and translocated to the cell membrane through amplifying pathways, activated by metabolic coupling factors such as NADPH, pyruvate, malate, isocitrate, and glutamate [226,228]. Insulin and insulin vesicles are also produced during the second phase of insulin secretion [226,228].

For the *in vivo* GSIS test, mice of both genotypes were injected with a glucose bolus after overnight starvation, and blood was collected before, as well as 2 minutes (first phase) or 30 minutes (second phase) after injection (for details refer to methods section 2.2.6). Plasma insulin and C-peptide levels were measured using ELISA (Table 6). C-peptide measurement was employed as a control for insulin determination, as both C-peptide and insulin are cleaved from proinsulin and secreted in equimolar concentrations [229,230]. Notably, C-peptide bypasses hepatic degradation, exhibiting a longer half-life and steadier metabolic rate than insulin [229,230].

Both insulin (Figure 11 A, B) and C-peptide (Figure 11 C, D) levels exhibited a decrease 2 or 30 minutes after glucose injection. In contrast, basal insulin concentrations remained unaffected, although basal C-peptide levels in mutant mice tended towards a decrease (Figure 11 C, D). Given that C-peptide provides a more

accurate measurement of insulin secretion, these findings suggest a general deficiency in insulin secretion in SORCS2-deficient mice.

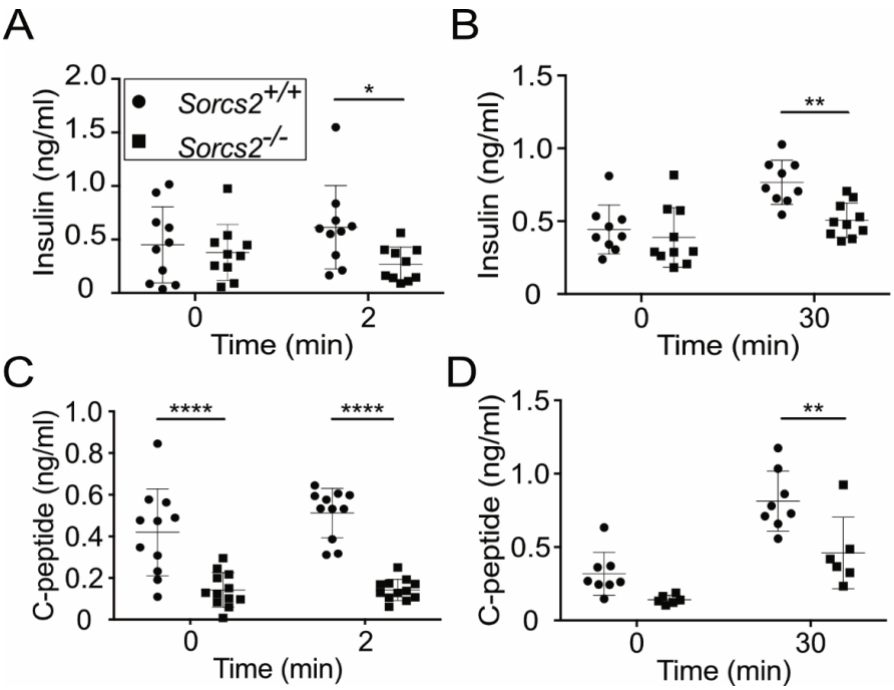

Figure 11: SORCS2 deficiency blunts insulin secretion *in vivo*

(A-B) Insulin (A, B) levels were determined in plasma by ELISA under basal conditions, or 2 or 30 minutes after i.p. injection of 2 g/kg body weight of glucose (n = 9-10) animals per group).
(C-D) C-peptide levels were determined in plasma by ELISA under basal conditions, or 2 or 30 minutes after i.p. injection of 2 g/kg body weight of glucose (n = 6-12) animals per group).
The significance of data was determined using two-way ANOVA followed by Sidak's or Tukey's multiple comparisons tests. *, $p \leq 0.05$; **, $p \leq 0.01$.

3.5 SORCS2 deficiency dampens islet insulin secretion *in vitro*

To validate the *in vivo* insulin secretion findings and rule out any impact of SORCS2 deficiency on the central regulation of insulin secretion via the sympathetic and parasympathetic systems [231], I performed GSIS tests on isolated and overnight-cultured pancreatic islets from both genotypes.

To emulate the conditions of *in vivo* GSIS, where insulin secretion was analyzed post-fasting and after high glucose injection, low (1.6 mM) and high (16 mM) concentrations of glucose were utilized to stimulate insulin secretion. A 1-hour incubation with 1.6 mM glucose represented the fasting or basal condition, followed by treatment with high glucose (16 mM) for an additional hour, encompassing both the first and second phases of insulin secretion. Islet supernatants from each step were analyzed for insulin and C-peptide levels using ELISA. As measurement was performed only after one hour

of stimulation with high glucose (16 mM), discrimination between the first and second phases was not feasible (Figure 12 A).

The results revealed a significant decrease in secreted levels of insulin (Figure 12 B) and C-peptide (Figure 12 C) after glucose stimulation, while basal levels remained unaffected. This decrease in glucose-stimulated insulin/C-peptide release corroborated the *in vivo* GSIS findings (Figure 11) and indicated pancreatic islet-specific defects in insulin secretion. However, the comparable basal insulin/C-peptide secretion rates in wild-type mice contradicted the *in vivo* results (Figure 11 C, D). This inconsistency could be attributed to the uptake of C-peptide in muscle cells, where C-peptide acts as a glycogen synthesis stimulator [232,233], or in endothelial cells, where C-peptide protects against oxidative stress [234].

I conducted islet perifusion studies to explore phase-wise differences in insulin secretion due to SORCS2 deficiency. Islets were perifused consecutively with 1.6 mM glucose KRBH for 1 hour and 18 minutes and 16 mM glucose KRBH for 1 hour at a flow rate of 100 µL/min (Figure 12 D, for more details please refer to 2.3.4). No difference was observed in basal (3-18 minutes) and first phase (20-26 minutes) insulin secretion, but a clear distinction was apparent in second phase insulin secretion (28-79 minutes) ($F(1,4) = 10.33$, $p = 0.0038$) (Figure 12 E).

While the decreased glucose-stimulated insulin secretion during the second phase aligned with *in vivo* results (Figure 11 B), the decrease in insulin secretion during the first phase in *in vivo* experiments did not correspond with the perifusion experiment results (Figure 11 A and Figure 12 E). This discrepancy might be explained by a possible faster insulin uptake and degradation rate in other tissues, such as the liver in *Sorcs2*$^{-/-}$ mouse model, which does not occur in the isolated islet perifusion setting [229,230].

To investigate the possibility of a general secretion defect in *Sorcs2*$^{-/-}$ pancreatic islets, islets were stimulated with KCl, a known insulin secretion secretagogue [235–237]. KCl depolarizes β-cell membranes, activating Ca^{2+} L-channels, resulting in calcium influx and, subsequently, insulin secretion [238].

I subjected islets to low (1.6 mM) and high (16 mM) glucose concentrations for an hour, followed by an additional hour with 1.6 mM glucose and a 30-minute stimulation with 30 mM KCl (Figure 12 A). Islet supernatants from each step were analyzed for insulin and C-peptide levels by ELISA (Table 6).

A trend towards decreased insulin secretion after KCl stimulation in *Sorcs2*$^{-/-}$ islets was observed, suggesting a potential generalized defect in insulin release (Figure 12 B). Such global defects may involve membrane depolarization machinery, Ca^{2+} uptake, vesicle docking, or insulin production [235].

Finally, to explore potential insulin production defects in overnight-cultured islets, insulin, C-peptide, and proinsulin protein content were measured. The islet content of insulin (Figure 12 F) and proinsulin (Figure 12 H) was comparable between genotypes. However, the total islet C-peptide content (Figure 12 G) was diminished. The non-equimolar decrease in C-peptide versus insulin levels in SORCS2-deficient tissue suggested disruptions in C-peptide and insulin synthesis, increased lysosomal degradation of C-peptide, and defective insulin/C-peptide vesicle packaging as potential underlying reasons [103,125,239].

3.6 SORCS2 deficiency does not affect pancreatic islet morphology

Given the observed reduction in insulin secretion upon KCl stimulation (Figure 12 B), a suspicion of potential morphological changes in pancreatic islets prompted further investigation.

To assess this hypothesis, I initially analyzed the distribution of distinct cell types within pancreatic islets. Imbalances in the number of cell types could contribute to aberrations in insulin secretion, as hormones secreted from α-cells, PP-cells, or δ-cells play regulatory roles in insulin secretion [127,240–242]. Furthermore, a decrease in β-cell area and mass in *Sorcs2*$^{-/-}$ samples might suggest β cell death.

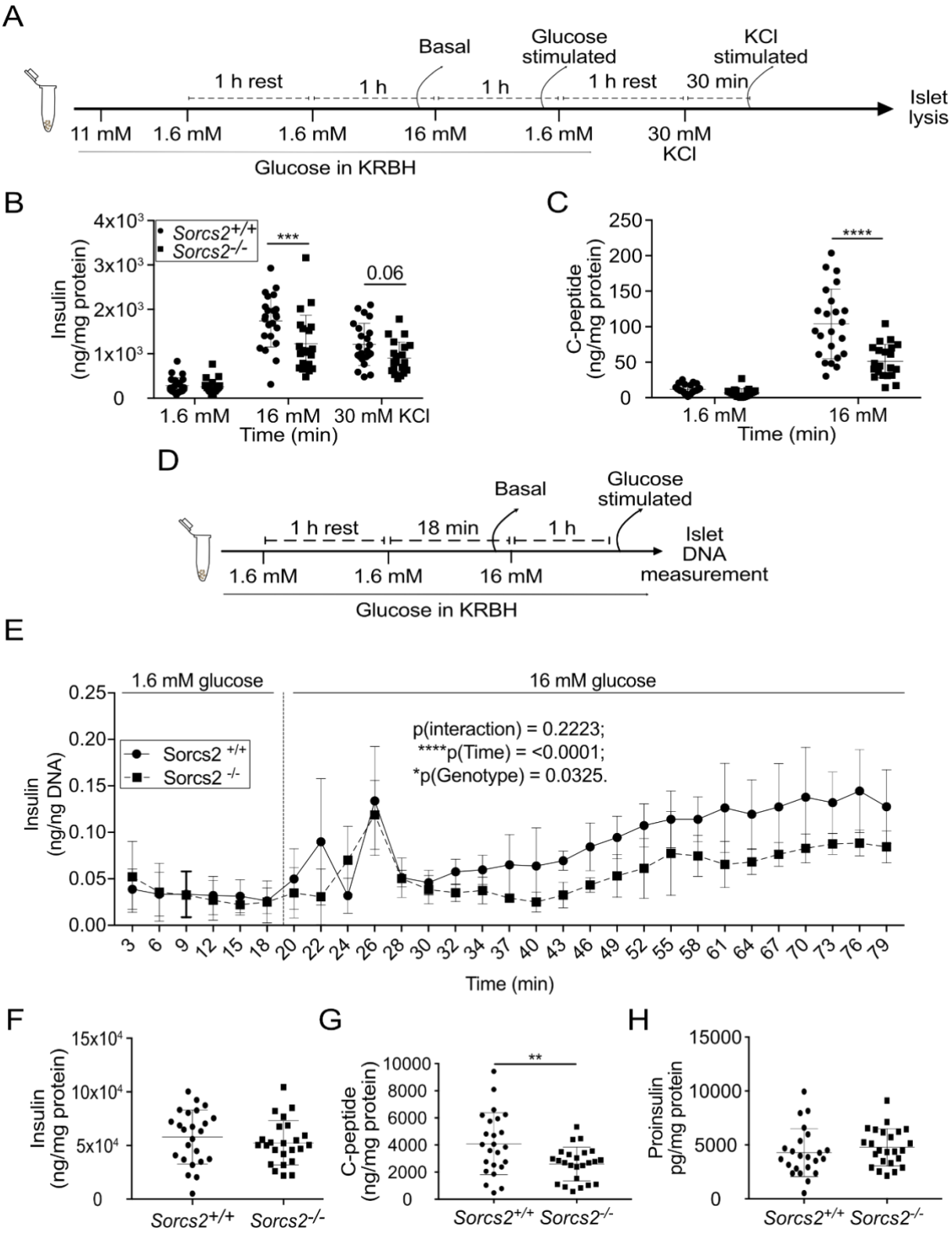

Figure 12: SORCS2 deficiency in pancreatic islets dampens insulin secretion

(A) Protocol for glucose stimulation in isolated pancreatic islets.
(B - C) Insulin and C-peptide levels normalized to total islet protein as determined by ELISA in supernatants of isolated *Sorcs2*$^{+/+}$ and *Sorcs2*$^{-/-}$ islets treated consecutively for one hour with 1.6 mM and 16 mM glucose and one hour with 30 mM KCl in Krebs-Ringer-Bicarbonate Hepes buffer (KRBH) (n = 21-23 animals per genotype)
(D) Protocol for perifusion study for isolated pancreatic islets.

(E) Insulin levels were normalized to the DNA content as determined by ELISA in flow-through of isolated *Sorcs2*$^{+/+}$ (filled circles) and *Sorcs2*$^{-/-}$ (filled squares) islets treated for 18 min with 1.6 mM (basal) and for one hour with 16 mM glucose in KRBH (glucose-stimulated) (n = 3 animals per genotype).
(F-H) Insulin (F), C-peptide (G), and Proinsulin (H) levels were determined by ELISA in lysates of isolated islets from *Sorcs2*$^{+/+}$ and *Sorcs2*$^{-/-}$ animals cultured overnight (n = 24 animals per genotype).
The significance of data was determined using two-way ANOVA followed by Sidak's or Tukey's multiple comparisons tests (B, C, E), or unpaired t-test (F-H), **, $p \leq 0.01$, ***, $p \leq 0.001$; ****, $p \leq 0.0001$;

To evaluate the percentage of pancreatic cell areas occupied by α, δ, PP, or β cells, pancreatic islets were stained with cell-type markers (glucagon for α-cells, insulin for β-cells, polypeptide Y for PP-cells, and somatostatin for δ-cells). The areas covered by specific markers were measured using ImageJ, and this area was divided by the total area of the pancreatic islet in which it was measured.

It was observed that *Sorcs2*$^{-/-}$ pancreatic islets exhibited comparable percentages of areas assigned to different cell types as *Sorcs2*$^{+/+}$ islets, along with a similar pancreatic islet area (Figure 13).

While these results suggest that areas of all cell types in *Sorcs2*$^{-/-}$ pancreatic islets were within the normal range, indicating no apoptotic events or aberrant development among cell types, it is important to note that this analysis was conducted on a single plane of pancreatic islets. Given the irregular spheroid shape of islets, an assay accounting for different planes of the pancreas would provide additional insight.

To corroborate the findings from the cell types area analysis and account for the spheroid shape of pancreatic islets, I analyzed β cell mass in the entire pancreatic tissue between genotypes. Additionally, to elucidate the decrease in *in vivo* basal C-peptide levels, I analyzed the number of pancreatic islets in *Sorcs2*$^{+/+}$ and *Sorcs2*$^{-/-}$ pancreatic tissue. For this analysis, I weighed the pancreatic tissue before processing, cut it into six slices 200 µm apart, and stained it for the β cell marker insulin. β cell area was quantified by dividing the insulin-immunopositive area by the total tissue area, and the total β cell mass in the pancreas was quantified by dividing the β cell area by the pancreas weight (please refer to methods section 2.2.5.3 for more details).

A

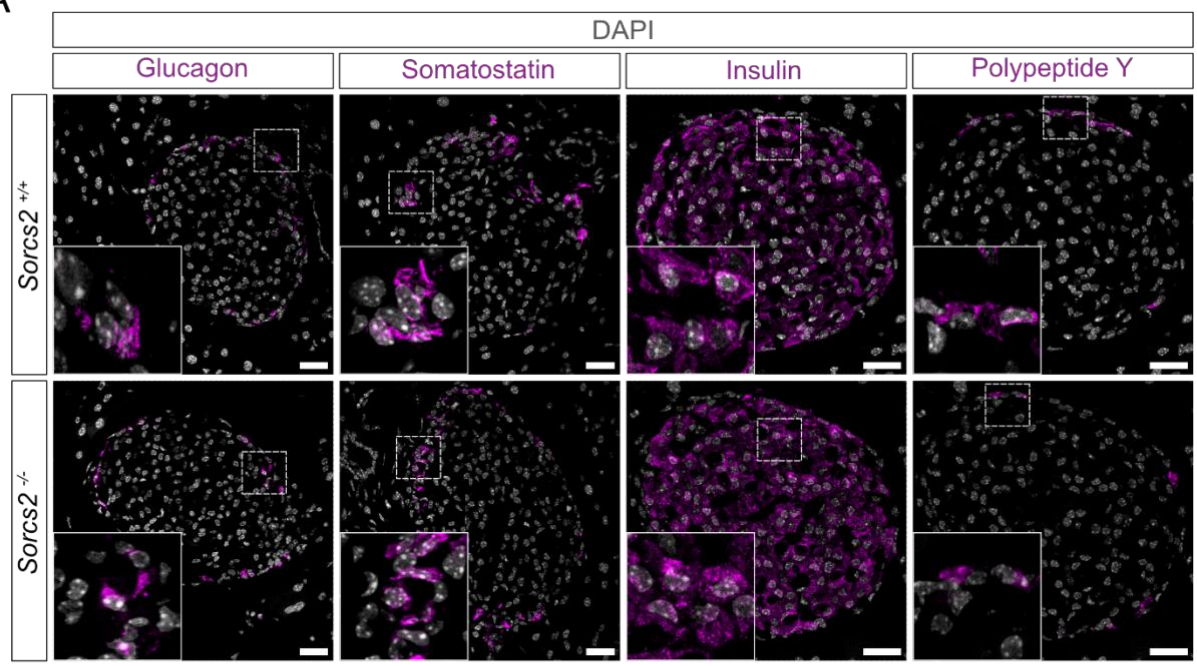

B

% Cell area	mean ± SD		df	t	p
	Sorcs2 $^{+/+}$	*Sorcs2* $^{-/-}$			
Glucagon	6.76 ± 2.6	5.3 ± 2.5	10	0.99	0.3452
Somatostatin	3.57 ± 0.94	3.5 ± 0.7	10	0.12	0.9072
Insulin	58.3 ± 12	55.1 ± 5.93	10	0.6	0.5696
Polypeptide Y	2.74 ± 0.69	3.23 ± 0.99	10	0.998	0.3418
Islet area (pixels)	209175 ± 60844	234180 ± 58412	10	0.73	0.4844

Figure 13: Cell type composition of wild-type and SORCS2-deficient murine pancreatic islets

(**A**) Representative images of murine islets of the indicated *Sorcs2* genotypes immunostained for insulin, glucagon, somatostatin, and polypeptide Y (purple). Nuclei were counterstained with DAPI (grey).
(**B**) Area covered by cells expressing insulin, glucagon, polypeptide Y, or somatostatin in *Sorcs2*$^{+/+}$ and *Sorcs2*$^{-/-}$ pancreatic islets were quantified based on immunohistological stainings for the various hormones (as exemplified in A) and expressed as % of the total islet cell area. For each mouse, 30-35 pancreatic islets were analyzed (n = 6 animals per genotype).
Stippled boxes in A indicate the area of sections shown in the higher magnification insets in the respective panels. Scale bars: 25 µm. Statistical significance was tested by unpaired t-test with $p \leq 0.05$ considered significant. p, p-value.

In these studies, no changes in β cell area or β cell mass were observed when comparing genotypes (Figure 14 B), suggesting that the reduced insulin secretion does not stem from altered β cell number or mass. However, a trend towards a decrease in the number of pancreatic islets in *Sorcs2*$^{-/-}$ pancreases was noted (Figure 14 B). This reduction in the number of pancreatic islets might explain the basal and first-phase C-peptide decrease observed in the *in vivo* GSIR analysis (Figure 11 C, D).

A

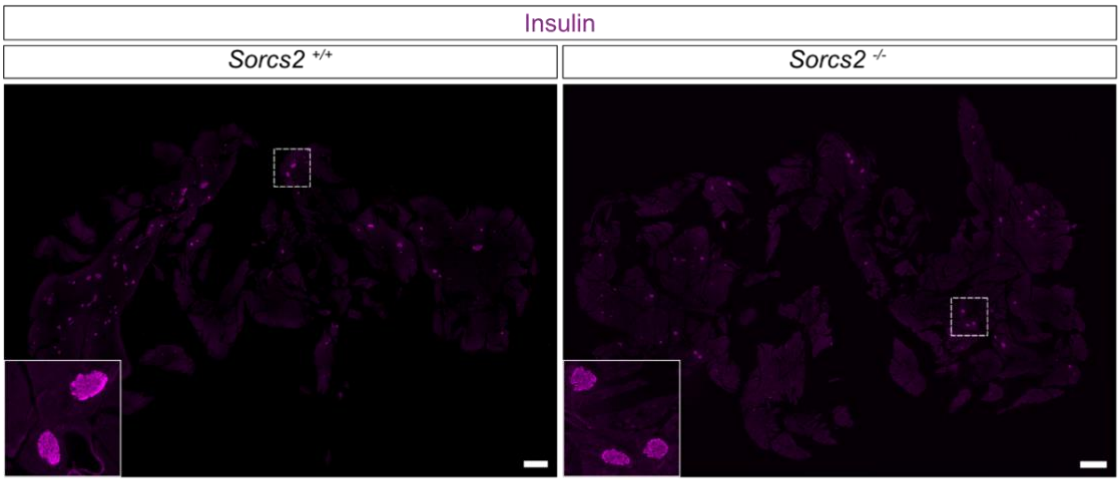

B

	mean ± SD		df	t	p
	Sorcs2 $^{+/+}$	*Sorcs2* $^{-/-}$			
Beta cell area (%)	0.112 ± 0.025	0.09 ± 0.019	9	0.11	0.1073
Beta cell mass (mg)	162.2 ± 36.27	149.4 ± 33.2	9	0.61	0.5564
Islet number	546.8 ± 39.5	471.2 ± 65.15	9	2.26	0.0501

Figure 14: SORCS2 deficiency doesn't affect β cell mass

(A) Representative images of murine pancreatic sections of the indicted *Sorcs2* genotypes immunostained for insulin (purple).
(**B**) Quantitative analysis of β cell area and mass in wild-type and SORCS2-deficient islets based on immunostainings for insulin (as exemplified in A). The β cell area was quantified as insulin+ area per total pancreas area of each section. The β cell mass was quantified as β cell area multiplied by the weight of the respective pancreatic tissue. Islet numbers were manually counted on six histological sections per pancreas, spaced 200 µm apart (n = 5-6 animals per genotype).
Stippled boxes in A indicate the area of sections shown in the higher magnification insets in the respective panels. Scale bars: 1000 µm. Statistical significance was tested by unpaired t-test with $p \leq 0.05$ considered significant. p, p-value.

3.7 SORCS2 deficiency affects the maturation of insulin granules in β cells

To further explore morphological changes of *Sorcs2*$^{-/-}$ pancreatic islets, an analysis of the vesicle composition of β cells was undertaken. In light of the subdued response of *Sorcs2*$^{-/-}$ islets to KCl stimulation (Figure 12 B) and the decrease in total islet C-peptide content (Figure 12 E), I formulated a hypothesis that *Sorcs2*$^{-/-}$ pancreases might exhibit impaired insulin vesicle maturation or docking.

The synthesis of insulin involves multiple steps, including the production of preproinsulin on the rough endoplasmic reticulum, conversion to proinsulin with the removal of the amino-terminal signal sequence, packaging of proinsulin into immature vesicles on the trans-Golgi network, and subsequent vesicle maturation [243,244]. Vesicle maturation encompasses processes such as acidification of the granule lumen,

conversion to insulin and C-peptide in equimolar concentrations through proteolysis with endoproteases PC1/2 and PC2, removal of carboxypeptidase E carboxyl terminal, and the elimination of clathrin [243,244]. Mature vesicles contain a crystalline form of insulin: $(Zn^{2+})_2(Ca^{2+})$ $(Insulin)_6$, forming a dense core [245]. Increased Zn^{2+} availability within immature vesicles can lead to the formation of slow-dissolving insulin crystals: $(Zn^{2+})_4(Ca^{2+})(Cl)(Insulin)_6$ [246,247].

To analyze β cell vesicle patterns, I isolated overnight-cultured pancreatic islets and subjected them to 1.6 mM or 16 mM glucose conditions for one hour and fixed in 4% (w/v) paraformaldehyde plus 2.5% (v/v) glutaraldehyde in 0.1 M phosphate buffer for 2 hours at room temperature. Subsequent fixation, sectioning, and imaging were conducted in collaboration with Dr. Séverine Kunz from the Technology Platform for Electron Microscopy at the Max Delbrueck Centre for Molecular Medicine.

Islet β cells were distinguished based on vesicle morphology: a white halo and a dense, dark, round core [248]. On replicate electron microscopy images of islet β cells, I conducted manual counts for the numbers of total and docked vesicles (vesicles within 0.2 µm proximity to the plasma membrane [192]) of different types (empty (EG), crystal-containing (CG), immature (IG), and mature (MG) [193,194,249,250]). Vesicles were categorized as follows: EG had no dense core; CG had a rod-like core; IG had a large light grey core with a thin halo; MG had a dense dark-grey to black core with a wide halo (Figure 15 A and C). [192,248,251,252].

The amounts of total as well as docked vesicles were comparable between genotypes under both glucose conditions (Figure 15 B and D). The numbers of total and docked vesicles, as well as empty and mature vesicles, were also comparable between genotypes under both conditions (Figure 15 B and D). However, the number of total immature vesicles significantly increased in SORCS2-deficient β cells under 1.6 mM glucose stimulation (Figure 15 B) and showed a trend towards an increase under 16 mM glucose stimulation (Figure 15 D). Additionally, the numbers of docked immature vesicles in *Sorcs2*$^{-/-}$ β cells tended towards an increase (Figure 15 B, D), while the total number of crystal-containing vesicles in SORCS2-deficient β cells decreased under both glucose conditions compared to control tissue (Figure 15 B, D). Conversely, the

number of docked crystal-containing vesicles showed a trend toward reduction under both glucose conditions (Figure 15 B, D).

In summary, changes in the numbers of immature and crystal-containing vesicles in *Sorcs2*$^{-/-}$ β cells suggested a defect in vesicle maturation as the cause for insulin secretion defects. Additionally, the decrease in the number of crystal-containing vesicles may indicate a reduction in Zn^{2+} in β cells.

Due to the exclusive expression of SORCS2 in non-β cell types, SORCS2 deficiency is expected to impact the insulin release machinery through a non-cell-autonomous mechanism. One potential mode of operation could involve the secretion of factors by α, δ, or PP cells that promote insulin secretion by β cells.

3.8 SORCS2 deficiency does not affect hormonal secretion or content in α, δ or PP cells

Insulin secretion from β cells is intricately regulated by non-β cell types within islets. Notably, α cells release glucagon and GLP-1. Glucagon stimulates insulin secretion by activating G-protein coupled glucagon receptors, subsequently triggering adenylate cyclase activation [127,240]. GLP-1 functions as an amplification factor for insulin secretion, acting through the inhibition of K_{ATP} channels to maintain β-cell membrane depolarization and enhancing adenylate cyclase activity, leading to increased Ca^{2+} influx [103,127,253,254]. δ cells, on the other hand, secrete somatostatin-28 [241], which exerts inhibitory effects on insulin secretion [241]. This inhibition occurs through the blockade of adenylate cyclase and activation of K^+ channels, resulting in hyperpolarization and closure of Ca^{2+} channels [242]. Some studies also propose somatostatin's inhibitory action on insulin gene expression [241].

Additionally, PP cells secrete pancreatic PPY, PYY, and NPY [255]. PPY increases insulin sensitivity by regulating hepatic insulin receptor expression and availability [256,257]. NPY inhibits insulin secretion through the Ca^{2+}-independent pathway actin on G_α subunit [136], while PYY regulates glucose homeostasis by controlling β cell mass [102]. Epsilon cells, the rarest islet cell subtype, secrete ghrelin, which inhibits insulin secretion by hyperpolarizing the β cell membrane [258].

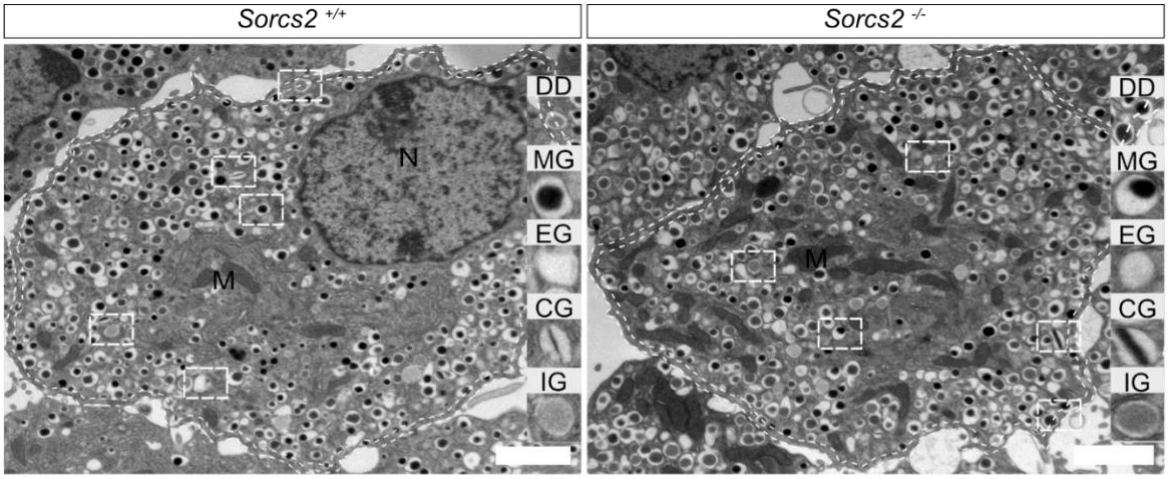

	Vesicle type/µm²	mean ± SD / median [25; 75]		df	t	U	p
		Sorcs2 +/+	*Sorcs2* -/-				
Total	Mature	2.4 ± 0.16	2.28 ± 0.14	6	1.15		0.2933
	Empty	0.89 [0.63; 1]	0.82 [0.81; 0.95]			6	0.6857
	Immature	0.17 ± 0.01	0.28 ± 0.05	6	3.9		0.0081
	Crystallized	0.1 ± 0.022	0.05 ± 0.0043	6	4.9		0.026
	Total	3.5 ± 0.4	3.47 ± 0.13	6	0.35		0.7401
Docked	Mature	0.52 ± 0.08	0.55 ± 0.074	6	0.65		0.5366
	Empty	0.16 ± 0.05	0.18 ± 0.016	6	0.9		0.4001
	Immature	0.03 ± 0.01	0.05 ± 0.019	6	2.05		0.0860
	Crystallized	0.018 ± 0.01	0.008 ± 0.002	6	1.9		0.1074
	Total	0.72 ± 0.16	0.79 ± 0.09	6	0.97		0.3703

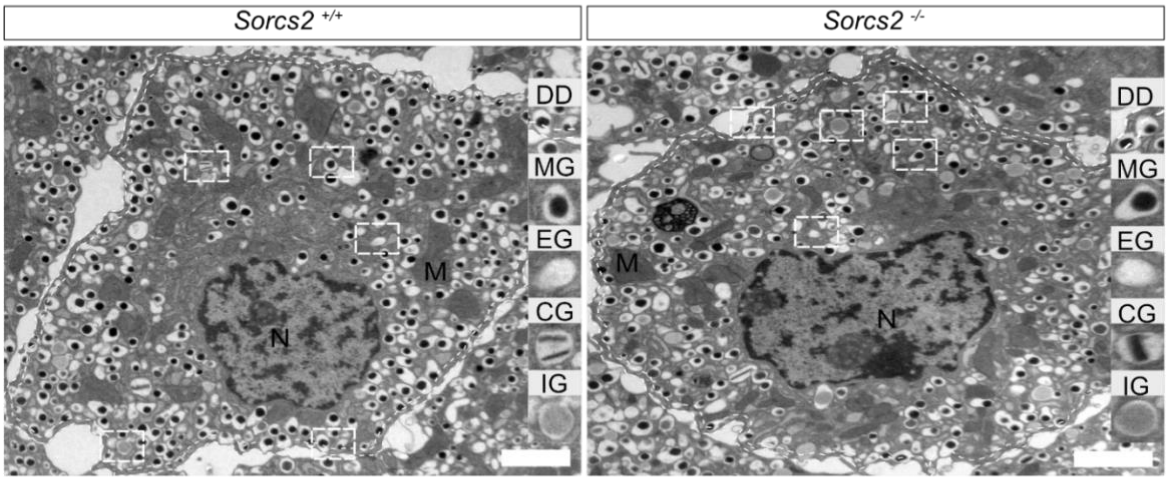

	Vesicle type/µm²	mean ± SD / median [25; 75]		df	t	U	p
		Sorcs2 +/+	*Sorcs2* -/-				
Total	Mature	2.3 ± 0.11	2.15 ± 0.24	6	0.8		0.4624
	Empty	0.8 [0.77; 1]	0.8 [0.8; 0.93]			4	0.3429
	Immature	0.16 ± 0.07	0.25 ± 0.1	6	1.5		0.1863
	Crystallized	0.08 ± 0.01	0.06 ± 0.009	6	2.9		0.0291
	Total	3.3 ± 0.09	3.34 ± 0.3	6	0.04		0.9671
Docked	Mature	0.49 ± 0.03	0.53 ± 0.1	6	0.8		0.4658
	Empty	0.18 ± 0.04	0.18 ± 0.013	6	0.21		0.8392
	Immature	0.03 ± 0.01	0.06 ± 0.03	6	1.76		0.1286
	Crystallized	0.014 [0.01; 0.02]	0.012 [0.01; 0.015]			7	0.8857
	Total	0.72 ± 0.05	0.78 ± 0.14	6	0.98		0.3636

Figure 15: SORCS2 deficiency affects insulin vesicle maturation in β cells

(**A**) Representative transmission electron microscopic (EM) images of β cells in isolated *Sorcs2*$^{+/+}$ and *Sorcs2*$^{-/-}$ islets treated for one hour with 1.6 mM glucose. Stippled boxes highlight the different types of secretory granules shown in the higher magnification insets and identified as mature granules (MG), empty granules (EG), crystallized granules (GC), as well as immature granules (IM). Inset DD indicates exemplary vesicles with a docking distance of 0.2 µm from the plasma membrane. Scale bar: 2 µm.
(**B**) Quantification of different types of granules per cell area identified on EM sections from *Sorcs2*$^{+/+}$ and *Sorcs2*$^{-/-}$ islets treated for one hour with 1.6 mM glucose. (n = 4 animals, 14-27 quantified cells per animal).
(**C**) Representative EM images of β cells in isolated *Sorcs2*$^{+/+}$ and *Sorcs2*$^{-/-}$ islets treated for one hour with 16 mM glucose. Scale bar: 2 µm.
(**D**) Quantification of different types of granules per cell area identified on EM sections from *Sorcs2*$^{+/+}$ and *Sorcs2*$^{-/-}$ islets treated for one hour with 16 mM glucose. (n = 4 animals, 17-27 quantified cells per animal).
Statistical significance was determined using an unpaired t-test or Mann Whitney U test with $p \leq 0.05$ considered significant. df, degrees of freedom; t, degree of difference in relation to variability; p, p-value).

Considering the predominant expression of SORCS2 in non-β cell types of pancreatic islets (Figure 10 B), I hypothesized that the absence of SORCS2 expression may lead to dysregulated hormonal secretion from α, δ, PP, or ghrelin-expressing epsilon cells, subsequently impacting insulin secretion from β cells. To test this hypothesis, an analysis of *in vivo* basal and *in vitro* glucose-stimulated hormone secretion, as well as the total islet content of various hormones released by non-β cells, was conducted.

For *in vivo* hormone secretion evaluation, I starved mice overnight, and collected blood before and after a 30-minute injection of 2 g/kg glucose. Concentrations of GLP-1, glucagon, PYY, NPY, total somatostatin, and somatostatin-28 were determined with ELISA. To analyze the secreted concentration of these hormones and ghrelin in isolated pancreatic islets, islets were subjected to low (1.6 mM) and high (16 mM) glucose concentrations for an hour. The islet supernatants from each step were subjected to the determination of hormone levels by ELISA (Table 6). Additionally, the total islet hormone content of these hormones was determined in unstimulated islets with ELISA (Table 6).

The data revealed unchanged levels of plasma and islet-secreted glucagon, GLP-1, somatostatin, or somatostatin-28 under basal or glucose-stimulated conditions (Table 10 and Table 11). Similarly, the islet total content of glucagon, somatostatin, and somatostatin-28 was comparable between genotypes (Table 12).

NPY levels were significantly increased in SORCS2-deficient mice under basal and glucose-stimulated conditions *in vivo* (Table 10). However, islet-secreted NPY levels were not altered under either condition (Table 11). PYY levels were decreased under basal and glucose-stimulated conditions *in vivo* (Table 10), whereas islet-secreted levels were not altered (Table 11). The normal secretion of non-β cell hormones in SORCS2 mutant islets suggests that the observed insulin secretion defects *in vitro* result from a non-hormonal mechanism.

It is noteworthy that altered plasma levels of NPY and PYY *in vivo*, but not in overnight cultured islets *in vitro*, suggest changes in NPY secretion coming from the hypothalamus [259,260] and PYY secretion from the intestine [261] in SORCS2-deficient mice. While these alterations may contribute to the metabolic changes seen in these mice *in vivo*, they do not explain impaired insulin secretion observed in islets *in vitro*. Similarly, an increased islet content of GLP-1 or decreased islet content of PYY (Table 12) did not translate into chan9ged rates of secretion (Table 11) and, therefore, do not provide an explanation for impaired insulin secretion in receptor mutant islets.

3.9 SORCS2 deficiency causes alterations in fatty acid levels in the pancreas

Considering the alterations in lipid levels observed in the liver of SORCS2-deficient mice compared to controls (Table 8), I hypothesized that a similar situation in the pancreas might affect β cell function.

Lipids can impact insulin secretion and β cell health in two different ways. On one hand, free fatty acids are essential for glucose-stimulated insulin secretion. Particularly, palmitic acids and oleic acids stimulate insulin secretion via the activation of the FFA1/GPR40 cell surface receptor on β cells [262–265]. Additionally, the metabolism of free fatty acids in β cells produces metabolic coupling factors (malonyl-CoA), which also stimulate insulin secretion by inhibiting carnitine-palmitoyltransferase 1 (CPT-1), reducing fatty oxidation and consequently increasing the concentration of long-chain acyl-CoA esters [263,265,266]. This activation enhances insulin release [263,265,266].

Table 10: Plasma levels of pancreatic hormones in wild-type and SORCS2-deficient mice

Hormone levels in plasma were determined by ELISA (Table 6) under basal conditions or 30 minutes after i.p. injection of 2 g/kg body weight of glucose (glc). Data are given as mean ± standard deviation (SD). The significance of data was evaluated using repeated measures two-way ANOVA followed by Sidak's multiple comparisons tests. F, F-test; p, p-value.

	Sorcs2$^{+/+}$			*Sorcs2*$^{-/-}$		
	basal	glc	n	basal	glc	n
	mean ± SD	mean ± SD		mean ± SD	mean ± SD	
Glucagon (pg/ml)	7.88 ± 3.72	5.53 ± 2.29	8	7.41 ± 3.36	5.22 ± 4.21	6
GLP-1 (pM)	44.55 ± 42.6	49.39 ± 51.4	12	59.8 ± 78.49	58.09 ± 69.8	10
Somatostatin (ng/ml)	1.16 ± 0.139	1.28 ± 0.27	8	1.23 ± 0.17	1.24 ± 0.11	8
Somatostatin-28 (pg/ml)	181.3 ± 37.1	244.1 ± 78.22	8	160.2 ± 24.45	185.7 ± 25.12	5
NPY (ng/ml)	1.367 ± 0.21	1.726 ± 0.1	10	1.758 ± 0.19	1.779 ± 0.18	10
PYY (ng/ml)	1.182 ± 0.15	1.416 ± 0.53	10	1.099 ± 0.13	0.957 ± 0.09	10

Two-Way ANOVA

	Interaction (condition vs genotype)		Condition (basal or glc)		Genotype (*Sorcs2*$^{-/-}$ and *Sorcs2*$^{+/+}$)	
	F	p	F	p	F	p
Glucagon (pg/ml)	F (1, 12) = 0.008	0.9290	F (1, 12) = 6.51	0.0254	F (1, 12) = 0.058	0.8132
GLP-1 (pM)	F (1, 20) = 0.55	0.4660	F (1, 20) = 0.13	0.7255	F (1, 20) = 0.22	0.6463
Somatostatin (ng/ml)	F (1, 14) = 0.75	0.4014	F (1, 14) = 1.24	0.2842	F (1, 14) = 0.85	0.8537
Somatostatin-28 (pg/ml)	F (1, 11) = 1.89	0.1971	F (1, 11) = 10.55	0.0078	F (1, 11) = 2.38	0.1510
NPY (ng/ml)	F (1, 18) = 15.93	0.0009	F (1, 18) = 20.08	0.0003	F (1, 18) = 11.74	0.0030
PYY (ng/ml)	F (1, 18) = 7.68	0.0126	F (1, 18) = 0.83	0.3753	F (1, 18) = 8.25	0.0101

Table 11: Levels of hormones released from wild-type and SORCS2-deficient pancreatic islets

Hormone levels were determined by ELISA (Table 6) in supernatants of isolated *Sorcs2*$^{+/+}$ and *Sorcs2*$^{-/-}$ pancreatic islets treated for 1 hour with 1.6 mM or 16 mM glucose in Krebs-Ringer-Bicarbonate Hepes buffer. Data are given as mean ± standard deviation (SD). The significance of data was determined using repeated measures two-way ANOVA followed by Sidak's multiple comparisons tests. p, p-value; F, F-test.

	Sorcs2$^{+/+}$			*Sorcs2*$^{-/-}$		
	1.6 mM	16 mM	n	1.6 mM	16 mM	n
	mean ± SD	mean ± SD		mean ± SD	mean ± SD	
Glucagon (pg/mg protein)	1593 ± 1243.25	1870 ± 1708.65	23	1470 ± 1152.31	2271 ± 3688.84	23
GLP-1 (pM/mg protein)	1151 ± 712.74	1326 ± 950.35	21	1058 ± 439.6	1192 ± 745.84	21
Somatostatin (ng/mg protein)	0.81 ± 0.49	1.18 ± 0.51	16	0.81 ± 0.51	1.316 ± 0.54	16
Somatostatin-28 (pg/mg protein)	580.9 ± 131.42	858.3 ± 353.56	7	475.4 ± 453.61	1306 ± 1218.63	7
NPY (ng/mg protein)	0.03 ± 0.03	0.07 ± 0.05	12	0.06 ± 0.05	0.111 ± 0.09	13
PYY (ng/mg protein)	0.64 ± 0.26	0.46 ± 0.21	18	0.76 ± 0.41	0.574 ± 0.28	18
Ghrelin (ng/mg protein)	1.45 ± 1.03	1.23 ± 1.05	16	1.1 ±0.9	0.99 ± 0.79	15

Two-Way ANOVA

	Interaction (condition vs genotype)		Condition (1.6 mM or 16 mM glucose)		Genotype (*Sorcs2*$^{-/-}$ and *Sorcs2*$^{+/+}$)	
	F	p	F	p	F	p
Glucagon (pg/mg protein)	F (1, 44) = 0.55	0.4625	F (1, 44) = 2.3	0.1337	F (1, 44) = 0.065	0.7999
GLP-1 (pM/mg protein)	F (1, 40) = 0.03	0.8560	F (1, 40) = 1.9	0.1792	F (1, 40) = 0.33	0.5685
Somatostatin (ng/mg protein)	F (1, 30) = 0.79	0.3818	F (1, 30) = 35.6	< 0.0001	F (1, 30) = 0.16	0.6039
Somatostatin-28 (pg/mg protein)	F (1, 12) = 2.65	0.1295	F (1, 12) = 10.6	0.0068	F (1, 12) = 0.29	0.6018
NPY (ng/mg protein)	F (1, 23) = 0.22	0.6434	F (1, 23) = 23.5	< 0.0001	F (1, 23) = 2.47	0.1296
PYY (ng/mg protein)	F (1, 34) = 0.01	0.9218	F (1, 34) = 17.5	0.0002	F (1, 34) = 1.72	0.1989
Ghrelin (ng/mg protein)	F (1, 29) = 1.3	0.2563	F (1, 29) = 14.7	0.0006	F (1, 29) = 0.8358	0.3682

Table 12: Total hormone content in isolated wild-type and SORCS2-deficient pancreatic islets

Hormone levels were determined by ELISA (Table 6) in lysates of unstimulated isolated pancreatic islets from Sorcs2+/+ and Sorcs2-/- animals cultured over-night. Data are given as mean ± standard deviation (SD) (Glucagon, Somatostatin, Somatostatin-28, NPY, PYY) or median with 25 and 75 quartiles (GLP-1). The significance of data was determined using an unpaired t-test (Glucagon, Somatostatin, Somatostatin-28, NPY, PYY) or Mann-Whitney U test (GLP-1). df, degrees of freedom; t, t-test; U, U-test; p, p-value.

	Sorcs2$^{+/+}$		*Sorcs2*$^{-/-}$					
	mean ± SD median [25; 75 quartiles]	n	mean ± SD/ median [25; 75 quartiles]	n	df	t	U	p
Glucagon (pg/mg protein)	576652 ± 439302	12	653183 ± 337616	12	22	0.48		0.6370
GLP-1 (pM/mg protein)	23301 [17255; 31839]	11	32508 [24954, 40701]	12			37	0.0449
Somatostatin (ng/mg protein)	403.5 ± 315.5	13	462.8 ± 386	13	24	0.43		0.6720
Somatostatin-28 (pg/mg protein)	20782 ± 9628	11	26735 ± 11589	11	20	1.3		0.2049
NPY (ng/mg protein)	1.203 ± 0.1873	8	1.359 ± 0.3711	8	14	1.06		0.3066
PYY (ng/mg protein)	1.616 ± 0.5495	8	0.992 ± 0.1609	8	14	3.08		0.0081

On the other hand, excess saturated fatty acids can lead to lipotoxicity and β cell failure through the activation of stress pathways, including ER stress, mitochondrial dysfunction, and oxidative stress [265,267].

To test this hypothesis, I extracted lipids from either total pancreas tissue isolated from overnight-fasted mice or from isolated islets following the Free Fatty Acid Quantification Kit protocol (refer to the methods section 2.2.3).

The data indicated a trend towards a decrease in free fatty acid levels in SORCS2-deficient pancreases (Figure 16 A). However, no such changes were detected in isolated islets when comparing genotypes (Figure 16 B). As mentioned above, changes in free fatty acid levels observed in mutant pancreas might affect insulin secretion from β cells. However, the unchanged levels in isolated islets argued against a lipid-mediated effect on insulin secretion seen *in vitro*.

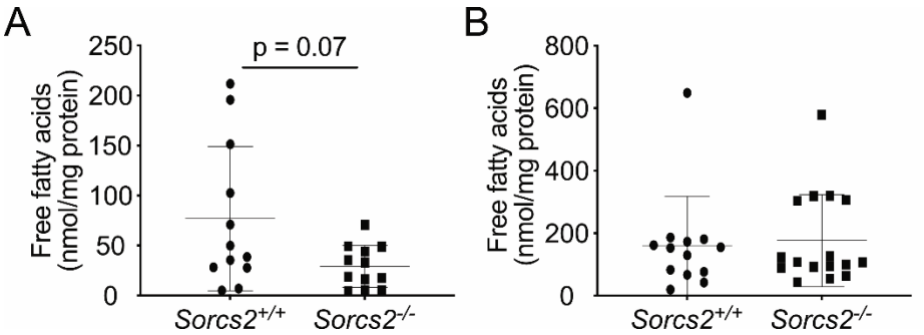

Figure 16: Pancreas and isolated pancreatic islets free fatty acids levels in *Sorcs2*$^{+/+}$ and *Sorcs2*$^{-/-}$ mice.

(A) Free fatty acids levels in the pancreas of overnight starved *Sorcs2*$^{+/+}$ and *Sorcs2*$^{-/-}$ mice.
(B) Free fatty acids levels in pancreatic islets isolated from overnight starved *Sorcs2*$^{+/+}$ and *Sorcs2*$^{-/-}$ mice. The statistical significance was tested by the Mann-Whitney U test, with $p \leq 0.05$ considered significant. p, p-value.

3.10 Cluster analysis of *Sorcs2*$^{-/-}$ and *Sorcs2*$^{+/+}$ pancreatic islets

To understand the intrinsic mechanisms by which SORCS2 may affect insulin secretion, I performed single-cell RNA sequencing (scRNA-seq) on dispersed overnight cultured pancreatic islets isolated from *Sorcs2*$^{+/+}$ and *Sorcs2*$^{-/-}$ mice.

Pancreatic islets consist of distinct cell types, with a predominant composition of 70% β cells, 20% α cells, less than 10% δ cells, less than 5% PP cells, and a minimal presence

(1-2%) of ghrelin-producing ε cells [219]. Current Fluorescence-Activated Cell Sorting (FACs) protocols for pancreatic isles, reliant on surface markers ($CD24^{low}$, $CD71^{-}$ - α; $CD24^{low}$, $CD71^{+}$ - β; $CD24^{high}$ - δ), pose challenges due to significant sample loss and demand for large quantities of a sample [268–270]. In contrast, scRNA-seq facilitates the discrimination of all cell types, revealing rare populations and unique differences between them through single-cell barcoding in a minuscule sample volume [269–271].

In brief, the scRNA-seq process involves applying a single-cell suspension to the Next Gem Chip G (10x Genomics Inc., USA), capturing individual cells in oil droplets with unique barcodes. This barcoded cDNA is subsequently sequenced, generating a distinct transcriptome for each cell. The analysis involves clustering cells based on gene counts, followed by DEG analysis for comparing clusters [269–271] (for details, please refer to methods section 2.3.11).

A meticulous method was devised to address challenges such as high apoptosis and aggregation rates in pancreatic single-cell suspensions. I employed Accutase as a gentle dissociation medium and DNAse1 to cleave released DNA from dead cells, preventing cell clumping. Additionally, the use of HBSS buffer with EDTA and without Ca^{2+}/Mg^{2+} minimized cation-dependent cell-cell adhesion [195,272–274] (for details, please refer to methods section 2.3.10).

The resulting single-cell suspension underwent library preparation and sequencing at the Genomics Technical Platform of Max Delbrueck Centre for Molecular Medicine. Data analysis, including sequence alignment, gene-level count analysis, data normalization, and dimensional reduction, was conducted collaboratively with Per Qvist, an associate professor at the Department of Biomedicine of Aarhus University.

In summary, sequenced reads were rigorously filtered for per sequence GC, N, adaptor content, and duplication levels [275–278], aligned to the mouse genome [276–278], and counted to create a gene count matrix per cell [275–278]. Unsupervised clustering using UMAP was applied [279], followed by Seurat clustering for annotating and understanding cluster functions based on marker genes [200,280]. An alternative approach involving supervised clustering, utilizing markers identified in prior pancreatic islet scRNA-seq analyses, could have been employed. However, this method might have compromised

the identification of unique clusters resulting from *Sorcs2*$^{-/-}$. In the final step, gene counts from the corresponding clusters of *Sorcs2*$^{+/+}$ and *Sorcs2*$^{-/-}$ samples were compared using differential gene expression analysis, employing limma. This analysis aimed to unveil DEGs in *Sorcs2*$^{-/-}$ samples compared to *Sorcs2*$^{+/+}$ samples (for details, please refer to the methods section 2.3.11.3.4).

Unsupervised cell clustering analysis identified eighteen cell clusters with fourteen clusters (1, 2, 3, 4, 5, 7, 8, 9, 10, 12, 13, 15, 17, 18) exhibiting high expression of genes associated with β cell functions, such as *Ins1*, *Ins2*, *Chromogranin (Chg)* a and *Chgb* (Figure 17 A, B; Figure 18). *Ins1* and *Ins2* are two genes encoding preproinsulin 1 and preproinsulin 2 respectively which function in a sex-dimorphic way [281,282]. Chromogranin B regulates insulin vesicle trafficking from the Golgi, while Chromogranin A regulates vesicle storage and modifies β cell mitochondrial function to increase insulin secretion [283,284].

Cluster 6 was designated as α cells due to high expression of glucagon (*Gcg*) and transthyretin (*Ttr)* (Figure 17 A, B; Figure 18). Transthyretin was previously found to be regulating glucagon expression [285]. However, the mechanism is yet unknown [285].

Cluster 16, exhibiting high expression of polypeptide Y (*Ppy*) and *Peptide YY* (*Pyy*), was identified as the PP cell cluster, while cluster 11 was defined as δ cell cluster based on upregulation of somatostatin (*Sst*) transcripts (Figure 17 A, B; Figure 18).

Cluster 14 displayed characteristics of both β cells (*Ins1, Ins2*, *ChgB, ChgA*) and non- β cell types (*Gcg, Ttr, Ppy, Pyy*), suggesting a progenitor or transdifferentiating pancreatic cell type (Figure 17 A, B; Figure 18) [286,287].

Subsequent confirmation of *Sorcs2* transcripts being confined to α, δ, and PP cell type clusters (Figure 17 C), as supported by previous immunohistological analyses (Figure 10 B), indicated the selective expression of *Sorcs2* in specific islet cell populations. Notably, the presence of *Sorcs2* transcripts in cluster 14 suggested a potential influence of *Sorcs2* in the context of the transdifferentiating or multi-hormonal nature of this cluster (Figure 17 C).

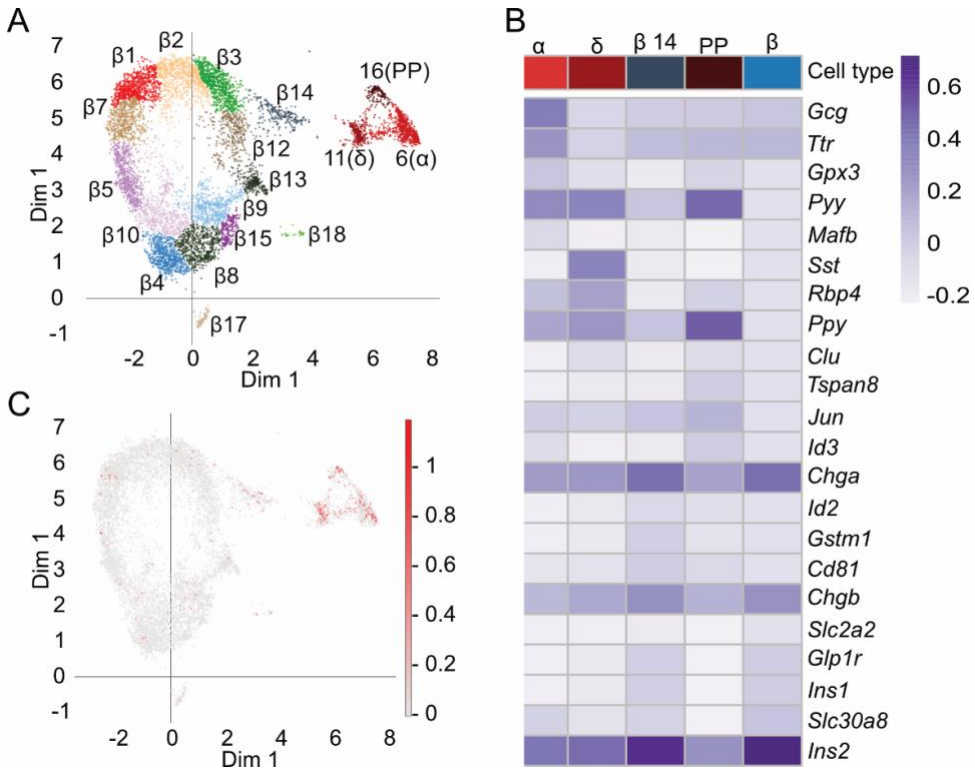

Figure 17: Unsupervised clustering analysis of single-cell RNA sequencing identifies eighteen cell clusters in combined Sorcs2$^{+/+}$ with Sorcs2$^{-/-}$ pancreatic islet samples.

(A) Cell transcripts from pancreatic islets of *Sorcs2*$^{+/+}$ and *Sorcs2*$^{-/-}$ mice were analyzed by unsupervised clustering and visualized using uniform manifold approximation and projection for dimension reduction (UMAP) plot. A total of 18 distinct cell clusters were identified in the pooled data set.
(B) Heatmap for *Sorcs2*$^{+/+}$ samples shows the top five most unique identifiers per cluster according to the adjusted p-value and fold change for α, δ, all β, β cluster 14, and PP clusters.
(C) UMAP plot localizing *Sorcs2* transcripts (red) indicating receptor gene transcription in clusters of α, δ, and PP cells, as well as cluster 14.
The significance of data was determined using a non-parametric Wilcoxson rank sum test with p≤0.05 considered significant.

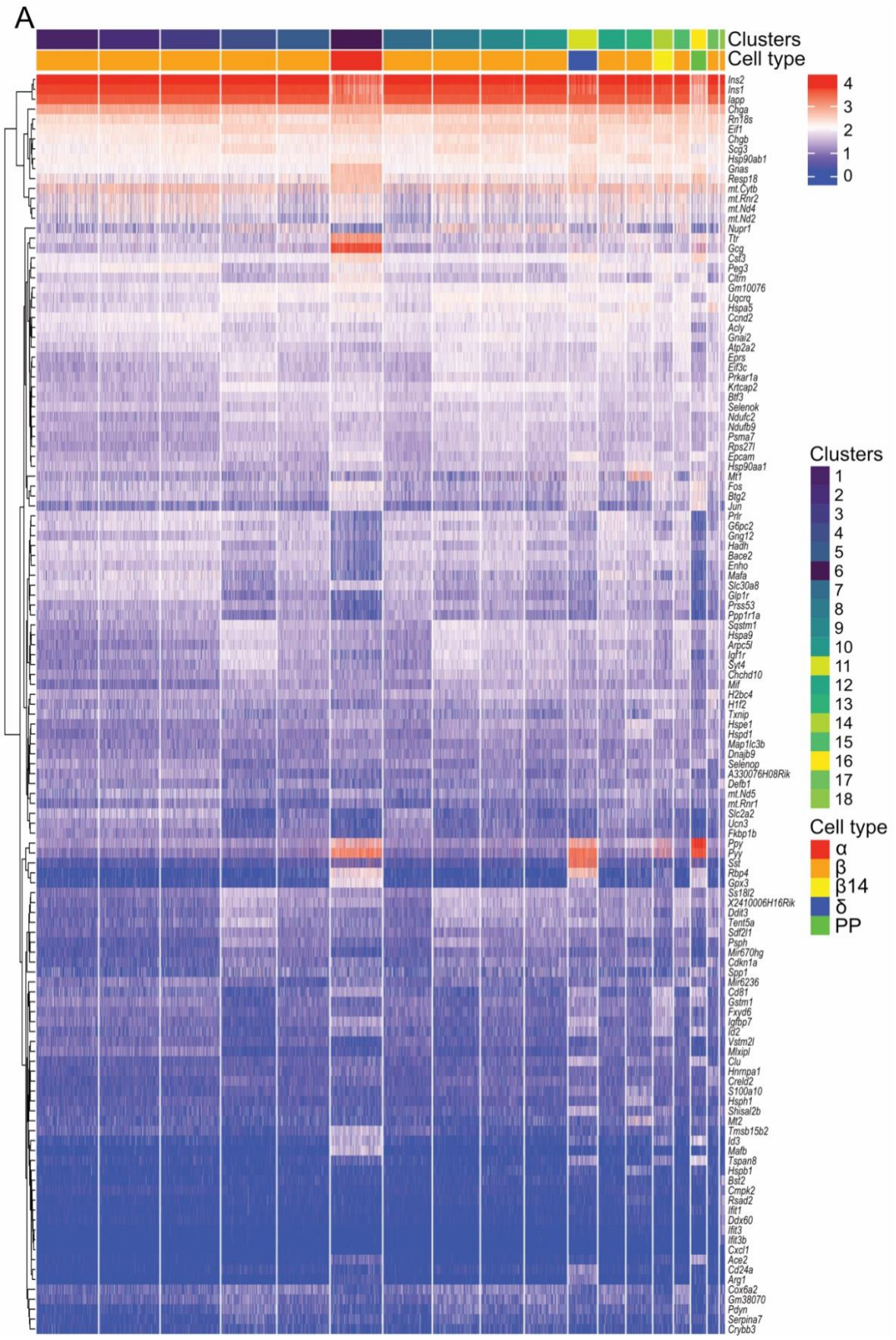

Figure 18: A single-cell heatmap separating all eighteen pancreatic islet clusters with the ten most upregulated genes calculated with Seurat clustering

(A) Heatmap for *Sorcs2*$^{+/+}$ samples showing the top 10 unique identifiers per cluster according to the adjusted p-value and fold change. Gene counts were logarithmically transformed. Euclidean distance was applied for the clustering of rows. No clustering was applied to columns.
The significance of data was determined using a non-parametric Wilcoxson rank sum test with $p \leq 0.05$ considered significant.

3.11 Distribution of β cell clusters based on capacity for insulin secretion

Our understanding of β cell subtypes is limited, with previous studies categorizing β cells into high and low insulin-secreting, as well as fast or slow responders to glucose [288–290]. Notably, "Hub" β cells, constituting only 1-10% of all islet β cells, have been identified as fast responders with low insulin secretion. These cells play a crucial role in directing and regulating other β cell subtypes, referred to as "Followers" [290].

Additional studies have classified β cells into subtypes based on the expression of ST8SIA1 and CD9, where low expression of both markers correlated with the highest glucose-stimulated insulin secretion, while high expression correlated with high basal insulin secretion but the lowest glucose-stimulated insulin secretion [289].

Another classification based on the levels of the epigenetic factor H3K27me3 revealed that higher levels of H3K27me3 were associated with increased insulin secretion and mitochondrial mass [291].

While markers for different β subtypes exist, their intrinsic functions in β cells are often unclear. For instance, high flattop (FLTP)-expressing β cells, associated with high maturity and insulin secretion, did not show adverse effects upon FLTP deletion [292,293].

It is essential to note that scRNA-seq analysis, while capable of identifying β cell subtypes based on unique gene expression patterns, may also detect cell states due to changes in transcription, potentially leading to the identification of faulty subtypes [292]. Additionally, "Hub" cell types, crucial for regulating β cell populations, may be more susceptible to ER stress, impacting their viability and detection through scRNA-seq [290,292].

Thus, in this study, I focused primarily on identifying low and high insulin-producing cell types based on previous research.

To discern differences between β cell clusters, DEGs were extracted from fourteen β clusters (1, 2, 3, 4, 5, 7, 8, 9, 10, 12, 13, 15, 17, 18) obtained after Seurat clusters DEG analysis, revealing up- and down-regulated genes for each cluster for *Sorcs2*$^{+/+}$ and *Sorcs2*$^{-/-}$ samples combined. The degree of overlap between clusters based on up- and downregulated DEGs was assessed.

Analysis indicated that β clusters 15, 9, 8, 13, 12, 3 have the most similar up-regulated genes (Figure 19 A), while β clusters 1, 7, 2, 3, 5, 4, 10, 17 share the most similarity in down-regulated genes (Figure 19 B).

To unravel the functional significance of these distinct cluster groups, I isolated DEGs prevalent in each cluster. Specifically, I focused on genes that appeared in a minimum of 5 clusters for up-regulated genes (clusters 15, 9, 8, 13, 12, 3) (Figure 19 A) and in at least 6 clusters for down-regulated genes (clusters 1, 7, 2, 3, 5, 4, 10, 17) (Figure 19 C). Subsequently, ORA was conducted to discern GO terms associated with the shared differentially expressed genes.

This meticulous approach aimed to identify common molecular signatures across multiple clusters and shed light on the biological processes and pathways implicated in each group. The ORA analysis provided insights into the enriched functional categories, aiding in the interpretation of the roles played by these gene sets in the context of β cell diversity and insulin secretion dynamics.

Clusters 15, 9, 8, 13, 12, 3, characterized by up-regulated overlapping genes, were associated with GO terms such as "Membrane docking," "Membrane fusion," "Vesicle docking," "Insulin secretion," and "Peptide secretion," indicative of high insulin-secreting subtypes (Figure 19 B).

Clusters 1, 7, 2, 3, 5, 4, 10, and 17, sharing down-regulated overlapping genes, were associated with GO terms like "Protein folding," "mRNA processing," "Regulation of insulin secretion," "Potassium ion transport," "Regulation of calcium ion transport," and

"Translation initiation," suggesting a possibly low insulin-secreting subgroup (Figure 19 D).

Interestingly, DEGs from β cluster 18 exhibited minimal overlap with other clusters (Figure 19 A, C). To understand the function of β cluster 18, up-regulated DEGs were compared to all β clusters. Unique DEGs were extracted and subjected to ORA analysis, revealing GO terms associated with upregulated immune response: "Regulation of type I/II interferon production" and "Regulation of innate immune response" (Figure 19 E).

Previous research indicates a potential shift in cell state to antigen-presenting-like for β cells under intrinsic (endoplasmic reticulum stress, reactive oxygen species) or external stress (stimulation with cytokines) [161]. Antigen-presenting β cells interact with plasmacytoid dendritic cells and activate autoreactive CD4 and CD8 T cells [161]. These cells are found in elevated quantities in pancreatic islets from Type I Diabetes donors and diabetic NOD mice, suggesting a potential link between immune response and β cell dysfunction [161].

In conclusion, the β cell clusters in combined *Sorcs2*$^{+/+}$ and *Sorcs2*$^{-/-}$ samples encompass both low and high insulin-producing β cell populations, along with a distinctive β cell population exhibiting characteristics reminiscent of antigen-presenting cells.

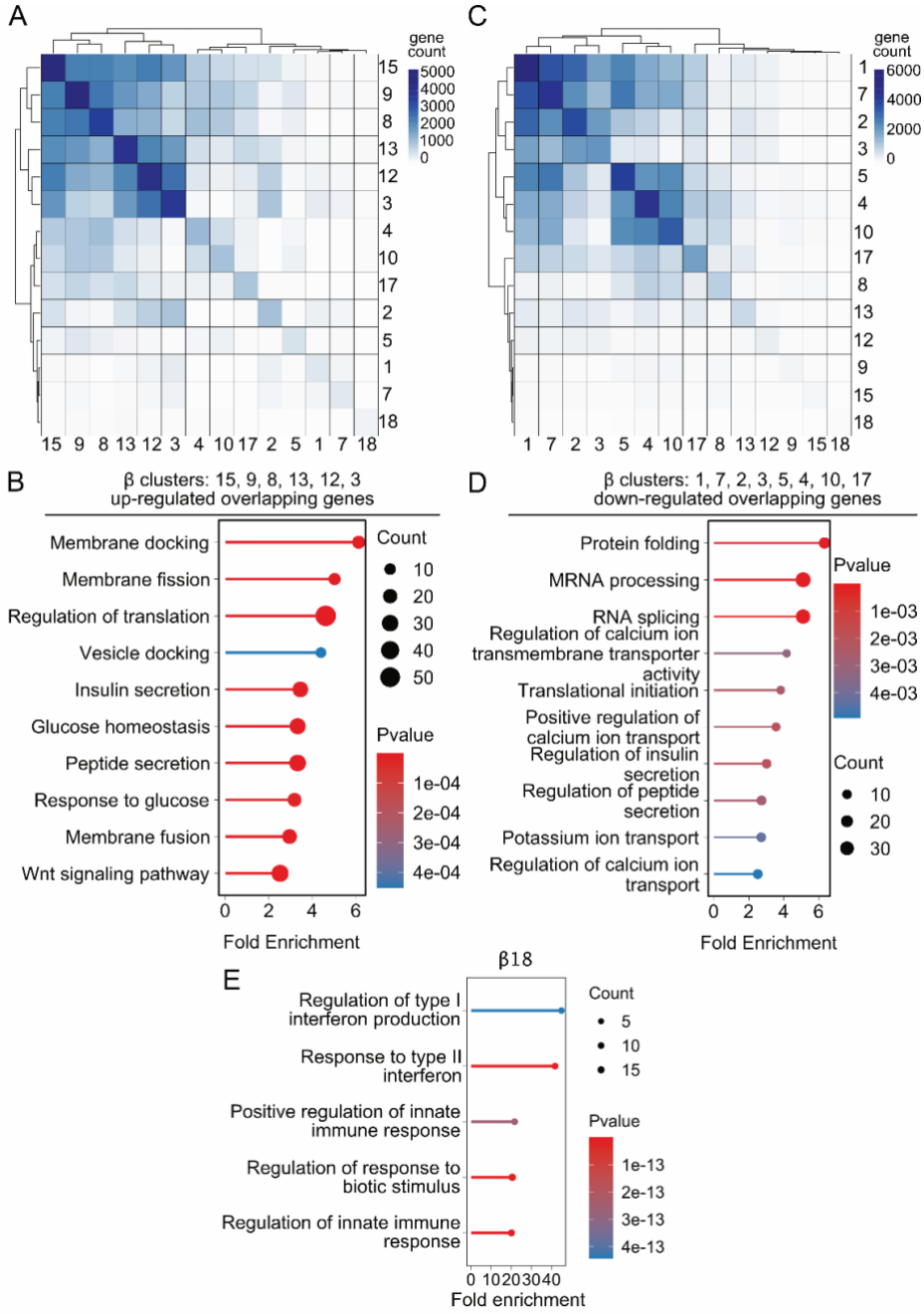

Figure 19: β cell clusters are divided into two separate groups with opposite functions.

(A) A heatmap showing numbers of up-regulated genes overlapping between β clusters in combined *Sorcs2*$^{+/+}$ and *Sorcs2*$^{-/-}$ samples.
(B) A heatmap showing numbers of down-regulated genes overlapping between β clusters in combined *Sorcs2*$^{+/+}$ and *Sorcs2*$^{-/-}$ samples.
(C) A graph representing biological processes of overlapping up-regulated genes for β clusters 15, 9, 8, 13, 12, 3 in combined *Sorcs2*$^{+/+}$ and *Sorcs2*$^{-/-}$ samples.
(D) A graph representing biological processes of overlapping down-regulated genes for β clusters 1, 7, 2, 3, 5, 4, 10, 17 in combined *Sorcs2*$^{+/+}$ and *Sorcs2*$^{-/-}$ samples.
(E) A graph representing biological processes of unique up-regulated genes for β cluster 18 in combined *Sorcs2*$^{+/+}$ and *Sorcs2*$^{-/-}$ samples.
The significance of data was determined using Seurat with $p \leq 0.05$ considered significant. Gene ontology analysis was performed with the clusterProfiler R package [208]. Adjusted p-values (p.adjust) were calculated with the Benjamini-Hochberg test with $p \leq 0.05$ considered significant.

3.12 Distribution of β cell clusters based on the level of maturity

The categorization of β cell clusters extends beyond functional distinctions, encompassing variations in the level of maturity. Although both mature and immature β cells can secrete insulin, mature β cells exhibit greater sensitivity to glucose, allowing insulin secretion even in response to lower glucose levels [294].

Shared transcription factors in both mature and immature β cells include pancreatic and duodenal homeobox 1 (*Pdx1*), NK6 Homebox1 (*Nkx6.1*), NK2 homeobox 2 (*Nkx2.2*), ISL LIM homeobox1 (*Isl1*) and paired box 6 (*Pax6*) [294–297]. However, mature β cells express higher levels of *Pdx1*, *Nkx6.1,* and *Foxo1,* crucial for the generation of mono-hormonal β cells [294–297].

Markers indicating β cell maturity include MAF BZIP transcription factor A (*Mafa*), urocortin 3 (*Ucn3,*) and neuronal differentiation 1 (*Neurod1*) [294]. *Mafa,* in collaboration with *Pdx1*, facilitates the conversion of immature into mature β cells [298]. *Ucn3*, part of the corticotropin-releasing family, regulates glucose-stimulated insulin secretion, while *Neurod1*, a transcription factor, influences the maturity phenotype, with its deficiency leading to immature-like characteristics [294].

Mature β cells exhibit suppressed expression of hexokinase 1 (*Hk1*), lactate dehydrogenase A (*Ldha*), monocarboxylate carrier 1 (*Mct1*), and repressor element 1 silencing transcription factor (*Rest*) [294]. *Rest* downregulation in mature β cells is essential for proper insulin exocytotic machinery expression [294]. The downregulation of *Mct1* and *Ldha* in mature β cells ensures primary insulin secretion in response to glucose rather than lactate [294]. The downregulation of *Hk1* enhances β cell sensitivity to glucose with glucokinase instead of hexokinase [294].

β cells can also be classified as mature or immature based on the expression of *Ins1* and *Pdx1* genes [299]. Those with high expression of both *Ins1* and *Pdx1* are considered the most mature [299]. However, a subset with high *Pdx1* and low *Ins1* expression exhibits immature characteristics, including high proliferative and apoptotic markers and a polyhormonal gene profile [299].

Another perspective on assessing the maturity level of β cells involves scrutinizing the expression of genes responsible for glucose and insulin handling. The glucose 2 transporter (*Slc2a2*) is crucial for facilitating glucose uptake in β cells. *G6pc2* encodes the G6P catalytic subunit isoform located in the ER, converting G6P into glucose and inorganic phosphate [300]. Studies have demonstrated that *G6pc2* serves as a negative regulator of basal glucose-stimulated insulin secretion, influencing the finely tuned balance of insulin release [300]. Glucokinase (*Gck*) assumes the role of a glucose-sensing enzyme within β cells, converting glucose to G6P [301]. Its activity is fundamental to the intricate mechanisms by which β cells respond to glucose levels. Proprotein convertase subtilisin/kexin type 1 (*Pcsk1*) plays a pivotal role in prohormone convertase 1/3-mediated proinsulin processing [302,303]. The deficiency of *Pcsk1* has been associated with an increased susceptibility to diabetes in mice, underscoring its significance in maintaining proper insulin production and secretion [303].

Conducting an in-depth examination of gene expression within β cell clusters, I focused on markers of maturity (*Mafa, Neurod1, Ucn3*) and immaturity (*Hk1, Ldha, Mct1, Rest*), along with genes associated with both immature and mature populations (P*dx1, Nkx6.1, Nkx2.2, Isl1, Pax6*), heterogeneity (*Cd9, Cfap126, St8sia1*), and functionality (*Slc2a2, G6pc2, Gck, Ins1, Ins2, Pcsk1*). For the analysis I aligned the metadata file (containing information about the genotype and cluster number for each sequenced cell) and gene count matrix by cell names and extracted gene counts for the above-mentioned genes. I specifically extracted *Sorcs2*$^{+/+}$ cells to avoid the effect of *Sorcs2* deficiency. Subsequently, I performed MAST test [304], to analyze difference in expression of these markers among β cell populations. The MAST test was chosen over the limma test due to the low number of genes analyzed and the nature of MAST, which assesses the rate and level of expression independently for each gene in a cell [304] (for more details please refer to methods section 2.3.11.3.4).

No marked distinctions were observed in the expression of genes linked to β cell heterogeneity (*Cfap125, Cd9, St8sia1*), except for an elevated expression of *St8sia1* in clusters 1, 2, and 3 (Figure 20 A). This concurs with my prior analysis designating clusters 1, 2, and 3 as exhibiting a low insulin-producing profile (Figure 19 D). Furthermore, clusters 1 and 2 displayed reduced expression of the insulin processing gene *Pcsk1* (Figure 20 C), reinforcing the likelihood of a low insulin production phenotype for these

clusters. Notably, clusters 2 and 3 exhibited heightened expression of *G6pc2*, a negative regulator of glucose-stimulated insulin secretion, pointing towards a low insulin-secreting phenotype (Figure 20 B). Intriguingly, cluster 3 also demonstrated increased expression of *Gck*, a feature associated with highly functional β cells (Figure 20 B), providing an explanation for its dual classification as both low and high insulin-secreting clusters (Figure 19 B, D).

Clusters exhibited notable differences in *Slc2a2* expression, with clusters 1-3 and 7 displaying increased *Slc2a2* levels, whereas clusters 4, 5, 8, 9, 10, and 15 demonstrated decreased *Slc2a2* expression (Figure 20 B). Additionally, cluster 5 presented elevated *G6pc2* expression and low *Pcsk1* expression, indicating a low insulin-secreting phenotype, consistent with the previous analysis (Figure 19 D, Figure 20 B, C). Cluster 4 showed further reduced *G6pc2* expression, potentially compensating for the low *Slc2a2* expression (Figure 20 B). Clusters 8, 9, and 15 displayed decreased expression of *Ins1* and *Ins2* (cluster 9) genes (Figure 20 C). Intriguingly, despite being previously categorized as part of the high insulin-secreting cluster, clusters 8 and 9 exhibited increased insulin processing gene expression *Pcsk1*, suggesting the involvement of other factors in determining their phenotype (Figure 20 C).

None of the clusters exhibited high expression of disallowed genes (*MCT1, Rest, Ldha,* and *Hk*), signifying the absence of true immature β cells in our dataset (Figure 21 A). Nevertheless, clusters demonstrated variability in terms of maturation markers (*Mafa, Ucn3, Neurod1*) (Figure 21 A) and transcription factors (*Pdx1, Foxo1, Nkx6.1, Pax6, Isl1, Nkx2-2*) (Figure 21 B). Clusters 1, 2, 3, and 12 displayed increased expression of at least two maturation markers, while clusters 4, 5, 7, 10, 14, and 17 exhibited lower expression of maturation markers compared to other clusters (Figure 21 A, B). Moreover, clusters 1, 2, 3, 12, and 13 showed heightened expression of transcription factors, indicating a fully mature phenotype (Figure 21 B). Although cluster 14 demonstrated increased expression of transcription factors *Pdx1, Foxo1, Pax6*, and *Isl1* (Figure 21 B), it also displayed decreased expression of the maturation gene *Mafa* (Figure 21 A) and expressed *Pyy* and *Ppy* genes (Figure 17 B, Figure 18), suggesting a multi-hormonal phenotype typical of immature or transdifferentiating β-cells [305].

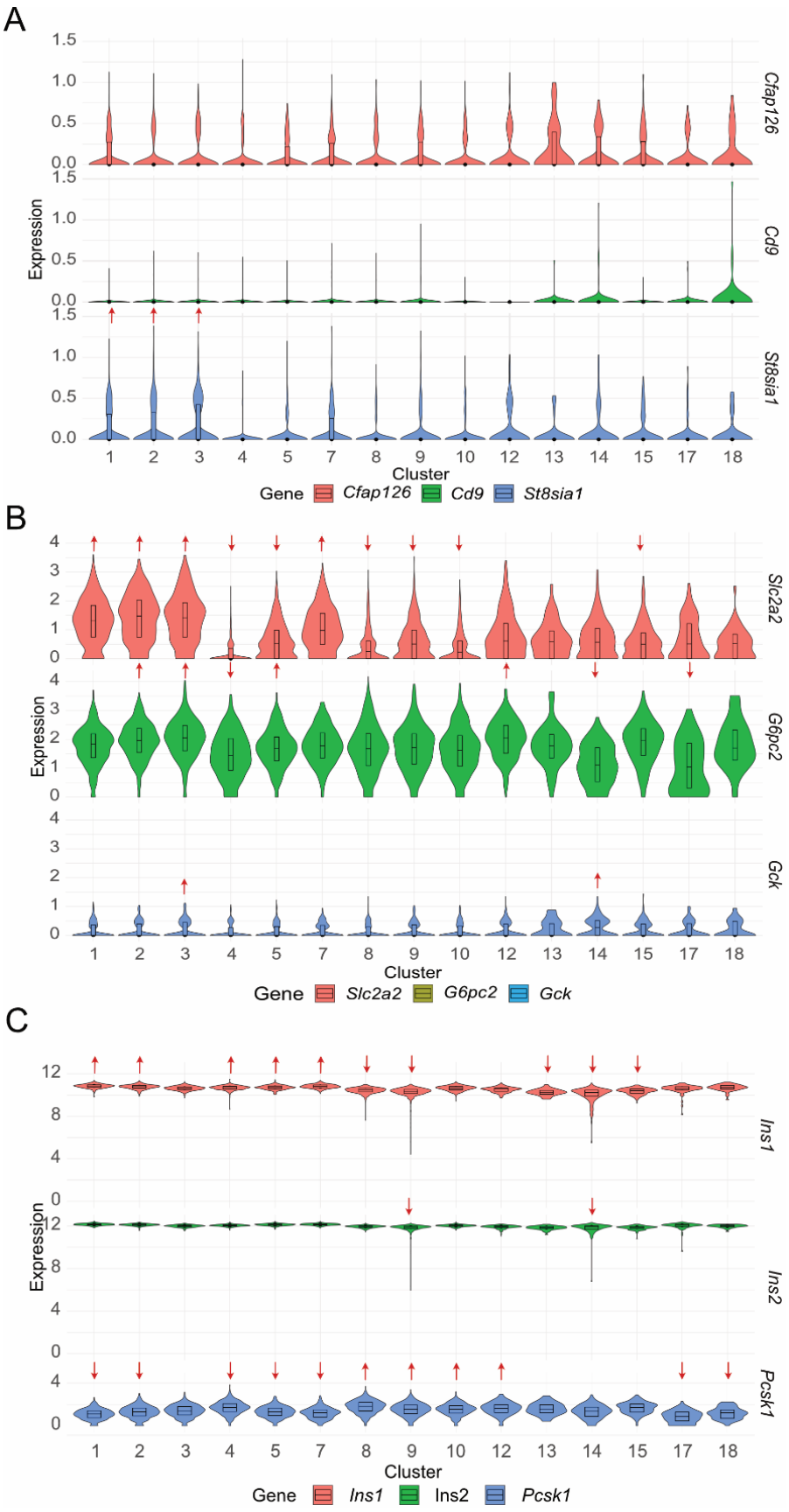

Figure 20: β cell clusters are heterogeneous according to glucose and insulin-related gene expression.

(A) Stacked violin plot comparing gene expression for genes previously associated with β cell heterogeneity among all β cell clusters in *Sorcs2*$^{+/+}$ pancreatic islets.
(B) Stacked violin plot comparing gene expression for genes involved in insulin synthesis (*Ins1*, *Ins2)* and processing (*Pcsk1*) among all β cell clusters in *Sorcs2*$^{+/+}$ pancreatic islets.
(C) Stacked violin plot comparing gene expression for genes involved in glucose handling (*Slc2a2, G6pc2, G6pc3,* and *Gck*) among all β cell clusters in *Sorcs2*$^{+/+}$ pancreatic islets.
Arrows up or down indicate significant up- or down-regulation, respectively, in one cluster compared to all the cells from other clusters. The significance of data was determined using Seurat and model-based analysis of single-cell transcriptomics (MAST) for differential gene expression with $p \leq 0.05$ considered significant.

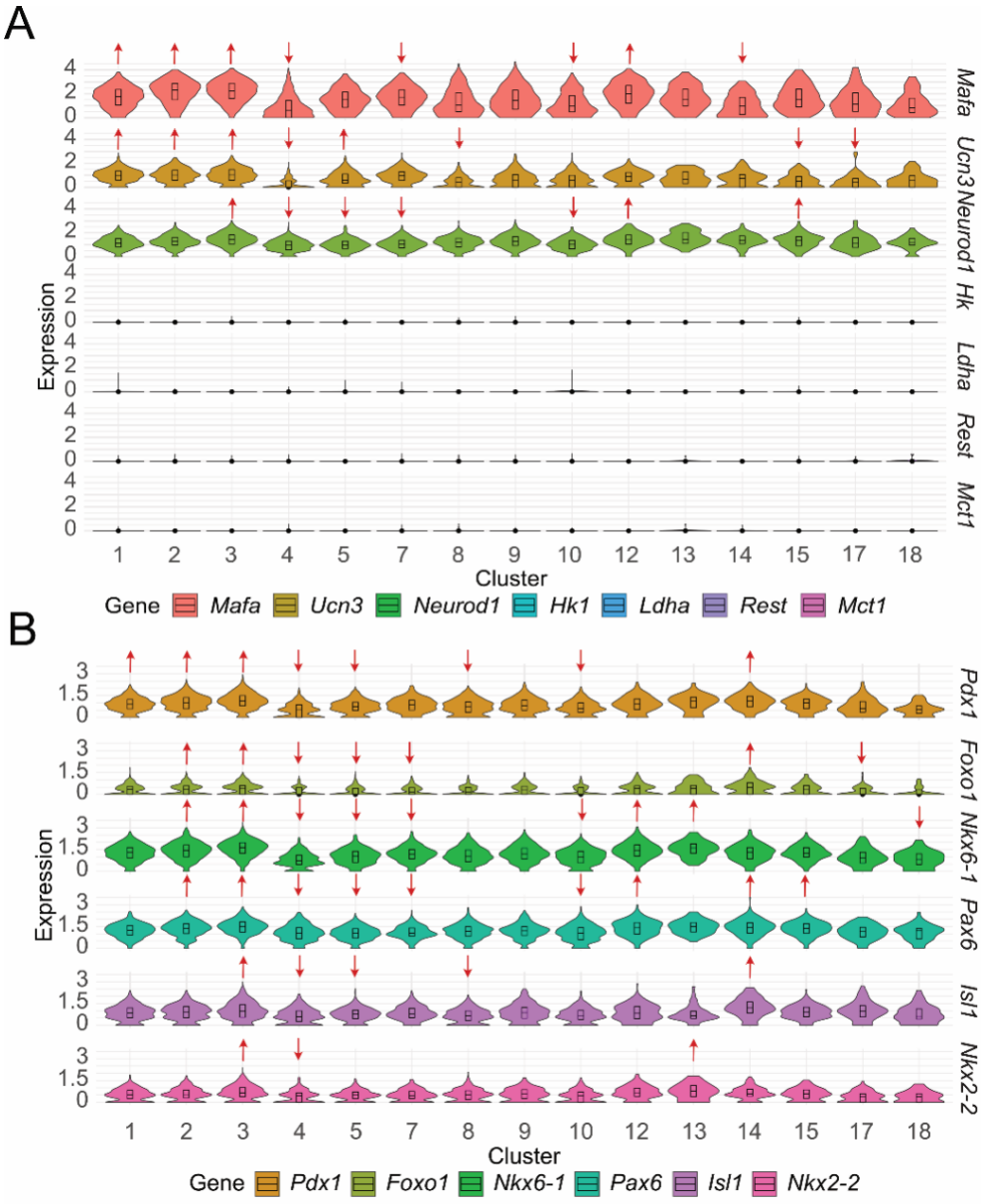

Figure 21: β cell clusters are heterogeneous according to the expression of β cell maturation genes and transcription factors involved in the maturation of β cells.

(A) Stacked violin plot comparing gene expression of markers for mature (*Mafa, Ucn3, Neurod1, Esrrg*) and immature (*Hk, Ldha, Rest, Slc16a1*) β cells among all β cell clusters in *Sorcs2*$^{+/+}$ pancreatic islets.
(B) Stacked violin plot comparing expression of transcription markers involved in maturation of β cell among all β cell clusters in *Sorcs2*$^{+/+}$ pancreatic islets.
Arrows up or down indicate significant up- or down-regulation, respectively, in one cluster compared to all the cells from other clusters. The significance of data was determined using Seurat and model-based analysis of single-cell transcriptomics (MAST) for differential gene expression with $p \leq 0.05$ considered significant.

Clusters 4, 7, 8, 10, 17, and 18 exhibited decreased expression of transcription factors and maturation markers, indicating an immature phenotype for these clusters (Figure 21). Cluster 5 displayed reduced expression of nearly all transcription factors and the *Neurod1* maturation marker, with decreased *Ucn3*, suggesting an immature phenotype for this cluster as well (Figure 21).

In summary, my analysis indicates that clusters 1, 2, 3, 9, 13, and 12 exhibit a mature phenotype. However, clusters 1 and 2 might have a low insulin-secreting profile due to low *Pcsk1* expression and high *St8sia1* expression (Figure 20). Cluster 3, characterized by elevated expression of all maturation markers and glucose handling genes, especially *Gck*, a key glucose-sensing enzyme in β cells, may signify a fast-responding phenotype (Figure 20). Conversely, clusters 4, 5, 7, 8, 10, and 15 display decreased expression of maturation markers, transcription factors, and glucose-handling genes, suggesting a less mature phenotype for these clusters (Figure 20, Figure 21).

3.13 SORCS2 deficiency affected the composition of β cell clusters

I next compared cluster composition between genotypes by extracting the number of cells belonging to each cluster and genotype from the metadata and gene count cell matrix.

Clusters 1, 2, 3, 4, 5, 6, 7, 9, 11, 16, 17, and 18 exhibited a similar number of cells between genotypes, while β clusters 8, 10, and 15 displayed an average 68% decrease in cell number in *Sorcs2*$^{-/-}$ samples (Figure 22 A). In contrast, β clusters 12 and 13 demonstrated a substantial increase of 103% and 1320% in cell numbers, respectively (Figure 22 A).

Previous analyses indicated a less mature nature for clusters 8, 10, and 15, attributing cluster 10 to low insulin secretion and clusters 8 and 15 to high insulin secretion (Figure

19 B, D; Figure 20; Figure 21). Clusters 12 and 13 were identified as mature and characterized by high insulin secretion (Figure 19 B; Figure 20; Figure 21).

To gain deeper insights into the differences between β clusters with altered and unchanged cell numbers, I performed a limma moderated t-test [203] between unchanged β clusters (1, 2, 3, 4, 5, 7, 9, 17, 18) and β clusters with high (12, 13) or low (8, 10, 15) cell numbers, followed by GO analysis with the "clusterProfiler" R package [208]. In brief, I aligned the metadata file (containing information for the cluster, genotype, batch, and cell type accessory for each cell) and gene counts matrix by cell names and extracted gene counts for the specified groups of clusters. I specifically extracted *Sorcs2*$^{+/+}$ cells to mitigate the impact of *Sorcs2* deficiency. Subsequently, I conducted differential gene expression analysis using the limma test (for details, please refer to the methods section 2.3.11.3.4) [203].

Sorcs2$^{+/+}$ β clusters 12 and 13, which exhibited an increased number of cells upon *Sorcs2* deficiency, were associated with GO terms such as "positive/negative regulation of cell differentiation," "regulation of mitotic cycle," "regulation of cell population proliferation," "positive regulation of cell cycle G1/S phase transition," as well as "pancreatic α cell differentiation" (Figure 22 B), suggesting a potential transdifferentiating or proliferative nature of these clusters [287,305,306]. Hypothetically, clusters 12-13 may be increased in mutant islets to compensate for potential β cell loss in *Sorcs2*$^{-/-}$ samples, providing a rationale for the overall unchanged β cell mass in mutant islets.
β clusters with decreased cell numbers in *Sorcs2*$^{-/-}$ samples (clusters 8, 10, and 15) were characterized by GO terms such as "response to ER stress," "response to unfolded proteins," "response to topologically incorrect proteins," and "oxidative phosphorylation" (Figure 22 C). These GO terms suggest elevated cell stress and metabolic activity in clusters 8, 10, and 15.

ER stress is common in pancreatic β cells due to high rates of insulin production, triggering adaptive UPR mechanisms to maintain cellular proteostasis and enhance tolerance to ER stress by downregulating genes identifying β cells (*Pdx1, Gck, Neurod1*, etc.), as well as proinsulin expression and processing [307]. However, chronic or unresolved ER stress, coupled with increased production of reactive oxygen species and inflammation, can initiate maladaptive UPR, leading to cell death [307].

Consequently, I inferred that the loss of clusters 8, 10, and 15 in mutant islets may be associated with maladaptive cell stress and UPR, suggesting a potential role for SORCS2 in a protective stress response.

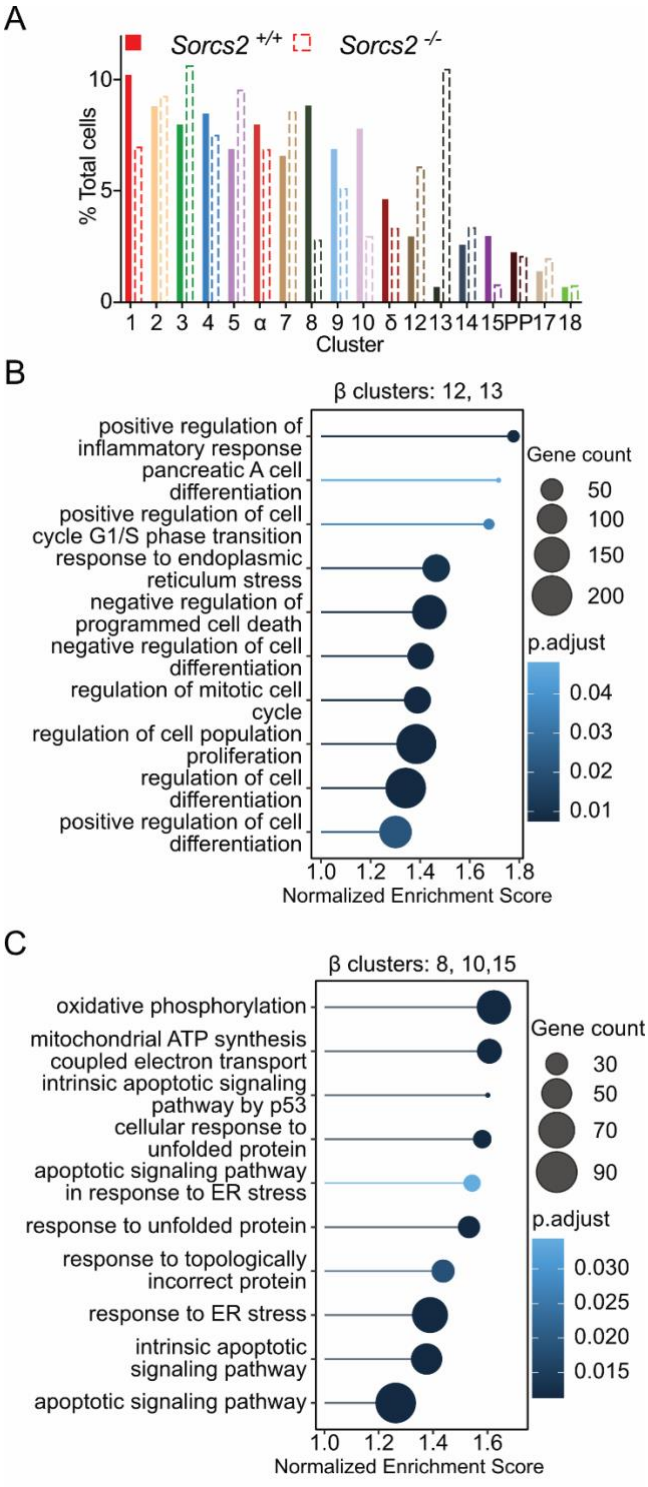

Figure 22: *Sorcs2*$^{-/-}$ pancreatic islets have an altered β cluster cell composition.

(A) Quantitative contribution of individual cell clusters to the total cell counts in *Sorcs2*$^{+/+}$ (solid bars) and *Sorcs2*$^{-/-}$ (stippled bars) islets.

(B) Graph representing biological processes of genes differentially expressed when comparing β clusters 1, 2, 3, 4, 5, 7, 9, 17, 18 against β clusters 12 and 13 in *Sorcs2*$^{+/+}$ pancreatic islets.
(C) Graph representing biological processes of genes differentially expressed when comparing β clusters 1, 2, 3, 4, 5, 7, 9, 17, 18 against β clusters 8, 10, and 15 of *Sorcs2*$^{+/+}$ pancreatic islets.
The significance of data was determined using limma moderated t-statistics with $p \leq 0.05$ considered significant. Gene ontology analysis was performed with the clusterProfiler R package. Adjusted p-value (p.adjust) calculated with the Benjamini-Hochberg test with $p \leq 0.05$ considered significant.

3.14 Single-cell RNA sequencing suggests increased cell stress in SORCS2-deficient pancreatic islets

To delve deeper into the impact of receptor deficiency on pancreatic islet cell types, differential gene expression analysis using the limma test was conducted, comparing *Sorcs2*$^{+/+}$ and *Sorcs2*$^{-/-}$ samples across combined β clusters, as well as separately for α, δ, and PP clusters.

Among all cell types, β cells exhibited the most significant alterations in response to pancreatic islet *Sorcs2* deficiency, with 2507 upregulated and 1739 downregulated genes (Figure 23 A). α cells were comparatively less affected, showing approximately 100 genes both up- and down-regulated. In contrast, PP and δ cells exhibited minimal impact due to *Sorcs2* deficiency (Figure 23 A).

Across all four cell types, 10 differentially expressed genes were identified in common, primarily associated with mitochondrial function (*Cox7c, Cox6c, mt-Nd3*), ribosomal function (*Rpl39, Rpl41, Rn18s*), transcription (*IER2, Jun*), or pseudogenes (*Gm28438, Mir6236*) (Figure 23 B, C).

Both α and β cell types shared 170 differentially expressed genes, primarily linked to cell stress response, as indicated by GO terms such as "oxidative phosphorylation," "aerobic respiration," "response to oxidative stress," and "response to reactive oxygen species." These shared findings suggested a potential role for SORCS2 as a protective stress response factor in both cell types (Figure 23 B, C).

For further insight, GSEA was employed specifically for β and α cells. This gene ontology method discriminates between up- and down-regulated genes, assigning them to GO terms based on their fold change [211] (for details, refer to the methods section 2.3.11.3.6).

GSEA for combined β clusters identified GO terms associated with "Cellular response to unfolded proteins," "Cellular response to topologically incorrect proteins," and "Response to oxidative stress," indicating a suppressed cell stress response in *Sorcs2*$^{-/-}$ samples (Figure 24 A).

Furthermore, *Sorcs2*$^{-/-}$ β cells displayed distinct gene expression patterns associated with GO terms such as "suppressed protein and vesicle transport," "retrograde protein transport ER to the cytosol," and "endoplasmic reticulum to Golgi vesicle-mediated transport" (Figure 24 A). This observation was supported by corresponding data indicating altered vesicle structure obtained through EM analysis (Figure 15). Notably, the GO term "COPI-coated vesicle budding" also exhibited differences in transcriptomes (Figure 24 A), with particular relevance to the export of proinsulin from the ER and the formation of mature insulin [308]. Additionally, an upregulation of genes involved in insulin secretion was identified (Figure 24 A), suggesting a potential compensatory mechanism in response to impaired insulin release machinery in mutant β cells.

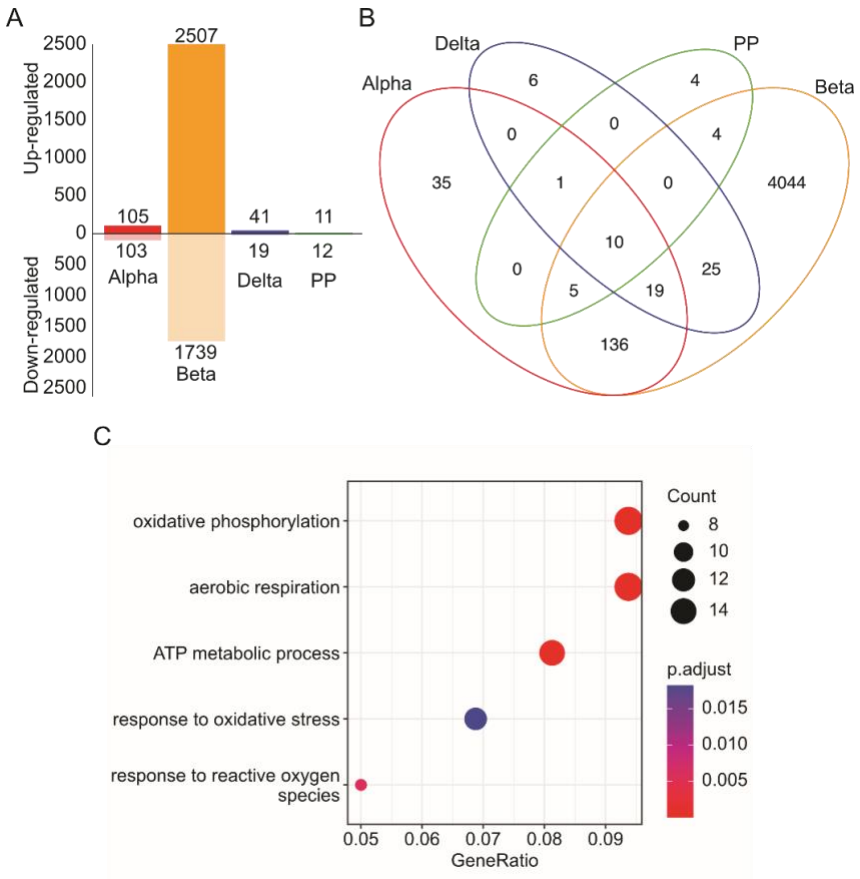

Figure 23: *Sorcs2* deficiency affects gene expression of α and β, but not δ and PP cell types of pancreatic islets

(A) Bar graph comparing numbers of up- or down-regulated genes in α, β, δ, and PP cell types.
(B) A Venn diagram showing numbers of differentially expressed genes common between all cell types identified by comparing gene counts between *Sorcs2*$^{+/+}$ and *Sorcs2*$^{-/-}$ in α, β, δ, and PP cell types.
(C) Graph representing biological processes common to α and β cell types of differentially expressed genes identified by comparing gene counts between *Sorcs2*$^{+/+}$ and *Sorcs2*$^{-/-}$.
The significance of data was determined using limma moderated t-statistics with p≤0.05 considered significant. Gene ontology analysis was performed with the clusterProfiler R package. Adjusted p-values (p.adjust) were calculated with the Benjamini-Hochberg test with p≤0.05 considered significant.

Among the genes associated with these GO terms, *Nupr1*, a stress-inducible chromatin protein [309], emerged as the most consistently and significantly downregulated gene, linking ER stress, oxidative stress, and COPI-coated vesicle budding pathways (Figure 24 A, B). Previous studies have demonstrated that *Nupr1* inactivation in pancreatic islets led to a diminished ER stress response, resulting in reduced oxidative phosphorylation, ATP production, mitochondrial failure, and eventual cell death [309].

Another intriguing target associated with GO terms in β cells is *Manf* (mesencephalic astrocyte-derived neurotrophic factor) (Figure 24 B). Originally identified as a trophic factor for dopamine neurons, *Manf* is expressed in various peripheral tissues, including the pancreas and specifically β cells [310]. MANF localizes to the ER in response to ER stress and plays a crucial role in protecting against ER stress-induced damage [310].

Furthermore, *Manf*$^{-/-}$ mice exhibited insulin-deficient diabetes characterized by decreased β cell proliferation and increased β cell apoptosis due to unresolved ER stress [310]. Overexpression studies of *Manf* confirmed its role in stimulating β cell proliferation and providing protection against ER stress [310].

The proposed mechanism of MANF action involves the inactivation of PERK/EIF2α activation, leading to the suppression of *Trib3* expression and the activation of AKT-CDK4-cyclinD1 activity, thereby regulating proliferation [310,311].

The downregulation of *Manf* and *Nupr1* in *Sorcs2*$^{-/-}$ β cells suggests potential unresolved ER stress in *Sorcs2*$^{-/-}$ pancreatic islets. Consistent with this evidence, *Sorcs2*$^{-/-}$ β cells may experience heightened cellular stress, resulting in unresolved stress responses in the ER and mitochondria. These defects are known to adversely affect insulin vesicle formation, ultimately leading to attenuated glucose-stimulated insulin secretion. Given

that SORCS2 is not expressed in β cells, the cellular stress observed in this cell type likely originates from mechanisms *in trans*.

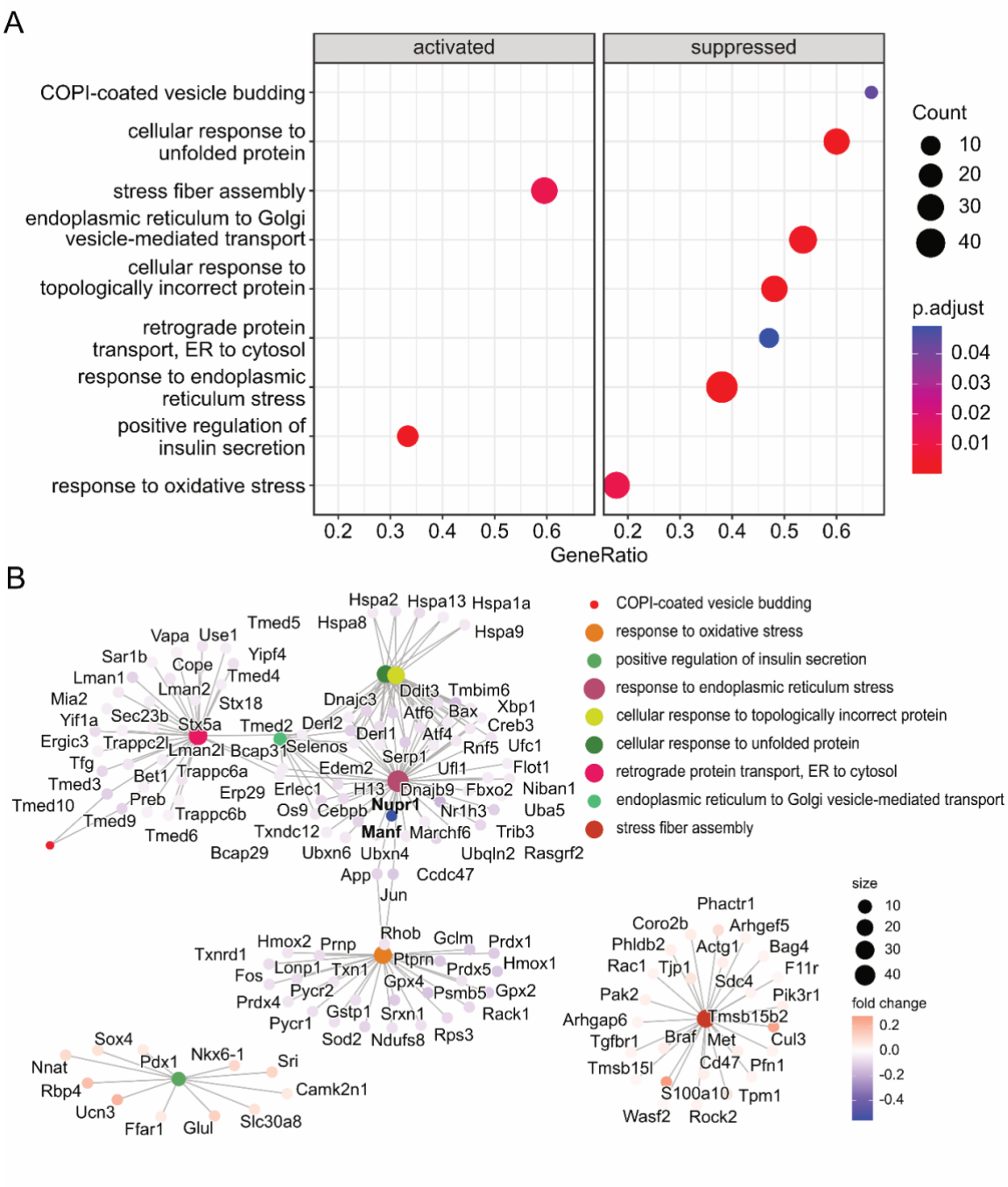

Figure 24: *Sorcs2* deficiency in pancreatic β cell type leads to suppressed cell stress response and dysregulation of vesicle formation

(A) GSEA analysis performed on genes differentially expressed comparing *Sorcs2*$^{-/-}$ and *Sorcs2*$^{+/+}$ pancreatic islet β cell type using clusterProfiler R package.
(B) Category gene net plot showing gene associated with gene ontology terms in GSEA analysis.
The significance of data was determined using limma moderated t-statistics with $p \leq 0.05$ considered significant. Gene ontology analysis was performed with the clusterProfiler R package. Adjusted p-value (p.adjust) was calculated with the Benjamini-Hochberg test with $p \leq 0.05$ considered significant.

Subsequently, changes in gene expression between *Sorcs2*$^{+/+}$ and *Sorcs2*$^{-/-}$ α cells were analyzed. The GSEA analysis of differentially expressed genes in α cells revealed a trend similar to that observed in β cells, indicating a decreased cell stress response, as evidenced by GO terms such as "response to stress," "response to oxidative stress," and "regulation of response to stress" (Figure 25 A). Moreover, *Sorcs2*$^{-/-}$ α cells exhibited alterations in gene expression associated with GO terms related to the "regulation of DNA-templated transcription from RNA polymerase" and "regulation of gene expression," suggesting a potential suppression of the transcription machinery (Figure 25 A).

Furthermore, *Sorcs2*-deficient α cells displayed downregulation of genes encoding transcription factors implicated in pancreatic islet maturation and proliferation, including *Klf4, Klf6, Jun, JunD, Fos,* and *FosB* (Figure 25 B) [221,312–314]. Considering the documented high expression of SORCS2 in human stem cell α and β cells and the dysregulation in the expression of pancreatic islet-related transcription factors, the suppression of stress response in *Sorcs2*$^{-/-}$ α cells may have developmental implications [221].

Moreover, the mitogen-activated protein kinase (MAPK) cascade was observed to be downregulated in *Sorcs2*$^{-/-}$ α cells (Figure 25 A). MAP kinases can be categorized into three families: extracellular-signal-regulated kinases (ERK), Jun amino-terminal kinases (JNK), and stress-activated protein kinases (p38/SAPK) [315]. The MAPK signaling pathway serves as a double-edged sword in response to ER stress. ERK1/2 activation promotes cell survival by increasing the expression of anti-apoptotic proteins such as MCL-1 [316], BCL2 [317], and BCL-XL [318] while simultaneously reducing the expression of pro-apoptotic proteins like BIM, PUMA, and BMF [319,320]. Conversely, JNK activation in response to ER stress induces cell death by acting on cell death receptors, their ligands, and components of the BCL2 family [320]. The activation of p38, also triggered by cellular stressors, can lead to either cell proliferation or cell cycle arrest. ER stress primarily targets p38 and JNK, highlighting their involvement in the UPR [320]. Some studies even propose suppressed UPR upon the inactivation of JNK [321,322].

α cells exhibit lower susceptibility to ER stress compared to β cells, primarily because of their elevated expression of Bcl-xL, an anti-apoptotic protein that enhances cell survival by inhibiting proapoptotic proteins Bax and Bak [323,324]. Given that the MAPK cascade

is a known stimulator of Bcl-xL expression, and *Sorcs2*$^{-/-}$ α cells display suppressed MAPK signaling, it is conceivable that *Sorcs2*$^{-/-}$ α cells may experience compromised ER stress responses owing to the inhibition of MAPK signaling.

A gene net plot depicting differentially expressed genes associated with GO terms for α cells revealed another MAPK signaling and stress-related gene, *Spp1* (osteopontin) (Figure 25 B). SPP1 expression is induced through AKT, ERK, JNK, STAT3, and Rac1 pathways in response to various stressors, including DNA damage, ER stress, and high glucose levels [325–327]. SPP1 functions include the promotion of cell survival, stimulation of proliferation, and modulation of pro- or anti-inflammatory processes [328]. Notably, externally added SPP1 can stimulate insulin secretion in pancreatic β cells in a calcium-dependent manner, facilitating insulin vesicle docking upon glucose stimulation [329–331]. I propose a mechanism in which SORCS2 stimulates the MAPK pathway, leading to increased SPP1 expression and secretion in α cells, thereby promoting cell survival through MAPK signaling. The secreted SPP1, in turn, enhances insulin secretion from β cells upon glucose stimulation.

Similar to α cells, *Sorcs2*-deficient δ and PP cells exhibited changes in gene expression profiles related to altered gene transcription machinery and gene expression (Figure 26 A, B), suggesting a common mechanism of action for SORCS2 in α, δ, and PP cell types.

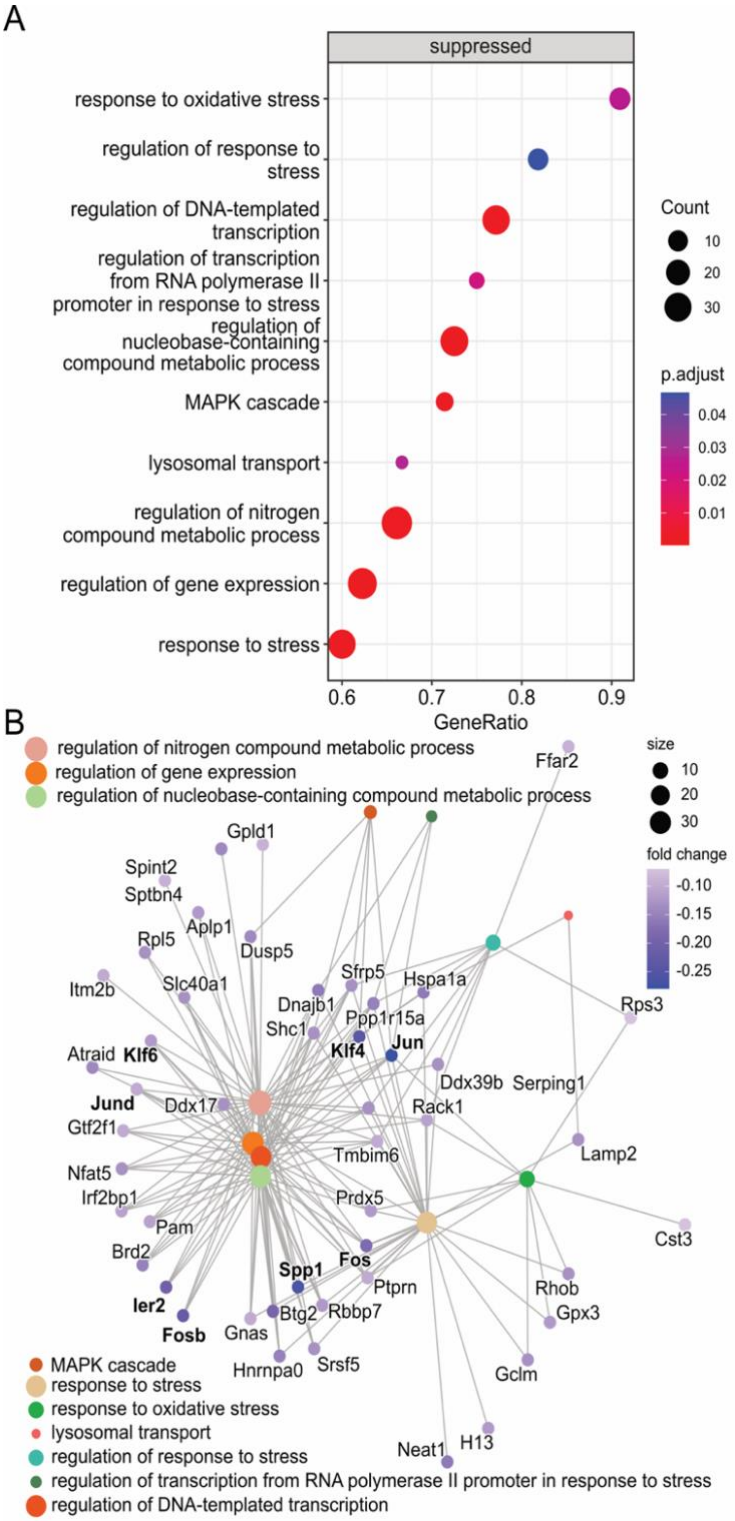

Figure 25: *Sorcs2* deficiency affects the transcription machinery and suppresses cellular stress response in α cells.

(A) GSEA analysis performed on genes differentially expressed comparing *Sorcs2*$^{-/-}$ and *Sorcs2*$^{+/+}$ pancreatic islet α cell type.
(B) Category gene net plot showing genes associated with gene ontology terms in GSEA analysis.

The significance of data was determined using limma moderated t-statistics with p≤0.05 considered significant. Gene ontology analysis was performed with the clusterProfiler R package. Adjusted p-value (p.adjust) calculated with the Benjamini-Hochberg test with p≤0.05 considered significant.

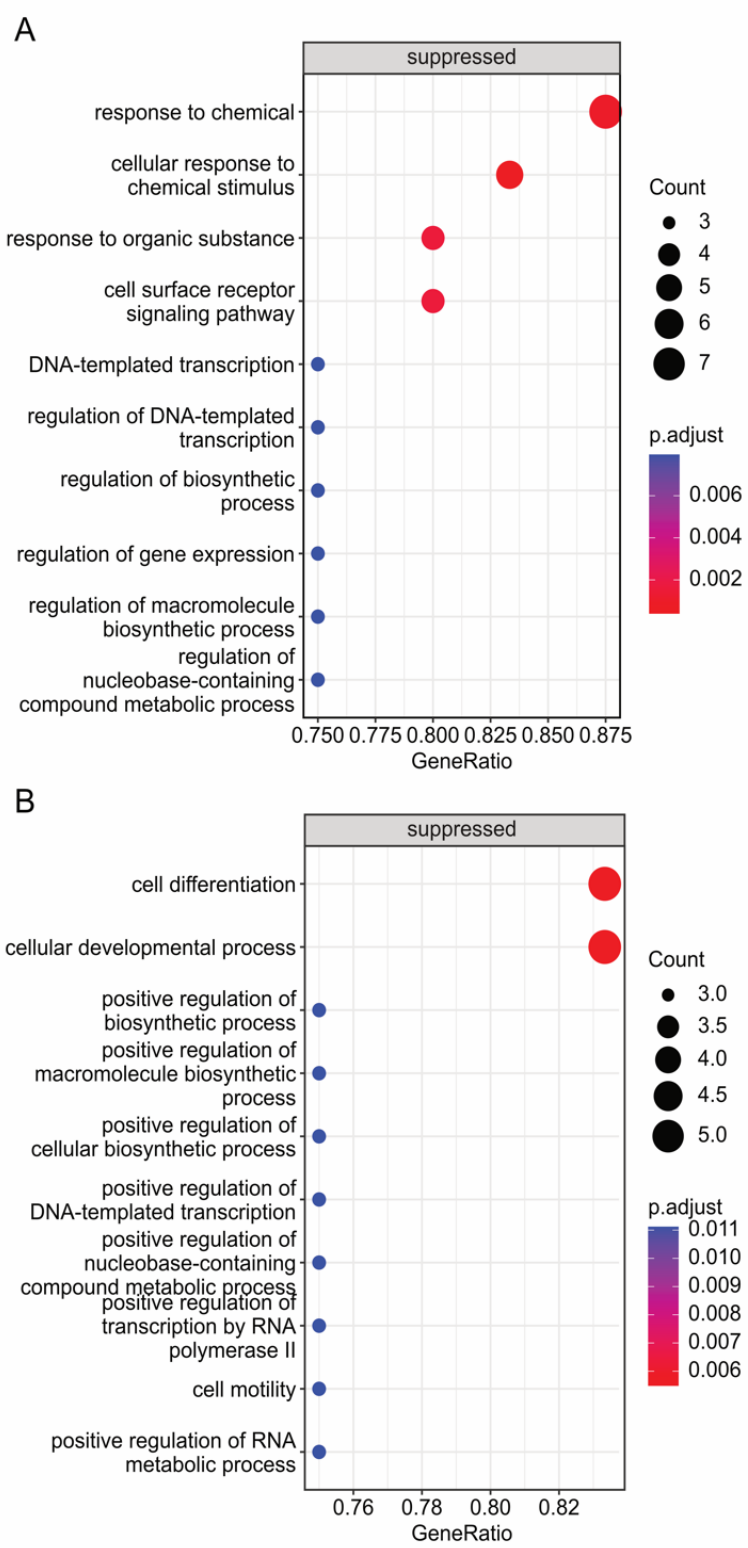

Figure 26: *Sorcs2* deficiency affects the transcription machinery in δ and PP cells.

(A) GSEA analysis performed on genes differentially expressed in *Sorcs2*$^{-/-}$ versus *Sorcs2*$^{+/+}$ pancreatic islet δ cell type using clusterProfiler R package.
(B) GSEA analysis performed on genes differentially expressed in *Sorcs2*$^{-/-}$ versus *Sorcs2*$^{+/+}$ pancreatic islet PP cell type using the clusterProfiler R package.
The significance of data was determined using limma moderated t-statistics with p≤0.05 considered significant. Gene ontology analysis was performed with the clusterProfiler R package. Adjusted p-value (p.adjust) calculated with the Benjamini-Hochberg test with p≤0.05 considered significant.

3.15 SORCS2 deficiency does not induce inflammatory responses in pancreatic islets

Excessive ER stress, mediated through the activation of the nuclear factor-κB or MAPK pathway, has the potential to induce the overproduction of reactive oxygen species, leading to inflammation [332]. GO analysis of differentially expressed genes in α and β cells revealed alterations in GO terms associated with the response to oxidative stress in mutant cells (Figure 24 A and Figure 25 A). Consequently, I performed an analysis of freshly isolated pancreatic islets to assess the transcript levels of inflammatory cell markers and cytokines using RT-qPCR. Specifically, I examined the abundance of transcripts related to M1 macrophages (*Nos2, IL-6*), M2 macrophages (*Arg1, CD32, Iba1*), T-cells (*CD3*) [333], B-cells (*CD40*) [334], as well as pro-inflammatory cytokines *TNF-α* and *IL-6* [166].

However, results did not indicate any changes in the transcript levels of the tested genes (Figure 27). Therefore, SORCS2 deficiency does not directly promote inflammation.

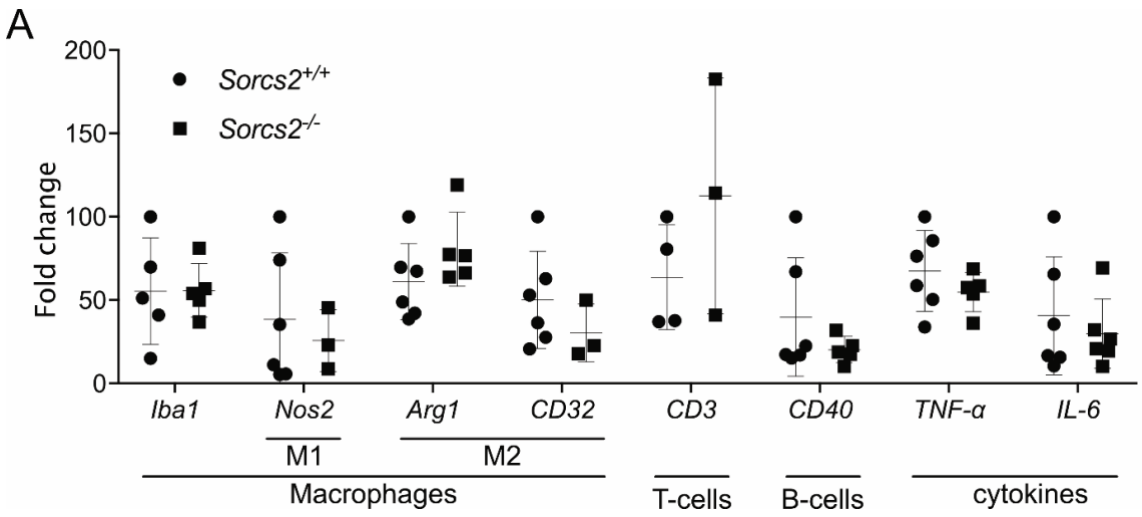

Figure 27: SORCS2-deficient islets do not promote inflammation

(A) Fold changes in transcripts encoding the indicated inflammatory markers comparing freshly isolated Sorcs2$^{+/+}$ and Sorcs2$^{-/-}$ islets (n = 3-6 animals per genotype) using q RT-PCR.
The significance of data was determined using an unpaired Student's t-test.

3.16 SORCS2 deficiency alters osteopontin expression through the AKT pathway

One gene that exhibited strong downregulation in α cells was *Spp1* (secreted phosphoprotein 1) (Figure 25 B). Secreted phosphoprotein 1, also known as osteopontin, belongs to the small integrin-binding ligand N-linked glycoprotein (SIBLING) family. It plays a crucial role in various biological processes, including bone remodeling, inflammation, cellular stress responses, and cancer [335,336]. Osteopontin is widely expressed in diverse tissues, and its significance has been well-established in bone, lung, gastrointestinal tissues, and inflammatory cells, where it activates anti-apoptotic pathways in response to stress [335,336].

Osteopontin, acting on integrin receptors, can activate several signaling pathways, including protein kinase B (AKT), Janus kinase 2 (Jak2), and mitogen-activated kinase (MEK), which, in turn, activate anti-apoptotic pathways [335]. Additionally, osteopontin can directly interact with the apoptosis regulator factor B-cell lymphoma-2 (Bcl-2) to promote cell survival (Figure 28) [335]. In pancreatic islets, osteopontin has a specific function of inhibiting nitric oxide synthase (iNOS), preventing the accumulation of nitric oxide (NO) in response to cellular stress (Figure 28) [335].

Beyond its role in stress responses, the expression product of osteopontin is implicated in potentiating glucose-stimulated insulin secretion. This dual functionality makes osteopontin an intriguing target for further investigation [329,330].

To validate the findings from scRNA-seq results, I conducted a comprehensive analysis of osteopontin expression at both the transcript and protein levels in isolated pancreatic islets, using RT-qPCR and ELISA, respectively.

The results clearly demonstrated a significant reduction in both osteopontin transcript and protein levels in SORCS2-deficient samples compared to *Sorcs2*$^{+/+}$ samples (Figure 29 A, B). Furthermore, to assess the impact of SORCS2 deficiency on osteopontin secretion, *Sorcs2*$^{+/+}$ and *Sorcs2*$^{-/-}$ pancreatic islets were cultured overnight, and the culture medium for secreted osteopontin was analyzed using ELISA.

This additional experiment revealed a noticeable decrease in osteopontin secretion in *Sorcs2*$^{-/-}$ samples (Figure 29 C). These findings provide robust support for the hypothesis that SORCS2 plays a crucial role in influencing glucose-stimulated insulin secretion from β cells through the regulation of osteopontin release from α cells.

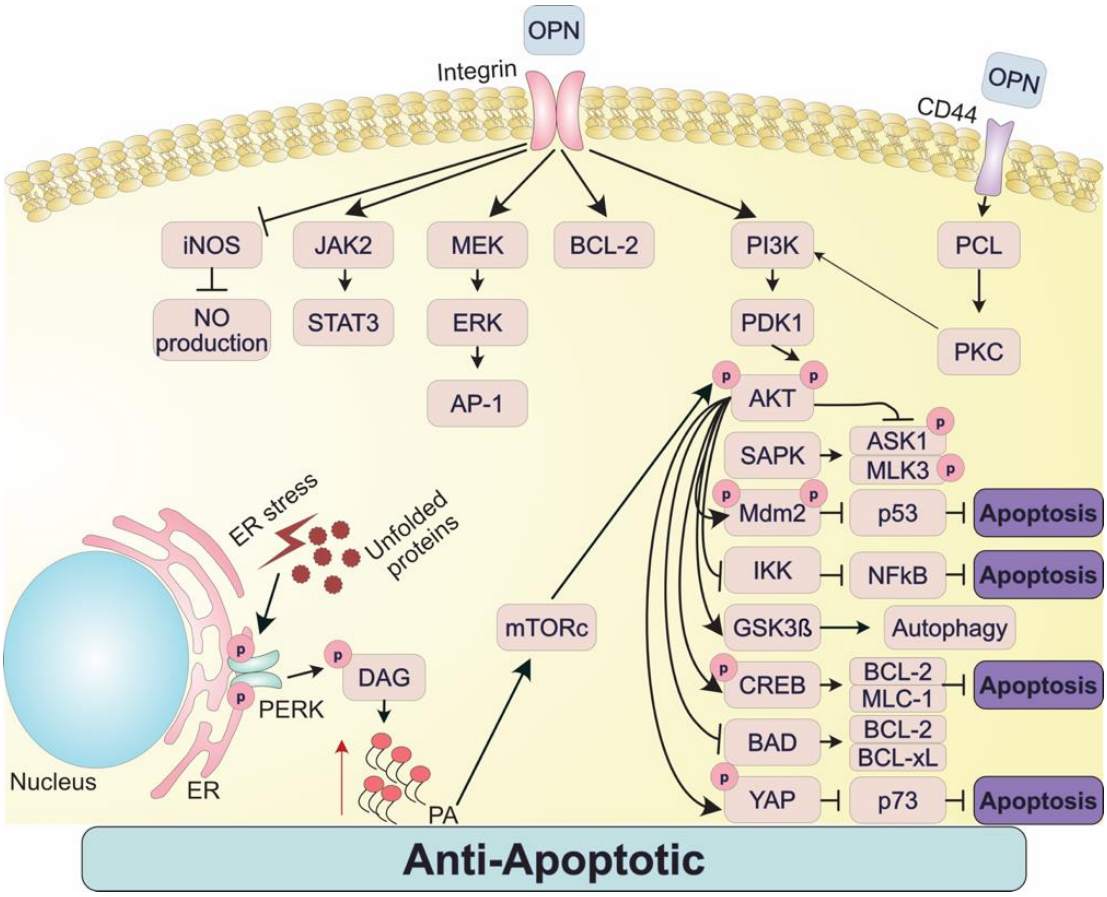

Figure 28: Molecular mechanisms involved in osteopontin (OPN) regulation of apoptosis and ER stress regulation of AKT pathway.

OPN can act through integrin and CD44 receptors in order to activate anti-apoptotic signaling. By acting on the integrin receptor, OPN activates Jak2-STAT3, ERK, and PI3K pathways. Additionally, OPN activates BCL-2 and inhibits iNOS action. By acting on the CD44 receptor, OPN activates PKC, which further potentiates PI3K pathway activation.

AKT (protein kinase B), AP-1 (activator protein-1), ASK1 (apoptosis signal-regulating kinase 1); BCL-2 (B-cell lymphoma-2), CREB (cAMP response element-binding protein), DAG (diacylglycerol), ER (endoplasmic reticulum), ERK (extracellular-signal regulated kinases), GSK3ß (glycogen synthase kinase β), iNOS (nitric oxide synthase), JAK2 (Janus Kinase 2), Mdm2 (Murine double minute 2); MEK (mitogen-activated protein kinase kinase), MLK3 (mixed lineage kinase 3); mTORc (mammalian target of rapamycin complex), NFkB (nuclear factor kappa light chain enhancer of activated B cells), NO (nitric oxide), PA (phosphatidic acid), PERK (protein kinase R (PKR)-like endoplasmic reticulum kinase), PI3K (phosphoinositide 3-kinase), PKC (protein kinase C), PCL (polycomb-like protein), SAPK (stress-activated protein kinase), STAT3 (signal transducer and activator of transcription 3), YAP (yes-associated protein 1).

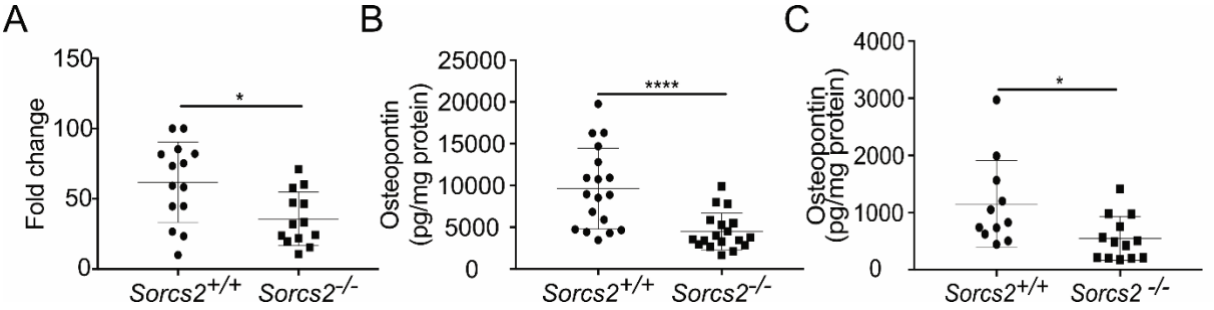

Figure 29: Impaired osteopontin expression in SORCS2-deficient islets

(A) Fold change for *Spp1* transcript levels was determined by quantitative RT-PCR in *Sorcs2*$^{+/+}$ and *Sorcs2*$^{-/-}$ islets cultured overnight (n = 12-13 animals per genotype).
(B) Osteopontin levels were determined by ELISA in lysates of isolated *Sorcs2*$^{+/+}$ and *Sorcs2*$^{-/-}$ islets cultured overnight (n = 18 animals per genotype).
(C) Secreted osteopontin levels were determined by ELISA in the supernatant of isolated *Sorcs2*$^{+/+}$ and *Sorcs2*$^{-/-}$ islets cultured overnight (n = 11-13 animals per genotype).
The significance of data was determined using an unpaired Student's t-test (A) or Mann-Whitney U test (B, C). *, $p < 0.05$; ****, $p < 0.0001$.

To explore how SORCS2 activity may influence osteopontin expression and secretion, pathways known to be associated with the control of osteopontin expression were investigated. These pathways include protein kinase B (AKT), extracellular signal-regulated kinases (ERK), signal transducer and activator of transcription (STAT3), and p38 mitogen-activated protein kinases (p38 MAPK) pathways (Figure 28).

For the analysis of AKT, ERK, STAT3, and p38 MAPK pathway activation, I isolated and cultured overnight pancreatic islets from *Sorcs2*$^{+/+}$ and *Sorcs2*$^{-/-}$ mice. Western blotting was then employed to assess total levels of proteins (AKT, ERK1/2, STAT3, and p38) as well as their phosphorylated counterparts (pAKT-Thr308, pAKT-Ser473, pERK1/2, pSTAT3, pp38). The ratio of phosphorylated to total protein served as an indicator of pathway activity.

The results demonstrated a reduced activation of the AKT pathway (Figure 30 A, B) and a tendency towards decreased activation of the p38 pathway (Figure 30 C, A).

Notably, the ERK1/2 and STAT3 pathways were not significantly affected by SORCS2 deficiency.

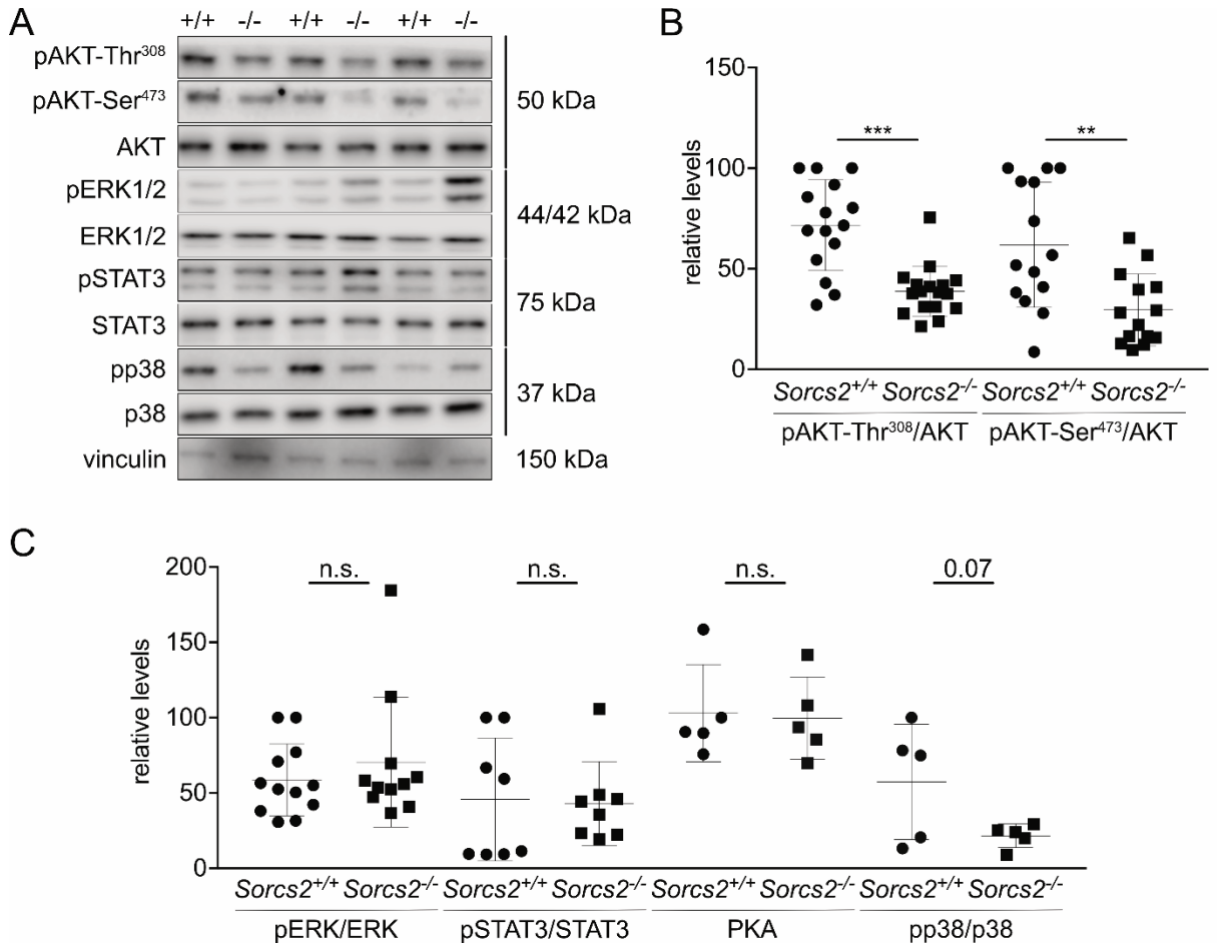

Figure 30: Impaired AKT signaling in SORCS2 deficient islet samples

(A) Levels of the indicated proteins in lysates of isolated *Sorcs2*$^{+/+}$ (WT) and *Sorcs2*$^{-/-}$ (KO) islets were detected using western blotting analysis. The blots show representative data of three individual pools of islet preparation for each genotype (approximately 250 islets per pool). Detection of vinculin served as loading control. p, phosphorylated.
(B, C) Quantitative analysis of protein levels based on densitometric scanning of replicate blots (as exemplified in A) of a total of 13-18 pools of isolated islets per genotype.
The significance of data was determined using an unpaired Student's t-test (B, C). **, $p < 0.01$; ***, $p < 0.001$; ****, $p < 0.0001$; n.s., not significant.

The AKT pathway, similar to MAPK, is activated by ER stress. Specifically, ER stress triggers the activation of protein kinase RNA-like ER kinase (PERK), which, through its lipid kinase activity, enhances the production of phosphatidic acids (PA) (Figure 28) [337]. Elevated PA levels activate the mTOR complex, leading to the phosphorylation of AKT on Ser473, partially activating the AKT pathway [338]. Additionally, the mTOR complex inhibits the phosphorylation of insulin receptor substrate, activating the PI3K pathway and, subsequently, its downstream target, phosphoinositide-dependent kinase-1 (PDK1), which phosphorylates AKT on Thr308, fully activating the AKT pathway [338,339].

Phosphorylated AKT, in its turn, promotes cell survival in various ways [340] (Figure 28). Firstly, via activation of glycogen synthase kinase-3 β (GSK3β), which promotes autophagy via 60-kDa tat-interactive protein (TIP60) – unc-51 like autophagy activating kinase 1 (ULK1) pathway [341]. Secondly, by phosphorylating and consequently inactivating proapoptotic protein of Bcl-2 family Bcl-2-associated death promoter (BAD) on Ser136, which activates Bcl-2 and Bcl-xL proteins [340] (Figure 28). Thirdly, via phosphorylation and consequent inhibition of upstream kinases of stress-activated protein kinase (SAPK) pathway, which regulate responses to stress: MAP kinase kinase (MKKK) on Ser83, mixed lineage kinase 3 (MLK3) on Ser674 and dual specificity mitogen-activated protein kinase SEK1 (SEK1) on Ser78 [340] (Figure 28). AKT also activates cyclic AMP (cAMP)-response element binding protein (CREB) through phosphorylation at Ser133, which consequentially activates antiapoptotic Bcl-2 and Mcl-1 proteins [340] (Figure 28). AKT may also phosphorylate and increase ligase activity of murine double minute 2 (Mdm2), which leads to deactivation of p53 pro-apoptotic response. Finally, AKT can activate YES-associated protein (YAP) via phosphorylation at Ser127, which in turn suppresses p73-mediated apoptosis [340] (Figure 28).

This data supports the hypothesis that SORCS2 deficiency in α cells disrupts AKT and MAPK pathways, leading to an inadequate UPR, decreased cell survival mechanisms, and a subsequent reduction in the secretion of SPP1, thereby dampening glucose-stimulated insulin secretion in β cells.

4 Discussion

4.1 Effects of SORCS2 deficiency on glucose metabolism

Glucose is a primary metabolic fuel in mammalian organisms, and precise regulation of glucose metabolism is vital for survival, given that both its deficiency and excess can lead to severe complications or even death.

The genetic association of *SORCS2* with both T2DM [54] and BMI [342], coupled with its close structural resemblance to SORCS1 — a protein integral to β-cell vesicle formation [343] — prompted an investigation into the potential role of SORCS2 in glucose metabolism, particularly its involvement in insulin secretion from pancreatic islets.

Sorcs2$^{-/-}$ mice exhibited decreased glucose tolerance but not affected insulin tolerance, as determined by Dr. Vanessa Schmidt-Krüger [185]. Moreover, *Sorcs2*$^{-/-}$ mice exhibited decreased body weight and reduced lipid and glycogen content in the liver and muscles, further supporting our hypothesis of defective insulin secretion in these mice (Figure **9** A; Table 8; Table 9). Intraperitoneal injection of glucose in *Sorcs2*$^{-/-}$ mice revealed a diminished insulin secretion response compared to *Sorcs2*$^{+/+}$ mice (Figure 11 A). Additionally, high glucose stimulation of isolated *Sorcs2*$^{-/-}$ pancreatic islets confirmed a reduced insulin secretion response (Figure 12 B, E). Notably, electron microscopy analysis of pancreatic β cells revealed suppressed insulin vesicle maturation (Figure 15). However, morphological characteristics, such as β cell mass and areas of α, δ and PP cell types, of *Sorcs2*$^{-/-}$ pancreases were not affected (Figure 13; Figure 14).

Intriguingly, despite exclusive SORCS2 protein expression to α, δ and PP cells (Figure 10 B), basal or glucose-stimulated secretion of insulin-release regulatory hormones (glucagon, GLP-1, somatostatin, NPY, and PYY) released from α, δ, PP, or ε pancreatic islet cell types remained unaffected by SORCS2 deficiency, both *in vivo* and *in vitro* (Table 10; Table 11; Table 12)

Further insights from single-cell RNA sequencing analysis of *Sorcs2*$^{-/-}$ and *Sorcs2*$^{+/+}$ isolated pancreatic islets indicated a blunted stress response in *Sorcs2*$^{-/-}$ α and β cells, possibly linked to reduced expression of the stress response molecule osteopontin from

α cells (Figure 24; Figure 25; Figure 29). Osteopontin protein levels and secreted levels were also found to be diminished in *Sorcs2*$^{-/-}$ pancreatic islets (Figure 29). Moreover, the AKT signaling pathway, known to regulate SPP1 expression [335], was inhibited by SORCS2 deficiency (Figure 30 B).

Given osteopontin's crucial role in enhancing the distribution of β-cell insulin granules [344] and its stimulatory impact on glucose-stimulated insulin secretion within pancreatic islets [345], I posit that SORCS2 in α cells indirectly modulates the expression of SPP1 by influencing the AKT pathway. Upon secretion, osteopontin is likely to augment glucose-stimulated insulin secretion, as well as potentiate stress response in pancreatic β cells. Stress potentiation, in turn, facilitates the proper maturation of insulin vesicles, thereby ensuring their correct functionality.

4.2 SORCS2 promotes systemic glucose metabolism

Our understanding of SORCS2's involvement in glucose metabolism is reinforced by findings from Dr. V. Schmidt-Krüger, demonstrating distinct metabolic alterations in *Sorcs2*$^{-/-}$ mice compared to their *Sorcs2*$^{+/+}$ counterparts [185].

Notably, *Sorcs2*$^{-/-}$ mice exhibited reduced glucose tolerance without a concurrent impairment in tissue insulin sensitivity, indicating an insulin-deficient phenotype rather than insulin resistance [185]. Dr. V. Schmidt-Krüger's investigation also revealed a decrease in the respiratory exchange ratio during the day in *Sorcs2*$^{-/-}$ mice [185], suggesting an increased reliance on lipids as the primary energy source — an observation commonly associated with insulin deficiency [346,347] .

Despite elevated lipid oxidation being a hallmark of decreased insulin availability [348,349], I acknowledge that other factors may contribute to the altered metabolic fuel consumption in *Sorcs2*$^{-/-}$ mice. Notably, the increased activity observed in these mice, reminiscent of an ADHD-like phenotype [350], could potentially influence higher lipid utilization, as documented in humans following endurance training [351].
My investigation further substantiates SORCS2's role in systemic glucose metabolism by revealing reduced levels of glycogen, cholesterol, and free fatty acids in the liver (Table 8) and decreased levels of glycogen in skeletal muscles (Table 9) of *Sorcs2*$^{-/-}$ mice

compared to *Sorcs2*$^{+/+}$. These observations align with the characteristic blunting of insulin stimulation on lipogenesis and glycogen synthesis [215–217].

In tandem with diminished muscle and liver glycogen and lipid stores, *Sorcs2*$^{-/-}$ mice exhibited a reduced body weight compared to *Sorcs2*$^{+/+}$ mice (Figure **9**), mirroring established phenotypes of Type 1 Diabetes (T1D). In early T1D stages, insulin deficiency leads to attenuated tissue glucose uptake, prompting increased reliance on fat and glycogen as primary metabolic fuel sources [352,353].

4.3 SORCS2 expression is specific to non- β pancreatic cell types

To substantiate the potential involvement of SORCS2 in insulin secretion, I present evidence of its predominant expression in pancreatic α, δ, and PP cells, distinctly absent from β cells (Figure 10). Single-cell RNA sequencing (scRNA-seq) analysis further supports this observation, highlighting heightened *Sorcs2* expression in α, δ, and PP cells, while acknowledging some presence in the β cell cluster 14 (Figure 17 C). Notably, cluster 14 exhibits characteristics indicative of a multi-hormonal, transdifferentiating-like, or progenitor-like nature (Figure 17 B, Figure 21 A, B).

The complexity arises when considering the nature of cluster 14, prompting a discussion on the ongoing debate surrounding the presence of transdifferentiating or immature cells within adult pancreatic islets. Numerous studies affirm the ability of α [354], δ [355], and β [286] cells to undergo de-differentiation or reprogramming. During the onset of Type 1 Diabetes (T1D), pancreatic β cells were demonstrated to dedifferentiate, characterized by impaired oxidative phosphorylation and heightened expression of progenitor cell markers [286,356]. In a diphtheria toxin-induced acute selective near-total β cell ablation transgenic mouse model, pancreatic α cells transdifferentiated into β cells, displaying an intermediate stage of bi-hormonal (glucagon+, insulin+) cells attempting to augment β cell mass after total ablation [354]. Additionally, pancreatic δ cells were found to reprogram into insulin-producing cells in a FOXO1-dependent manner, and pharmacological FOXO1 inhibition stimulated δ to β cell reprogramming [355].

Our findings align with previously published mouse pancreas scRNA-seq analyses, emphasizing *Sorcs2*'s predominant expression in α, δ, and PP cell types [222,223].

Notably, these studies reported slight *Sorcs2* expression in β cell populations, though they did not distinguish between different types of β cell clusters, leaving the nature of *Sorcs2* expression in predominantly transdifferentiating or progenitor-like clusters undetermined [222,223]. In human pancreatic islet scRNA-seq, *SORCS2* exhibited its highest expression in α cells [219]. Conversely, scRNA-seq analysis of induced pluripotent stem-derived pancreatic islets demonstrated *SORCS2* expression in adult α, δ, and β cells [222,223]. Intriguingly, the highest expression of *SORCS2* was identified in early stem-cell α and β cell clusters, characterized by a multi-hormonal nature secreting both glucagon and insulin, as well as in stem-cell enterochromaffin cells cluster secreting serotonin [221,357]. These findings not only affirm our results of *Sorcs2* expression in multi-hormonal, progenitor-like cell types (β cell cluster 14, Figure 17 C) but also raise questions about SORCS2's potential involvement in pancreatic islet development.

4.4 SORCS2 promotes insulin secretion from beta cells

Building upon the observed reductions in glucose tolerance, liver and muscle glycogen, and lipid levels in *Sorcs2*$^{-/-}$ mice, this section provides a comprehensive analysis of insulin secretion and the underlying mechanisms influenced by SORCS2 deficiency.

The *in vivo* and *in vitro* assessments of insulin and C-peptide secretion during high-glucose stimulation clearly indicate a significant reduction in *Sorcs2*$^{-/-}$ samples compared to *Sorcs2*$^{+/+}$ controls (Figure 11 A, B; Figure 12 B). Notably, even under basal conditions, C-peptide secretion was diminished in *Sorcs2*$^{-/-}$ mice (Figure 11 C, D), emphasizing the importance of considering basal insulin secretion. The argument for decreased insulin secretion under basal conditions is further supported by the slower degradation rate of C-peptide, making it a more accurate reflection of *in vivo* insulin secretion [358].

However, the nuanced findings related to the first phase of glucose-stimulated insulin secretion warrant discussion. While the *in vivo* setting revealed a decrease, isolated *Sorcs2*$^{-/-}$ pancreatic islets did not exhibit altered insulin secretion during the first phase (Figure 12 C, D, E). The proposed explanation involving a faster rate of insulin clearance in the liver, kidney, muscles, and other tissues highlights the importance of considering physiological context in interpreting *in vitro* results [359].

The attenuation of insulin secretion in response to KCl stimulation, which depolarizes β cell membrane and allows secretion from all primed and docked vesicles, further strengthens the argument for a generalized insulin release defect in *Sorcs2*$^{-/-}$ β cells (Figure 12 B). Morphological examination of pancreatic islets supports this observation, revealing abnormalities in secretory insulin granule formation in mutant beta cells, particularly evident in the increased numbers of immature vesicles and decreased numbers of crystallized mature vesicles (Figure 15).

An intriguing aspect to explore is the plausible connection between the observed reduction in insulin secretion upon KCl stimulation and potential alterations in Ca^{2+} channels in the context of SORCS2 deficiency. However, detailed scrutiny of the scRNA-seq data from *Sorcs2*$^{-/-}$ β cell clusters (for details please refer to methods section 2.3.11.3.5) revealed no significant changes in the genes associated with Ca^{2+} channels. Furthermore, the absence of SORCS2 expression in β cells (Figure 10 B) rules out the possibility of its direct involvement in the trafficking of calcium channels. This suggests that the diminished insulin secretion in response to KCl stimulation observed in SORCS2-deficient conditions may be mediated through alternative pathways or factors not directly linked to Ca^{2+} channel regulation.

The comparable total content of insulin and proinsulin in isolated pancreatic islets between genotypes (Figure 12 F, H), alongside reduced C-peptide content in *Sorcs2*$^{-/-}$ samples (Figure 12 G), raises intriguing questions. The 1:1 ratio of cleavage of insulin and C-peptide from proinsulin suggests the possibility of proinsulin processing defects or increased lysosomal degradation of C-peptide [103,125,126].

Furthermore, previous studies provide valuable insights into the fate of C-peptide compared to insulin. A faster rate of degradation of C-peptide compared to insulin by crinophagy, involving the fusion of vesicles with lysosomes, has been documented [239]. Additionally, the C-peptide pulse-chase approach in INS1 cells demonstrated an alternative degradation route for C-peptide from immature vesicles [360]. This pathway involves the sorting of C-peptide in immature vesicles and its transportation to lysosomes [360]. Both of these studies suggest that the reduction in C-peptide seen in *Sorcs2*$^{-/-}$ samples may be attributed to increased lysosomal degradation of C-peptide as compared to mature insulin.

The elevated presence of immature vesicles observed in *Sorcs2*$^{-/-}$ mice may find its roots in the disrupted maturation of ER-derived insulin, potentially induced by chronic ER stress [307] (Figure 24 A). This phenomenon mirrors findings in MIN6 cells treated with cyclopiazonic acid (CPA), an inhibitor of ER Ca^{2+} ATPases, leading to an imbalance in ER Ca^{2+} homeostasis, triggering the unfolded protein response (UPR) and chronic stress [307]. Notably, CPA-treated MIN6 cells demonstrated a mislocalization of proinsulin to cytoplasmic granules, similar to the distribution observed in *Sorcs2*$^{-/-}$ β cells [307]. The scRNA-seq analysis revealed distinct alterations in ER stress-related genes in *Sorcs2*$^{-/-}$ β cells (Figure 24 A), suggesting a potential link between the disrupted ER stress response and the aberrant proinsulin processing, ultimately culminating in the accumulation of immature vesicles in *Sorcs2*$^{-/-}$ β cells (Figure 15).

Alternatively, despite the absence of SORCS2 protein expression in mouse β cells, the scRNA-seq data indicating its presence in human progenitor β cells opens avenues for exploring SORCS2's potential role in the developmental formation of vesicle machinery [221].

Insulin secretion on the other hand, can be influence by SORCS2 in a paracrine manner by regulating the secretion of factors from α, δ or PP cells. These factors may include hormones such as glucagon [127,240], somatostatin [136], ghrelin [258], NPY [136], GLP-1 [103,127,253,254], or PYY [256,257].

Moreover, the influence of extracellular vesicles on insulin secretion should be considered. Studies in NOD scid gamma (NGS) mice treated with extracellular vesicles derived from the breast cancer cell line MDA-MB-231 revealed a decrease in glucose-stimulated insulin secretion [361]. Specifically, miR-122 secreted from the MDA-MB-231 cell line reduced pyruvate kinase M1/2 (PKM) expression, thereby suppressing glycolysis and ATP-dependent insulin secretion from isolated pancreatic islets derived from NGS mice and the MIN6 cell line [361]. These findings contribute to the intricate regulatory network involved in insulin secretion, providing an additional layer of complexity.

Furthermore, ER stress emerges as a crucial consideration. As highly metabolically active cell types, all pancreatic cell types are prone to ER stress, initiated by the high demand

for secreted hormones in response to glucose or other nutrients [177]. ER stress onset in one type of cell can be transmitted to the cell in close proximity through the secretion of factors of yet unknown nature [362,363]. Previous studies have demonstrated ER stress transmission between stressed cancer cells and macrophages, leading to the up-regulation of ER stress signaling pathways [362]. The nature of the secreted molecules, described as protein kinase K resistant lipid-like substances, emphasizes the complexity of intercellular communication in response to ER stress [363]. Similarly, ER-stressed astrocytes were shown to transmit ER stress to neuronal cells, further highlighting the intricate network of signaling molecules involved in stress responses [363].

4.5 Involvement of SORCS2 in global regulation of glucose metabolism

Central to the intricate web of glucose metabolism is the hypothesis that SORCS2's activity promotes insulin secretion through the controlled release of hormones from α, δ, or PP cells. This orchestrated release involves hormones that either inhibit (somatostatin [136], NPY [136], ghrelin [258]) or augment (glucagon [127,240], GLP-1 [103,127,253,254], PYY [256,257]) glucose-stimulated insulin secretion.

However, as the investigation unfolded, this hypothesis faced disproof. Documented levels of glucagon, GLP-1, and somatostatin *in vivo* (Table 10) and glucagon, GLP-1, somatostatin, NPY, PYY, and ghrelin *in vitro* (Table 11) remained comparable between mutant and control islets.

Yet, the dynamics of NPY and PYY secretion *in vivo* unveiled intriguing insights. Notably, NPY levels increased under basal conditions in *Sorcs2*$^{-/-}$ mice, while PYY levels decreased (Table 10). These alterations were not mirrored in isolated pancreatic islets *in vitro*, hinting at a broader role for SORCS2 beyond the islet microenvironment. This argues against a direct involvement of SORCS2 in hormone release from islet cell types but suggests additional roles in systemic control of metabolism, potentially in the hypothalamus or intestine.

4.5.1 Role for SORCS2 in hypothalamic regulation of glucose metabolism

Beyond the pancreatic realm, NPY's presence in the brain cortex, hippocampus, hindbrain, and hypothalamus unveils its multifaceted role in central metabolic regulation

[364]. Arcuate nucleus neurons in the hypothalamus, abundant sources of NPY, play pivotal roles in neuroendocrine regulation, appetite control, and insulin secretion [364].

NPY secretion responds to various factors, such as circulating elements (glucose, ghrelin, asprosin, glucocorticoids, etc.), synaptic inputs from the paraventricular nucleus of the hypothalamus (thyrotropin-releasing hormone, and pituitary adenylate cyclase-activating polypeptide), and inputs through neuropeptide FF receptor 2 signaling [365,366]. Secreted NPY orchestrates appetite control by acting on Y1 receptors on proopiomelanocortin (POMC) and cocaine-amphetamine-regulated transcript (CART) neurons in the arcuate nucleus, inhibiting their satiety outputs [365]. Without this inhibition, POMC neurons, responding to satiety signals (leptin, insulin, etc.), release the α-melanocyte-stimulating hormone [366]. This, in turn, acts on melanocortin receptors 3 and 4 to reduce food intake [366]. NPY neurons project to various brain regions, promoting feeding [366]. In regard to insulin secretion control, NPY is produced by the sympathetic nervous system, which is known to inhibit insulin and stimulate glucagon secretion [367].

scRNA-seq and mass spectrometry showcased the expression of SORCS2 in hypothalamic [368] and sympathetic neurons [369]. Additionally, increased *in vivo* NPY levels in *Sorcs2*$^{-/-}$ mice hint at SORCS2 involvement in neuronal NPY secretion (Table 10). Intriguingly, the role of NPY in stimulating food intake, which typically leads to obesity, contrasts with our data showing decreased body weight in *Sorcs2*$^{-/-}$ compared with *Sorcs2*$^{+/+}$ mice (Figure 9). This discrepancy might be attributed to increased activity due to an ADHD-like phenotype in *Sorcs2*$^{-/-}$ mice [185,186].

Another plausible explanation for decreased body weight alongside elevated NPY levels could be cellular desensitization in mutant mice due to persistent NPY signaling [370]. Studies showed that stimulation of the human neuropeptide Y2 receptor (hY_2R) with NPY leads to receptor internalization, preventing continuous stimulation until agonist removal [370]. Prolonged cellular stimulation with NPY persistently activates the Gαi pathway and depletes G-protein stores, dampening signaling through hY_2R even after agonist removal [370].

4.5.2 Role of SORCS2 in gut regulation of glucose metabolism

Turning attention to a possible role for SORCS2 in intestinal PYY release, this hormone exists in two forms [137]. Full-length PYY_{1-36}, predominantly expressed and secreted in the brain, and PYY_{3-36}, lacking the N-terminal dipeptide, secreted by enteroendocrine cells and intestinal L cells [137]. PYY_{1-36} directly inhibits insulin secretion by activating NPY receptors Y1 or Y4 on β cells [137]. Conversely, PYY_{3-36} may protect β cells from apoptosis by acting on Y1 receptors and inhibiting NF-κB in pancreatic islets [137]. Additional functions include inhibiting food intake and reducing weight gain [137]. Although the ELISA used did not discriminate between the two forms, considering PYY_{3-36} as the major circulating variant in *Sorcs2*$^{-/-}$ mice suggests a reduction in plasma PYY_{3-36} (Table 10).

scRNA-seq analysis revealed SORCS2 expression in small intestine tissue [371]. Hence, the impact of SORCS2 deficiency on PYY expression and/or secretion from this tissue is conceivable [371]. Unfortunately, the analysis did not distinguish specific cell types in the small intestine, limiting conclusions regarding *Sorcs2* expression in PYY-secreting L-cells [371].

Notably, the unchanged feeding behavior of *Sorcs2*$^{-/-}$ mice, as communicated by V. Schmidt [185], argues against a significant impact of altered NPY and PYY levels on the body metabolism of these mice (Table 10).

4.6 Heterogeneity of β-cell clusters in wildtype and SORCS2-deficient murine islets

In a quest to unravel the nuanced cellular mechanisms that link SORCS2 deficiency to alterations in insulin secretion within pancreatic islets, scRNA-seq experiments were conducted on pancreatic islets derived from both *Sorcs2*$^{-/-}$ and *Sorcs2*$^{+/+}$ mice. The findings unveiled a rich diversity, identifying fourteen β-cell clusters and single clusters for α, δ, and PP cell types (Figure 17 A, B).

A comparative gene expression analysis categorized the β-cell clusters into three distinctive groups. The first group showcased high insulin-secreting cells (clusters 15, 9,

8, 13, 12, 3) (Figure 19 B). The second group exhibited low insulin-secreting cells (1, 7, 2, 3, 5, 4, 10, 17) (Figure 19 D). Intriguingly, a unique cluster emerged, identified as antigen-producing β cells (cluster 18) (Figure 19 E). Furthermore, these β clusters were differentiated based on the expression of genes associated with β -cell maturation (*Mafa, Ucn3, Neurod1*) and functionality (*Slc2a2, G6pc2, Gck, Ins1, Ins2, Pcsk1*) (Figure 20; Figure 21).

The investigation illuminated the diverse nature of β-cell clusters. Clusters 1, 2, 3, 9, 13, and 12 exhibited maturity and high functionality, characterized by elevated expression of maturation markers and genes related to glucose and insulin handling (Figure 20, Figure 21). In contrast, clusters 1 and 2 represented low insulin-secreting cells, showcasing high expression of St9sia1 and low expression of *Pcsk1* (Figure 19 D, Figure 20). Clusters 4, 5, 6, 7, 8, 10, and 15 exhibited decreased expression of maturation markers and insulin and glucose handling genes, suggesting an immature β-cell state (Figure 20, Figure 21).

While SORCS2-deficient islets retained the same categories of β cell clusters, a quantitative analysis uncovered a substantial loss of cell numbers in clusters 8, 10, and 15, coupled with a gain in cell numbers in clusters 12 and 13 (Figure 22 A). Notably, clusters 8, 10, and 15 in mutant islets were marked by high ER stress, oxidative phosphorylation, and UPR (Figure 22 C). These features, indicative of highly metabolically active β cells, are also known to accompany unresolved ER stress and UPR, leading to cellular loss [178–180]. Thus, cell death due to unresolved cell stress caused by SORCS2 deficiency is a likely explanation for the decrease in cell numbers seen in mutant islets.

Clusters 12 and 13, exhibiting increased cell numbers in mutant islets, displayed markers of cell proliferation and differentiation (Figure 22 B). This suggests a compensatory mechanism, where proliferative cell types rise in numbers to offset the loss of mature β-cells in clusters 8, 10, and 15.

4.7 SORCS2 deficiency coincides with suppressed ER stress response

In a meticulous exploration of the genetic landscape, differential gene expression analysis between *Sorcs2*$^{+/+}$ and *Sorcs2*$^{-/-}$ revealed that β cells stood as the primary domain profoundly impacted by Sorcs2 deficiency, having over 1000 differentially expressed

genes (Figure 23 A). Downregulated genes, intricately associated with vesicle formation, not only reinforced our earlier morphological analyses indicating impaired vesicle maturation in *Sorcs2*$^{-/-}$ β cells (Figure 24; Figure 15) but also laid the groundwork for a deeper understanding of the ramifications of SORCS2 absence.

In the realm of ER stress and UPR, a noticeable suppression unfolded in SORCS2-deficient β cells, aligning with the loss observed in highly metabolic clusters 8, 10, and 15 (Figure 24 A, Figure 22 A, C). Down-regulation of *Manf* and *Nupr1*, both responsive to ER stress and linked to insulin-deficient diabetes, β cell apoptosis, and ER stress suppression, further underscored the intricate dance between SORCS2 and cellular stress responses (Figure 24 B). Intriguingly, the upregulation of genes tied to the regulation of insulin secretion hinted at a compensatory response to the altered second phase of insulin secretion and perturbed vesicle maturation (Figure 12 B, E; Figure 15; Figure 24)

Contrastingly, cell types expressing SORCS2 were comparatively less impacted by its deficiency than the non-receptor expressing β cells, emphasizing a pivotal role of the receptor in mediating communication between insulin-secreting and non-secreting cell types (Figure 23 A; Figure **17** C). Notably, δ and PP cells exhibited minor impacts, suggesting resilience in the face of SORCS2 deficiency (Figure 23 A, Figure 26). A nuanced picture emerged for α cells, displaying over 200 differentially expressed genes associated with the suppression of stress response, paralleling observations in β cells, and suppression of transcription akin to δ and PP cells (Figure 23 A, Figure 25). This resonates with prior studies indicating a role for SORCS2 in cellular stress response in neurons [47].

In the realm of neuroscience, SORCS2 emerges as a defender against oxidative stress. Studies on epileptic patients and a mouse model of seizures revealed increased SORCS2 expression in neurons three days after prolonged seizures (status epilepticus) induced by pentylenetetrazol [47]. Remarkably, neurons bearing SORCS2 were more resistant to seizure-induced death, underscoring the receptor's importance in stress protection [47]. The study highlighted SORCS2's role in sorting glutamate and cysteine transporter EAAT3, facilitating neuronal cysteine uptake crucial for synthesizing the reactive oxygen

species scavenger glutathione, shielding neurons from oxidative stress-induced death [47].

Akin to its protective role in seizures, SORCS2 demonstrated significance in a stroke mouse model, a condition associated with oxidative stress [49]. Activated astrocytes surrounding ischemic lesions exhibited increased SORCS2 expression, emphasizing its importance in tissue healing, particularly post-stroke angiogenesis [49]. SORCS2's modulated enhancement of endostatin release showcased its role in promoting angiogenesis [49].

Adding to its protective role, a recent study applied hypoosmotic shock to cell lines expressing SORCS2 (HepG2, SH-SY5Y, HEK293, primary mouse hippocampal neurons) [49]. The study revealed either a change in the expression of SORCS2 isoforms or an increase in total Sorcs2 transcripts, further supporting the involvement of SORCS2 in stress response across various cell types [372].

The primary function of pancreatic β cells involves the intricate orchestration of insulin production in response to varied stimuli, necessitating a high metabolic pace [175–177]. While short-term ER stress and UPR can benefit β cell survival, prolonged exposure may lead to apoptosis [175–177]. Additionally, high glucose stimulation activates oxidative stress, initially supporting insulin secretion through activating ryanodine receptors and consequent increase in intracellular Ca^{2+}, but culminating in β cell apoptosis over time [373]. Interestingly, ER stress may potentiate oxidative stress [373].

In the intricate landscape of pancreatic islets, α cells, akin to their β cell counterparts, grapple with ER stress due to the constant production of hormones such as glucagon and GLP-1 [374]. Intriguingly, studies suggest that α cells exhibit a remarkable resilience to ER or oxidative stress, surviving even in the late stages of diabetes [374]. This resilience is attributed to the increased expression of the antiapoptotic gene *BCL2L1*, the protective ER stress-related chaperone BiP (*HSPA5*), and the decreased expression of pro-apoptotic URP response gene *CHOP* [374].
I envisage two potential mechanisms by which SORCS2 may contribute to ER stress response in α cells, specifically by regulating MAPK (p38) or PI3K-AKT pathways (Figure 30).

Analysis of differentially expressed genes in α cells suggested the suppression of the MAPK pathway in the absence of SORCS2, supported by the downregulation of genes such as *Sfrp5, Shc1, Dusp5, Klf4*, and *Jun* (Figure 25). Western blotting further confirmed the suppressed activation of p38 (Figure 30 C). The MAPK cascade stimulates the expression of Bcl-xL, an anti-apoptotic protein crucial for the survival of differentiating pancreatic cells [375,376]. SORCS2 appears to play an essential role in promoting stress-related p38 activity, the loss of which in receptor-deficient α cells may compromise Bcl-xL expression, rendering them more susceptible to ER stress [323,324]. Additionally, p38 activates the transcription factor ATF6, which stimulates the expression of UPR components like ER-associated protein degradation components XBP1 and CHOP [320]. The involvement of SORCS2 in regulating p38 activation may explain the observed suppression of UPR and stress response in mutant α cells (Figure 25 A). Further exploration of the JNK pathway, another significant cascade of the MAPK signaling pathway activated by mitogen-activated protein kinases 4 and 7 [377,378], may provide valuable insights, given its pivotal role in UPR activation [321,322].

The AKT pathway, activated in response to ER stress, was similarly suppressed in SORCS2-deficient pancreatic islets (Figure 30 B). This pathway primarily promotes cell survival by activating CREB, YAP, MDM2 and inhibiting BAD [340]. AKT phosphorylates CREB on Ser133, enhancing the transcriptional activation of CREB and mediating the expression of anti-apoptotic genes *Bcl-2* and *Mcl-1* [340]. Moreover, AKT phosphorylated YAP on Ser127 suppresses the transcriptional activity of pro-apoptotic p73 [340]. The oncogene product MDM2, usually induced by p53, undergoes phosphorylation by AKT on Ser166 and Ser186, leading to its enhanced nuclear import and ubiquitin ligase activity, eventually inactivating and degrading p53, a major proapoptotic agent [340]. AKT phosphorylation of BAD on Ser136 releases it from the protein complex with Bcl2-Bcl-X in the mitochondrial membrane, thereby inhibiting its proapoptotic function [340].

Adding an intriguing layer, AKT can potentiate UPR. Specifically, the AKT upstream regulator PI3K, particularly its regulatory subunit p85α, can modulate UPR via the regulation of nuclear translocation of XBP-1s [84]. Confirmation of SORCS2's involvement in UPR regulation through the modulation of p85α action necessitates an in-depth analysis of PI3K and p85α expression.

4.8 Loss of SORCS2 in α cells impacts stress response and insulin secretion capacity of β cells

Delineating the intricate web of transcellular control in ER stress response, various examples in different biological contexts offer profound insights. In the nematode *Caenorhabditis elegans*, nervous system, particularly amphid single-ciliated endings sensory neurons (ASH and ASI), orchestrates UPR induction in intestinal cells by releasing neuronal small core vesicles [379]. Another noteworthy instance involves the interplay between the intestinal tissue and surrounding tissues, where up-regulation of *daf-16*, a FOXO protein, in the C. elegans intestine induces increased *daf-16* expression in neighboring tissues by releasing insulin-like peptide ins-7 [379].

Similar transmissible ER stress phenomena have been documented in other systems. For instance, ER-stressed murine prostate cancer TRAMP-C1 (TC1) cells induced ER stress in macrophages and dendritic cells incubated in their conditioned medium [362]. Subsequent studies extended this phenomenon to different prostate cancer cell types, such as PC3, LNCaP, DU145, and TC1, revealing that the survival of recipient cancer cells was enhanced, potentially through the secretion of ER stress-inducing factors in the medium [380]. Secreted ER stress-inducing factors in the medium lead to decreased PERK-ATF4 activation in receiving cancer cells, which ordinarily activate CHOP and consequent apoptosis, thereby adapting cancer cells to ER stress and promoting their survival [380].

Likewise, when applied to neurons, the cultural medium of ER-stressed astrocytes shielded them from enhanced ER stress upon thapsigargin stimulation, indicative of cell communication that prepares cell types for stressors [363]. This communication involved the secretion of proteinase K-resistant lipid-like molecules, although the precise nature of these molecules is still under investigation [363].

In the realm of pancreatic islets, recent finding underscored the protective interplay between α and β cells during oxidative stress [381]. In a three-dimensional co-culture of alphaTC1 and INS1E cell lines, a balanced ratio of 50:50 prevented oxidative stress-induced cell death in both cell types when exposed to hydrogen peroxide [381]. This novel

evidence points to a protective communication from α to β cells, echoing research on the defensive role of astrocytes for ER-stressed neurons [363].

While transmissible ER stress has yet to be investigated in pancreatic islet cells, the recurring theme of ER stress in these cells and the myriad examples in other tissues prompt the hypothesis that transmissible ER stress might be a pertinent aspect of pancreatic islet cellular dynamics. Furthermore, given the interconnectedness of α and β cells in the pancreatic islets, the role of SORCS2 in mediating transmissible ER stress from α to β cells becomes an intriguing avenue for exploration.

In my investigation, despite the elusive nature of the anti-stress factors released in a SORCS2-dependent manner, circumstantial evidence points towards osteopontin as a potential candidate. scRNA-seq analysis revealed *Spp1*, the gene encoding osteopontin, as the most downregulated gene in SORCS2-deficient α cells (Figure 25 B). This was corroborated by quantification of *Spp1* transcripts and osteopontin protein levels in isolated islets, demonstrating decreased expression in SORCS2-deficient tissue (Figure 29 A, B). Furthermore, suppressed osteopontin secretion in *Sorcs2*$^{-/-}$ pancreatic islets (Figure 29 C) aligned with the observed downregulation. Pathway analysis indicated compromised AKT activation and a trend towards decreased p38 activation in osteopontin regulation (Figure 30 A, B) [326,382].

Osteopontin, a multifaceted protein, has been extensively studied for its diverse functions encompassing the regulation of apoptosis, ER stress, oxidative stress, and, more recently, insulin secretion and signaling [325,326,328,383,384].

In the realm of cancer progression, osteopontin's influence on hepatocellular carcinoma, small-cell lung cancer, and colorectal cancer is noteworthy, manipulating cell proliferation, migration, and survival through intricate signaling pathways [326]. In hepatocellular carcinoma, osteopontin controls cell proliferation and migration by increasing JAK2/STAT3/NADPH oxidase 1 (NOX1) signaling, thereby elevating ROS production [326]. Additionally, osteopontin induces proliferation in small-cell lung cancer and colorectal cancer through autophagy and apoptosis inhibition [326]. Notably, *Spp1* mRNA expression and osteopontin protein expression can be induced in multiple cancer cell

lines (A549, MLE12, HPAEpic) in response to ER stress stimulators like tunicamycin and thapsigargin through activation of the ERK-dependent signaling pathway [325].

In the central nervous system, osteopontin responds to injury, neuronal damage, or pro-inflammatory stimuli [328]. A study suggests the importance of osteopontin in the secretion of the adrenocorticotropic hormone (ACTH), thus influencing cortisol secretion and the functionality of the hypothalamic-pituitary-adrenal axis responsible for reactions to stress, such as anti-inflammatory responses, pro-to anti-inflammatory cytokine balance, digestion, etc. [90,93]. However, the mode of action of osteopontin on ACTH secretion is currently unknown [328].

In the peripheral tissues, osteopontin promotes ER stress [383]. It induced ER stress in human liver cell culture upon treatment and in mouse liver tissue upon intraperitoneal osteopontin injection [383]. Specifically, three ER signaling branches were induced upon osteopontin treatment: PERK-eIF2α, ATF6-p50, and XBP1 [383]. The study showed upregulation of JNK phosphorylation and consequent reduction in IRS-1 tyrosine phosphorylation and insulin signaling upon osteopontin treatment [383]. Similarly, osteopontin stimulates apoptosis in cardiac myocytes via the involvement of oxidative and ER stress and mitochondrial death pathways through binding to CD44 receptors [384].

Within pancreatic islets, osteopontin emerges as a shield against IL-1β-mediated cytotoxicity [345]. In detail, osteopontin, by binding to, yet unknown, integrin inhibits kappa light polypeptide gene enhancer in B-cells inhibitor α (IκBα), thereby preventing translocation of NF-κB to the nucleus [345]. As a result, osteopontin inhibits NF-κB-regulated transcription of nitric oxide synthase mRNA and, thus, nitric oxide production, thereby alleviating the effect of IL-1β on rat pancreatic islet cells [345].

Besides being involved in cell stress regulation, previous studies also implicated osteopontin in regulating glucose-stimulated insulin secretion [330]. In particular, externally added osteopontin augmented glucose-stimulated insulin secretion [330]. The proposed osteopontin mechanism of action suggests the elevation of intracellular Ca^{2+} through currently unknown integrin binding [330]. Interestingly, intrinsic β cell osteopontin

expression changes did not affect insulin secretion but affected vesicle docking in β cells, however the mechanism of osteopontin control of vesicles localization is unknown [344].

Another compelling illustration of osteopontin's pivotal role in insulin secretion lies in its function as a ligand for integrin β1 [328,385,386]. Upon activation of β1, a cascade is initiated involving ETS-domain-containing proteins (ELKS) and cell division control protein 42 (CDC42) [387,388]. ELKS, instrumental in defining insulin vesicle fusion sites and regulating Ca^{2+} influx, plays a crucial role in the intricate process of insulin secretion [387]. This significance is further highlighted by studies demonstrating that mice deficient in ELKS exhibit a reduction in first-phase glucose-stimulated insulin secretion, coupled with impaired Ca^{2+} influx in β cells [387,388]. The MIN6 cell line deficient for ELKS similarly shows a substantial 58% decrease in glucose-stimulated insulin secretion [387,389].

Moreover, CDC42, recruited to focal adhesion points upon β1 integrin activation, is not confined to the β cell plasma membrane but extends to insulin vesicles [387]. Through its association with syntaxin 1 and vesicle-associated membrane protein 2 (VAMP2), CDC42 plays a pivotal role in regulating insulin vesicle docking and, consequently, insulin secretion [387]. Studies have provided evidence of the colocalization of CDC42 and VAMP2 at the plasma membrane following glucose stimulation in the MIN6 cell line [387]. Interestingly, VAMP2-deficient MIN6 cells exhibit a diminished response in glucose-stimulated insulin secretion, attributed to their inability to form a CDC42-VAMP2-syntaxin-1 complex, crucial for the regulation of insulin vesicle docking [387,390]. This intricate interplay underscores the multifaceted involvement of osteopontin and its downstream effectors in modulating insulin secretion dynamics.

With decreased osteopontin expression and secretion in SORCS2-deficient pancreatic islets, a compelling hypothesis emerges. SORCS2, by regulating osteopontin secretion in α cells, is postulated to play a pivotal role in promoting glucose-stimulated insulin secretion in β cells while affording protection from ER stress (Figure 31). The putative mechanism involves the regulation of the AKT pathway in α cells (Figure 31). Notably, ER stress and glucose-stimulated insulin secretion promotion in β cells by osteopontin are most likely mediated through the CD44 receptor and β1 integrins, respectively (Figure 31). Further elucidating the intricate interplay between SORCS2, osteopontin, and

pancreatic islet dynamics promises to unravel novel facets of cellular communication and homeostasis in the context of metabolic regulation and stress response.

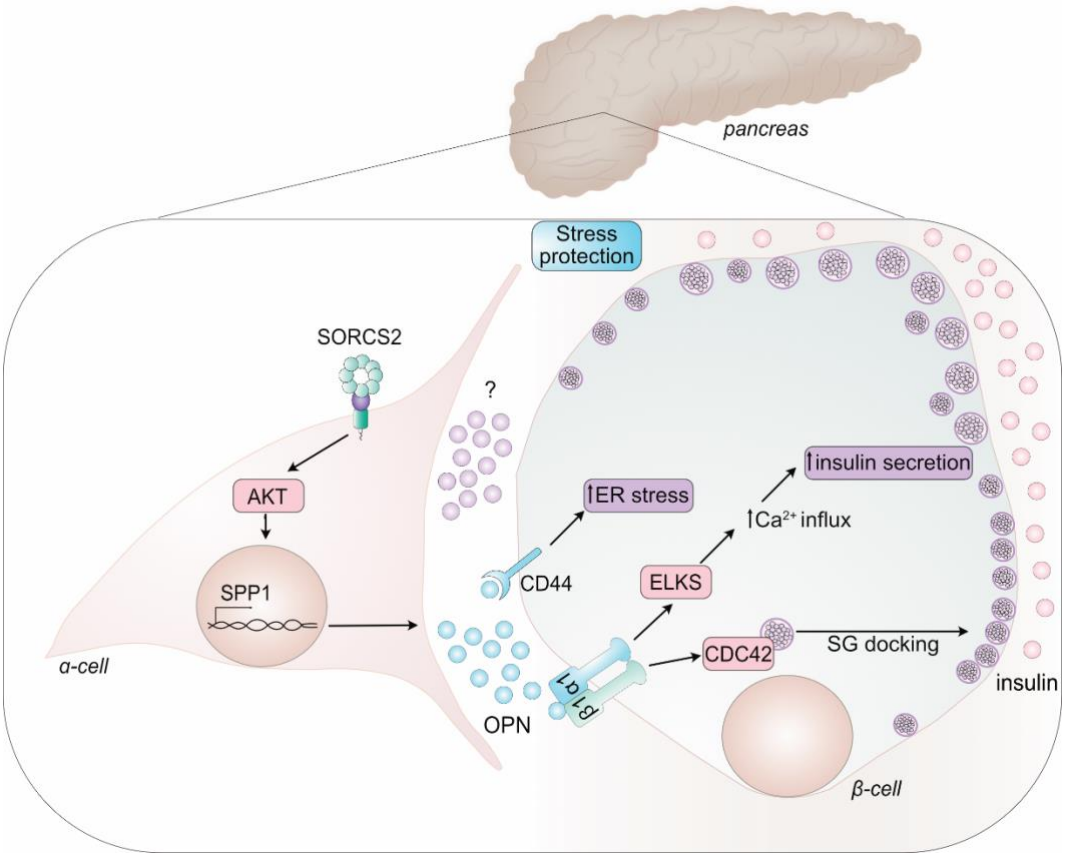

Figure 31: SORCS2 regulates osteopontin secretion in α cells, thereby modulating insulin secretion in β cells.

SORCS2, a versatile receptor with multifaceted functions, exerts its influence on α cells through complex and yet-to-be-uncovered pathways. Its activity triggers stress-induced activation of the AKT signaling pathway, leading to the expression and secretion of anti-stress response factors, prominently osteopontin. These factors, operating in a transcellular manner, extend their protective effects to neighboring β cells. Osteopontin, a pivotal component in this intricate mechanism, likely engages in calcium-dependent processes during insulin granule formation by binding to the β1 integrin receptor and activating ELKS. Simultaneously, it promotes protection against endoplasmic reticulum (ER) stress through the CD44 receptor. Osteopontin may further regulate vesicle docking by influencing the β1 integrin receptor and, consequently, the CDC42 effector protein. This intricate interplay involving SORCS2, secreted factors, and cellular responses highlights a pivotal role in modulating the dynamics of stress response and insulin secretion within pancreatic islets.

AKT, protein kinase B; CDC42, cell division control protein 42; ELKS, ETS-domain-containing proteins; ER stress, endoplasmic Reticulum Stress; OPN, osteopontin; SG, secretory granules; SORCS2, sortilin related VPS10 domain containing receptor 2.

5 Conclusions and Outlook

In summary, my research has delved into the intricate role of SORCS2 in glucose metabolism. I have demonstrated that SORCS2 plays a crucial, albeit indirect, role in potentiating insulin secretion in β cells and is involved in the regulation of vesicle maturation (Figure 11; Figure 12; Figure 15). Moreover, the expression of SORCS2 in α cells suggests its contribution to the activation of the AKT pathway, leading to increased expression and secretion of osteopontin (Figure 10; Figure 29; Figure 30).

This secreted osteopontin, in turn, has the potential to adapt β cells to ER stress by binding to CD44 receptors, thereby facilitating the correct maturation pattern of insulin vesicles [384]. Additionally, the interaction of osteopontin with β1 integrin may further potentiate insulin secretion potentially through the activation of ELKS and the subsequent increase in Ca^{2+} influx [387,388]. Furthermore, osteopontin's binding to β1 integrin could activate CDC42, regulating secretory granule docking in β cells [387,388]. Thus, SORCS2 emerges as a guardian and enhancer of insulin secretion in pancreatic β cells by fostering the secretion of stress-protective factors such as osteopontin from α cells (Figure ***31***).

Beyond its role in insulin secretion, my work uncovers a novel non-hormonal paracrine interaction between α and β cells, enhancing our understanding of the physiology and connectivity of pancreatic islets. This novel paracrine interplay not only refines our comprehension of islet cell dynamics but also opens avenues for investigating potential therapeutic targets rooted in the delicate balance maintained by SORCS2.

While my investigation has shed light on a fascinating case of non-hormonal paracrine regulation of β cells, in part mediated by SORCS2, there are limitations to a full-body mouse SORCS2 knockout, which do not allow to exclude the effect from other tissues expressing SORCS2. To validate and extend these findings, a pancreatic α cell-specific SORCS2 knockout in mice using CRISPR/Cas9 technology is recommended.

To confirm the impact of α cell-specific SORCS2 knock-out on insulin secretion, co-culture experiments involving *Sorcs2*$^{-/-}$ or *Sorcs2*$^{+/+}$ αTC1-6 alpha cell lines with β TC-1 cell lines, or incubation of β TC-1 cell lines in medium from *Sorcs2*$^{-/-}$ and *Sorcs2*$^{+/+}$ αTC1-

6 alpha cell lines with subsequent analysis of glucose-stimulated insulin secretion, could provide valuable insights [391]. Moreover, employing pull-down assay in these experiments can help identify potential binding partners for SORCS2 in α cells. By honing in on α cell-specific knockout models and intricate cell culture setups, we can uncover the nuanced molecular mechanisms that underpin SORCS2-mediated effects on insulin secretion.

While my research suggests osteopontin as a potent factor regulated by SORCS2, it is essential to recognize that undiscovered factors from α cells may also contribute to the intricate dynamics of paracrine signaling within pancreatic islets. Further investigation and comparison of the *Sorcs2*$^{-/-}$ and *Sorcs2*$^{+/+}$ αTC1-6 cell line secretome can uncover hidden players in the orchestration of pancreatic islet communication.

Additionally, the substantial expression of SORCS2 in stem β and α cells [221] opens a new avenue for exploring its role in the development of pancreatic islets, and may shed light on how SORCS2 may mediate vesicles maturation in β cells. Extending the scope of our exploration, delving into the role of SORCS2 in stem β cells could offer a fresh perspective on the developmental aspects of pancreatic islets, with potential implications for regenerative medicine.

In conclusion, while obstacles remain in fully understanding the importance of SORCS2 in pancreatic islets' physiology and organismal glucose metabolism, my research unveils a captivating aspect of communication among pancreatic islet cells, partly mediated by SORCS2. In the final analysis, this research not only contributes to our understanding of pancreatic islet function but also sparks curiosity and enthusiasm for the avenues of research that lie ahead in unraveling the complexities of SORCS2's influence.

Reference list

1. Willnow TE, Petersen CM, Nykjaer A. VPS10P-domain receptors - Regulators of neuronal viability and function. Nat Rev Neurosci. 2008;9(12):899–909.
2. Blondeau N, Béraud-Dufour S, Lebrun P, Hivelin C, Coppola T. Sortilin in glucose homeostasis: From accessory protein to key player? Front Pharmacol. 2019;9(JAN):1–7.
3. Malik AR, Willnow TE. VPS10P Domain Receptors: Sorting Out Brain Health and Disease. Trends Neurosci [Internet]. 2020;43(11):870–85. Available from: https://doi.org/10.1016/j.tins.2020.08.003
4. Cereghino JL, Marcusson EG, Emr SD. The cytoplasmic tail domain of the vacuolar protein sorting receptor Vps10p and a subset of VPS gene products regulate receptor stability, function, and localization. Mol Biol Cell. 1995;6(9):1089–102.
5. Marcusson EG, Horazdovsky BF, Cereghino JL. The Sorting Receptor for Yeast Vacuolar Carboxypeptidase Y Is Encoded by the VFW0 Gene. 1994;77.
6. Hampe W, Urny J, Franke I, Hoffmeister-Ullerich SAH, Herrmann D, Petersen CM, Lohmann J, Schaller HC. A head-activator binding protein is present in hydra in a soluble and a membrane-anchored form. Development [Internet]. 1999 Sep 15;126(18):4077–86. Available from: https://journals.biologists.com/dev/article/126/18/4077/40331/A-head-activator-binding-protein-is-present-in
7. Valk V, Kaaij RM van der, Dijkhuizen L. The evolutionary origin and possible functional roles of FNIII domains in two Microbacterium aurum B8.A granular starch degrading enzymes, and in other carbohydrate acting enzymes. Amylase. 2017;1(1):1–11.
8. Andersen OM, Schmidt V, Spoelgen R, Gliemann J, Behlke J, Galatis D, McKinstry WJ, Parker MW, Masters CL, Hyman BT, Cappai R, Willnow TE. Molecular dissection of the interaction between amyloid precursor protein and its neuronal trafficking receptor SorLA/LR11. Biochemistry. 2006;45(8):2618–28.
9. Leloup N, Chataigner LMP, Janssen BJC. Structural insights into SorCS2–Nerve Growth Factor complex formation. Nat Commun [Internet]. 2018;9(1):1–10. Available from: http://dx.doi.org/10.1038/s41467-018-05405-z
10. Petersen CM, Nielsen MS, Jacobsen C, Tauris J, Jacobsen L, Gliemann J, Moestrup SK, Madsen P. Propeptide cleavage conditions sortilin/neurotensin

receptor-3 for ligand binding. EMBO J. 1999;18(3):595–604.

11. Nykjaer A, Willnow TE. Sortilin: A receptor to regulate neuronal viability and function. Trends Neurosci [Internet]. 2012;35(4):261–70. Available from: http://dx.doi.org/10.1016/j.tins.2012.01.003
12. Mitok KA, Keller MP, Attie AD. Sorting through the extensive and confusing roles of sortilin in metabolic disease. J Lipid Res [Internet]. 2022;63(8):100243. Available from: https://doi.org/10.1016/j.jlr.2022.100243
13. Schmidt V, Willnow TE. Protein sorting gone wrong - VPS10P domain receptors in cardiovascular and metabolic diseases. Atherosclerosis [Internet]. 2016;245:194–9. Available from: http://dx.doi.org/10.1016/j.atherosclerosis.2015.11.027
14. Moreno-Grau S, de Rojas I, Hernández I, Quintela I, Montrreal L, Alegret M, Hernández-Olasagarre B, Madrid L, González-Perez A, Maroñas O, Rosende-Roca M, Mauleón A, Vargas L, Lafuente A, Abdelnour C, Rodríguez-Gómez O, Gil S, Santos-Santos MÁ, Espinosa A, Ortega G, Sanabria Á, Pérez-Cordón A, Cañabate P, Moreno M, Preckler S, Ruiz S, Aguilera N, Pineda JA, Macías J, Alarcón-Martín E, Sotolongo-Grau O, Abdelnour C, Alarcon E, Benaque A, Boada M, Buendia M, Carracedo A, Corbatón A, Diego S, Gailhajenet A, García González P, Guitart M, Ibarria M, Martín E, Martínez MT, Marquié M, Monté-Rubio G, Orellana A, Pancho A, Pelejà E, Real LM, Ruiz A, Ruiz S, Sáez ME, Sanabria A, Serrano-Rios M, Tárraga L, Valero S, Adarmes-Gómez AD, Álvarez I, Álvarez V, Amer-Ferrer G, Antequera M, Antúnez C, Baquero M, Bernal M, Blesa R, Buiza-Rueda D, Bullido MJ, Burguera JA, Calero M, Carrillo F, Carrión-Claro M, Casajeros MJ, Clarimón J, Cruz-Gamero JM, de Pancorbo MM, del Ser T, Diez-Fairen M, Fortea J, Franco E, Frank-García A, García-Alberca JM, Garcia Madrona S, Garcia-Ribas G, Gómez-Garre P, Hevilla S, Jesús S, Espinosa L, Lage C, Legaz A, Lleó A, López de Munáin A, López-García S, Macias D, Manzanares S, Marín M, Marín-Muñoz J, Marín T, Martín Montes A, Martínez B, Martínez C, Martínez V, Martínez-Lage Álvarez P, Medina M, Mendioroz Iriarte M, Menéndez-González M, Mir P, Molinuevo JL, Pastor AB, Pástor P, Pérez Tur J, Periñán-Tocino T, Piñol Ripoll G, Rábano A, Real de Asúa D, Rodrigo S, Rodríguez-Rodríguez E, Royo JL, Ruiz A, Sanchez del Valle Díaz R, Sánchez-Juan P, Sastre I, Vicente MP, Vivancos L, García-Ribas G, Piñol-Ripoll G, Ávila J. Genome-wide association analysis of dementia and its clinical endophenotypes reveal novel loci associated with Alzheimer's disease and three causality networks: The GR@ACE project.

Alzheimer's Dement. 2019;15(10):1333–47.

15. Marioni RE, Harris SE, Zhang Q, McRae AF, Hagenaars SP, Hill WD, Davies G, Ritchie CW, Gale CR, Starr JM, Goate AM, Porteous DJ, Yang J, Evans KL, Deary IJ, Wray NR, Visscher PM. GWAS on family history of Alzheimer's disease. Transl Psychiatry [Internet]. 2018;8(1):0–6. Available from: http://dx.doi.org/10.1038/s41398-018-0150-6

16. Bellenguez C, Küçükali F, Jansen IE, Kleineidam L, Moreno-Grau S, Amin N, Naj AC, Campos-Martin R, Grenier-Boley B, Andrade V, Holmans PA, Boland A, Damotte V, van der Lee SJ, Costa MR, Kuulasmaa T, Yang Q, de Rojas I, Bis JC, Yaqub A, Prokic I, Chapuis J, Ahmad S, Giedraitis V, Aarsland D, Garcia-Gonzalez P, Abdelnour C, Alarcón-Martín E, Alcolea D, Alegret M, Alvarez I, Álvarez V, Armstrong NJ, Tsolaki A, Antúnez C, Appollonio I, Arcaro M, Archetti S, Pastor AA, Arosio B, Athanasiu L, Bailly H, Banaj N, Baquero M, Barral S, Beiser A, Pastor AB, Below JE, Benchek P, Benussi L, Berr C, Besse C, Bessi V, Binetti G, Bizarro A, Blesa R, Boada M, Boerwinkle E, Borroni B, Boschi S, Bossù P, Bråthen G, Bressler J, Bresner C, Brodaty H, Brookes KJ, Brusco LI, Buiza-Rueda D, Bûrger K, Burholt V, Bush WS, Calero M, Cantwell LB, Chene G, Chung J, Cuccaro ML, Carracedo Á, Cecchetti R, Cervera-Carles L, Charbonnier C, Chen HH, Chillotti C, Ciccone S, Claassen JAHR, Clark C, Conti E, Corma-Gómez A, Costantini E, Custodero C, Daian D, Dalmasso MC, Daniele A, Dardiotis E, Dartigues JF, de Deyn PP, de Paiva Lopes K, de Witte LD, Debette S, Deckert J, del Ser T, Denning N, DeStefano A, Dichgans M, Diehl-Schmid J, Diez-Fairen M, Rossi PD, Djurovic S, Duron E, Düzel E, Dufouil C, Eiriksdottir G, Engelborghs S, Escott-Price V, Espinosa A, Ewers M, Faber KM, Fabrizio T, Nielsen SF, Fardo DW, Farotti L, Fenoglio C, Fernández-Fuertes M, Ferrari R, Ferreira CB, Ferri E, Fin B, Fischer P, Fladby T, Fließbach K, Fongang B, Fornage M, Fortea J, Foroud TM, Fostinelli S, Fox NC, Franco-Macías E, Bullido MJ, Frank-García A, Froelich L, Fulton-Howard B, Galimberti D, García-Alberca JM, García-González P, Garcia-Madrona S, Garcia-Ribas G, Ghidoni R, Giegling I, Giorgio G, Goate AM, Goldhardt O, Gomez-Fonseca D, González-Pérez A, Graff C, Grande G, Green E, Grimmer T, Grünblatt E, Grunin M, Gudnason V, Guetta-Baranes T, Haapasalo A, Hadjigeorgiou G, Haines JL, Hamilton-Nelson KL, Hampel H, Hanon O, Hardy J, Hartmann AM, Hausner L, Harwood J, Heilmann-Heimbach S, Helisalmi S, Heneka MT, Hernández I, Herrmann MJ, Hoffmann P, Holmes C, Holstege H, Vilas RH,

Hulsman M, Humphrey J, Biessels GJ, Jian X, Johansson C, Jun GR, Kastumata Y, Kauwe J, Kehoe PG, Kilander L, Ståhlbom AK, Kivipelto M, Koivisto A, Kornhuber J, Kosmidis MH, Kukull WA, Kuksa PP, Kunkle BW, Kuzma AB, Lage C, Laukka EJ, Launer L, Lauria A, Lee CY, Lehtisalo J, Lerch O, Lleó A, Longstreth W, Lopez O, de Munain AL, Love S, Löwemark M, Luckcuck L, Lunetta KL, Ma Y, Macías J, MacLeod CA, Maier W, Mangialasche F, Spallazzi M, Marquié M, Marshall R, Martin ER, Montes AM, Rodríguez CM, Masullo C, Mayeux R, Mead S, Mecocci P, Medina M, Meggy A, Mehrabian S, Mendoza S, Menéndez-González M, Mir P, Moebus S, Mol M, Molina-Porcel L, Montrreal L, Morelli L, Moreno F, Morgan K, Mosley T, Nöthen MM, Muchnik C, Mukherjee S, Nacmias B, Ngandu T, Nicolas G, Nordestgaard BG, Olaso R, Orellana A, Orsini M, Ortega G, Padovani A, Paolo C, Papenberg G, Parnetti L, Pasquier F, Pastor P, Peloso G, Pérez-Cordón A, Pérez-Tur J, Pericard P, Peters O, Pijnenburg YAL, Pineda JA, Piñol-Ripoll G, Pisanu C, Polak T, Popp J, Posthuma D, Priller J, Puerta R, Quenez O, Quintela I, Thomassen JQ, Rábano A, Rainero I, Rajabli F, Ramakers I, Real LM, Reinders MJT, Reitz C, Reyes-Dumeyer D, Ridge P, Riedel-Heller S, Riederer P, Roberto N, Rodriguez-Rodriguez E, Rongve A, Allende IR, Rosende-Roca M, Royo JL, Rubino E, Rujescu D, Sáez ME, Sakka P, Saltvedt I, Sanabria Á, Sánchez-Arjona MB, Sanchez-Garcia F, Juan PS, Sánchez-Valle R, Sando SB, Sarnowski C, Satizabal CL, Scamosci M, Scarmeas N, Scarpini E, Scheltens P, Scherbaum N, Scherer M, Schmid M, Schneider A, Schott JM, Selbæk G, Seripa D, Serrano M, Sha J, Shadrin AA, Skrobot O, Slifer S, Snijders GJL, Soininen H, Solfrizzi V, Solomon A, Song Y, Sorbi S, Sotolongo-Grau O, Spalletta G, Spottke A, Squassina A, Stordal E, Tartan JP, Tárraga L, Tesí N, Thalamuthu A, Thomas T, Tosto G, Traykov L, Tremolizzo L, Tybjærg-Hansen A, Uitterlinden A, Ullgren A, Ulstein I, Valero S, Valladares O, Broeckhoven C Van, Vance J, Vardarajan BN, van der Lugt A, Dongen J Van, van Rooij J, van Swieten J, Vandenberghe R, Verhey F, Vidal JS, Vogelgsang J, Vyhnalek M, Wagner M, Wallon D, Wang LS, Wang R, Weinhold L, Wiltfang J, Windle G, Woods B, Yannakoulia M, Zare H, Zhao Y, Zhang X, Zhu C, Zulaica M, Laczo J, Matoska V, Serpente M, Assogna F, Piras F, Piras F, Ciullo V, Shofany J, Ferrarese C, Andreoni S, Sala G, Zoia CP, Zompo M Del, Benussi A, Bastiani P, Takalo M, Natunen T, Laatikainen T, Tuomilehto J, Antikainen R, Strandberg T, Lindström J, Peltonen M, Abraham R, Al-Chalabi A, Bass NJ, Brayne C, Brown KS, Collinge J, Craig D, Deloukas P, Fox N, Gerrish A, Gill M, Gwilliam

R, Harold D, Hollingworth P, Johnston JA, Jones L, Lawlor B, Livingston G, Lovestone S, Lupton M, Lynch A, Mann D, McGuinness B, McQuillin A, O'Donovan MC, Owen MJ, Passmore P, Powell JF, Proitsi P, Rossor M, Shaw CE, Smith AD, Gurling H, Todd S, Mummery C, Ryan N, Lacidogna G, Adarmes-Gómez A, Mauleón A, Pancho A, Gailhajenet A, Lafuente A, Macias-García D, Martín E, Pelejà E, Carrillo F, Merlín IS, Garrote-Espina L, Vargas L, Carrion-Claro M, Marín M, Labrador M, Buendia M, Alonso MD, Guitart M, Moreno M, Ibarria M, Periñán M, Aguilera N, Gómez-Garre P, Cañabate P, Escuela R, Pineda-Sánchez R, Vigo-Ortega R, Jesús S, Preckler S, Rodrigo-Herrero S, Diego S, Vacca A, Roveta F, Salvadori N, Chipi E, Boecker H, Laske C, Perneczky R, Anastasiou C, Janowitz D, Malik R, Anastasiou A, Parveen K, Lage C, López-García S, Antonell A, Mihova KY, Belezhanska D, Weber H, Kochen S, Solis P, Medel N, Lisso J, Sevillano Z, Politis DG, Cores V, Cuesta C, Ortiz C, Bacha JI, Rios M, Saenz A, Abalos MS, Kohler E, Palacio DL, Etchepareborda I, Kohler M, Novack G, Prestia FA, Galeano P, Castaño EM, Germani S, Toso CR, Rojo M, Ingino C, Mangone C, Rubinsztein DC, Teipel S, Fievet N, Deramerourt V, Forsell C, Thonberg H, Bjerke M, Roeck E De, Martínez-Larrad MT, Olivar N, Aguilera N, Cano A, Cañabate P, Macias J, Maroñas O, Nuñez-Llaves R, Olivé C, Pelejá E, Adarmes-Gómez AD, Alonso MD, Amer-Ferrer G, Antequera M, Burguera JA, Carrillo F, Carrión-Claro M, Casajeros MJ, Martinez de Pancorbo M, Escuela R, Garrote-Espina L, Gómez-Garre P, Hevilla S, Jesús S, Espinosa MAL, Legaz A, López-García S, Macias-García D, Manzanares S, Marín M, Marín-Muñoz J, Marín T, Martínez B, Martínez V, Martínez-Lage Álvarez P, Iriarte MM, Periñán-Tocino MT, Pineda-Sánchez R, Real de Asúa D, Rodrigo S, Sastre I, Vicente MP, Vigo-Ortega R, Vivancos L, Epelbaum J, Hannequin D, campion D, Deramecourt V, Tzourio C, Brice A, Dubois B, Williams A, Thomas C, Davies C, Nash W, Dowzell K, Morales AC, Bernardo-Harrington M, Turton J, Lord J, Brown K, Vardy E, Fisher E, Warren JD, Rossor M, Ryan NS, Guerreiro R, Uphill J, Bass N, Heun R, Kölsch H, Schürmann B, Lacour A, Herold C, Johnston JA, Passmore P, Powell J, Patel Y, Hodges A, Becker T, Warden D, Wilcock G, Clarke R, Deloukas P, Ben-Shlomo Y, Hooper NM, Pickering-Brown S, Sussams R, Warner N, Bayer A, Heuser I, Drichel D, Klopp N, Mayhaus M, Riemenschneider M, Pinchler S, Feulner T, Gu W, van den Bussche H, Hüll M, Frölich L, Wichmann HE, Jöckel KH, O'Donovan M, Owen M, Bahrami S, Bosnes I, Selnes P, Bergh S, Palotie A, Daly M, Jacob H, Matakidou A, Runz H, John S,

Plenge R, McCarthy M, Hunkapiller J, Ehm M, Waterworth D, Fox C, Malarstig A, Klinger K, Call K, Behrens T, Loerch P, Mäkelä T, Kaprio J, Virolainen P, Pulkki K, Kilpi T, Perola M, Partanen J, Pitkäranta A, Kaarteenaho R, Vainio S, Turpeinen M, Serpi R, Laitinen T, Mäkelä J, Kosma VM, Kujala U, Tuovila O, Hendolin M, Pakkanen R, Waring J, Riley-Gillis B, Liu J, Biswas S, Diogo D, Marshall C, Hu X, Gossel M, Graham R, Cummings B, Ripatti S, Schleutker J, Arvas M, Carpén O, Hinttala R, Kettunen J, Mannermaa A, Laukkanen J, Julkunen V, Remes A, Kälviäinen R, Peltola J, Tienari P, Rinne J, Ziemann A, Waring J, Esmaeeli S, Smaoui N, Lehtonen A, Eaton S, Lahdenperä S, van Adelsberg J, Michon J, Kerchner G, Bowers N, Teng E, Eicher J, Mehta V, Gormley P, Linden K, Whelan C, Xu F, Pulford D, Färkkilä M, Pikkarainen S, Jussila A, Blomster T, Kiviniemi M, Voutilainen M, Georgantas B, Heap G, Rahimov F, Usiskin K, Lu T, Oh D, Kalpala K, Miller M, McCarthy L, Eklund K, Palomäki A, Isomäki P, Pirilä L, Kaipiainen-Seppänen O, Huhtakangas J, Lertratanakul A, Hochfeld M, Bing N, Gordillo JE, Mars N, Pelkonen M, Kauppi P, Kankaanranta H, Harju T, Close D, Greenberg S, Chen H, Betts J, Ghosh S, Salomaa V, Niiranen T, Juonala M, Metsärinne K, Kähönen M, Junttila J, Laakso M, Pihlajamäki J, Sinisalo J, Taskinen MR, Tuomi T, Challis B, Peterson A, Chu A, Parkkinen J, Muslin A, Joensuu H, Meretoja T, Aaltonen L, Mattson J, Auranen A, Karihtala P, Kauppila S, Auvinen P, Elenius K, Popovic R, Schutzman J, Loboda A, Chhibber A, Lehtonen H, McDonough S, Crohns M, Kulkarni D, Kaarniranta K, Turunen JA, Ollila T, Seitsonen S, Uusitalo H, Aaltonen V, Uusitalo-Järvinen H, Luodonpää M, Hautala N, Loomis S, Strauss E, Chen H, Podgornaia A, Hoffman J, Tasanen K, Huilaja L, Hannula-Jouppi K, Salmi T, Peltonen S, Koulu L, Harvima I, Wu Y, Choy D, Pussinen P, Salminen A, Salo T, Rice D, Nieminen P, Palotie U, Siponen M, Suominen L, Mäntylä P, Gursoy U, Anttonen V, Sipilä K, Davis JW, Quarless D, Petrovski S, Wigmore E, Chen CY, Bronson P, Tsai E, Huang Y, Maranville J, Shaikho E, Mohammed E, Wadhawan S, Kvikstad E, Caliskan M, Chang D, Bhangale T, Pendergrass S, Holzinger E, Chen X, Hedman Å, King KS, Wang C, Xu E, Auge F, Chatelain C, Rajpal D, Liu D, Call K, Xia T he, Brauer M, Kurki M, Karjalainen J, Havulinna A, Jalanko A, Palta P, della Briotta Parolo P, Zhou W, Lemmelä S, Rivas M, Harju J, Lehisto A, Ganna A, Llorens V, Laivuori H, Rüeger S, Niemi ME, Tukiainen T, Reeve MP, Heyne H, Palin K, Garcia-Tabuenca J, Siirtola H, Kiiskinen T, Lee J, Tsuo K, Elliott A, Kristiansson K, Hyvärinen K, Ritari J, Koskinen M, Pylkäs K, Kalaoja M, Karjalainen

M, Mantere T, Kangasniemi E, Heikkinen S, Laakkonen E, Sipeky C, Heron S, Karlsson A, Jambulingam D, Rathinakannan VS, Kajanne R, Aavikko M, Jiménez MG, della Briotta Parola P, Lehistö A, Kanai M, Kaunisto M, Kilpeläinen E, Sipilä TP, Brein G, Awaisa G, Shcherban A, Donner K, Loukola A, Laiho P, Sistonen T, Kaiharju E, Laukkanen M, Järvensivu E, Lähteenmäki S, Männikkö L, Wong R, Mattsson H, Hiekkalinna T, Paajanen T, Pärn K, Gracia-Tabuenca J, Abner E, Adams PM, Aguirre A, Albert MS, Albin RL, Allen M, Alvarez L, Apostolova LG, Arnold SE, Asthana S, Atwood CS, Ayres G, Baldwin CT, Barber RC, Barnes LL, Barral S, Beach TG, Becker JT, Beecham GW, Beekly D, Below JE, Benchek P, Benitez BA, Bennett D, Bertelson J, Margaret FE, Bird TD, Blacker D, Boeve BF, Bowen JD, Boxer A, Brewer J, Burke JR, Burns JM, Bush WS, Buxbaum JD, Cairns NJ, Cao C, Carlson CS, Carlsson CM, Carney RM, Carrasquillo MM, Chasse S, Chesselet MF, Chesi A, Chin NA, Chui HC, Craft S, Crane PK, Cribbs DH, Crocco EA, Cruchaga C, Cullum M, Darby E, Davis B, De Jager PL, DeCarli C, DeToledo J, Dick M, Dickson DW, Dombroski BA, Doody RS, Duara R, Ertekin-Taner N, Evans DA, Fairchild TJ, Fallon KB, Farlow MR, Farrell JJ, Fernandez-Hernandez V, Ferris S, Frosch MP, Fulton-Howard B, Galasko DR, Gamboa A, Gearing M, Geschwind DH, Ghetti B, Gilbert JR, Grabowski TJ, Graff-Radford NR, Grant SFA, Green RC, Growdon JH, Haines JL, Hakonarson H, Hall J, Hamilton RL, Harari O, Harrell LE, Haut J, Head E, Henderson VW, Hernandez M, Hohman T, Honig LS, Huebinger RM, Huentelman MJ, Hulette CM, Hyman BT, Hynan LS, Ibanez L, Jarvik GP, Jayadev S, Jin LW, Johnson K, Johnson L, Kamboh MI, Karydas AM, Katz MJ, Kaye JA, Keene CD, Khaleeq A, Kim R, Knebl J, Kowall NW, Kramer JH, Kuksa PP, LaFerla FM, Lah JJ, Larson EB, Lee CY, Lee EB, Lerner A, Leung YY, Leverenz JB, Levey AI, Li M, Lieberman AP, Lipton RB, Logue M, Lyketsos CG, Malamon J, Mains D, Marson DC, Martiniuk F, Mash DC, Masliah E, Massman P, Masurkar A, McCormick WC, McCurry SM, McDavid AN, McDonough S, McKee AC, Mesulam M, Mez J, Miller BL, Miller CA, Miller JW, Montine TJ, Monuki ES, Morris JC, Myers AJ, Nguyen T, O'Bryant S, Olichney JM, Ory M, Palmer R, Parisi JE, Paulson HL, Pavlik V, Paydarfar D, Perez V, Peskind E, Petersen RC, Phillips-Cremins JE, Pierce A, Polk M, Poon WW, Potter H, Qu L, Quiceno M, Quinn JF, Raj A, Raskind M, Reiman EM, Reisberg B, Reisch JS, Ringman JM, Roberson ED, Rodriguear M, Rogaeva E, Rosen HJ, Rosenberg RN, Royall DR, Sager MA, Sano M, Saykin AJ, Schneider JA, Schneider LS, Seeley WW, Slifer SH, Small S,

Smith AG, Smith JP, Song YE, Sonnen JA, Spina S, George-Hyslop PS, Stern RA, Stevens AB, Strittmatter SM, Sultzer D, Swerdlow RH, Tanzi RE, Tilson JL, Trojanowski JQ, Troncoso JC, Tsuang DW, Valladares O, Van Deerlin VM, van Eldik LJ, Vassar R, Vinters H V., Vonsattel JP, Weintraub S, Welsh-Bohmer KA, Whitehead PL, Wijsman EM, Wilhelmsen KC, Williams B, Williamson J, Wilms H, Wingo TS, Wisniewski T, Woltjer RL, Woon M, Wright CB, Wu CK, Younkin SG, Yu CE, Yu L, Zhang Y, Zhao Y, Zhu X, Adams H, Akinyemi RO, Ali M, Aparicio HJ, Bahadori M, Becker JT, Breteler M, Chasman D, Chauhan G, Comic H, Cox S, Cupples AL, Davies G, DeCarli CS, Duperron MG, Dupuis J, Evans T, Fan F, Fitzpatrick A, Fohner AE, Ganguli M, Geerlings M, Glatt SJ, Gonzalez HM, Goss M, Grabe H, Habes M, Heckbert SR, Hofer E, Hong E, Hughes T, Kautz TF, Knol M, Kremen W, Lacaze P, Lahti J, Grand Q Le, Litkowski E, Li S, Liu D, Liu X, Loitfelder M, Manning A, Maillard P, Marioni R, Mazoyer B, van Lent DM, Mei H, Mishra A, Nyquist P, O'Connell J, Patel Y, Paus T, Pausova Z, Raikkonen-Talvitie K, Riaz M, Rich S, Rotter J, Romero J, Roshchupkin G, Saba Y, Sargurupremraj M, Schmidt H, Schmidt R, Shulman JM, Smith J, Sekhar H, Rajula R, Shin J, Simino J, Sliz E, Teumer A, Thomas A, Tin A, Tucker-Drob E, Vojinovic D, Wang Y, Weinstein G, Williams D, Wittfeld K, Yanek L, Yang Y, Farrer LA, Psaty BM, Ghanbari M, Raj T, Sachdev P, Mather K, Jessen F, Ikram MA, de Mendonça A, Hort J, Tsolaki M, Pericak-Vance MA, Amouyel P, Williams J, Frikke-Schmidt R, Clarimon J, Deleuze JF, Rossi G, Seshadri S, Andreassen OA, Ingelsson M, Hiltunen M, Sleegers K, Schellenberg GD, van Duijn CM, Sims R, van der Flier WM, Ruiz A, Ramirez A, Lambert JC. New insights into the genetic etiology of Alzheimer's disease and related dementias. Nat Genet. 2022;54(4):412–36.

17. Lambert JC, Ibrahim-Verbaas CA, Harold D, Naj AC, Sims R, Bellenguez C, Jun G, DeStefano AL, Bis JC, Beecham GW, Grenier-Boley B, Russo G, Thornton-Wells TA, Jones N, Smith A V., Chouraki V, Thomas C, Ikram MA, Zelenika D, Vardarajan BN, Kamatani Y, Lin CF, Gerrish A, Schmidt H, Kunkle B, Fiévet N, Amouyel P, Pasquier F, Deramecourt V, De Bruijn RFAG, Amin N, Hofman A, Van Duijn CM, Dunstan ML, Hollingworth P, Owen MJ, O'Donovan MC, Jones L, Holmans PA, Moskvina V, Williams J, Baldwin C, Farrer LA, Choi SH, Lunetta KL, Fitzpatrick AL, Harris TB, Psaty BM, Gilbert JR, Hamilton-Nelson KL, Martin ER, Pericak-Vance MA, Haines JL, Gudnason V, Jonsson P V., Eiriksdottir G, Bihoreau MT, Lathrop M, Valladares O, Cantwell LB, Wang LS, Schellenberg GD, Ruiz A,

Boada M, Reitz C, Mayeux R, Ramirez A, Maier W, Hanon O, Kukull WA, Buxbaum JD, Campion D, Wallon D, Hannequin D, Crane PK, Larson EB, Becker T, Cruchaga C, Goate AM, Craig D, Johnston JA, Mc-Guinness B, Todd S, Passmore P, Berr C, Ritchie K, Lopez OL, De Jager PL, Evans D, Lovestone S, Proitsi P, Powell JF, Letenneur L, Barberger-Gateau P, Dufouil C, Dartigues JF, Morón FJ, Rubinsztein DC, St. George-Hyslop P, Sleegers K, Bettens K, Van Broeckhoven C, Huentelman MJ, Gill M, Brown K, Morgan K, Kamboh MI, Keller L, Fratiglioni L, Green R, Myers AJ, Love S, Rogaeva E, Gallacher J, Bayer A, Clarimon J, Lleo A, Tsuang DW, Yu L, Bennett DA, Tsolaki M, Bossù P, Spalletta G, Collinge J, Mead S, Sorbi S, Nacmias B, Sanchez-Garcia F, Deniz Naranjo MC, Fox NC, Hardy J, Bosco P, Clarke R, Brayne C, Galimberti D, Mancuso M, Matthews F, Moebus S, Mecocci P, Del Zompo M, Hampel H, Pilotto A, Bullido M, Panza F, Caffarra P, Mayhaus M, Pichler S, Gu W, Riemenschneider M, Lannfelt L, Ingelsson M, Hakonarson H, Carrasquillo MM, Zou F, Younkin SG, Beekly D, Alvarez V, Coto E, Razquin C, Pastor P, Mateo I, Combarros O, Faber KM, Foroud TM, Soininen H, Hiltunen M, Blacker D, Mosley TH, Graff C, Holmes C, Montine TJ, Rotter JI, Brice A, Nalls MA, Kauwe JSK, Boerwinkle E, Schmidt R, Rujescu D, Tzourio C, Nöthen MM, Launer LJ, Seshadri S. Meta-analysis of 74,046 individuals identifies 11 new susceptibility loci for Alzheimer's disease. Nat Genet. 2013;45(12):1452–8.

18. Jun G, Ibrahim-Verbaas CA, Vronskaya M, Lambert JC, Chung J, Naj AC, Kunkle BW, Wang LS, Bis JC, Bellenguez C, Harold D, Lunetta KL, Destefano AL, Grenier-Boley B, Sims R, Beecham GW, Smith A V, Chouraki V, Hamilton-Nelson KL, Ikram MA, Fievet N, Denning N, Martin ER, Schmidt H, Kamatani Y, Dunstan ML, Valladares O, Laza AR, Zelenika D, Ramirez A, Foroud TM, Choi SH, Boland A, Becker T, Kukull WA, van der Lee SJ, Pasquier F, Cruchaga C, Beekly D, Fitzpatrick AL, Hanon O, Gill M, Barber R, Gudnason V, Campion D, Love S, Bennett DA, Amin N, Berr C, Tsolaki M, Buxbaum JD, Lopez OL, Deramecourt V, Fox NC, Cantwell LB, Tárraga L, Dufouil C, Hardy J, Crane PK, Eiriksdottir G, Hannequin D, Clarke R, Evans D, Mosley TH, Letenneur L, Brayne C, Maier W, De Jager P, Emilsson V, Dartigues JF, Hampel H, Kamboh MI, de Bruijn RFAG, Tzourio C, Pastor P, Larson EB, Rotter JI, O'Donovan MC, Montine TJ, Nalls MA, Mead S, Reiman EM, Jonsson P V, Holmes C, St George-Hyslop PH, Boada M, Passmore P, Wendland JR, Schmidt R, Morgan K, Winslow AR, Powell JF, Carasquillo M, Younkin SG, Jakobsdóttir J, Kauwe JSK, Wilhelmsen KC, Rujescu

D, Nöthen MM, Hofman A, Jones L, Adams PM, Albert MS, Albin RL, Apostolova LG, Arnold SE, Asthana S, Atwood CS, Baldwin CT, Barmada MM, Barnes LL, Beach TG, Becker JT, Bigio EH, Bird TD, Blacker D, Boeve BF, Bowen JD, Boxer A, Burke JR, Cairns NJ, Cao C, Carlson CS, Carlsson CM, Carney RM, Carrasquillo MM, Carroll SL, Chui HC, Clark DG, Corneveaux J, Cribbs DH, Crocco EA, Cruchaga C, De Jager PL, DeCarli C, DeKosky ST, Demirci FY, Dick M, Dickson DW, Doody RS, Duara R, Ertekin-Taner N, Faber KM, Fairchild TJ, Fallon KB, Farlow MR, Ferris S, Frosch MP, Galasko DR, Gearing M, Geschwind DH, Ghetti B, Gilbert JR, Glass JD, Graff-Radford NR, Green RC, Growdon JH, Hakonarson H, Hamilton RL, Hardy J, Harrell LE, Head E, Honig LS, Huebinger RM, Huentelman MJ, Hulette CM, Hyman BT, Jarvik GP, Jicha GA, Jin LW, Karydas A, Kauwe JS, Kaye JA, Kim R, Koo EH, Kowall NW, Kramer JH, LaFerla FM, Lah JJ, Leverenz JB, Levey AI, Li G, Lieberman AP, Lin CF, Lopez OL, Lyketsos CG, Mack WJ, Marson DC, Martiniuk F, Mash DC, Masliah E, McCormick WC, McCurry SM, McDavid AN, McKee AC, Mesulam M, Miller BL, Miller CA, Miller JW, Morris JC, Mukherjee S, Murrell JR, Myers AJ, O'Bryant S, Olichney JM, Pankratz VS, Parisi JE, Partch A, Paulson HL, Perry W, Peskind E, Petersen RC, Pierce A, Poon WW, Potter H, Quinn JF, Raj A, Raskind M, Reisberg B, Reisch JS, Reitz C, Ringman JM, Roberson ED, Rogaeva E, Rosen HJ, Rosenberg RN, Royall DR, Sager MA, Sano M, Saykin AJ, Schneider JA, Schneider LS, Seeley WW, Smith AG, Sonnen JA, Spina S, Stern RA, Tanzi RE, Thornton-Wells TA, Trojanowski JQ, Troncoso JC, Tsuang DW, Van Deerlin VM, Van Eldik LJ, Vardarajan BN, Vinters H V, Vonsattel JP, Weintraub S, Welsh-Bohmer KA, Williamson J, Wishnek S, Woltjer RL, Wright CB, Wu CK, Yu CE, Yu L, Au R, Wolf PA, Beiser A, Satizabal C, Uitterlinden AG, Rivadeneira F, Koudstaal PJ, Longstreth Jr WT, Becker JT, Kuller LH, Lumley T, Rice K, Harris TB, Nalls M, Marksteiner JJM, Dal-Bianco P, Töglhofer AM, Freudenberger P, Ransmayr G, Benke T, Toeglhofer AM, Boerwinkle E, Bressler J, Fornage M, Morón FJ, Hernández I, Roca MR, Mauleón A, Alegret M, Ramírez-Lorca R, González-Perez A, Alpérovitch A, Alvarez V, Barberger-Gateau P, Bettens K, Bossù P, Brice A, Bullido M, Caffara P, Clarimon J, Combarros O, Coto E, Zampo M del, Delepine M, Deniz Naranjo MC, Epelbaum J, Fratiglioni L, Galimberti D, Graff C, Hiltunen M, Ingelsson M, Keller L, Lannfelt L, Llèo A, Mancuso M, Mateo I, Mecocci P, Nacmias B, Panza F, Pilotto A, Garcia FS, Scarpini E, Seripa D, Sleegers K, Soininen H, Sorbi S, Spalletta G, Wallon D,

Thomas C, Gerrish A, Chapman J, Stretton A, Morgan A, Oldham H, Owen MJ, Kehoe PG, Medway C, Brown K, Lord J, Turton J, Hooper NM, Vardy E, Warren JD, Schott JM, Uphill J, Hollingworth P, Psy Dc, Ryan N, Rossor M, Collinge J, Ben-Shlomo Y, Makrina D, Gkatzima O, Lupton M, Koutroumani M, Avramidou D, Germanou A, Jessen F, Riedel-Heller S, Dichgans M, Heun R, Kölsch H, Schürmann B, Herold C, Lacour A, Drichel D, Hoffmann P, Kornhuber J, Gu W, Feulner T, Mayhaus M, Pichler S, Riemenschneider M, Bussche H van den, Lawlor B, Lynch A, Mann D, Smith AD, Warden D, Wilcock G, Heuser I, Wiltfang J, Frölich L, Hüll M, Mayo K, Livingston G, Bass NJ, Gurling H, McQuillin A, Gwilliam R, Deloukas P, Al-Chalabi A, Shaw CE, Singleton AB, Guerreiro R, Russo G, Jöckel KH, Moebus S, Klopp N, Wichmann HE, Dickson DW, Graff-Radford NR, Ma L, Bisceglio G, Fisher E, Warner N, Pickering-Brown S, Craig D, Johnston JA, McGuinness B, Todd S, Rubinsztein DC, Lovestone S, Bayer A, Gallacher J, Proitsi P, Ortega-Cubero S, Haines JL, Psaty BM, Van Broeckhoven C, Holmans P, Launer LJ, Mayeux R, Lathrop M, Goate AM, Escott-Price V, Seshadri S, Pericak-Vance MA, Amouyel P, Williams J, van Duijn CM, Schellenberg GD, Farrer LA. A novel Alzheimer disease locus located near the gene encoding tau protein. Mol Psychiatry [Internet]. 2016 Jan 17;21(1):108–17. Available from: http://www.nature.com/mp/journal/v21/n1/abs/mp201523a.html

19. Grupe A, Li Y, Rowland C, Nowotny P, Hinrichs AL, Smemo S, Kauwe JSK, Maxwell TJ, Cherny S, Doil L, Tacey K, Van Luchene R, Myers A, Wavrant-De Vrièze F, Kaleem M, Hollingworth P, Jehu L, Foy C, Archer N, Hamilton G, Holmans P, Morris CM, Catanese J, Sninsky J, White TJ, Powell J, Hardy J, O'Donovan M, Lovestone S, Jones L, Morris JC, Thal L, Owen M, Williams J, Goate A. A scan of chromosome 10 identifies a novel locus showing strong association with late-onset Alzheimer disease. Am J Hum Genet. 2006;78(1):78–88.
20. Lu T, Pan Y, Kao SY, Li C, Kohane I, Chan J, Yankner BA. Gene regulation and DNA damage in the ageing human brain. Nature. 2004;429(6994):883–91.
21. Sonia Gaur, BS1,2, Baris Turkbey, MD1 and PC. Sex-Dependent Shared and Non-Shared Genetic Architecture Across Mood and Psychotic Disorders. Alzheimer's Dement [Internet]. 2018;14(4):535–62. Available from: https://www.ncbi.nlm.nih.gov/pmc/articles/PMC5958625/pdf/nihms960157.pdf
22. Yao X, Glessner JT, Li J, Qi X, Hou X, Zhu C, Li X, March ME, Yang L, Mentch FD, Hain HS, Meng X, Xia Q, Hakonarson H, Li J. Integrative analysis of genome-wide

association studies identifies novel loci associated with neuropsychiatric disorders. Transl Psychiatry [Internet]. 2021;11(1). Available from: http://dx.doi.org/10.1038/s41398-020-01195-5

23. Wu Y, Cao H, Baranova A, Huang H, Li S, Cai L, Rao S, Dai M, Xie M, Dou Y, Hao Q, Zhu L, Zhang X, Yao Y, Xu M, Wang Q, Zhang F. Multi-trait analysis for genome-wide association study of five psychiatric disorders. Transl Psychiatry [Internet]. 2020;10(1). Available from: http://dx.doi.org/10.1038/s41398-020-00902-6
24. Watanabe K, Jansen PR, Savage JE, Nandakumar P, Wang X, Agee M, Aslibekyan S, Auton A, Bell RK, Bryc K, Clark SK, Elson SL, Fletez-Brant K, Fontanillas P, Furlotte NA, Gandhi PM, Heilbron K, Hicks B, Huber KE, Jewett EM, Jiang Y, Kleinman A, Lin KH, Litterman NK, McCreight JC, McIntyre MH, McManus KF, Mountain JL, Mozaffari S V., Noblin ES, Northover CAM, O'Connell J, Pitts SJ, Poznik GD, Sathirapongsasuti JF, Shelton JF, Shi J, Shringarpure S, Tian C, Tung JY, Tunney RJ, Vacic V, Wang W, Hinds DA, Gelernter J, Levey DF, Polimanti R, Stein MB, Van Someren EJW, Smit AB, Posthuma D. Genome-wide meta-analysis of insomnia prioritizes genes associated with metabolic and psychiatric pathways. Nat Genet. 2022;54(8):1125–32.
25. Huang EJ, Reichardt LF. Neurotrophins: Roles in neuronal development and function. Annu Rev Neurosci. 2001;24:677–736.
26. Miranda M, Morici JF, Zanoni MB, Bekinschtein P. Brain-Derived Neurotrophic Factor: A Key Molecule for Memory in the Healthy and the Pathological Brain. Front Cell Neurosci. 2019;13(August):1–25.
27. Huang EJ, Reichardt LF. Trk receptors: Roles in neuronal signal transduction. Annu Rev Biochem. 2003;72:609–42.
28. Yang M, Lim Y, Li X, Zhong JH, Zhou XF. Precursor of brain-derived neurotrophic factor (proBDNF) forms a complex with huntingtin-associated protein-1 (HAP1) and sortilin that modulates proBDNF trafficking, degradation, and processing. J Biol Chem [Internet]. 2011;286(18):16272–84. Available from: http://dx.doi.org/10.1074/jbc.M110.195347
29. Chen ZY, Ieraci A, Teng H, Dall H, Meng CX, Herrera DG, Nykjaer A, Hempstead BL, Lee FS. Sortilin controls intracellular sorting of brain-derived neurotrophic factor to the regulated secretory pathway. J Neurosci. 2005;25(26):6156–66.
30. Nykjaer A, Lee R, Kenneth K. Teng, Jansen P, Madsen P, Nielsen MS, Jacobsen C, Kliemannel M, Schwarz E, Willnow TE, Hempstead BL, Petersen CM. Sortilin is

essential for proNGF- induced neuronal cell death. Nature. 2004;427(6977):839–43.

31. Vaegter CB, Jansen P, Fjorback AW, Glerup S, Skeldal S, Kjolby M, Richner M, Erdmann B, Nyengaard JR, Tessarollo L, Lewin GR, Willnow TE, Chao M V., Nykjaer A. Sortilin associates with Trk receptors to enhance anterograde transport and neurotrophin signaling. Nat Neurosci. 2011;14(1):54–63.
32. Andersen OM, Reiche J, Schmidt V, Gotthardt M, Spoelgen R, Behlke J, Von Arnim CAF, Breiderhoff T, Jansen P, Wu X, Bales KR, Cappai R, Masters CL, Gliemann J, Mufson EJ, Hyman BT, Paul SM, Nykjsær A, Willnow TE. Neuronal sorting protein-related receptor sorLA/LR11 regulates processing of the amyloid precursor protein. Proc Natl Acad Sci U S A. 2005;102(38):13461–6.
33. Offe K, Dodson SE, Shoemaker JT, Fritz JJ, Gearing M, Levey AI, Lah JJ. The lipoprotein receptor LR11 regulates amyloid β production and amyloid precursor protein traffic in endosomal compartments. J Neurosci. 2006;26(5):1596–603.
34. Shih AZL, Chen YC, Speckmann T, Søndergaard E, Schürmann A, Verchere CB, Willnow TE. SORLA mediates endocytic uptake of proIAPP and protects against islet amyloid deposition. Mol Metab [Internet]. 2022;65(August):101585. Available from: https://doi.org/10.1016/j.molmet.2022.101585
35. Díaz-Alonso J, Nicoll RA. AMPA receptor trafficking and LTP: Carboxy-termini, amino-termini and TARPs. Neuropharmacology [Internet]. 2021;197:108710. Available from: https://doi.org/10.1016/j.neuropharm.2021.108710
36. Chater TE, Goda Y. The role of AMPA receptors in postsynaptic mechanisms of synaptic plasticity. Front Cell Neurosci. 2014;8(NOV):1–14.
37. Mateos-Aparicio P, Rodríguez-Moreno A. The impact of studying brain plasticity. Front Cell Neurosci. 2019;13(February):1–5.
38. Gomez AM, Traunmüller L, Scheiffele P. Neurexins: molecular codes for shaping neuronal synapses. Nat Rev Neurosci [Internet]. 2021;22(3):137–51. Available from: http://dx.doi.org/10.1038/s41583-020-00415-7
39. Südhof TC. Neuroligins and neurexins link synaptic function to cognitive disease. Nature. 2008;455(7215):903–11.
40. Christiane Reitz1, 2, 3, Shinya Tokuhiro8, Lorraine N. Clark1, 5, Christopher Conrad1, 5, JeanPaul Vonsattel1, 5, Lili-Naz Hazrati8, András Palotás20, Raphael Lantigua1, 6, Martin Medrano18, Ivonne Z. Jiménez-Velázquez19, Badri Vardarajan10, Irene Simkin1 6. SORCS1 Alters Amyloid Precursor Protein

Processing and Variants May Increase Alzheimer's Disease Risk. 2009;6(11):1249–54.

41. Hur JY. γ-Secretase in Alzheimer's disease. Exp Mol Med. 2022;54(4):433–46.
42. Alemany S, Ribasés M, Vilor-Tejedor N, Bustamante M, Sánchez-Mora C, Bosch R, Richarte V, Cormand B, Casas M, Ramos-Quiroga JA, Sunyer J. New suggestive genetic loci and biological pathways for attention function in adult attention-deficit/hyperactivity disorder. Am J Med Genet Part B Neuropsychiatr Genet. 2015;168(6):459–70.
43. Fabbri C, Serretti A. Genetics of long-term treatment outcome in bipolar disorder. Prog Neuro-Psychopharmacology Biol Psychiatry [Internet]. 2016;65:17–24. Available from: http://dx.doi.org/10.1016/j.pnpbp.2015.08.008
44. Yang J, Ma Q, Dincheva I, Giza J, Jing D, Marinic T, Milner TA, Rajadhyaksha A, Lee FS, Hempstead BL. SorCS2 is required for social memory and trafficking of the NMDA receptor. Mol Psychiatry [Internet]. 2021;26(3):927–40. Available from: http://dx.doi.org/10.1038/s41380-020-0650-7
45. Hermey G, Sjøgaard SS, Petersen CM, Nykjær A, Gliemann J. Tumour necrosis factor α-converting enzyme mediates ectodomain shedding of Vps10p-domain receptor family members. Biochem J. 2006;395(2):285–93.
46. Ma Q, Yang J, Milner TA, Vonsattel JPG, Palko ME, Tessarollo L, Hempstead BL. SorCS2-mediated NR2A trafficking regulates motor deficits in Huntington's disease. JCI insight. 2017;2(9):1–16.
47. Malik AR, Szydlowska K, Nizinska K, Asaro A, van Vliet EA, Popp O, Dittmar G, Fritsche-Guenther R, Kirwan JA, Nykjaer A, Lukasiuk K, Aronica E, Willnow TE. SorCS2 Controls Functional Expression of Amino Acid Transporter EAAT3 and Protects Neurons from Oxidative Stress and Epilepsy-Induced Pathology. Cell Rep [Internet]. 2019;26(10):2792-2804.e6. Available from: https://doi.org/10.1016/j.celrep.2019.02.027
48. Steve TA, Jirsch JD, Gross DW. Quantification of subfield pathology in hippocampal sclerosis: A systematic review and meta-analysis. Epilepsy Res [Internet]. 2014;108(8):1279–85. Available from: http://dx.doi.org/10.1016/j.eplepsyres.2014.07.003
49. Malik AR, Lips J, Gorniak-Walas M, Broekaart DWM, Asaro A, Kuffner MTC, Hoffmann CJ, Kikhia M, Dopatka M, Boehm-Sturm P, Mueller S, Dirnagl U, Aronica E, Harms C, Willnow TE. SorCS2 facilitates release of endostatin from astrocytes

and controls post-stroke angiogenesis. Glia. 2020;68(6):1304–16.

50. Goodarzi MO, Lehman DM, Taylor KD, Guo X, Cui J, Quiñones MJ, Clee SM, Yandell BS, Blangero J, Hsueh WA, Attie AD, Stern MP, Rotter JI. SORCS1: A novel human type 2 diabetes susceptibility gene suggested by the mouse. Diabetes. 2007;56(7):1922–9.
51. Clee SM, Yandell BS, Schueler KM, Rabaglia ME, Richards OC, Raines SM, Kabara EA, Klass DM, Mui ETK, Stapleton DS, Gray-Keller MP, Young MB, Stoehr JP, Lan H, Boronenkov I, Raess PW, Flowers MT, Attie AD. Positional cloning of Sorcs1, a type 2 diabetes quantitative trait locus. Nat Genet. 2006;38(6):688–93.
52. Florez JC, Manning AK, Dupuis J, McAteer J, Irenze K, Gianniny L, Mirel DB, Fox CS, Cupples LA, Meigs JB. A 100K genome-wide association scan for diabetes and related traits in the Framingham Heart Study: Replication and integration with other genome-wide datasets. Diabetes. 2007;56(12):3063–74.
53. Dupuis J, Langenberg C, Prokopenko I, Saxena R, Soranzo N, Jackson AU, Wheeler E, Glazer NL, Bouatia-Naji N, Gloyn AL, Lindgren CM, Mägi R, Morris AP, Randall J, Johnson T, Elliott P, Rybin D, Thorleifsson G, Steinthorsdottir V, Henneman P, Grallert H, Dehghan A, JanHottenga J, Franklin CS, Navarro P, Song K, Goel A, Perry JRB, Egan JM, Lajunen T, Grarup N, Sparsø T, Doney A, Voight BF, Stringham HM, Li M, Kanoni S, Shrader P, Cavalcanti-Proença C, Kumari M, Qi L, Timpson NJ, Gieger C, Zabena C, Rocheleau G, Ingelsson E, An P, O'Connell J, Luan J, Elliott A, McCarroll SA, Payne F, Roccasecca RM, Pattou F, Sethupathy P, Ardlie K, Ariyurek Y, Balkau B, Barter P, Beilby JP, Ben-Shlomo Y, Benediktsson R, Bennett AJ, Bergmann S, Bochud M, Boerwinkle E, Bonnefond A, Bonnycastle LL, Borch-Johnsen K, Böttcher Y, Brunner E, Bumpstead SJ, Charpentier G, Der IdaChen Y, Chines P, Clarke R, McOin LJ, Cooper MN, Cornelis M, Crawford G, Crisponi L, Day INM, De Geus EJC, Delplanque J, Dina C, Erdos MR, Fedson AC, Fischer-Rosinsky A, Forouhi NG, Fox CS, Frants R, GraziaFranzosi M, Galan P, Goodarzi MO, Graessler J, Groves CJ, Grundy S, Gwilliam R, Gyllensten U, Hadjadj S, Hallmans G, Hammond N, Han X, -LiisaHartikainen A, Hassanali N, Hayward C, Heath SC, Hercberg S, Herder C, Hicks AA, Hillman DR, Hingorani AD, Hofman A, Hui J, Hung J, Isomaa B, Johnson PRV, Jørgensen T, Jula A, Kaakinen M, Kaprio J, AnteroKesaniemi Y, Kivimaki M, Knight B, Koskinen S, Kovacs P, Kyvik KO, Lathrop GM, Lawlor DA, Bacquer O Le, Lecoeur C, Li Y, Lyssenko V, Mahley R, Mangino M, Manning AK, TeresaMartínez-Larrad M,

McAteer JB, McCulloch LJ, McPherson R, Meisinger C, Melzer D, Meyre D, Mitchell BD, Morken MA, Mukherjee S, Naitza S, Narisu N, Neville MJ, Oostra BA, Orrù M, Pakyz R, APalmer CN, Paolisso G, Pattaro C, Pearson D, Peden JF, Pedersen NL, Perola M, Pfeiffer AFH, Pichler I, Polasek O, Posthuma D, Potter SC, Pouta A, Province MA, Psaty BM, Rathmann W, Rayner NW, Rice K, Ripatti S, Rivadeneira F, Roden M, Rolandsson O, Sandbaek A, Sandhu M, Sanna S, Sayer AA, Scheet P, Scott LJ, Seedorf U, Sharp SJ, Shields B, Sigursson G, Sijbrands EJG, Silveira A, Simpson L, Singleton A, Smith NL, Sovio U, Swift A, Syddall H, -ChristineSyvänen A, Tanaka T, Thorand B, Tichet J, Tönjes A, Tuomi T, Uitterlinden AG, Van Dijk KW, Hoek M Van, Varma D, Visvikis-Siest S, Vitart V, Vogelzangs N, Waeber G, Wagner PJ, Walley A, BragiWalters G, Ward KL, Watkins H, Weedon MN, Wild SH, Willemsen G, MWitteman JC, GYarnell JW, Zeggini E, Zelenika D, Zethelius B, Zhai G, Zhao JH, Zillikens MC, Borecki IB, Loos RJF, Meneton P, Magnusson PKE, Nathan DM, Williams GH, Hattersley AT, Silander K, Salomaa V, Smith GD, Bornstein SR, Schwarz P, Spranger J, Karpe F, Shuldiner AR, Cooper C, Dedoussis G V., Serrano-Ríos M, Morris AD, Lind L, Palmer LJ, Hu FB, Franks PW, Ebrahim S, Marmot M, Linda Kao WH, Pankow JS, Sampson MJ, Kuusisto J, Laakso M, Hansen T, Pedersen O, Pramstaller PP, Wichmann HE, Illig T, Rudan I, Wright AF, Stumvoll M, Campbell H, Wilson JF, Bergman RN, Buchanan TA, Collins FS, Mohlke KL, Tuomilehto J, Valle TT, Altshuler D, Rotter JI, Siscovick DS, Penninx BWJH, Boomsma DI, Deloukas P, Spector TD, Frayling TM, Ferrucci L, Kong A, Thorsteinsdottir U, Stefansson K, Van Duijn CM, Aulchenko YS, Cao A, Scuteri A, Schlessinger D, Uda M, Ruokonen A, -RiittaJarvelin M, Waterworth DM, Vollenweider P, Peltonen L, Mooser V, Abecasis GR, Wareham NJ, Sladek R, Froguel P, Watanabe RM, Meigs JB, Groop L, Boehnke M, McCarthy MI, Florez JC, Barroso I. New genetic loci implicated in fasting glucose homeostasis and their impact on type 2 diabetes risk. Nat Genet. 2010;42(2):105–16.

54. Pipal K V., Mamtani M, Patel AA, Jaiswal SG, Jaisinghani MT, Kulkarni H. Susceptibility Loci for Type 2 Diabetes in the Ethnically Endogamous Indian Sindhi Population: A Pooled Blood Genome-Wide Association Study. Genes (Basel). 2022;13(8).

55. Strachan DP, Rudnicka AR, Power C, Shepherd P, Fuller E, Davis A, Gibb I, Kumari M, Rumley A, Macfarlane GJ, Rahi J, Rodgers B, Stansfeld S. Lifecourse influences

on health among British adults: Effects of region of residence in childhood and adulthood. Int J Epidemiol. 2007;36(3):522–31.

56. Wen W, Cho YS, Zheng W, Dorajoo R, Kato N, Qi L, Chen CH, Delahanty RJ, Okada Y, Tabara Y, Gu D, Zhu D, Haiman CA, Mo Z, Gao YT, Saw SM, Go MJ, Takeuchi F, Chang LC, Kokubo Y, Liang J, Hao M, Le Marchand L, Zhang Y, Hu Y, Wong TY, Long J, Han BG, Kubo M, Yamamoto K, Su MH, Miki T, Henderson BE, Song H, Tan A, He J, Ng DPK, Cai Q, Tsunoda T, Tsai FJ, Iwai N, Chen GK, Shi J, Xu J, Sim X, Xiang YB, Maeda S, Ong RTH, Li C, Nakamura Y, Aung T, Kamatani N, Liu JJ, Lu W, Yokota M, Seielstad M, Fann CSJ, Wu JY, Lee JY, Hu FB, Tanaka T, Tai ES, Shu XO. Meta-analysis identifies common variants associated with body mass index in east Asians. Nat Genet. 2012;44(3):307–11.
57. Cheng CF, Hsieh AR, Liang WM, Chen CC, Chen CH, Wu JY, Lin TH, Liao CC, Huang SM, Huang YC, Ban B, Lin YJ, Tsai FJ. Genome-Wide and Candidate Gene Association Analyses Identify a 14-SNP Combination for Hypertension in Patients with Type 2 Diabetes. Am J Hypertens. 2021;34(6):651–61.
58. Namjou B, Lingren T, Huang Y, Parameswaran S, Cobb BL, Stanaway IB, Connolly JJ, Mentch FD, Benoit B, Niu X, Wei WQ, Carroll RJ, Pacheco JA, Harley ITW, Divanovic S, Carrell DS, Larson EB, Carey DJ, Verma S, Ritchie MD, Gharavi AG, Murphy S, Williams MS, Crosslin DR, Jarvik GP, Kullo IJ, Hakonarson H, Li R, Xanthakos SA, Harley JB. GWAS and enrichment analyses of non-alcoholic fatty liver disease identify new trait-associated genes and pathways across eMERGE Network. BMC Med. 2019;17(1):1–19.
59. Thorleifsson G, Walters GB, Gudbjartsson DF, Steinthorsdottir V, Sulem P, Helgadottir A, Styrkarsdottir U, Gretarsdottir S, Thorlacius S, Jonsdottir I, Jonsdottir T, Olafsdottir EJ, Olafsdottir GH, Jonsson T, Jonsson F, Borch-Johnsen K, Hansen T, Andersen G, Jorgensen T, Lauritzen T, Aben KK, Verbeek ALM, Roeleveld N, Kampman E, Yanek LR, Becker LC, Tryggvadottir L, Rafnar T, Becker DM, Gulcher J, Kiemeney LA, Pedersen O, Kong A, Thorsteinsdottir U, Stefansson K. Genome-wide association yields new sequence variants at seven loci that associate with measures of obesity. Nat Genet. 2009;41(1):18–24.
60. Meyre D, Delplanque J, Chèvre JC, Lecoeur C, Lobbens S, Gallina S, Durand E, Vatin V, Degraeve F, Proença C, Gaget S, Körner A, Kovacs P, Kiess W, Tichet J, Marre M, Hartikainen AL, Horber F, Potoczna N, Hercberg S, Levy-Marchal C, Pattou F, Heude B, Tauber M, McCarthy MI, Blakemore AIF, Montpetit A,

Polychronakos C, Weill J, Coin LJM, Asher J, Elliott P, Järvelin MR, Visvikis-Siest S, Balkau B, Sladek R, Balding D, Walley A, Dina C, Froguel P. Genome-wide association study for early-onset and morbid adult obesity identifies three new risk loci in European populations. Nat Genet. 2009;41(2):157–9.

61. Willer CJ, Speliotes EK, Loos RJF, Li S, Lindgren CM, Heid IM, Berndt SI, Elliott AL, Jackson AU, Lamina C, Lettre G, Lim N, Lyon HN, McCarroll SA, Papadakis K, Qi L, Randall JC, Roccasecca RM, Sanna S, Scheet P, Weedon MN, Wheeler E, Zhao JH, Jacobs LC, Prokopenko I, Soranzo N, Tanaka T, Timpson NJ, Almgren P, Bennett A, Bergman RN, Bingham SA, Bonnycastle LL, Brown M, Burtt NP, Chines P, Coin L, Collins FS, Connell JM, Cooper C, Smith GD, Dennison EM, Deodhar P, Elliott P, Erdos MR, Estrada K, Evans DM, Gianniny L, Gieger C, Gillson CJ, Guiducci C, Hackett R, Hadley D, Hall AS, Havulinna AS, Hebebrand J, Hofman A, Isomaa B, Jacobs KB, Johnson T, Jousilahti P, Jovanovic Z, Khaw KT, Kraft P, Kuokkanen M, Kuusisto J, Laitinen J, Lakatta EG, Luan J, Luben RN, Mangino M, McArdle WL, Meitinger T, Mulas A, Munroe PB, Narisu N, Ness AR, Northstone K, O'Rahilly S, Purmann C, Rees MG, Ridderstråle M, Ring SM, Rivadeneira F, Ruokonen A, Sandhu MS, Saramies J, Scott LJ, Scuteri A, Silander K, Sims MA, Song K, Stephens J, Stevens S, Stringham HM, Tung YCL, Valle TT, Van Duijn CM, Vimaleswaran KS, Vollenweider P, Waeber G, Wallace C, Watanabe RM, Waterworth DM, Watkins N, Witteman JCM, Zeggini E, Zhai G, Zillikens MC, Altshuler D, Caulfield MJ, Chanock SJ, Farooqi IS, Ferrucci L, Guralnik JM, Hattersley AT, Hu FB, Jarvelin MR, Laakso M, Mooser V, Ong KK, Ouwehand WH, Salomaa V, Samani NJ, Spector TD, Tuomi T, Tuomilehto J, Uda M, Uitterlinden AG, Wareham NJ, Deloukas P, Frayling TM, Groop LC, Hayes RB, Hunter DJ, Mohlke KL, Peltonen L, Schlessinger D, Strachan DP, Wichmann HE, McCarthy MI, Boehnke M, Barroso I, Abecasis GR, Hirschhorn JN. Six new loci associated with body mass index highlight a neuronal influence on body weight regulation. Nat Genet. 2009;41(1):25–34.

62. Kebede MA, Oler AT, Gregg T, Balloon AJ, Johnson A, Mitok K, Rabaglia M, Schueler K, Stapleton D, Thorstenson C, Wrighton L, Floyd BJ, Richards O, Raines S, Eliceiri K, Seidah NG, Rhodes C, Keller MP, Coon JL, Audhya A, Attie AD. SORCS1 is necessary for normal insulin secretory granule biogenesis in metabolically stressed β cells. J Clin Invest. 2014;124(10):4240–56.

63. Schmidt V, Schulz N, Yan X, Schürmann A, Kempa S, Kern M, Blüher M, Poy MN,

Olivecrona G, Willnow TE. SORLA facilitates insulin receptor signaling in adipocytes and exacerbates obesity. J Clin Invest. 2016;126(7):2706–20.

64. Shi J, Kandror K V. Sortilin is essential and sufficient for the formation of glut4 storage vesicles in 3T3-L1 adipocytes. Dev Cell. 2005;9(1):99–108.
65. Leto D, Saltiel AR. Regulation of glucose transport by insulin: Traffic control of GLUT4. Nat Rev Mol Cell Biol. 2012;13(6):383–96.
66. Stöckli J, Fazakerley DJ, James DE. GLUT4 exocytosis. J Cell Sci. 2011;124(24):4147–59.
67. Pan X, Zaarur N, Singh M, Morin P, Kandror K V. Sortilin and retromer mediate retrograde transport of Glut4 in 3T3-L1 adipocytes. Mol Biol Cell. 2017;28(12):1667–75.
68. Li J, Matye DJ, Wang Y, Li T. Sortilin 1 knockout alters basal adipose glucose metabolism but not diet-induced obesity in mice. FEBS Lett. 2017;591(7):1018–28.
69. Rabinowich L, Fishman S, Hubel E, Thurm T, Park WJ, Pewzner-Jung Y, Saroha A, Erez N, Halpern Z, Futerman AH, Zvibel I. Sortilin deficiency improves the metabolic phenotype and reduces hepatic steatosis of mice subjected to diet-induced obesity. J Hepatol [Internet]. 2015;62(1):175–81. Available from: http://dx.doi.org/10.1016/j.jhep.2014.08.030
70. Owen K, Turner H, Wass J. Oxford Handbook of Endocrinology and Diabetes 4e [Internet]. 4th ed. Owen K, Turner H, Wass J, editors. Oxford Handbook of Endocrinology & Diabetes 4e. Oxford: Oxford University PressOxford; 2022. Available from: https://academic.oup.com/book/37188
71. Reno CM, Skinner A, Bayles J, Chen YS, Daphna-Iken D, Fisher SJ. Severe hypoglycemia-induced sudden death is mediated by both cardiac arrhythmias and seizures. Am J Physiol - Endocrinol Metab. 2018;315(2):E240–9.
72. Nishihama K, Eguchi K, Maki K, Okano Y, Tanaka S, Inoue C, Uchida A, Uemura M, Suzuki T, Yasuma T, D'alessandro-Gabazza CN, Gabazza EC, Yano Y. Sudden death associated with severe hypoglycemia in a diabetic patient during sensor-augmented pump therapy with the predictive low glucose management system. Am J Case Rep. 2021;22(1):1–5.
73. Weant KA, Bailey AM, Baker SN. Hyperglycemia in critical illness. Adv Emerg Nurs J. 2013;35(3):209–16.
74. Mouri M, Badireddy M. Hyperglycemia. In Treasure Island (FL): StatPearls Publishing; 2023. Available from: https://www.ncbi.nlm.nih.gov/books/NBK430900/

75. Mouri M, Badireddy M. Hyperglycemia. In Treasure Island (FL): StatPearls Publishing; 2023.
76. Aronoff SL, Berkowitz K, Shreiner B, Want L. Glucose Metabolism and Regulation: Beyond Insulin and Glucagon. Diabetes Spectr. 2004;17(3):183–90.
77. Nakrani MN, Wineland RH, Anjum F. Physiology, Glucose Metabolism [Internet]. Treasure Island (FL): StatPearls Publishing; 2022. Available from: https://www.ncbi.nlm.nih.gov/books/NBK560599/%0A
78. Nakrani MN, Wineland RH, Anjum F. Physiology, Glucose Metabolism. Treasure Island (FL): StatPearls Publishing; 2022.
79. Kuo, Taiyi; McQueen, Allison; Chen, Tzu-Chieh; Wang JC. Regulation of Glucose Homeostasis by Glucocorticoids Taiyi. 2018;99–126.
80. Sherwin RS, Sacca L. Effect of epinephrine on glucose metabolism in humans: Contribution of the liver. Am J Physiol - Endocrinol Metab. 1984;10(2).
81. Resmini E, Minuto F, Colao A, Ferone D. Secondary diabetes associated with principal endocrinopathies: The impact of new treatment modalities. Acta Diabetol. 2009;46(2):85–95.
82. Hyun U, Sohn JW. Autonomic control of energy balance and glucose homeostasis. Exp Mol Med. 2022;54(4):370–6.
83. Deng D, Yan N. GLUT, SGLT, and SWEET: Structural and mechanistic investigations of the glucose transporters. Protein Sci. 2016;25(3):546–58.
84. Thorens B, Mueckler M. The SLC2 (GLUT) Family of Membrane Transporters. Mol Aspects Med. 2014;34(0):121–38.
85. Chadt A, Al-Hasani H. Glucose transporters in adipose tissue, liver, and skeletal muscle in metabolic health and disease. Pflugers Arch Eur J Physiol. 2020;472(9):1273–98.
86. Siska PJ, Rathmell JC. PKCs Sweeten Cell Metabolism by Phosphorylation of Glut1. Mol Cell [Internet]. 2015;58(5):711–2. Available from: http://dx.doi.org/10.1016/j.molcel.2015.05.025
87. Wu N, Zheng B, Shaywitz A, Dagon Y, Tower C, Bellinger G, Shen CH, Wen J, Asara J, McGraw TE, Kahn BB, Cantley LC. AMPK-Dependent Degradation of TXNIP upon Energy Stress Leads to Enhanced Glucose Uptake via GLUT1. Mol Cell [Internet]. 2013;49(6):1167–75. Available from: http://dx.doi.org/10.1016/j.molcel.2013.01.035
88. Thorens B. GLUT2, glucose sensing and glucose homeostasis. Diabetologia.

2015;58(2):221–32.

89. Wu N, Zheng B, Shaywitz A, Dagon Y, Tower C, Bellinger G, Shen CH, Wen J, Asara J, McGraw TE, Kahn BB, Cantley LC. AMPK-Dependent Degradation of TXNIP upon Energy Stress Leads to Enhanced Glucose Uptake via GLUT1. Mol Cell. 2013;49(6):1167–75.
90. Prada PO, Pauli JR, Ropelle ER, Zecchin HG, Carvalheira JBC, Velloso LA, Saad MJA. Selective modulation of the CAP/Cbl pathway in the adipose tissue of high fat diet treated rats. FEBS Lett. 2006;580(20):4889–94.
91. Kong S, Zhang YH, Zhang W. Regulation of intestinal epithelial cells properties and functions by amino acids. Biomed Res Int. 2018;2018(Figure 1).
92. Nicoletti C. Unsolved mysteries of intestinal M cells. Gut. 2000;47(5):735–9.
93. Alcaino C, Knutson KR, Treichel AJ, Yildiz G, Strege PR, Linden DR, Li JH, Leiter AB, Szurszewski JH, Farrugia G, Beyder A. A population of gut epithelial enterochromaffin cells is mechanosensitive and requires Piezo2 to convert force into serotonin release. Proc Natl Acad Sci U S A. 2018;115(32):E7632–41.
94. Gribble FM, Reimann F. Function and mechanisms of enteroendocrine cells and gut hormones in metabolism. Nat Rev Endocrinol [Internet]. 2019;15(4):226–37. Available from: http://dx.doi.org/10.1038/s41574-019-0168-8
95. Kalafatakis K, Triantafyllou K. Contribution of neurotensin in the immune and neuroendocrine modulation of normal and abnormal enteric function. Regul Pept [Internet]. 2011;170(1–3):7–17. Available from: http://dx.doi.org/10.1016/j.regpep.2011.04.005
96. Afroze S, Meng F, Jensen K, McDaniel K, Rahal K, Onori P, Gaudio E, Alpini G, Glaser SS. The physiological roles of secretin and its receptor. Ann Transl Med. 2013;1(3):1–14.
97. Gutierrez-Aguilar R, Woods SC. Nutrition and L and K-enteroendocrine cells. Curr Opin Endocrinol Diabetes Obes. 2011;18(1):35–41.
98. Drucker DJ. Glucagon-Like Peptide 2. J Clin Endocrinol Metab [Internet]. 2001 Mar;86(4):1759–64. Available from: https://academic.oup.com/jcem/article-lookup/doi/10.1210/jcem.86.4.7386
99. Karra E, Chandarana K, Batterham RL. The role of peptide YY in appetite regulation and obesity. J Physiol. 2009;587(1):19–25.
100. Stümpel F, Burcelin R, Jungermann K, Thorens B. Normal kinetics of intestinal glucose absorption in the absence of GLUT2: Evidence for a transport pathway

requiring glucose phosphorylation and transfer into the endoplasmic reticulum. Proc Natl Acad Sci U S A. 2001;98(20):11330–5.

101. Reimann F, Habib AM, Tolhurst G, Parker HE, Rogers GJ, Gribble FM. Glucose Sensing in L Cells: A Primary Cell Study. Cell Metab. 2008;8(6):532–9.
102. Shi YC, Loh K, Bensellam M, Lee K, Zhai L, Lau J, Cantley J, Luzuriaga J, Laybutt DR, Herzog H. Pancreatic PYY is critical in the control of insulin secretion and glucose homeostasis in female mice. Endocrinology. 2015;156(9):3122–36.
103. Fu Z, R. Gilbert E, Liu D. Regulation of Insulin Synthesis and Secretion and Pancreatic Beta-Cell Dysfunction in Diabetes. Curr Diabetes Rev. 2012;9(1):25–53.
104. Suckale J, Solimena M. Pancreas islets in metabolic signaling - focus on the β -cell Pancreatic islet microorgan. Bioscience. 2007;
105. Zechner R, Kienesberger PC, Haemmerle G, Zimmermann R, Lass A. Adipose triglyceride lipase and the lipolytic catabolism of cellular fat stores. J Lipid Res [Internet]. 2009;50(1):3–21. Available from: http://dx.doi.org/10.1194/jlr.R800031-JLR200
106. Rorsman P, Braun M, Zhang Q. Regulation of calcium in pancreatic α- and β-cells in health and disease. Cell Calcium [Internet]. 2012;51(3–4):300–8. Available from: http://dx.doi.org/10.1016/j.ceca.2011.11.006
107. Müller TD, Finan B, Clemmensen C, Di Marchi RD, Tschöp MH. The new biology and pharmacology of glucagon. Vol. 97, Physiological Reviews. 2017. 721–766 p.
108. Verberne AJM, Korim WS, Sabetghadam A, Llewellyn-Smith IJ. Adrenaline: Insights into its metabolic roles in hypoglycaemia and diabetes. Br J Pharmacol. 2016;173(9):1425–37.
109. Ramracheya R, Ward C, Shigeto M, Walker JN, Amisten S, Zhang Q, Johnson PR, Rorsman P, Braun M. Membrane potential-dependent inactivation of voltage-gated ion channels in α-cells inhibits glucagon secretion from human islets. Diabetes. 2010;59(9):2198–208.
110. Rorsman P, Braun M, Zhang Q. Regulation of calcium in pancreatic α- and β-cells in health and disease. Cell Calcium. 2012;51(3–4):300–8.
111. Zhao YF. Free fatty acid receptors in the endocrine regulation of glucose metabolism: Insight from gastrointestinal-pancreatic-adipose interactions. Front Endocrinol (Lausanne). 2022;13(September):1–13.
112. Staehr P, Hother-Nielsen O, Landau BR, Chandramouli V, Holst JJ, Beck-Nielsen

H. Effects of free fatty acids per se on glucose production, gluconeogenesis, and glycogenolysis. Diabetes. 2003;52(2):260–7.

113. Rui L. Energy metabolism in the liver. Vol. 4, Comprehensive Physiology. 2014. p. 177–97.
114. Vatner DF, Majumdar SK, Kumashiro N, Petersen MC, Rahimi Y, Gattu AK, Bears M, Camporez JPG, Cline GW, Jurczak MJ, Samuel VT, Shulman GI. Insulin-independent regulation of hepatic triglyceride synthesis by fatty acids. Proc Natl Acad Sci U S A. 2015;112(4):1143–8.
115. Edgerton DS, Lautz M, Scott M, Everett CA, Stettler KM, Neal DW, Chu CA, Cherrington AD. Insulin's direct effects on the liver dominate the control of hepatic glucose production. J Clin Invest. 2006;116(2):521–7.
116. Han HS, Kang G, Kim JS, Choi BH, Koo SH. Regulation of glucose metabolism from a liver-centric perspective. Exp Mol Med. 2016;48(3):1–10.
117. Ramnanan CJ, Edgerton DS, Kraft G, Cherrington AD. Physiologic action of glucagon on liver glucose metabolism. Diabetes, Obes Metab [Internet]. 2011 Oct 8;13(s1):118–25. Available from: https://dom-pubs.pericles-prod.literatumonline.com/doi/10.1111/j.1463-1326.2011.01454.x
118. Pelley JW. Membranes and Intracellular Signal Transduction. Elsevier's Integr Rev Biochem. 2012;39–48.
119. Jiang G, Zhang BB. Glucagon and regulation of glucose metabolism. Am J Physiol - Endocrinol Metab. 2003;284(4 47-4).
120. Titchenell PM, Lazar MA, Birnbaum MJ. Unraveling the Regulation of Hepatic Metabolism by Insulin. Trends Endocrinol Metab [Internet]. 2017;28(7):497–505. Available from: http://dx.doi.org/10.1016/j.tem.2017.03.003
121. Bakan I, Laplante M. Connecting mTORC1 signaling to SREBP-1 activation. Curr Opin Lipidol. 2012;23(3):226–34.
122. DeBose-Boyd RA, Ye J. SREBPs in Lipid Metabolism, Insulin Signaling, and Beyond. Trends Biochem Sci [Internet]. 2018;43(5):358–68. Available from: http://dx.doi.org/10.1016/j.tibs.2018.01.005
123. DeBose-Boyd RA, Ye J. SREBPs in Lipid Metabolism, Insulin Signaling, and Beyond. Trends Biochem Sci. 2018;43(5):358–68.
124. Galsgaard KD, Pedersen J, Knop FK, Holst JJ, Albrechtsen NJW. Glucagon receptor signaling and lipid metabolism. Front Physiol. 2019;10(APR):1–11.
125. Vasiljević J, Torkko JM, Knoch KP, Solimena M. The making of insulin in health

and disease. Diabetologia. 2020;63(10):1981–9.

126. Lipson KL, Fonseca SG, Ishigaki S, Nguyen LX, Foss E, Bortell R, Rossini AA, Urano F. Regulation of insulin biosynthesis in pancreatic beta cells by an endoplasmic reticulum-resident protein kinase IRE1. Cell Metab. 2006;4(3):245–54.
127. Svendsen B, Larsen O, Gabe MBN, Christiansen CB, Rosenkilde MM, Drucker DJ, Holst JJ. Insulin Secretion Depends on Intra-islet Glucagon Signaling. Cell Rep [Internet]. 2018;25(5):1127-1134.e2. Available from: https://doi.org/10.1016/j.celrep.2018.10.018
128. Dickerson MT, Vierra NC, Milian SC, Dadi PK, Jacobson DA. Osteopontin activates the diabetes-associated potassium channel TALK-1 in pancreatic β- Cells. PLoS One. 2017;12(4):1–21.
129. Henquin JC. Regulation of insulin secretion: A matter of phase control and amplitude modulation. Diabetologia. 2009;52(5):739–51.
130. la Vega-Monroy MLL de, Fernandez-Meji C. Beta-Cell Function and Failure in Type 1 Diabetes. Type 1 Diabetes - Pathog Genet Immunother. 2011;(May 2014).
131. Ämmälä C, Eliasson L, Bokvist K, Berggren PO, Honkanen RE, Sjöholm Å, Rorsman P. Activation of protein kinases and inhibition of protein phosphatases play a central role in the regulation of exocytosis in mouse pancreatic β cells. Proc Natl Acad Sci U S A. 1994;91(10):4343–7.
132. Kang G, Chepurny OG, Malester B, Rindler MJ, Rehmann H, Bos JL, Schwede F, Coetzee WA, Holz GG. cAMP sensor Epac as a determinant of ATP-sensitive potassium channel activity in human pancreatic β cells and rat INS-1 cells. J Physiol. 2006;573(3):595–609.
133. Wan QF, Dong Y, Yang H, Lou X, Ding J, Xu T. Protein kinase activation increases insulin secretion by sensitizing the secretory machinery to Ca2+. J Gen Physiol. 2004;124(6):653–62.
134. Strowski MZ, Parmar RM, Blake AD, Schaeffer JM. Somatostatin inhibits insulin and glucagon secretion via two receptor subtypes: An in vitro study of pancreatic islets from somatostatin receptor 2 knockout mice. Endocrinology. 2000;141(1):111–7.
135. Daunt M, Dale O, Smith PA. Somatostatin inhibits oxidative respiration in pancreatic β-cells. Endocrinology. 2006;147(3):1527–35.
136. Schwetz TA, Ustione A, Piston DW. Neuropeptide Y and somatostatin inhibit insulin

secretion through different mechanisms. Vol. 304, American Journal of Physiology - Endocrinology and Metabolism. 2013.

137. Persaud SJ, Bewick GA. Peptide YY: More than just an appetite regulator. Diabetologia. 2014;57(9):1762–9.
138. Meyer C. Final answer: Ghrelin can suppress insulin secretion in humans, but is it clinically relevant? Diabetes. 2010;59(11):2726–8.
139. Abdalla MMI. Ghrelin - Physiological functions and regulation. Eur Endocrinol. 2015;11(2):90–5.
140. Malaisse W, Malaisse-Lagae F, Wright PH, Ashmore J. Effects of adrenergic and cholinergic agents upon insulin secretion in vitro. Endocrinology. 1967;80(5):975–8.
141. Hamamdzic D, Duzic E, Sherlock JD, Lanier SM. Regulation of α2-adrenergic receptor expression and signaling in pancreatic β-cells. Am J Physiol - Endocrinol Metab. 1995;269(1 32-1).
142. Hampton RF, Jimenez-Gonzalez M, Stanley SA. Unravelling innervation of pancreatic islets. Diabetologia. 2022;65(7):1069–84.
143. Liu M tsai, KIRCHGESSNER AL. Pituitary Adenylate Cyclase Activating Peptide (PACAP) in the Enteropancreatic Innervation. Pancreas. 2001;100(September 2000):91–100.
144. Winzell MS, Ahrén B. Role of VIP and PACAP in islet function. Peptides. 2007;28(9):1805–13.
145. Karlsson S, Sundler F, Ahrén B. Insulin secretion by gastrin-releasing peptide in mice: Ganglionic versus direct islet effect. Am J Physiol - Endocrinol Metab. 1998;274(1 37-1).
146. Pørksen N. The in vivo regulation of pulsatile insulin secretion. Diabetologia. 2002;45(1):3–20.
147. Papazoglou I, Lee JH, Cui Z, Li C, Fulgenzi G, Bahn YJ, Staniszewska-Goraczniak HM, Piñol RA, Hogue IB, Enquist LW, Krashes MJ, Rane SG. A distinct hypothalamus-to-β cell circuit modulates insulin secretion. Cell Metab. 2022;34(2):285-298.e7.
148. Washabau RJ. Integration of Gastrointestinal Function. Canine Feline Gastroenterol. 2012;1–31.
149. Kim JD, Toda C, D'Agostino G, Zeiss CJ, DiLeone RJ, Elsworth JD, Kibbey RG, Chan O, Harvey BK, Richie CT, Savolainen M, Myöhännen T, Jeong JK, Diano S.

Hypothalamic prolyl endopeptidase (PREP) regulates pancreatic insulin and glucagon secretion in mice. Proc Natl Acad Sci U S A. 2014;111(32):11876–81.

150. Deutsch AJ, Ahlqvist E, Udler MS. Phenotypic and genetic classification of diabetes. Diabetologia. 2022;65(11):1758–69.

151. Gouda P, Zheng S, Peters T, Fudim M, Randhawa VK, Ezekowitz J, Mavrakanas TA, Giannetti N, Tsoukas M, Lopes R, Sharma A. Clinical Phenotypes in Patients With Type 2 Diabetes Mellitus: Characteristics, Cardiovascular Outcomes and Treatment Strategies. Curr Heart Fail Rep [Internet]. 2021;18(5):253–63. Available from: https://doi.org/10.1007/s11897-021-00527-w

152. Dysted MP, Esztergályos B, Gautam S, Helman B, Pinkepank M, Randi A, Salim A, Wallis K, Jiménez BY, Ysebaert M. IDF Diabetes Atlas. 10th ed. Boyko EJ, Karuranga DJMS, Piemonte L, Saeedi PRP, Sun H, editors. International Diabetes Federation; 2021. 1–135 p.

153. Ong KL, Stafford LK, McLaughlin SA, Boyko EJ, Vollset SE, Smith AE, Dalton BE, Duprey J, Cruz JA, Hagins H, Lindstedt PA, Aali A, Abate YH, Abate MD, Abbasian M, Abbasi-Kangevari Z, Abbasi-Kangevari M, Abd ElHafeez S, Abd-Rabu R, Abdulah DM, Abdullah AYM, Abedi V, Abidi H, Aboagye RG, Abolhassani H, Abu-Gharbieh E, Abu-Zaid A, Adane TD, Adane DE, Addo IY, Adegboye OA, Adekanmbi V, Adepoju AV, Adnani QES, Afolabi RF, Agarwal G, Aghdam ZB, Agudelo-Botero M, Aguilera Arriagada CE, Agyemang-Duah W, Ahinkorah BO, Ahmad D, Ahmad R, Ahmad S, Ahmad A, Ahmadi A, Ahmadi K, Ahmed A, Ahmed A, Ahmed LA, Ahmed SA, Ajami M, Akinyemi RO, Al Hamad H, Al Hasan SM, AL-Ahdal TMA, Alalwan TA, Al-Aly Z, AlBataineh MT, Alcalde-Rabanal JE, Alemi S, Ali H, Alinia T, Aljunid SM, Almustanyir S, Al-Raddadi RM, Alvis-Guzman N, Amare F, Ameyaw EK, Amiri S, Amusa GA, Andrei CL, Anjana RM, Ansar A, Ansari G, Ansari-Moghaddam A, Anyasodor AE, Arabloo J, Aravkin AY, Areda D, Arifin H, Arkew M, Armocida B, Ärnlöv J, Artamonov AA, Arulappan J, Aruleba RT, Arumugam A, Aryan Z, Asemu MT, Asghari-Jafarabadi M, Askari E, Asmelash D, Astell-Burt T, Athar M, Athari SS, Atout MM d. W, Avila-Burgos L, Awaisu A, Azadnajafabad S, B DB, Babamohamadi H, Badar M, Badawi A, Badiye AD, Baghcheghi N, Bagheri N, Bagherieh S, Bah S, Bahadory S, Bai R, Baig AA, Baltatu OC, Baradaran HR, Barchitta M, Bardhan M, Barengo NC, Bärnighausen TW, Barone MTU, Barone-Adesi F, Barrow A, Bashiri H, Basiru A, Basu S, Basu S, Batiha AMM, Batra K, Bayih MT, Bayileyegn NS, Behnoush AH, Bekele AB, Belete

MA, Belgaumi UI, Belo L, Bennett DA, Bensenor IM, Berhe K, Berhie AY, Bhaskar S, Bhat AN, Bhatti JS, Bikbov B, Bilal F, Bintoro BS, Bitaraf S, Bitra VR, Bjegovic-Mikanovic V, Bodolica V, Boloor A, Brauer M, Brazo-Sayavera J, Brenner H, Butt ZA, Calina D, Campos LA, Campos-Nonato IR, Cao Y, Cao C, Car J, Carvalho M, Castañeda-Orjuela CA, Catalá-López F, Cerin E, Chadwick J, Chandrasekar EK, Chanie GS, Charan J, Chattu VK, Chauhan K, Cheema HA, Chekol Abebe E, Chen S, Cherbuin N, Chichagi F, Chidambaram SB, Cho WCS, Choudhari SG, Chowdhury R, Chowdhury EK, Chu DT, Chukwu IS, Chung SC, Coberly K, Columbus A, Contreras D, Cousin E, Criqui MH, Cruz-Martins N, Cuschieri S, Dabo B, Dadras O, Dai X, Damasceno AAM, Dandona R, Dandona L, Das S, Dascalu AM, Dash NR, Dashti M, Dávila-Cervantes CA, De la Cruz-Góngora V, Debele GR, Delpasand K, Demisse FW, Demissie GD, Deng X, Denova-Gutiérrez E, Deo S V., Dervišević E, Desai HD, Desale AT, Dessie AM, Desta F, Dewan SMR, Dey S, Dhama K, Dhimal M, Diao N, Diaz D, Dinu M, Diress M, Djalalinia S, Doan LP, Dongarwar D, dos Santos Figueiredo FW, Duncan BB, Dutta S, Dziedzic AM, Edinur HA, Ekholuenetale M, Ekundayo TC, Elgendy IY, Elhadi M, El-Huneidi W, Elmeligy OAA, Elmonem MA, Endeshaw D, Esayas HL, Eshetu HB, Etaee F, Fadhil I, Fagbamigbe AF, Fahim A, Falahi S, Faris MAIEM, Farrokhpour H, Farzadfar F, Fatehizadeh A, Fazli G, Feng X, Ferede TY, Fischer F, Flood D, Forouhari A, Foroumadi R, Foroutan Koudehi M, Gaidhane AM, Gaihre S, Gaipov A, Galali Y, Ganesan B, Garcia-Gordillo MA, Gautam RK, Gebrehiwot M, Gebrekidan KG, Gebremeskel TG, Getacher L, Ghadirian F, Ghamari SH, Ghasemi Nour M, Ghassemi F, Golechha M, Goleij P, Golinelli D, Gopalani SV, Guadie HA, Guan SY, Gudayu TW, Guimarães RA, Guled RA, Gupta R, Gupta K, Gupta VB, Gupta VK, Gyawali B, Haddadi R, Hadi NR, Haile TG, Hajibeygi R, Haj-Mirzaian A, Halwani R, Hamidi S, Hankey GJ, Hannan MA, Haque S, Harandi H, Harlianto NI, Hasan SMM, Hasan SS, Hasani H, Hassanipour S, Hassen MB, Haubold J, Hayat K, Heidari G, Heidari M, Hessami K, Hiraike Y, Holla R, Hossain S, Hossain MS, Hosseini MS, Hosseinzadeh M, Hosseinzadeh H, Huang J, Huda MN, Hussain S, Huynh HH, Hwang BF, Ibitoye SE, Ikeda N, Ilic IM, Ilic MD, Inbaraj LR, Iqbal A, Islam SMS, Islam RM, Ismail NE, Iso H, Isola G, Itumalla R, Iwagami M, Iwu CCD, Iyamu IO, Iyasu AN, Jacob L, Jafarzadeh A, Jahrami H, Jain R, Jaja C, Jamalpoor Z, Jamshidi E, Janakiraman B, Jayanna K, Jayapal SK, Jayaram S, Jayawardena R, Jebai R, Jeong W, Jin Y, Jokar M, Jonas JB, Joseph N, Joseph A, Joshua CE,

Joukar F, Jozwiak JJ, Kaambwa B, Kabir A, Kabthymer RH, Kadashetti V, Kahe F, Kalhor R, Kandel H, Karanth SD, Karaye IM, Karkhah S, Katoto PD, Kaur N, Kazemian S, Kebede SA, Khader YS, Khajuria H, Khalaji A, Khan MA, Khan M, Khan A, Khanal S, Khatatbeh MM, Khater AM, Khateri S, khorashadizadeh F, Khubchandani J, Kibret BG, Kim MS, Kimokoti RW, Kisa A, Kivimäki M, Kolahi AA, Komaki S, Kompani F, Koohestani HR, Korzh O, Kostev K, Kothari N, Koyanagi A, Krishan K, Krishnamoorthy Y, Kuate Defo B, Kuddus M, Kuddus MA, Kumar R, Kumar H, Kundu S, Kurniasari MD, Kuttikkattu A, La Vecchia C, Lallukka T, Larijani B, Larsson AO, Latief K, Lawal BK, Le TTT, Le TTB, Lee SWH, Lee M, Lee WC, Lee PH, Lee S woong, Lee SW, Legesse SM, Lenzi J, Li Y, Li MC, Lim SS, Lim LL, Liu X, Liu C, Lo CH, Lopes G, Lorkowski S, Lozano R, Lucchetti G, Maghazachi AA, Mahasha PW, Mahjoub S, Mahmoud MA, Mahmoudi R, Mahmoudimanesh M, Mai AT, Majeed A, Majma Sanaye P, Makris KC, Malhotra K, Malik AA, Malik I, Mallhi TH, Malta DC, Mamun AA, Mansouri B, Marateb HR, Mardi P, Martini S, Martorell M, Marzo RR, Masoudi R, Masoudi S, Mathews E, Maugeri A, Mazzaglia G, Mekonnen T, Meshkat M, Mestrovic T, Miao Jonasson J, Miazgowski T, Michalek IM, Minh LHN, Mini GK, Miranda JJ, Mirfakhraie R, Mirrakhimov EM, Mirza-Aghazadeh-Attari M, Misganaw A, Misgina KH, Mishra M, Moazen B, Mohamed NS, Mohammadi E, Mohammadi M, Mohammadian-Hafshejani A, Mohammadshahi M, Mohseni A, Mojiri-forushani H, Mokdad AH, Momtazmanesh S, Monasta L, Moniruzzaman M, Mons U, Montazeri F, Moodi Ghalibaf AA, Moradi Y, Moradi M, Moradi Sarabi M, Morovatdar N, Morrison SD, Morze J, Mossialos E, Mostafavi E, Mueller UO, Mulita F, Mulita A, Murillo-Zamora E, Musa KI, Mwita JC, Nagaraju SP, Naghavi M, Nainu F, Nair TS, Najmuldeen HHR, Nangia V, Nargus S, Naser AY, Nassereldine H, Natto ZS, Nauman J, Nayak BP, Ndejjo R, Negash H, Negoi RI, Nguyen HTH, Nguyen DH, Nguyen PT, Nguyen VT, Nguyen HQ, Niazi RK, Nigatu YT, Ningrum DNA, Nizam MA, Nnyanzi LA, Noreen M, Noubiap JJ, Nzoputam OJ, Nzoputam CI, Oancea B, Odogwu NM, Odukoya OO, Ojha VA, Okati-Aliabad H, Okekunle AP, Okonji OC, Okwute PG, Olufadewa II, Onwujekwe OE, Ordak M, Ortiz A, Osuagwu UL, Oulhaj A, Owolabi MO, Padron-Monedero A, Padubidri JR, Palladino R, Panagiotakos D, Panda-Jonas S, Pandey A, Pandey A, Pandi-Perumal SR, Pantea Stoian AM, Pardhan S, Parekh T, Parekh U, Pasovic M, Patel J, Patel JR, Paudel U, Pepito VCF, Pereira M, Perico N, Perna S, Petcu IR, Petermann-Rocha FE, Podder V, Postma MJ, Pourali G, Pourtaheri N, Prates

EJS, Qadir MMF, Qattea I, Raee P, Rafique I, Rahimi M, Rahimifard M, Rahimi-Movaghar V, Rahman MO, Rahman MA, Rahman MHU, Rahman M, Rahman MM, Rahmani M, Rahmani S, Rahmanian V, Rahmawaty S, Rahnavard N, Rajbhandari B, Ram P, Ramazanu S, Rana J, Rancic N, Ranjha MMAN, Rao CR, Rapaka D, Rasali DP, Rashedi S, Rashedi V, Rashid AM, Rashidi MM, Ratan ZA, Rawaf S, Rawal L, Redwan EMM, Remuzzi G, Rengasamy KR, Renzaho AMN, Reyes LF, Rezaei N, Rezaei N, Rezaeian M, Rezazadeh H, Riahi SM, Rias YA, Riaz M, Ribeiro D, Rodrigues M, Rodriguez JAB, Roever L, Rohloff P, Roshandel G, Roustazadeh A, Rwegerera GM, Saad AMA, Saber-Ayad MM, Sabour S, Sabzmakan L, Saddik B, Sadeghi E, Saeed U, Saeedi Moghaddam S, Safi S, Safi SZ, Saghazadeh A, Saheb Sharif-Askari N, Saheb Sharif-Askari F, Sahebkar A, Sahoo SS, Sahoo H, Saif-Ur-Rahman KM, Sajid MR, Salahi S, Salahi S, Saleh MA, Salehi MA, Salomon JA, Sanabria J, Sanjeev RK, Sanmarchi F, Santric-Milicevic MM, Sarasmita MA, Sargazi S, Sathian B, Sathish T, Sawhney M, Schlaich MP, Schmidt MI, Schuermans A, Seidu AA, Senthil Kumar N, Sepanlou SG, Sethi Y, Seylani A, Shabany M, Shafaghat T, Shafeghat M, Shafie M, Shah NS, Shahid S, Shaikh MA, Shanawaz M, Shannawaz M, Sharfaei S, Shashamo BB, Shiri R, Shittu A, Shivakumar KM, Shivalli S, Shobeiri P, Shokri F, Shuval K, Sibhat MM, Silva LMLR, Simpson CR, Singh JA, Singh P, Singh S, Siraj MS, Skryabina AA, Sohag AAM, Soleimani H, Solikhah S, Soltani-Zangbar MS, Somayaji R, Sorensen RJD, Starodubova A V., Sujata S, Suleman M, Sun J, Sundström J, Tabarés-Seisdedos R, Tabatabaei SM, Tabatabaeizadeh SA, Tabish M, Taheri M, Taheri E, Taki E, Tamuzi JJL, Tan KK, Tat NY, Taye BT, Temesgen WA, Temsah MH, Tesler R, Thangaraju P, Thankappan KR, Thapa R, Tharwat S, Thomas N, Ticoalu JHV, Tiyuri A, Tonelli M, Tovani-Palone MR, Trico D, Trihandini I, Tripathy JP, Tromans SJ, Tsegay GM, Tualeka AR, Tufa DG, Tyrovolas S, Ullah S, Upadhyay E, Vahabi SM, Govindaraj Vaithinathan A, Valizadeh R, van Daalen KR, Vart P, Varthya SB, Vasankari TJ, Vaziri S, Verma M verma, Verras GI, Vo DC, Wagaye B, Waheed Y, Wang Z, Wang Y, Wang C, Wang F, Wassie GT, Wei MYW, Weldemariam AH, Westerman R, Wickramasinghe ND, Wu YF, Wulandari RD, Xia J, Xiao H, Xu S, Xu X, Yada DY, Yang L, Yatsuya H, Yesiltepe M, Yi S, Yohannis HK, Yonemoto N, You Y, Zaman S Bin, Zamora N, Zare I, Zarea K, Zarrintan A, Zastrozhin MS, Zeru NG, Zhang ZJ, Zhong C, Zhou J, Zielińska M, Zikarg YT, Zodpey S, Zoladl M, Zou Z, Zumla A, Zuniga YMH, Magliano DJ, Murray CJL, Hay SI, Vos T. Global,

regional, and national burden of diabetes from 1990 to 2021, with projections of prevalence to 2050: a systematic analysis for the Global Burden of Disease Study 2021. Lancet. 2023;402(10397):203–34.

154. Magliano DJ, Martin VJ, Owen AJ, Zomer E, Liew D. The Productivity Burden of Diabetes at a Population Level. Diabetes Care. 2018;41(5):979–84.
155. Zajec A, Trebušak Podkrajšek K, Tesovnik T, Šket R, Čugalj Kern B, Jenko Bizjan B, Šmigoc Schweiger D, Battelino T, Kovač J. Pathogenesis of Type 1 Diabetes: Established Facts and New Insights. Genes (Basel). 2022;13(4).
156. Katsarou A, Gudbjörnsdottir S, Rawshani A, Dabelea D, Bonifacio E, Anderson BJ, Jacobsen LM, Schatz DA, Lernmark A. Type 1 diabetes mellitus. Nat Rev Dis Prim [Internet]. 2017;3:1–18. Available from: http://dx.doi.org/10.1038/nrdp.2017.16
157. Artasensi A, Pedretti A, Vistoli G, Fumagalli L. Type 2 diabetes mellitus: A review of multi-target drugs. Molecules [revista en Internet] 2020 [acceso 7 de marzo de 2022]; 25(8): 1-20. 2020;1–20. Available from: https://www.ncbi.nlm.nih.gov/pmc/articles/PMC7221535/
158. Westman EC. Type 2 Diabetes Mellitus: A Pathophysiologic Perspective. Front Nutr. 2021;8(August):1–5.
159. Hansen T. Genetics of type 2 diabetes. Curr Sci. 2002;83(12):1477–82.
160. Goodarzi MO, Lehman DM, Taylor KD, Guo X, Cui J, Quiñones MJ, Clee SM, Yandell BS, Blangero J, Hsueh WA, Attie AD, Stern MP, Rotter JI. SORCS1: A novel human type 2 diabetes susceptibility gene suggested by the mouse. Diabetes. 2007;56(7):1922–9.
161. Li Y, Sun F, Yue TT, Wang FX, Yang CL, Luo JH, Rong SJ, Xiong F, Zhang S, Wang CY. Revisiting the Antigen-Presenting Function of β Cells in T1D Pathogenesis. Front Immunol. 2021;12(July):1–8.
162. Pugliese A. Autoreactive T cells in type 1 diabetes. J Clin Invest. 2017;127(8):2881–91.
163. al. R et. Beta-cell specific autoantibodies: Are they just an indicator of type 1 diabetes? Physiol Behav. 2018;176(5):139–48.
164. Scherm MG, Wyatt RC, Serr I, Anz D, Richardson SJ, Daniel C. Beta cell and immune cell interactions in autoimmune type 1 diabetes: How they meet and talk to each other. Mol Metab [Internet]. 2022;64(August):101565. Available from: https://doi.org/10.1016/j.molmet.2022.101565
165. Newsholme P, Keane K, de Bittencourt PIH, Krause M. The Impact of Inflammation

on Pancreatic β-Cell Metabolism, Function and Failure in T1DM and T2DM: Commonalities and Differences. In: Escher AP, Li A, editors. Type 1 Diabetes [Internet]. InTech; 2013. p. 127–65. Available from: http://www.intechopen.com/books/type-1-diabetes/the-impact-of-inflammation-on-pancreatic-cell-metabolism-function-and-failure-in-t1dm-and-t2dm-commo

166. Zhang JM, An J. Cytokines, Inflammation, and Pain. Int Anesthesiol Clin [Internet]. 2007 Nov 15;45(2):27–37. Available from: https://www.hindawi.com/journals/ecam/2019/3612481/
167. Zhan Y, Carrington EM, Zhang Y, Heinzel S, Lew AM. Life and death of activated T cells: How are they different from naïve T Cells? Front Immunol. 2017;8(DEC):1–9.
168. Rosales C, Uribe-Querol E. Phagocytosis: A Fundamental Process in Immunity. Biomed Res Int. 2017;2017.
169. NORMAN P. T cell-mediated cytotoxicity. In: Immunobiology: The Immune System in Health and Disease [Internet]. 5th ed. New York: Garland Science; 2001. p. 274–274. Available from: https://www.ncbi.nlm.nih.gov/books/NBK27101/
170. Walker LSK, von Herrath M. CD4 T cell differentiation in type 1 diabetes. Clin Exp Immunol. 2016;183(1):16–29.
171. Weitz JR, Jacques-Silva C, Qadir MMF, Umland O, Pereira E, Qureshi F, Tamayo A, Dominguez-Bendala J, Rodriguez-Diaz R, Almaça J, Caicedo A. Secretory functions of macrophages in the human pancreatic islet are regulated by endogenous purinergic signaling. Diabetes. 2020;69(6):1206–18.
172. Weitz JR, Makhmutova M, Almaça J, Stertmann J, Aamodt K, Brissova M, Speier S, Rodriguez-Diaz R, Caicedo A. Mouse pancreatic islet macrophages use locally released ATP to monitor beta cell activity. Diabetologia. 2018;61(1):182–92.
173. Cosentino C, Regazzi R. Crosstalk between macrophages and pancreatic β-cells in islet development, homeostasis and disease. Int J Mol Sci. 2021;22(4):1–16.
174. Espinoza-Jiménez A, Peón AN, Terrazas LI. Alternatively activated macrophages in types 1 and 2 diabetes. Mediators Inflamm. 2012;2012.
175. Hasnain SZ, Prins JB, McGuckin MA. Oxidative and endoplasmic reticulum stress in β-cell dysfunction in diabetes. J Mol Endocrinol. 2016;56(2):R33–54.
176. Shrestha N, De Franco E, Arvan P, Cnop M. Pathological β-Cell Endoplasmic Reticulum Stress in Type 2 Diabetes: Current Evidence. Front Endocrinol (Lausanne). 2021;12(April):1–7.

177. Ghosh R, Colon-Negron K, Papa FR. Endoplasmic reticulum stress, degeneration of pancreatic islet β-cells, and therapeutic modulation of the unfolded protein response in diabetes. Mol Metab [Internet]. 2019;27:S60–8. Available from: https://doi.org/10.1016/j.molmet.2019.06.012
178. Fonseca SG, Gromada J, Urano F. Endoplasmic reticulum stress and pancreatic beta cell death Protein homeostasis in the β cell. Trends Endocrinol Metab. 2012;22(7):266–74.
179. Dhanasekaran DN, Reddy EP. JNK signaling in apoptosis. Oncogene. 2008;27(48):6245–51.
180. Brush MH, Weiser DC, Shenolikar S. Growth arrest and DNA damage-inducible protein GADD34 targets protein phosphatase 1 alpha to the endoplasmic reticulum and promotes dephosphorylation. Mol Cell Biol [Internet]. 2003;23(4):1292–303. Available from: http://scholar.google.com/scholar?hl=en&btnG=Search&q=intitle:Growth+Arrest+and+DNA+Damage-Inducible+Protein+GADD34+Targets+Protein+Phosphatase+1+alpha+to+the+Endoplasmic+Reticulum+and+Promotes+Dephosphorylation+of+the+alpha+Subunit+of+Eukaryotic+Translat
181. Eguchi N, Vaziri ND, Dafoe DC, Ichii H. The role of oxidative stress in pancreatic β cell dysfunction in diabetes. Int J Mol Sci. 2021;22(4):1–18.
182. Newsholme P, Keane KN, Carlessi R, Cruzat V. Oxidative stress pathways in pancreatic β-cells and insulin-sensitive cells and tissues: Importance to cell metabolism, function, and dysfunction. Am J Physiol - Cell Physiol. 2019;317(3):C420–33.
183. Leenders F, Groen N, de Graaf N, Engelse MA, Rabelink TJ, de Koning EJP, Carlotti F. Oxidative Stress Leads to β-Cell Dysfunction Through Loss of β-Cell Identity. Front Immunol. 2021;12(November).
184. Drews G, Krippeit-Drews P, Duïfer M. Oxidative stress and beta-cell dysfunction. Pflugers Arch Eur J Physiol. 2010;460(4):703–18.
185. Kalnytska O, Qvist P, Kunz S, Conrad T, Willnow TE, Schmidt V. SORCS2 activity in pancreatic α-cells safeguards insulin granule formation and release from glucose-stressed β-cells. iScience. 2024;27(1).
186. Glerup S, Olsen D, Vaegter CB, Gustafsen C, Sjoegaard SS, Hermey G, Kjolby M, Molgaard S, Ulrichsen M, Boggild S, Skeldal S, Fjorback AN, Nyengaard JR,

Jacobsen J, Bender D, Bjarkam CR, Sørensen ES, Füchtbauer EM, Eichele G, Madsen P, Willnow TE, Petersen CM, Nykjaer A. SorCS2 regulates dopaminergic wiring and is processed into an apoptotic two-chain receptor in peripheral glia. Neuron. 2014;82(5):1074–87.

187. Jiao Y, Sun Z, Lee T, Fusco FR, Kimble TD, Meade CA, Cuthbertson S, Reiner A. A simple and sensitive antigen retrieval method for free-floating and slide-mounted tissue sections. J Neurosci Methods. 1999;93(2):149–62.
188. McQuin C, Goodman A, Chernyshev V, Kamentsky L, Cimini BA, Karhohs KW, Doan M, Ding L, Rafelski SM, Thirstrup D, Wiegraebe W, Singh S, Becker T, Caicedo JC, Carpenter AE. CellProfiler 3.0: Next-generation image processing for biology. PLoS Biol. 2018;16(7):1–17.
189. Téllez N, Montanya E. Determining Beta Cell Mass, Apoptosis, Proliferation, and Individual Beta Cell Size in Pancreatic Sections. Methods Mol Biol. 2020;2128:313–37.
190. Zhang C, Moriguchi T, Kajihara M, Esaki R, Harada A, Shimohata H, Oishi H, Hamada M, Morito N, Hasegawa K, Kudo T, Engel JD, Yamamoto M, Takahashi S. MafA Is a Key Regulator of Glucose-Stimulated Insulin Secretion. Mol Cell Biol. 2005;25(12):4969–76.
191. Moynihan KA, Grimm AA, Plueger MM, Bernal-Mizrachi E, Ford E, Cras-Méneur C, Permutt MA, Imai SI. Increased dosage of mammalian Sir2 in pancreatic β cells enhances glucose-stimulated insulin secretion in mice. Cell Metab. 2005;2(2):105–17.
192. Speidel D, Salehi A, Obermueller S, Lundquist I, Brose N, Renström E, Rorsman P. CAPS1 and CAPS2 Regulate Stability and Recruitment of Insulin Granules in Mouse Pancreatic β Cells. Cell Metab. 2008;7(1):57–67.
193. Like AA, Chick WL. Studies in the diabetic mutant mouse: II. Electron microscopy of pancreatic islets. Diabetologia. 1970;6(3):216–42.
194. Obermüller S, Calegari F, King A, Lindqvist A, Lundquist I, Salehi A, Francolini M, Rosa P, Rorsman P, Huttner WB, Barg S. Defective secretion of islet hormones in chromogranin-B deficient mice. PLoS One. 2010;5(1).
195. Reichard A, Asosingh K. Best Practices for Preparing a Single Cell Suspension from Solid Tissues for Flow Cytometry. Cytom Part A. 2019;95(2):219–26.
196. Dobin A, Davis CA, Schlesinger F, Drenkow J, Zaleski C, Jha S, Batut P, Chaisson M, Gingeras TR. STAR: Ultrafast universal RNA-seq aligner. Bioinformatics.

2013;29(1):15–21.

197. Jalili V, Afgan E, Gu Q, Clements D, Blankenberg D, Goecks J, Taylor J, Nekrutenko A. The Galaxy platform for accessible, reproducible and collaborative biomedical analyses: 2020 update. Nucleic Acids Res. 2021;48(W1):W395–402.
198. Lun ATL, Riesenfeld S, Andrews T, Dao TP, Gomes T, Marioni JC. EmptyDrops: Distinguishing cells from empty droplets in droplet-based single-cell RNA sequencing data. Genome Biol. 2019;20(1):1–9.
199. Gardeux V, David FPA, Shajkofci A, Schwalie PC, Deplancke B. ASAP: A web-based platform for the analysis and interactive visualization of single-cell RNA-seq data. Bioinformatics. 2017;33(19):3123–5.
200. Hao Y, Hao S, Andersen-Nissen E, Mauck WM, Zheng S, Butler A, Lee MJ, Wilk AJ, Darby C, Zager M, Hoffman P, Stoeckius M, Papalexi E, Mimitou EP, Jain J, Srivastava A, Stuart T, Fleming LM, Yeung B, Rogers AJ, McElrath JM, Blish CA, Gottardo R, Smibert P, Satija R. Integrated analysis of multimodal single-cell data. Cell [Internet]. 2021;184(13):3573-3587.e29. Available from: https://doi.org/10.1016/j.cell.2021.04.048
201. McInnes L, Healy J, Melville J. UMAP: Uniform Manifold Approximation and Projection for Dimension Reduction. 2018; Available from: http://arxiv.org/abs/1802.03426
202. Waltman L, Van Eck NJ. A smart local moving algorithm for large-scale modularity-based community detection. Eur Phys J B. 2013;86(11).
203. Ritchie ME, Phipson B, Wu D, Hu Y, Law CW, Shi W, Smyth GK. limma powers differential expression analyses for RNA-sequencing and microarray studies. Nucleic Acids Res [Internet]. 2015 Apr 20;43(7):e47–e47. Available from: http://academic.oup.com/nar/article/43/7/e47/2414268/limma-powers-differential-expression-analyses-for
204. Finak G, McDavid A, Yajima M, Deng J, Gersuk V, Shalek AK, Slichter CK, Miller HW, McElrath MJ, Prlic M, Linsley PS, Gottardo R. MAST: A flexible statistical framework for assessing transcriptional changes and characterizing heterogeneity in single-cell RNA sequencing data. Genome Biol. 2015;16(1):1–13.
205. Evans C, Hardin J, Stoebel DM. Selecting between-sample RNA-Seq normalization methods from the perspective of their assumptions. Brief Bioinform. 2018;19(5):776–92.
206. Robinson MD, Oshlack A. A scaling normalization method for differential

expression analysis of RNA-seq data. Genome Biol [Internet]. 2010;11(3):1–9. Available from: http://genomebiology.com/2010/11/3/R25

207. Smyth GK. Linear models and empirical bayes methods for assessing differential expression in microarray experiments. Stat Appl Genet Mol Biol. 2004;3(1).
208. Yu G, Wang LG, Han Y, He QY. ClusterProfiler: An R package for comparing biological themes among gene clusters. Omi A J Integr Biol. 2012;16(5):284–7.
209. Wu T, Hu E, Xu S, Chen M, Guo P, Dai Z, Feng T, Zhou L, Tang W, Zhan L, Fu X, Liu S, Bo X, Yu G. clusterProfiler 4.0: A universal enrichment tool for interpreting omics data. Innovation [Internet]. 2021;2(3):100141. Available from: http://dx.doi.org/10.1016/j.xinn.2021.100141
210. Gentleman RC, Carey VJ, Bates DM, Bolstad B, Dettling M, Dudoit S, Ellis B, Gautier L, Ge Y, Gentry J, Hornik K, Hothorn T, Huber W, Iacus S, Irizarry R, Leisch F, Li C, Maechler M, Rossini AJ, Sawitzki G, Smith C, Smyth G, Tierney L, Yang JYH, Zhang J. Bioconductor: open software development for computational biology and bioinformatics. Genome Biol. 2004;5(10).
211. Subramanian A, Tamayo P, Mootha VK, Mukherjee S, Ebert BL, Gillette MA, Paulovich A, Pomeroy SL, Golub TR, Lander ES, Mesirov JP. Gene set enrichment analysis: A knowledge-based approach for interpreting genome-wide expression profiles. Proc Natl Acad Sci U S A. 2005;102(43):15545–50.
212. Chicco D, Agapito G. Nine quick tips for pathway enrichment analysis. PLoS Comput Biol [Internet]. 2022;18(8):1–15. Available from: http://dx.doi.org/10.1371/journal.pcbi.1010348
213. Bouskila M, Hirshman MF, Jensen J, Goodyear LJ, Sakamoto K. Insulin promotes glycogen synthesis in the absence of GSK3 phosphorylation in skeletal muscle. Vol. 294, American Journal of Physiology - Endocrinology and Metabolism. 2008.
214. Hatting M, Tavares CDJ, Sharabi K, Rines AK, Puigserver P. Insulin regulation of gluconeogenesis. Ann N Y Acad Sci. 2018;1411(1):21–35.
215. Dimitriadis G, Mitron P, Lambadiari V, Maratou E, Raptis SA. Insulin effects in muscle and adipose tissue. Diabetes Res Clin Pract. 2011;93(SUPPL. 1):52–9.
216. Leavens KF, Birnbaum MJ. Insulin signaling to hepatic lipid metabolism in health and disease. Crit Rev Biochem Mol Biol. 2011;46(3):200–15.
217. Xiao X, Luo Y, Peng D. Updated Understanding of the Crosstalk Between Glucose/Insulin and Cholesterol Metabolism. Front Cardiovasc Med. 2022;9(April):1–11.

218. Hayashi Y. Glucagon regulates lipolysis and fatty acid oxidation through inositol triphosphate receptor 1 in the liver. J Diabetes Investig. 2021;12(1):32–4.
219. Segerstolpe Å, Palasantza A, Eliasson P, Andersson EM, Andréasson AC, Sun X, Picelli S, Sabirsh A, Clausen M, Bjursell MK, Smith DM, Kasper M, Ämmälä C, Sandberg R. Single-Cell Transcriptome Profiling of Human Pancreatic Islets in Health and Type 2 Diabetes. Cell Metab. 2016;24(4):593–607.
220. Lawlor N, George J, Bolisetty M, Kursawe R, Sun L, Sivakamasundari V, Kycia I, Robson P, Stitzel ML. Single-cell transcriptomes identify human islet cell signatures and reveal cell-type-specific expression changes in type 2 diabetes. Genome Res. 2017;27(2):208–22.
221. Balboa D, Barsby T, Lithovius V, Saarimäki-vire J, Omar-hmeadi M, Dyachok O, Montaser H, Lund P eric, Yang M, Ibrahim H, Näätänen A, Chandra V, Vihinen H, Jokitalo E, Kvist J, Ustinov J, Nieminen AI, Kuuluvainen E, Hietakangas V, Katajisto P, Lau J, Carlsson P ola, Barg S, Tengholm A. Functional, metabolic and transcriptional maturation of human pancreatic islets derived from stem cells. Nat Biotechnol. 2022;40(July):1042–55.
222. Schaum N, Karkanias J, Neff NF, May AP, Quake SR, Wyss-Coray T, Darmanis S, Batson J, Botvinnik O, Chen MB, Chen S, Green F, Jones RC, Maynard A, Penland L, Pisco AO, Sit R V., Stanley GM, Webber JT, Zanini F, Baghel AS, Bakerman I, Bansal I, Berdnik D, Bilen B, Brownfield D, Cain C, Cho M, Cirolia G, Conley SD, Demers A, Demir K, de Morree A, Divita T, du Bois H, Dulgeroff LBT, Ebadi H, Espinoza FH, Fish M, Gan Q, George BM, Gillich A, Genetiano G, Gu X, Gulati GS, Hang Y, Hosseinzadeh S, Huang A, Iram T, Isobe T, Ives F, Kao KS, Karnam G, Kershner AM, Kiss BM, Kong W, Kumar ME, Lam JY, Lee DP, Lee SE, Li G, Li Q, Liu L, Lo A, Lu WJ, Manjunath A, May KL, May OL, McKay M, Metzger RJ, Mignardi M, Min D, Nabhan AN, Ng KM, Noh J, Patkar R, Peng WC, Puccinelli R, Rulifson EJ, Sikandar SS, Sinha R, Szade K, Tan W, Tato C, Tellez K, Travaglini KJ, Tropini C, Waldburger L, van Weele LJ, Wosczyna MN, Xiang J, Xue S, Youngyunpipatkul J, Zardeneta ME, Zhang F, Zhou L, Castro P, Croote D, DeRisi JL, Kuo CS, Lehallier B, Nguyen PK, Tan SY, Wang BM, Yousef H, Beachy PA, Chan CKF, Huang KC, Weinberg K, Wu SM, Barres BA, Clarke MF, Kim SK, Krasnow MA, Nusse R, Rando TA, Sonnenburg J, Weissman IL. Single-cell transcriptomics of 20 mouse organs creates a Tabula Muris. Nature. 2018;562(7727):367–72.
223. Hrovatin K, Bastidas-ponce A, Bakhti M, Zappia L, Büttner M. Delineating mouse β

-cell identity during lifetime and in diabetes with a single cell atlas. 2022;1–69.

224. Vogel C, Marcotte EM. Insights into the regulation of protein abundance from proteomic and transcriptomic analyses. Nat Rev Genet. 2012;13(4):227–32.
225. Bensellam M, Shi YC, Chan JY, Laybutt DR, Chae H, Abou-Samra M, Pappas EG, Thomas HE, Gilon P, Jonas JC. Metallothionein 1 negatively regulates glucose-stimulated insulin secretion and is differentially expressed in conditions of beta cell compensation and failure in mice and humans. Diabetologia. 2019;62(12):2273–86.
226. Caumo A, Luzi L. First-phase insulin secretion: Does it exist in real life? Considerations on shape and function. Am J Physiol - Endocrinol Metab. 2004;287(3 50-3):371–85.
227. Rorsman P, Eliasson L, Renström E, Gromada J, Barg S, Göpel S. The cell physiology of biphasic insulin secretion. News Physiol Sci. 2000;15(2):72–7.
228. Huang M, Joseph JW. Assessment of the metabolic pathways associated with glucose-stimulated biphasic insulin secretion. Endocrinology. 2014;155(5):1653–66.
229. Cobelli C, Pacini G. Insulin secretion and hepatic extraction in humans by minimal modeling of C-peptide and insulin kinetics. Diabetes. 1988;37(2):223–31.
230. Leighton E, Sainsbury CA, Jones GC. A Practical Review of C-Peptide Testing in Diabetes. Vol. 8, Diabetes Therapy. 2017. p. 475–87.
231. Thorens B. Brain glucose sensing and neural regulation of insulin and glucagon secretion. Diabetes, Obes Metab. 2011;13(SUPPL. 1):82–8.
232. Grunberger G, Sima AAF. The C-peptide signaling. Exp Diabesity Res. 2004;5(1):25–36.
233. VEJRAZKOVA D, VANKOVA M, LUKASOVA P, VCELAK J, BENDLOVA B. Insights Into the Physiology of C-peptide. Physiol Res. 2020;69:S237–43.
234. Luppi P, Drain P. C-peptide antioxidant adaptive pathways in β cells and diabetes. J Intern Med. 2017;281(1):7–24.
235. Belz M, Willenborg M, Görgler N, Hamada A, Schumacher K, Rustenbeck I. Insulinotropic effect of high potassium concentration beyond plasma membrane depolarization. Am J Physiol - Endocrinol Metab. 2014;306(6):697–706.
236. Brüning D, Reckers K, Drain P, Rustenbeck I. Glucose but not KCL diminishes submembrane granule turnover in mouse beta-cells. J Mol Endocrinol. 2017;59(3):311–24.

237. Seino S, Takahashi H, Fujimoto W, Shibasaki T. Roles of cAMP signalling in insulin granule exocytosis. Diabetes, Obes Metab. 2009;11(SUPPL. 4):180–8.
238. Hatlapatka K, Willenborg M, Rustenbeck I. Plasma membrane depolarization as a determinant of the first phase of insulin secretion. Am J Physiol - Endocrinol Metab. 2009;297(2):315–22.
239. Halban P, Renold AE, Perrelet A. Insulin, not C-peptide (proinsulin), is present in crinophagic bodies of the pancreatic B-cell. J Cell Biol. 1984;98(1):222–8.
240. Song G, Pacini G, Ahrén B, D'Argenio DZ. Glucagon increases insulin levels by stimulating insulin secretion without effect on insulin clearance in mice. Peptides [Internet]. 2017 Feb;88(12):74–9. Available from: https://linkinghub.elsevier.com/retrieve/pii/S0196978116302583
241. Patel YC, Liu JL, Galanopoulou A, Papachristou DN. Production, Action, and Degradation of Somatostatin. Compr Physiol. 2011;
242. Theodoropoulou M, Stalla GK. Somatostatin receptors: From signaling to clinical practice. Front Neuroendocrinol [Internet]. 2013;34(3):228–52. Available from: http://dx.doi.org/10.1016/j.yfrne.2013.07.005
243. June Chunqiu Hou, Le Min and JEP. Insulin Granule Biogenesis, Trafficking and Exocytosis June. NIH Public Access Author Manuscr. 2009;6729(1):1–7.
244. Nam D, Mantell J, Bull D, Verkade P, Achim A. A novel framework for segmentation of secretory granules in electron micrographs. Med Image Anal [Internet]. 2014;18(2):411–24. Available from: http://dx.doi.org/10.1016/j.media.2013.12.008
245. Asai S, Moravcová J, Žáková L, Selicharová I, Hadravová R, Brzozowski AM, Nováček J, Jiráček J. Characterization of insulin crystalline form in isolated β-cell secretory granules. Open Biol. 2022;12(12).
246. Smith GD, Swenson DC, Dodson EJ, Reynolds CD. Structural stability in the 4-zinc human insulin hexamer. Proc Natl Acad Sci U S A. 1984;81(22 I):7093–7.
247. Dodson, E.J. (Department of Chemistry University of York), Dodson GG (Department of CU of Y, Reynolds CD (Department of CU of Y, Vallely, D. (Department of Chemistry, York) U of. A COMPARISON BETWEEN THE INSULIN MOLECULES IN 2-ZINC AND 4-ZINC INSULIN CRYSTALS. Walter Gruyter Co. 1980;
248. Mohanasundaram D, Drogemuller C, Brealey J, Jessup CF, Milner C, Murgia C, Lang CJ, Milton A, Zalewski PD, Russ GR, Coates PT. Ultrastructural analysis, zinc transporters, glucose transporters and hormones expression in new world primate

(Callithrix jacchus) and human pancreatic islets. Gen Comp Endocrinol. 2011;174(2):71–9.

249. Dufurrena Q, Bäck N, Mains R, Hodgson L, Tanowitz H, Mandela P, Eipper B, Kuliawat R. Kalirin/Trio Rho GDP/GTP exchange factors regulate proinsulin and insulin secretion. J Mol Endocrinol. 2019;62(1):47–65.
250. Leapman R, Aronova M, Rao A, McBride E, Zhang G, Xu H, Notkins A, Cai T. Maturation Times of Pancreatic Beta Cell Secretory Granules Estimated from Serial Block-Face Electron Microscopy. Microsc Microanal. 2019;25(S2):1380–1.
251. Marchetti P, Bugliani M, De Tata VD, Suleiman M, Marselli L. Pancreatic beta cell identity in humans and the role of type 2 diabetes. Front Cell Dev Biol. 2017;5(MAY):1–8.
252. Karacay C, Prietl B, Harer C, Ehall B, Haudum CW, Bounab K, Franz J, Eisenberg T, Madeo F, Kolb D, Hingerl K, Hausl M, Magnes C, Mautner SI, Kotzbeck P, Pieber TR. The effect of spermidine on autoimmunity and beta cell function in NOD mice. Sci Rep [Internet]. 2022;12(1):1–15. Available from: https://doi.org/10.1038/s41598-022-08168-2
253. MacDonald PE, Salapatek AMF, Wheeler MB. Glucagon-like peptide-1 receptor activation antagonizes voltage-dependent repolarizing K+ currents in β-cells: A possible glucose-dependent insulinotropic mechanism. Diabetes. 2002;51(SUPPL. 3):443–7.
254. MacDonald PE, El-kholy W, Riedel MJ, Salapatek AMF, Light PE, Wheeler MB. The multiple actions of GLP-1 on the process of glucose-stimulated insulin secretion. Diabetes. 2002;51(SUPPL. 3).
255. Perez-Frances M, van Gurp L, Abate MV, Cigliola V, Furuyama K, Bru-Tari E, Oropeza D, Carreaux T, Fujitani Y, Thorel F, Herrera PL. Pancreatic Ppy-expressing γ-cells display mixed phenotypic traits and the adaptive plasticity to engage insulin production. Nat Commun [Internet]. 2021;12(1):1–16. Available from: http://dx.doi.org/10.1038/s41467-021-24788-0
256. Rabiee A, Galiatsatos P, Salas-Carrillo R, Thompson MJ, Andersen DK, Elahi D. Pancreatic polypeptide administration enhances insulin sensitivity and reduces the insnlin requirement of patients on insulin pump therapy. J Diabetes Sci Technol. 2011;5(6):1521–8.
257. Seymour NE, Volpert AR, Andersen DK. Regulation of hepatic insulin receptors by pancreatic polypeptide in fasting and feeding. J Surg Res. 1996;65(1):1–4.

258. Kaiser J, Krippeit-Drews P, Drews G. Acyl-Ghrelin Influences Pancreatic β-Cell Function by Interference with KATP Channels. Diabetes. 2021;70(2):423–35.
259. Evelina Sjöstedt, Wen Zhong, Linn Fagerberg, Max Karlsson, Nicholas Mitsios, Csaba Adori, Per Oksvold, Fredrik Edfors, Agnieszka Limiszewska, Feria Hikmet, Jinrong Huang, Yutao Du, Lin Lin, Zhanying Dong, Ling Yang, Xin Liu, Hui Jiang, Xun Xu, Jian Wang, JM. An atlas of the protein-coding genes in the human, pig, and mouse brain. Science (80-). 2020;367(6482).
260. Frankish HM, Dryden S, Hopkins D, Wang Q, Williams G. Neuropeptide Y, the hypothalamus, and diabetes: Insights into the central control of metabolism. Peptides. 1995;16(4):757–71.
261. Karlsson M, Zhang C, Méar L, Zhong W, Digre A, Katona B, Sjöstedt E, Butler L, Odeberg J, Dusart P, Edfors F, Oksvold P, von Feilitzen K, Zwahlen M, Arif M, Altay O, Li X, Ozcan M, Mardonoglu A, Fagerberg L, Mulder J, Luo Y, Ponten F, Uhlén M, Lindskog C. A single–cell type transcriptomics map of human tissues. Sci Adv. 2021;7(31):1–10.
262. Stein DT, Stevenson BE, Chester MW, Basit M, Daniels MB, Turley SD, McGarry JD. The insulinotropic potency of fatty acids is influenced profoundly by their chain length and degree of saturation. J Clin Invest. 1997;100(2):398–403.
263. Prentki M, Matschinsky FM, Madiraju SRM. Metabolic signaling in fuel-induced insulin secretion. Cell Metab [Internet]. 2013;18(2):162–85. Available from: http://dx.doi.org/10.1016/j.cmet.2013.05.018
264. Cen J, Sargsyan E, Bergsten P. Fatty acids stimulate insulin secretion from human pancreatic islets at fasting glucose concentrations via mitochondria-dependent and -independent mechanisms. Nutr Metab [Internet]. 2016;13(1):1–9. Available from: http://dx.doi.org/10.1186/s12986-016-0119-5
265. Imai Y, Cousins RS, Liu S, Phelps BM, Promes JA. Connecting pancreatic islet lipid metabolism with insulin secretion and the development of type 2 diabetes. Ann N Y Acad Sci. 2020;1461(1):53–72.
266. Roduit R, Nolan C, Alarcon C, Moore P, Barbeau A, Delghingaro-Augusto V, Przybykowski E, Morin J, Massé F, Massie B, Ruderman N, Rhodes C, Poitout V, Prentki M. A Role for the Malonyl-CoA/Long-Chain Acyl-CoA Pathway of Lipid Signaling in the Regulation of Insulin Secretion in Response to Both Fuel and Nonfuel Stimuli. Diabetes. 2004;53(4):1007–19.
267. Poitout V, Robertson RP. Glucolipotoxicity: Fuel excess and β-cell dysfunction.

Endocr Rev. 2008;29(3):351–66.

268. Berthault C, Staels W, Scharfmann R. Purification of pancreatic endocrine subsets reveals increased iron metabolism in beta cells. Mol Metab [Internet]. 2020;42:101060. Available from: https://doi.org/10.1016/j.molmet.2020.101060
269. Hwang B, Lee JH, Bang D. Single-cell RNA sequencing technologies and bioinformatics pipelines. Exp Mol Med [Internet]. 2018;50(8):1–14. Available from: http://dx.doi.org/10.1038/s12276-018-0071-8
270. Piñeros AR, Gao H, Wu W, Liu Y, Tersey SA, Mirmira RG. Single-cell transcriptional profiling of mouse islets following short-term obesogenic dietary intervention. Metabolites. 2020;10(12):1–12.
271. Tritschler S, Theis FJ, Lickert H, Böttcher A. Systematic single-cell analysis provides new insights into heterogeneity and plasticity of the pancreas. Mol Metab [Internet]. 2017;6(9):974–90. Available from: http://dx.doi.org/10.1016/j.molmet.2017.06.021
272. García-Piñeres AJ, Hildesheim A, Williams M, Trivett M, Strobl S, Pinto LA. DNAse treatment following thawing of Cryopreserved PBMC is a procedure suitable for lymphocyte functional studies. J Immunol Methods. 2006;313(1–2):209–13.
273. Zafar H, Li J, David GA, Coller BS. Inverse Effects of EDTA on αIIbβ3-Mediated Adhesion to Immobilized Fibrinogen Versus the D98 Plasmin Fragment of Fibrinogen. Blood [Internet]. 2015;126(23):1036–1036. Available from: http://dx.doi.org/10.1182/blood.V126.23.1036.1036
274. Garnotel R, Rittié L, Poitevin S, Monboisse JC, Nguyen P, Potron G, Maquart FX, Randoux A, Gillery P. Human Blood Monocytes Interact with Type I Collagen Through αxβ2 Integrin (CD11c-CD18, gp150-95). J Immunol. 2000;164(11):5928–34.
275. Maria Doyle, Belinda Phipson HD. RNA-Seq reads to counts. Galaxy Training Materials. 2023.
276. Hiltemann S, Rasche H, Gladman S, Hotz HR, Larivière D, Blankenberg D, Jagtap PD, Wollmann T, Bretaudeau A, Goué N, Griffin TJ, Royaux C, Bras Y Le, Mehta S, Syme A, Coppens F, Droesbeke B, Soranzo N, Bacon W, Psomopoulos F, Gallardo-Alba C, Davis J, Föll MC, Fahrner M, Doyle MA, Serrano-Solano B, Fouilloux AC, van Heusden P, Maier W, Clements D, Heyl F, Grüning B, Batut B. Galaxy Training: A powerful framework for teaching! PLoS Comput Biol. 2023;19(1):1–18.

277. Joachim Wolff, Bérénice Batut HR. Mapping [Internet]. Galaxy Training Materials. 2023. Available from: https://training.galaxyproject.org/training-material/topics/sequence-analysis/tutorials/mapping/tutorial.html
278. Batut B, Hiltemann S, Bagnacani A, Baker D, Bhardwaj V, Blank C, Bretaudeau A, Brillet-Guéguen L, Čech M, Chilton J, Clements D, Doppelt-Azeroual O, Erxleben A, Freeberg MA, Gladman S, Hoogstrate Y, Hotz HR, Houwaart T, Jagtap P, Larivière D, Le Corguillé G, Manke T, Mareuil F, Ramírez F, Ryan D, Sigloch FC, Soranzo N, Wolff J, Videm P, Wolfien M, Wubuli A, Yusuf D, Taylor J, Backofen R, Nekrutenko A, Grüning B. Community-Driven Data Analysis Training for Biology. Cell Syst. 2018;6(6):752-758.e1.
279. McInnes L, Healy J, Saul N, Großberger L. UMAP: Uniform Manifold Approximation and Projection. J Open Source Softw. 2018;3(29):861.
280. Patterson-Cross RB, Levine AJ, Menon V. Selecting single cell clustering parameter values using subsampling-based robustness metrics. BMC Bioinformatics [Internet]. 2021;22(1):1–13. Available from: https://doi.org/10.1186/s12859-021-03957-4
281. Shiao MS, Liao BY, Long M, Yu HT. Adaptive evolution of the insulin two-gene system in mouse. Genetics. 2008;178(3):1683–91.
282. Babaya N, Nakayama M, Moriyama H, Gianani R, Still T, Miao D, Yu L, Hutton JC, Eisenbarth GS. A new model of insulin-deficient diabetes: Male NOD mice with a single copy of Ins1 and no Ins2. Diabetologia. 2006;49(6):1222–8.
283. Bearrows SC, Bauchle CJ, Becker M, Haldeman JM, Swaminathan S, Stephens SB. Chromogranin B regulates early-stage insulin granule trafficking from the Golgi in pancreatic islet β-cells. J Cell Sci. 2019;132(13).
284. Wollam J, Mahata S, Riopel M, Hernandez-Carretero A, Biswas A, Bandyopadhyay GK, Chi NW, Eiden LE, Mahapatra NR, Corti A, Webster NJG, Mahata SK. Chromogranin A regulates vesicle storage and mitochondrial dynamics to influence insulin secretion. Cell Tissue Res. 2017;368(3):487–501.
285. Su Y, Jono H, Misumi Y, Senokuchi T, Guo J, Ueda M, Shinriki S, Tasaki M, Shono M, Obayashi K, Yamagata K, Araki E, Ando Y. Novel function of transthyretin in pancreatic alpha cells. FEBS Lett. 2012;586(23):4215–22.
286. Talchai C, Xuan S, Lin H V., Sussel L, Accili D. Pancreatic β cell dedifferentiation as a mechanism of diabetic β cell failure. Cell. 2012;150(6):1223–34.
287. van der Meulen T, Mawla AM, DiGruccio MR, Adams MW, Nies V, Dólleman S, Liu

S, Ackermann AM, Cáceres E, Hunter AE, Kaestner KH, Donaldson CJ, Huising MO. Virgin Beta Cells Persist throughout Life at a Neogenic Niche within Pancreatic Islets. Cell Metab. 2017;25(4):911-926.e6.

288. Landsman L, Parent A, Hebrok M. Elevated Hedgehog/Gli signaling causes β-cell dedifferentiation in mice. Proc Natl Acad Sci U S A. 2011;108(41):17010–5.
289. Dorrell C, Schug J, Canaday PS, Russ HA, Tarlow BD, Grompe MT, Horton T, Hebrok M, Streeter PR, Kaestner KH, Grompe M. Human islets contain four distinct subtypes of β cells. Nat Commun [Internet]. 2016;7:1–9. Available from: http://dx.doi.org/10.1038/ncomms11756
290. Johnston NR, Mitchell RK, Haythorne E, Pessoa MP, Semplici F, Ferrer J, Piemonti L, Marchetti P, Bugliani M, Bosco D, Berishvili E, Duncanson P, Watkinson M, Broichhagen J, Trauner D, Rutter GA, Hodson DJ. Beta Cell Hubs Dictate Pancreatic Islet Responses to Glucose. Cell Metab [Internet]. 2016;24(3):389–401. Available from: http://dx.doi.org/10.1016/j.cmet.2016.06.020
291. Dror E, Fagnocchi L, Wegert V, Apostle S, Grimaldi B, Gruber T, Panzeri I, Heyne S, Höffler KD, Kreiner V, Ching R, Tsai-Hsiu Lu T, Semwal A, Johnson B, Senapati P, Lempradl A, Schones D, Imhof A, Shen H, Pospisilik JA. Epigenetic dosage identifies two major and functionally distinct β cell subtypes. Cell Metab. 2023;35(5):821-836.e7.
292. Benninger RKP, Hodson DJ. New understanding of β-cell heterogeneity and in situ islet function. Diabetes. 2018;67(4):537–47.
293. Bader E, Migliorini A, Gegg M, Moruzzi N, Gerdes J, Roscioni SS, Bakhti M, Brandl E, Irmler M, Beckers J, Aichler M, Feuchtinger A, Leitzinger C, Zischka H, Sattler RW, Jastroch M, Tschöp M, Machicao F, Staiger H, Häring HU, Chmelova H, Chouinard JA, Oskolkov N, Korsgren O, Speier S, Lickert H. Identification of proliferative and mature β-cells in the islets of langerhans. Nature [Internet]. 2016;535(7612):430–4. Available from: http://dx.doi.org/10.1038/nature18624
294. Liu JSE, Hebrok M. All mixed up: Defining roles for β-cell subtypes in mature islets. Genes Dev. 2017;31(3):228–40.
295. Bensellam M, Jonas JC, Laybutt DR. Mechanisms of β-cell dedifferentiation in diabetes: Recent findings and future research directions. J Endocrinol. 2018;236(2):R109–43.
296. Aigha II, Abdelalim EM. NKX6.1 transcription factor: a crucial regulator of pancreatic β cell development, identity, and proliferation. Stem Cell Res Ther.

2020;11(1):1–14.

297. Casteels T, Zhang Y, Frogne T, Sturtzel C, Lardeau CH, Sen I, Liu X, Hong S, Pauler FM, Penz T, Brandstetter M, Barbieux C, Berishvili E, Heuser T, Bock C, Riedel CG, Meyer D, Distel M, Hecksher-Sørensen J, Li J, Kubicek S. An inhibitor-mediated beta-cell dedifferentiation model reveals distinct roles for FoxO1 in glucagon repression and insulin maturation. Mol Metab [Internet]. 2021;54(August):101329. Available from: https://doi.org/10.1016/j.molmet.2021.101329
298. Matsuoka TA, Kawashima S, Miyatsuka T, Sasaki S, Shimo N, Katakami N, Kawamori D, Takebe S, Herrera PL, Kaneto H, Stein R, Shimomura I. Mafa enables Pdx1 to effectively convert pancreatic islet progenitors and committed islet α-cells into β-cells in vivo. Diabetes. 2017;66(5):1293–300.
299. Aldous N, Moin ASM, Abdelalim EM. Pancreatic β-cell heterogeneity in adult human islets and stem cell-derived islets. Cell Mol Life Sci [Internet]. 2023;80(6):1–25. Available from: https://doi.org/10.1007/s00018-023-04815-7
300. Rahim M, Nakhe AY, Banerjee DR, Overway EM, Bosma KJ, Rosch JC, Oeser JK, Wang B, Lippmann ES, Jacobson DA, O'Brien RM, Young JD. Glucose-6-phosphatase catalytic subunit 2 negatively regulates glucose oxidation and insulin secretion in pancreatic β-cells. J Biol Chem [Internet]. 2022;298(4):101729. Available from: https://doi.org/10.1016/j.jbc.2022.101729
301. Matschinsky FM, Wilson DF. The central role of glucokinase in glucose homeostasis: A perspective 50 years after demonstrating the presence of the enzyme in islets of Langerhans. Front Physiol. 2019;10(MAR).
302. Ramzy A, Asadi A, Kieffer TJ. Revisiting proinsulin processing: Evidence that human β-cells process proinsulin with prohormone convertase (pc) 1/3 but not pc2. Diabetes. 2020;69(7):1451–62.
303. Li J, Mao Z, Huang J, Xiaa J. PICK1 is essential for insulin production and the maintenance of glucose homeostasis. Mol Biol Cell. 2018;29(5):587–96.
304. Finak G, McDavid A, Yajima M, Deng J, Gersuk V, Shalek AK, Slichter CK, Miller HW, McElrath MJ, Prlic M, Linsley PS, Gottardo R. MAST: A flexible statistical framework for assessing transcriptional changes and characterizing heterogeneity in single-cell RNA sequencing data. Genome Biol [Internet]. 2015;16(1):1–13. Available from: http://dx.doi.org/10.1186/s13059-015-0844-5
305. Talchai C, Xuan S, Lin H V., Sussel L, Accili D. Pancreatic β Cell Dedifferentiation

as a Mechanism of Diabetic β Cell Failure. Cell [Internet]. 2012 Sep;150(6):1223–34. Available from: https://linkinghub.elsevier.com/retrieve/pii/S0092867412009403

306. Dor Y. B-Cell Proliferation Is the Major Source of New Pancreatic B Cells. Nat Clin Pract Endocrinol Metab. 2006;2(5):242–3.
307. Chen CW, Guan BJ, Alzahrani MR, Gao Z, Gao L, Bracey S, Wu J, Mbow CA, Jobava R, Haataja L, Zalavadia AH, Schaffer AE, Lee H, LaFramboise T, Bederman I, Arvan P, Mathews CE, Gerling IC, Kaestner KH, Tirosh B, Engin F, Hatzoglou M. Adaptation to chronic ER stress enforces pancreatic β-cell plasticity. Nat Commun. 2022;13(1):1–18.
308. Fang J, Liu M, Zhang X, Sakamoto T, Taatjes DJ, Jena BP, Sun F, Woods J, Bryson T, Kowluru A, Zhang K, Chen X. COPII-dependent ER export: A critical component of insulin biogenesis and β-cell ER homeostasis. Mol Endocrinol. 2015;29(8):1156–69.
309. Santofimia-Castaño P, Lan W, Bintz J, Gayet O, Carrier A, Lomberk G, Neira JL, González A, Urrutia R, Soubeyran P, Iovanna J. Inactivation of NUPR1 promotes cell death by coupling ER-stress responses with necrosis. Sci Rep. 2018;8(1):1–16.
310. Danilova T, Lindahl M. Emerging roles for mesencephalic astrocyte-derived neurotrophic factor (MANF) in pancreatic beta cells and diabetes. Front Physiol. 2018;9(OCT):1–21.
311. Fatrai S, Elghazi L, Balcazar N, Cras-me C, Krits I, Kiyokawa H, Bernal-mizrachi E. Akt Induces Beta-Cell Proliferation by Regulating Cyclin D1, Cyclin D2, and p21 Levels and Cyclin-Dependent Kinase-4 Activity. Diabetes [Internet]. 2006;55(February):318–25. Available from: https://diabetesjournals.org/diabetes/article/55/2/318/12749/Akt-Induces-Cell-Proliferation-by-Regulating
312. Wei D, Wang L, Yan Y, Jia Z, Gagea M, Li Z, Zuo X, Kong X. KLF4 Is Essential for Induction of Cellular Identity Change and Acinar-to-Ductal Reprogramming during Early Pancreatic Carcinogenesis Article KLF4 Is Essential for Induction of Cellular Identity Change and Acinar-to-Ductal Reprogramming during Early Pancr. Cancer Cell [Internet]. 2016;29(3):324–38. Available from: http://dx.doi.org/10.1016/j.ccell.2016.02.005
313. Good AL, Cannon CE, Haemmerle MW, Yang J, Stanescu DE, Doliba NM,

Birnbaum MJ, Stoffers DA. JUND regulates pancreatic b cell survival during metabolic stress. Mol Metab [Internet]. 2019;25(April):95–106. Available from: https://doi.org/10.1016/j.molmet.2019.04.007

314. Dumayne C, Tarussio D, Sanchez-archidona AR, Picard A, Basco D, Berney XP, Ibberson M, Thorens B. Klf6 protects b -cells against insulin resistance- induced dedifferentiation. Mol Metab [Internet]. 2020;35(February):100958. Available from: https://doi.org/10.1016/j.molmet.2020.02.001
315. Kyriakis JM, Avruch J. MAP Kinase Pathways. Compend Inflamm Dis. 2016;892–908.
316. Widden H, Placzek WJ. The multiple mechanisms of MCL1 in the regulation of cell fate. Commun Biol [Internet]. 2021;4(1). Available from: http://dx.doi.org/10.1038/s42003-021-02564-6
317. Youle RJ, Strasser A. The BCL-2 protein family: Opposing activities that mediate cell death. Nat Rev Mol Cell Biol. 2008;9(1):47–59.
318. Stevens M, Oltean S. Modulation of the Apoptosis Gene Bcl-x Function Through Alternative Splicing. Front Genet. 2019;10(September):1–9.
319. Balmanno K, Cook SJ. Tumour cell survival signalling by the ERK1 / 2 pathway. Cell Death Differ. 2009;368–77.
320. Darling NJ, Cook SJ, Krebs J, Moreau M. The role of MAPK signalling pathways in the response to endoplasmic reticulum stress ☆. BBA - Mol Cell Res [Internet]. 2014;1843(10):2150–63. Available from: http://dx.doi.org/10.1016/j.bbamcr.2014.01.009
321. Verma G, Datta M. IL-1β induces ER stress in a JNK dependent manner that determines cell death in human pancreatic epithelial MIA PaCa-2 cells. Apoptosis. 2010;15(7):864–76.
322. Li X, Xu C, Yang P. c-Jun NH 2 -Terminal Kinase 1/2 and Endoplasmic Reticulum Stress as Interdependent and Reciprocal Causation in Diabetic Embryopathy. Diabetes. 2013;62(February):599–608.
323. Wali JA, Thomas HE. Pancreatic Alpha Cells Hold the Key to Survival. EBIOM [Internet]. 2015;2(5):368–9. Available from: http://dx.doi.org/10.1016/j.ebiom.2015.04.014
324. Marroqui L, Masini M, Merino B, Grieco FA, Millard I, Dubois C, Quesada I, Marchetti P, Cnop M, Eizirik DL. Pancreatic α Cells are Resistant to Metabolic Stress-induced Apoptosis in Type 2 Diabetes. EBioMedicine [Internet].

2015;2(5):378–85. Available from: http://dx.doi.org/10.1016/j.ebiom.2015.03.012

325. Kato A, Okura T, Hamada C, Miyoshi S, Katayama H, Higaki J, Ito R. Cell Stress Induces Upregulation of Osteopontin via the ERK Pathway in Type II Alveolar Epithelial Cells. 2014;9(6).
326. Kariya Y, Kariya Y, Virchow R. Osteopontin in Cancer : Mechanisms and Therapeutic Targets. Inernational J Transl Med. 2022;2:419–47.
327. Li T, Ni L, Liu X, Wang Z, Liu C. High glucose induces the expression of osteopontin in blood vessels in vitro and in vivo. Biochem Biophys Res Commun [Internet]. 2016;480(2):201–7. Available from: http://dx.doi.org/10.1016/j.bbrc.2016.10.027
328. Wang KX, Denhardt DT. Osteopontin: Role in immune regulation and stress responses. Cytokine Growth Factor Rev [Internet]. 2008 Oct;19(5–6):333–45. Available from: https://linkinghub.elsevier.com/retrieve/pii/S1359610108000658
329. Takemoto M, Yokote K, Yamazaki M, Ridall AL, Butler WT, Matsumoto T, Tamura K, Saito Y, Mori S. Enhanced Expression of Osteopontin by High Glucose in Cultured Rat Aortic Smooth Muscle Cells. 1999;726:722–6.
330. Cai M, Bompada P, Salehi A, Acosta JR, Prasad RB, Atac D, Laakso M, Groop L, De Marinis Y. Role of osteopontin and its regulation in pancreatic islet. Biochem Biophys Res Commun [Internet]. 2018;495(1):1426–31. Available from: https://doi.org/10.1016/j.bbrc.2017.11.147
331. Wendt A, Mollet IG, Knutsson A, Bolmgren VS, Hultgårdh-Nilsson A, Gomez MF, Eliasson L. Osteopontin Affects Insulin Vesicle Localization and Ca2+ Homeostasis in Pancreatic Beta Cells from Female Mice. Maedler K, editor. PLoS One [Internet]. 2017 Jan 20 [cited 2023 Feb 26];12(1):e0170498. Available from: https://dx.plos.org/10.1371/journal.pone.0170498
332. Zhang K, Kaufman RJ. From endoplasmic-reticulum stress to the inflammatory response. Nature. 2008;454(7203):455–62.
333. Szabo PA, Levitin HM, Miron M, Snyder ME, Senda T, Yuan J, Cheng YL, Bush EC, Dogra P, Thapa P, Farber DL, Sims PA. Single-cell transcriptomics of human T cells reveals tissue and activation signatures in health and disease. Nat Commun [Internet]. 2019;10(1). Available from: http://dx.doi.org/10.1038/s41467-019-12464-3
334. Elgueta R, Benson MJ, De Vries VC, Wasiuk A, Guo Y, Noelle RJ. Molecular mechanism and function of CD40/CD40L engagement in the immune system. Immunol Rev. 2009;229(1):152–72.

335. Iida T, Wagatsuma K, Hirayama D, Nakase H. Is osteopontin a friend or foe of cell apoptosis in inflammatory gastrointestinal and liver diseases? Int J Mol Sci. 2018;19(1).
336. Du Y, Mao L, Wang Z, Yan K, Zhang L, Zou J. Osteopontin - The stirring multifunctional regulatory factor in multisystem aging. Front Endocrinol (Lausanne). 2022;13(December):1–14.
337. Toschi A, Lee E, Xu L, Garcia A, Gadir N, Foster DA. Regulation of mTORC1 and mTORC2 Complex Assembly by Phosphatidic Acid: Competition with Rapamycin. Mol Cell Biol. 2009;29(6):1411–20.
338. Diehl JA, McQuiston A. Recent insights into PERK-dependent signaling from the stressed endoplasmic reticulum. F1000Research. 2017;6(0):1–11.
339. Fyffe C, Falasca M. 3-Phosphoinositide-Dependent Protein Kinase-1 As an Emerging Target in the Management of Breast Cancer. Cancer Manag Res. 2013;5(1):271–80.
340. Song G, Ouyang G, Bao S. The activation of Akt/PKB signaling pathway and cell survival. J Cell Mol Med. 2005;9(1):59–71.
341. Nie T, Yang S, Ma H, Zhang L, Lu F, Tao K, Wang R, Yang R, Huang L, Mao Z, Yang Q. Regulation of ER stress-induced autophagy by GSK3B-TIP60-ULK1 pathway. Cell Death Dis. 2016;7(12).
342. Wei WH, Hemani G, Gyenesei A, Vitart V, Navarro P, Hayward C, Cabrera CP, Huffman JE, Knott SA, Hicks AA, Rudan I, Pramstaller PP, Wild SH, Wilson JF, Campbell H, Hastie ND, Wright AF, Haley CS. Genome-wide analysis of epistasis in body mass index using multiple human populations. Eur J Hum Genet [Internet]. 2012;20(8):857–62. Available from: http://dx.doi.org/10.1038/ejhg.2012.17
343. Kebede MA, Oler AT, Gregg T, Balloon AJ, Johnson A, Mitok K, Rabaglia M, Schueler K, Stapleton D, Thorstenson C, Wrighton L, Floyd BJ, Richards O, Raines S, Eliceiri K, Seidah NG, Rhodes C, Keller MP, Coon JL, Audhya A, Attie AD. SORCS1 is necessary for normal insulin secretory granule biogenesis in metabolically stressed β cells. J Clin Invest. 2014 Oct 1;124(10):4240–56.
344. Wendt A, Mollet IG, Knutsson A, Bolmgren VS, Hultgårdh-Nilsson A, Gomez MF, Eliasson L. Osteopontin affects insulin vesicle localization and Ca2+ homeostasis in pancreatic beta cells from female mice. PLoS One. 2017;12(1):1–14.
345. Arafat HA, Katakam AK, Chipitsyna G, Gong Q, Vancha AR, Gabbeta J, Dafoe DC. Osteopontin protects the islets and β-cells from interleukin-1 β-mediated

cytotoxicity through negative feedback regulation of nitric oxide. Endocrinology. 2007;148(2):575–84.

346. Simonson DC, DeFronzo RA. Indirect calorimetry: Methodological and interpretative problems. Vol. 258, American Journal of Physiology - Endocrinology and Metabolism. 1990.
347. Turinese I, Marinelli P, Bonini M, Rossetti M, Statuto G, Filardi T, Paris A, Lenzi A, Morano S, Palange P. “Metabolic and cardiovascular response to exercise in patients with type 1 diabetes.” Vol. 40, Journal of Endocrinological Investigation. 2017. p. 999–1005.
348. Hamel FG, Bennett RG, Upward JL, Duckworth WC. Insulin inhibits peroxisomal fatty acid oxidation in isolated rat hepatocytes. Endocrinology. 2001;142(6):2702–6.
349. Gilbert M. Role of skeletal muscle lipids in the pathogenesis of insulin resistance of obesity and type 2 diabetes. J Diabetes Investig. 2021;12(11):1934–41.
350. Olsen D, Wellner N, Kaas M, de Jong IEM, Sotty F, Didriksen M, Glerup S, Nykjaer A. Altered dopaminergic firing pattern and novelty response underlie ADHD-like behavior of SorCS2-deficient mice. Transl Psychiatry [Internet]. 2021;11(1). Available from: http://dx.doi.org/10.1038/s41398-021-01199-9
351. Bergman BC, Brooks GA. Respiratory gas-exchange ratios during graded exercise in fed and fasted trained and untrained men. J Appl Physiol. 1999;86(2):479–87.
352. Röhling M, Martin K, Ellinger S, Schreiber M, Martin S, Kempf K. Weight reduction by the low-insulin-method— a randomized controlled trial. Nutrients. 2020;12(10):1–17.
353. Mottalib A, Kasetty M, Mar JY, Elseaidy T, Ashrafzadeh S, Hamdy O. Weight Management in Patients with Type 1 Diabetes and Obesity. Curr Diab Rep. 2017;17(10).
354. Thorel F, Népote V, Avril I, Kohno K, Desgraz R, Chera S, Herrera PL. Conversion of adult pancreatic α-cells to β-cells after extreme β-cell loss. Nature [Internet]. 2010 Apr 22;464(7292):1149–54. Available from: https://www.nature.com/articles/nature08894
355. Chera S, Baronnier D, Ghila L, Cigliola V, Jensen JN, Gu G, Furuyama K, Thorel F, Gribble FM, Reimann F, Herrera PL. Diabetes recovery by age-dependent conversion of pancreatic δ-cells into insulin producers. Nature [Internet]. 2014;514(7253):503–7. Available from: http://dx.doi.org/10.1038/nature13633

356. Kim-Muller JY, Fan J, Kim YJR, Lee SA, Ishida E, Blaner WS, Accili D. Aldehyde dehydrogenase 1a3 defines a subset of failing pancreatic β cells in diabetic mice. Nat Commun [Internet]. 2016;7:1–11. Available from: http://dx.doi.org/10.1038/ncomms12631
357. Veres A, Faust AL, Bushnell HL, Engquist EN, Kenty JHR, Harb G, Poh Y chuin, Sintov E, Gürtler M, Pagliuca FW, Peterson QP, Melton DA. Charting cellular identity during human in vitro β-cell differentiation. Nature [Internet]. 2019 May 8;569(7756):368–73. Available from: https://www.nature.com/articles/s41586-019-1168-5
358. Di Nardo F, Cogo CE, Faelli E, Morettini M, Burattini L, Ruggeri P. C-peptide-based assessment of insulin secretion in the Zucker fatty rat: A modelistic study. Vol. 10, PLoS ONE. 2015.
359. Duckworth WC, Bennett RG, Hamel FG. Insulin degradation: Progress and potential. Endocr Rev. 1998;19(5):608–24.
360. Neerman-Arbez M, Halban PA. Novel, non-crinophagic, degradation of connecting peptide in transformed pancreatic beta cells. J Biol Chem. 1993;268(22):16248–52.
361. Cao M, Isaac R, Yan W, Ruan X, Jiang L, Wan Y, Wang J, Wang E, Caron C, Neben S, Drygin D, Pizzo DP, Wu X, Liu X, Chin AR, Fong MY, Gao Z, Guo K, Fadare O, Schwab RB, Yuan Y, Yost SE, Mortimer J, Zhong W, Ying W, Bui JD, Sears DD, Olefsky JM, Wang SE. Cancer-cell-secreted extracellular vesicles suppress insulin secretion through miR-122 to impair systemic glucose homeostasis and contribute to tumour growth. Nat Cell Biol. 2022;24(6):954–67.
362. Mahadevan NR, Rodvold J, Sepulveda H, Rossi S, Drew AF, Zanetti M. Transmission of endoplasmic reticulum stress and pro-inflammation from tumor cells to myeloid cells. Proc Natl Acad Sci U S A. 2011;108(16):6561–6.
363. Sprenkle NT, Lahiri A, Simpkins JW, Meares GP. Endoplasmic reticulum stress is transmissible in vitro between cells of the central nervous system. J Neurochem [Internet]. 2019 Feb 18;148(4):516–30. Available from: https://onlinelibrary.wiley.com/doi/10.1111/jnc.14642
364. Beck B. Neuropeptide Y in normal eating and in genetic and dietary-induced obesity. Philos Trans R Soc B Biol Sci. 2006;361(1471):1159–85.
365. Zhang L, Hernandez-Sanchez D, Herzog H. Regulation of feeding-related behaviors by arcuate neuropeptide Y neurons. Endocrinology. 2019;160(6):1411–

20.

366. Baldini G, Phelan KD. The melanocortin pathway and control of appetite-progress and therapeutic implications. J Endocrinol. 2019;241(1):R1–33.
367. Lin EE, Scott-Solomon E, Kuruvilla R. Peripheral Innervation in the Regulation of Glucose Homeostasis. Trends Neurosci [Internet]. 2021 Mar;44(3):189–202. Available from: https://linkinghub.elsevier.com/retrieve/pii/S0166223620302484
368. Steuernagel L, Lam BYH, Klemm P, Dowsett GKC, Bauder CA, Tadross JA, Hitschfeld TS, del Rio Martin A, Chen W, de Solis AJ, Fenselau H, Davidsen P, Cimino I, Kohnke SN, Rimmington D, Coll AP, Beyer A, Yeo GSH, Brüning JC. HypoMap—a unified single-cell gene expression atlas of the murine hypothalamus. Nat Metab. 2022;4(10):1402–19.
369. Toma JS, Karamboulas K, Carr MJ, Kolaj A, Yuzwa SA, Mahmud N, Storer MA, Kaplan DR, Miller FD. Peripheral nerve single-cell analysis identifies mesenchymal ligands that promote axonal growth. eNeuro. 2020;7(3):1–70.
370. Ziffert I, Kaiser A, Babilon S, Mörl K, Beck-Sickinger AG. Unusually persistent Gαi-signaling of the neuropeptide Y2 receptor depletes cellular Gi/o pools and leads to a Gi-refractory state. Cell Commun Signal. 2020;18(1):1–16.
371. Haber AL, Biton M, Rogel N, Herbst RH, Shekhar K, Smillie C, Burgin G, Delorey TM, Howitt MR, Katz Y, Tirosh I, Beyaz S, Dionne D, Zhang M, Raychowdhury R, Garrett WS, Rozenblatt-Rosen O, Shi HN, Yilmaz O, Xavier RJ, Regev A. A single-cell survey of the small intestinal epithelium. Nature. 2017;551(7680):333–9.
372. Skeldal S, Voss LF, Lende J, Pedersen SB, Mølgaard S, Kaas M, Demange P, Bentsen AH, Fuglsang M, Sander MR, Buttenschøn H, Gustafsen C, Madsen P, Glerup S. Alternative splicing regulates adaptor protein binding, trafficking, and activity of the Vps10p domain receptor SorCS2 in neuronal development. J Biol Chem [Internet]. 2023;299(9):105102. Available from: https://doi.org/10.1016/j.jbc.2023.105102
373. Guan SS, Sheu ML, Yang R Sen, Chan DC, Wu CT, Yang TH, Chiang CK, Liu SH. The pathological role of advanced glycation end productsdownregulated heat shock protein 60 in islet β-cell hypertrophy and dysfunction. Oncotarget. 2016;7(17):23072–87.
374. Eizirik DL, Szymczak F, Mallone R. Why does the immune system destroy pancreatic β-cells but not α-cells in type 1 diabetes? Nat Rev Endocrinol. 2023;19(7):425–34.

375. Tai TW, Su FC, Chen CY, Jou IM, Lin CF. Activation of p38 MAPK-regulated Bcl-xL signaling increases survival against zoledronic acid-induced apoptosis in osteoclast precursors. Bone [Internet]. 2014;67:166–74. Available from: http://dx.doi.org/10.1016/j.bone.2014.07.003
376. Loo LSW, Soetedjo AAP, Lau HH, Ng NHJ, Ghosh S, Nguyen L, Krishnan VG, Choi H, Roca X, Hoon S, Teo AKK. BCL-xL/BCL2L1 is a critical anti-apoptotic protein that promotes the survival of differentiating pancreatic cells from human pluripotent stem cells. Cell Death Dis [Internet]. 2020;11(5). Available from: http://dx.doi.org/10.1038/s41419-020-2589-7
377. Yue J, López JM. Understanding MAPK signaling pathways in apoptosis. Int J Mol Sci. 2020;21(7).
378. Wagner EF, Nebreda ÁR. Signal integration by JNK and p38 MAPK pathways in cancer development. Nat Rev Cancer. 2009;9(8):537–49.
379. van Oosten-Hawle P, Morimoto RI. Organismal proteostasis: Role of cell-nonautonomous regulation and transcellular chaperone signaling. Genes Dev. 2014;28(14):1533–43.
380. Rodvold JJ, Chiu KT, Hiramatsu N, Nussbacher JK, Galimberti V, Mahadevan NR, Willert K, Lin JH, Zanetti M. Intercellular transmission of the unfolded protein response promotes survival and drug resistance in cancer cells. Sci Signal. 2017;10(482).
381. Sthijns MMJPE, Rademakers T, Oosterveer J, Geuens T, Van Blitterswijk CA, LaPointe VLS. The response of three-dimensional pancreatic alpha and beta cell co-cultures to oxidative stress. PLoS One [Internet]. 2022;17(3 March):1–15. Available from: http://dx.doi.org/10.1371/journal.pone.0257578
382. Kim HK, Kim MG, Leem KH. Collagen hydrolysates increased osteogenic gene expressions via a MAPK signaling pathway in MG-63 human osteoblasts. Food Funct. 2014;5(3):573–8.
383. Wu J, Wu D, Zhang L, Lin C, Liao J, Xie R, Li Z, Wu S, Liu A, Hu W, Xi Y, Bu S, Wang F. NK cells induce hepatic ER stress to promote insulin resistance in obesity through osteopontin production. J Leukoc Biol. 2020;107(4):589–96.
384. Dalal S, Zha Q, Singh M, Singh K. Osteopontin-stimulated apoptosis in cardiac myocytes involves oxidative stress and mitochondrial death pathway: role of a pro-apoptotic protein BIK. Mol Cell Biochem. 2016;418(1–2):1–11.
385. Kaido T, Yebra M, Cirulli V, Montgomery AM. Regulation of human β-cell adhesion,

motility, and insulin secretion by collagen IV and its receptor α1β1. J Biol Chem [Internet]. 2004;279(51):53762–9. Available from: http://dx.doi.org/10.1074/jbc.M411202200

386. Singh M, Dalal S, Singh K. Osteopontin: At the cross-roads of myocyte survival and myocardial function. Life Sci [Internet]. 2014 Nov;118(1):1–6. Available from: https://linkinghub.elsevier.com/retrieve/pii/S0024320514007632
387. Barillaro M, Schuurman M, Wang R. β1-Integrin - A Key Player in Controlling Pancreatic Beta-Cell Insulin Secretion via Interplay With SNARE Proteins. Endocrinol (United States) [Internet]. 2023;164(1):1–8. Available from: https://doi.org/10.1210/endocr/bqac179
388. Ohara-Imaizumi M, Aoyagi K, Yamauchi H, Yoshida M, Mori MX, Hida Y, Tran HN, Ohkura M, Abe M, Akimoto Y, Nakamichi Y, Nishiwaki C, Kawakami H, Hara K, Sakimura K, Nagamatsu S, Mori Y, Nakai J, Kakei M, Ohtsuka T. ELKS/Voltage-Dependent Ca2+ Channel-β Subunit Module Regulates Polarized Ca2+ Influx in Pancreatic β Cells. Cell Rep [Internet]. 2019;26(5):1213-1226.e7. Available from: https://doi.org/10.1016/j.celrep.2018.12.106
389. Ohara-Imaizumi M, Ohtsuka T, Matsushima S, Akimoto Y, Nishiwaki C, Nakamichi Y, Kikuta T, Nagai S, Kawakami H, Watanabe T, Nagamatsu S. ELKS, a Protein Structurally Related to the Active Zone-associated Protein CAST, Is Expressed in Pancreatic β Cells and Functions in Insulin Exocytosis: Interaction of ELKS with Exocytotic Machinery Analyzed by Total Internal Reflection Fluorescence Micro. Mol Biol Cell [Internet]. 2005 Jul;16(7):3289–300. Available from: https://www.molbiolcell.org/doi/10.1091/mbc.e04-09-0816
390. Nevins AK, Thurmond DC. A direct interaction between Cdc42 and vesicle-associated membrane protein 2 regulates SNARE-dependent insulin exocytosis. J Biol Chem [Internet]. 2005;280(3):1944–52. Available from: http://dx.doi.org/10.1074/jbc.M409528200
391. Kim SM, Lee EJ, Jung HS, Han N, Kim YJ, Kim TK, Kim TN, Kwon MJ, Lee SH, Park JH, Rhee BD, Kim MK. Co-Culture of α TC-6 cells and β TC-1 cells: Morphology and function. Endocrinol Metab. 2015;30(1):92–7.

Statutory Declaration

“I, Oleksandra Kalnytska by personally signing this document in lieu of an oath, hereby affirm that I prepared the submitted dissertation on the topic “SORCS2 activity in pancreatic α cells safeguards insulin secretion from pancreatic β cells under glucose stress / Die Aktivität von SORCS2 in den pankreatischen α-Zellen schützt die Insulinsekretion der pankreatischen β-Zellen bei Glukosebelastung” independently and without the support of third parties, and that I used no other sources and aids than those stated.

All parts which are based on the publications or presentations of other authors, either in letter or in spirit, are specified as such in accordance with the citing guidelines. The sections on methodology (in particular regarding practical work, laboratory regulations, statistical processing) and results (in particular regarding figures, charts and tables) are exclusively my responsibility.

Furthermore, I declare that I have correctly marked all of the data, the analyses, and the conclusions generated from data obtained in collaboration with other persons, and that I have correctly marked my own contribution and the contributions of other persons (cf. declaration of contribution). I have correctly marked all texts or parts of texts that were generated in collaboration with other persons.

My contributions to any publications to this dissertation correspond to those stated in the below joint declaration made together with the supervisor. All publications created within the scope of the dissertation comply with the guidelines of the ICMJE (International Committee of Medical Journal Editors; http://www.icmje.org) on authorship. In addition, I declare that I shall comply with the regulations of Charité – Universitätsmedizin Berlin on ensuring good scientific practice.

I declare that I have not yet submitted this dissertation in identical or similar form to another Faculty.

The significance of this statutory declaration and the consequences of a false statutory declaration under criminal law (Sections 156, 161 of the German Criminal Code) are known to me.”

Date Signature

Declaration of own contribution to the publication

Oleksandra Kalnytska contributed the following to the below listed publications:

Publication 1:

Kalnytska, O., Qvist, P., Kunz, S., Conrad, T., Willnow, T.E., Schmidt, V., 2024. SORCS2 activity in pancreatic α-cells safeguards insulin granule formation and release from glucose-stressed β-cells. IScience 27(1), Doi: 10.1016/j.isci.2023.108725.

Contribution:

In the preparation of this publication, I played a multifaceted role in designing experiments, acquiring experimental data, conducting data analysis, and contributing to manuscript writing. Specific contributions include:

- Figures 1 and 5 (A-D): I conducted immunostaining, performed confocal microscopy, and executed image analysis.
- Figures 2 (B-C), 3 (D-F), 4, 9, and Supplementary Tables 1-3: I designed and executed experiments, collected data, and conducted data analysis.
- Figure 5 (E-F): I was responsible for sample collection and image analysis.
- Figures 6 (B, D-E), 8 (A-C), and Supplementary Figure S1 and S2: I conducted GO analysis and generated graphs using the clusterProfiler R package.
- Figures 7 (C-D): I performed Differential DEG and GO analysis, and created corresponding graphs using the clusterProfiler R package.

Additionally, I took the lead in creating all figures, excluding the graphical abstract. I contributed to drafting the manuscript and played a role in addressing reviewers' comments.

_____

Signature, date and stamp of first supervising university professor / lecturer

_____

Signature of doctoral candidate

Publication list

1. Kalnytska O, Qvist P, Kunz S, Conrad T, Willnow TE, Schmidt V. SORCS2 activity in pancreatic α-cells safeguards insulin granule formation and release from glucose-stressed β-cells. iScience. 2024;27(1).
2. Asaro A, Sinha R, Bakun M, Kalnytska O, Carlo-Spiewok AS, Rubel T, Rozeboom A, Dadlez M, Kaminska B, Aronica E, Malik AR, Willnow TE. ApoE4 disrupts interaction of sortilin with fatty acid-binding protein 7 essential to promote lipid signaling. J Cell Sci. 2021;134(20).
3. Schraut KG, Kalnytska O, Lamp D, Jastroch M, Eder M, Hausch F, Gassen NC, Moore S, Nagaraj N, Lopez JP, Chen A, Schmidt MV. Loss of the psychiatric risk factor SLC6A15 is associated with increased metabolic functions in primary hippocampal neurons. Eur J Neurosci. 2021;53(2).
4. Xicoy H, Brouwers JF, Kalnytska O, Wieringa B, Martens GJM. Lipid Analysis of the 6-Hydroxydopamine-Treated SH-SY5Y Cell Model for Parkinson's Disease. Mol Neurobiol. 2020;57(2).

Acknowledgments

I would like to express my deepest gratitude to my supervisor, Prof. Dr. Thomas E. Willnow, for his unwavering support, invaluable guidance, and limitless patience throughout my entire thesis journey. His expertise and mentorship have been instrumental in shaping my research and academic growth. I would also like to thank my thesis advisory committee members Prof. Dr. Michael Gotthardt and Prof. Dr. Norbert Hübner whose guidance and insights have significantly enriched the development of this thesis.

I extend my sincere thanks to my lab members, each of whom has played a pivotal role in shaping the trajectory of this thesis. Dr. Vanessa Schmidt's generous contribution of preliminary results significantly enriched the foundation of this work. Her collaboration and insights were indispensable to the success of my research.

A special acknowledgment goes to our dedicated lab technicians, whose roles were instrumental in advancing my research endeavors. Tatjana Pasternack's teaching, Kristin Kampf's assistance with experiments, and Christine Kruse's unwavering support have been indispensable to the progression of my project.

Dr. Alexis Shih deserves heartfelt gratitude for sharing extensive knowledge and expertise in islet biology. Her guidance and teachings on various methods were pivotal to the experimental aspects of my research.

Mrs. Verona Kuhle, with her unwavering support in handling administrative tasks and aiding in my relocation to Berlin, deserves special mention. Her contributions went beyond measure, greatly easing the challenges of navigating administrative complexities.

I would also like to express my gratitude to my lab mates, Alexis, Rishabh, and Megan. Their camaraderie and friendship added excitement to the daily lab life, and I am truly grateful for their genuine companionship.

I extend my appreciation to all those in MDC who helped me with volunteering and collecting so needed resources for people in Ukraine at the beginning of the war. And I would like to thank my supervisor Prof. Dr. Thomas Willnow for allowing me to dedicate some time and space in the lab to create a hub for those who wanted to help Ukrainian people.

Lastly, I reserve my deepest gratitude for a remarkable woman who has been the unwavering force behind my Ph.D. journey — my mother, Tamara Palyvoda. Her unwavering support, boundless encouragement, and unshakeable belief in my abilities have been the true pillars of my strength. In the face of numerous challenges and setbacks, her guidance and patience were the guiding lights that helped me rise from every fall. Despite the harrowing circumstances of war in Ukraine, with each day marked by bomb shelling, she steadfastly remained a source of comfort and support whenever I needed it. The sacrifices she made to raise my brother and me, enabling us to pursue our dreams, are immeasurable.

As I reflect on the completion of this academic journey, I dedicate this thesis to my mother, who epitomizes resilience, love, and sacrifice. Her enduring spirit has not only shaped my character but has also fueled my pursuit of knowledge and excellence. This work stands as a tribute to her indomitable spirit and serves as a testament to the profound impact of a mother's love and sacrifice.

Certificate of the accredited statistician

CHARITÉ
UNIVERSITÄTSMEDIZIN BERLIN

Charité | Charitéplatz 1 | 10117 Berlin

Name, Vorname: Kalnytska, Oleksandra
Emailadresse: oleksandra.kalnytska@mdc-berlin.de
Matrikelnummer: 228102
Promotionsbetreuerin: Prof. Dr. Thomas E. Willnow
Promotionsinstitution / Klinik: Max Delbrueck Centre for Molecular Medicine

Institut für Biometrie und Klinische Epidemiologie

Institutsleiter (kommissarisch)
Prof. Dr. Frank Konietschke

Postadresse
Campus Charité Mitte
Charitéplatz 1 | 10117 Berlin

Besuchsadresse
Sauerbruchweg 3 | Ebene 2 | Raum 060

T +49 30 450 562 161
frank.konietschke@charite.de

Berlin, 2. Februar 2023

Bearbeitet von:
Dr.rer.medic. Pimrapat Gebert
T +49 30 450 562 173
pimrapat.gebert@charite.de

Bescheinigung

Hiermit bescheinige ich, dass *Frau Oleksandra Kalnytska* innerhalb der Service Unit Biometrie des Instituts für Biometrie und klinische Epidemiologie (iBikE) bei mir eine statistische Beratung zu einem Promotionsvorhaben wahrgenommen hat. Folgende Beratungstermine wurden wahrgenommen:

- Termin 1: 10.03.2023
- Termin 2: 02.02.2024

Folgende wesentliche Ratschläge hinsichtlich einer sinnvollen Auswertung und Interpretation der Daten wurden während der Beratung erteilt:

- Prüfung der Normalverteilung
- T-Test für unabhängige Stichproben oder Mann-Whitney-U-Test
- Two-way ANOVA und Two-way repeated measures ANOVA
- Post-hoc test

Diese Bescheinigung garantiert nicht die richtige Umsetzung der in der Beratung gemachten Vorschläge, die korrekte Durchführung der empfohlenen statistischen Verfahren und die richtige Darstellung und Interpretation der Ergebnisse. Die Verantwortung hierfür obliegt allein dem Promovierenden. Das Institut für Biometrie und klinische Epidemiologie übernimmt hierfür keine Haftung.

Datum: 02.02.2024 Name der Beraterin: Dr. Pimrapat Gebert

Pimrapat Gebert
Digital unterschrieben von Pimrapat Gebert
Datum: 2024.02.02 13:56:27 +01'00'

Unterschrift Beraterin, Institutsstempel

CHARITÉ
UNIVERSITÄTSMEDIZIN BERLIN
Institut für Biometrie und Klinische Epidemiologie
Campus Charité Mitte
Charitéplatz 1 | 10117 Berlin